Seismic site effects for the Island of Montreal

by

Mohammad Kamruzzaman Talukder, BSc Eng., M Eng. (with Thesis)

Department of Civil Engineering and Applied Mechanics

McGill University

Montreal, Quebec, Canada

July, 2017

A thesis submitted to McGill University in partial fulfillment of the requirements of the degree of

Doctor of Philosophy in Civil Engineering

TABLE OF CONTENTS

ACRONYMS

CENA: Central and Eastern North America

EPRI: Electric Power Research Institute

F_a: Foundation Factor for short periods, the 2010 National Building Code of Canada

F_v: Foundation Factor for long periods, the 2010 National Building Code of Canada

F(0.01 s): Site Factor corresponding to amplification of PGA at a period of T=0.01 s

F_0: Site Fundamental Frequency (Hz)

F_C= Site factor at a period of T (s) for class C site

F_D= Site factor at a period of T (s) for class D site

ENA: Eastern North America

EL: Equivalent Linear Analysis

G/G_{max}: Ratio of Secant Shear Modulus to Maximum Shear Modulus

NL: Non-linear Analysis

MASW: Multi-channel Analysis of Surface Wave

NBCC: The National Building Code of Canada

RQD: Rock Quality Designation

T_0: Site Fundamental Period (s)

USGS: The United States Geological Survey

V_s: shear wave Velocity (m/s)

V_{s30}: Shear Wave Average Velocity (m/s) in top thirty meters of a soil profile

$Vs30_{SS}$: V_{s30} (m/s) estimated from Seismic Survey (SS)

$Vs30_{SL}$: V_{s30} (m/s) estimated from depth to bedrock (single layer, SL) information

$Vs30_{ML}$: V_{s30} (m/s) estimated from Multiple-Layer (ML) information

$Vs30_{F0}$: V_{s30} (m/s) estimated from F_0 information

WNA: Western North America

LIST OF TABLES

LIST OF FIGURES

ABSTRACT

In most national building codes, site classification is based on the V_{s30} parameter, the average shear wave velocity for the first 30 m of soil below the surface, and defines the 2010 NBCC foundation factors (e.g. F_a and F_v) to be applied to ground motions for a reference condition. Seismic microzonation mapping is usually achieved by combining information from various sources, each with varying degrees of uncertainties. A preliminary microzonation can be derived from surface geology or surface elevation maps, while a more detailed and accurate map is usually based on extensive seismic surveys. A procedure is proposed that progressively allows the integration of information from various sources and to estimate the degree of uncertainty on the microzonation. This allows planners to determine where microzonation maps require further investigations given current or future urban development plans. The proposed procedure uses conditional second moment estimation and provides the best linear unbiased estimates of V_{s30} and its uncertainty. Next, these estimates are used to derive soil classification probability maps and to compute the expected values and variance of foundation factors F_a ad F_v to be used in probabilistic seismic risk analyses. The proposed procedure is demonstrated for the seismic microzonation of the island of Montreal.

The site factors of F(0.2 s), F(0.5 s) and F(1.0 s) for seismic structural design are dependent on soil sites classes A, B, C, D and E. The site factors in the 2015 NBCC were derived from field data on ground motions recorded during earthquakes and equivalent linear and nonlinear analyses, and represent average responses for a wide variety of soils and ground motions. For sites of Eastern North America, very few strong ground motion records are available in order to determine empirically the site factors for soil classes. Recently, NGA-East has compiled data and performed Equivalent linear dynamic analyses of one-dimensional soil columns in order to update these factors. Using a similar approach, database for soil profiles at 12 sites in Montreal were analyzed with the equivalent linear 1-D method for natural and synthetic rock input motions scaled to 0.1 g, 0.2 g, 0.3 g, 0.4 g, and 0.5 g. The site factors are computed from the 1-D response analyses. From the results of numerical predictions, new regression curves are derived for the relation between the site factors and V_{s30}, and for the relation between the site factors and fundamental site period. The site factors are compared to the factors of NBCC 2015. The results of this study indicate a large degree of scatter which may have an effect on overall hazards.

ABRÉGÉ

Dans la plupart des codes de construction nationaux, la classification des sites est basée sur le paramètre V_{s30}, la vitesse moyenne des ondes de cisaillement jusqu'à une profondeur de 30 m en dessous de la surface, et définit les facteurs de fondation (F_a et F_v) appliqués aux mouvements de référence. Un microzonage sismique délimite une règion en fonction des types de sols et est généralement obtenu en combinant l'information provenant de diverses sources, chacune ayant un degré d'incertitude variable. Un microzonage préliminaire peut être dérivé à partir des cartes de la géologie de la surface ou des cartes de l'élévation de la surface, tandis qu'un plan plus détaillé et spécifique est généralement basé sur des études sismiques plus approfondies. Une procédure est proposée pour l'intégration progressive de l'information provenant de diverses sources et l'estimation du degré d'incertitude sur le microzonage. Cette approche permet aux planificateurs de déterminer à quels emplacements la carte de microzonage nécessite des recherches plus approfondies considérant les plans de développement urbain actuels ou futurs. La procédure proposée utilise une estimation conditionnelle du second ordre et fournit les meilleures estimations linéaires non biaisées de V_{s30} et son incertitude. Ensuite, ces estimations sont utilisées pour dériver des cartes des probabilités de classification des sols et pour calculer la valeur moyenne et la variance des facteurs de fondation F_a et F_v qui sont plus appropriés dans les analyses probabilistes du risque sismique. La méthode proposée est démontrée pour le microzonage sismique de l'île de Montréal.

Les facteurs de site F(0,2 s), F(0,5 s) et F(1,0 s) sont définis pour chaque classe de sol A, B, C, D et E. Les facteurs de site dans le 2015 CNBC ont été obtenus à partir de données sur les mouvements des sols enregistrées durant des tremblements de terre et des analyses équivalentes linéaires et non-linéaires, et représentent des réponses moyennes pour une grande variété de sols ainsi qu'une grande variété de mouvements de terre. Pour les sites de l'Est de l'Amérique du Nord, très peu d'enregistrements des mouvements de sol forts sont disponibles afin de déterminer empiriquement des facteurs de site pour les différentes classes de sol. Récemment, NGA-Est a compilé des données et a effectué des analyses dynamiques linéaires équivalentes de colonnes de sol unidimensionnelles afin de mettre à jour ces facteurs En utilisant une approche similaire, une base de données des profils des sols pour le 12 sites à Montréal a été analysé avec la méthode linéaire équivalente unidimensionnelle. Des séismes naturels et synthétiques ont été utilisés. Les mouvements du sol sélectionnés couvrent une gamme des à 0,1 g, 0,2 g, 0,3 g, 0,4 g, et 0,50 g.

Les facteurs de site sont calculés par les analyses 1-D. Les résultats numériques sont utilisés pour dériver des nouvelles régressions pour la relation entre les facteurs de site et V_{s30} et pour la relation entre les facteurs de site et la période fondamentale du site. Les facteurs calculés sont comparés aux facteurs de CNBC 2015. Les résultats de cette étude indiquent un grand degré de dispersion qui peut avoir un effet sur les risques globaux.

DEDICATION

This Thesis is dedicated to the advancement of the study of science.

ACKNOWLEDGMENTS

I express my heartfelt gratitude to my doctoral Thesis supervisor Professor Dr. Luc Chouinard for his supervision of the Thesis. I am thankful to him for providing me with the Graduate Research Assistantship Award. I would like to thank Professor Dr. Luc Chouinard, Dr. Philippe Rosset, and Dr. Myriam Bour-Belvaux for providing me with data of geotechnical boreholes and seismic survey. I would like to thank Dr. Philippe Rosset for introducing me with the ArcMap software and the Tromino device. I am also thankful to McGill University for providing me with the McGill International Doctoral Award and Principal's Graduate Fellowship. Today, I am profoundly grateful to my parents, deceased grandmothers, deceased grandfathers, and caring brothers for their best wishes to my life. I sincerely thank my colleagues, my friends for encouraging me in the pursuit of my postgraduate studies. I thank the staff of McGill University for assisting me to navigate through the McGill University administrative procedures.

CONTRIBUTION OF AUTHORS

Chapter 3 of the thesis has been published as a journal article in the Bulletin of Earthquake Engineering (Probabilistic methods for the estimation of seismic Fa and Fv maps—application to Montreal, Bulletin of Earthquake Engineering, a journal of Springer, volume 14 (No. 2), pp. 345–372, DOI 10.1007/s10518-015-9832-0, 2016. Mohammad Kamruzzaman Talukder conducted the research under the supervision of Luc Chouinard. Mohammad Kamruzzaman Talukder is the primary author, and Luc Chouinard is the 2nd author.

Chapter 4 of the thesis is prepared as a manuscript to be submitted to a journal for publication. The details of the article are: titled 'Seismic Site Amplification Factors from Site Response Analysis for Typical Soil Profiles in Montreal', co-authored by Mohammad Kamruzzaman Talukder and Luc Chouinard. The authors are from McGill University. Mohammad Kamruzzaman Talukder conducted the research under the supervision of Luc Chouinard.

1 Introduction

1.1 Introduction

The 2015 National Building Code of Canada (NBCC), as in the 2010 NBCC, incorporates a seismic site classification system that characterizes the surface geology at a given location for the purpose of defining design ground motions (spectral accelerations for different fundamental periods of vibrations of structures) for that location. In classifying sites, the 2010 NBCC considered the average shear wave velocity in the top 30 m soil (V_{s30}). Five of the six site categories (or classes) correspond to hard rock (class A, V_{s30}>1500 m/s), rock (class B, 1500<V_{s30}<760 m/s), soft rock or very dense soil (class C, 760<V_{s30}<360 m/s), stiff soil (class D, 360<V_{s30}<180 m/s), and soft soil (class E, V_{s30}<180 m/s). The sixth class soil (F) is a special case that comprises liquefiable soil layers requiring dynamic site response analyses to find ground amplification. Building codes have recognized that the impact of geological conditions on seismic ground motions should be taken into consideration when performing seismic design of structures. For this reason, the need for improving the site classification for the Island of Montreal is of great importance.

The 2010 NBCC suggested two seismic foundation factors F_a and F_v in order to capture the amplification effects of local soil conditions on rock motions. The NBCC 2010 design (5 % damped) spectral accelerations are provided for site class C for four shaking periods of 0.2 s, 0.5 s, 1.0 s and 2.0 s at uniform probability of exceedance of 2 % in 50 years. The design spectral accelerations at periods of 0.2 s ($S_{a,0.2s}$) and 1.0 s ($S_{a,1.0s}$) for other site classes A, B, D and E are derived by modifying the corresponding class C spectral accelerations and this modification is done by the seismic foundation factors F_a and F_v. The design factor F_a is used to modify the value of $S_{a,0.2s}$ and the factor F_v modifies the value of $S_{a,1.0s}$. The 2010 NBCC code also recommended peak ground acceleration (PGA) value for class C sites. The PGA for class C site is modified by the amplification factor F_a to estimate the PGA for other site classes-A, B, D and E.

For a given site, the F_a and F_v factors are determined by first assigning a site classification based on V_{s30}. In some instances, this information can be obtained from seismic microzonation maps that define the site classification as a function of location. These maps are usually derived by combining information from various sources but do not provide any information of the degree of uncertainty associated with the classification. To address this case, this study proposes probabilistic site classification maps accounting for the uncertainties in the V_{s30} prediction models.

Mathematical models relating shear wave velocity (V_s) to depth for clay, sand and silt deposits in Montreal have been obtained through a limited number of seismic surveys (Rosset et al., 2014). In general, it is acknowledged that the shear wave velocity (V_s) profiles measured by seismic survey are the most accurate information on V_s-depth data. Recent literature also presents V_{s30} models for Montreal which are developed by linking soil stratigraphy data to the V_s-depth data (Rosset et al., 2014). Recently, V_{s30} models have also been developed using the site fundamental frequency as well as depth to bedrock. Each of these V_{s30} models has different degree of uncertainties. However, current site classification methodologies for microzonation maps do not express the degree of uncertainty in classifying a site. This study proposes new procedure that integrate data from different sources: detailed stratigraphy, site fundamental frequencies, depth to bedrock information and detailed seismic surveys into a site classification in order to improve the spatial resolution of microzonation maps and provide estimates of uncertainty in site classification in the form of site class (A, B, C, D or E) probabilities. The microzonation map is also used to derive mean values and standard deviations for site factors.

It is well recognized that the soft soils strongly affect the amplitudes of seismic waves travelling from bedrock to the surface. The magnitude 5.8 Saguenay Earthquake in Quebec in 1988 illustrates the extent of damage that can be caused even at distances up to 350 km from the epicenter due to site effects. In this instance, damage was observed when masonry from the façade of the Montreal East City Hall fell during the earthquake due to the amplification of ground motions at a site with 13 m of clay. This warrants for 1-D seismic response analyses with soil profiles and ground input motions relevant to the island of Montreal

The 2015 NBCC brings significant changes to the 2010 NBCC seismic design provisions. Between the time of publication of the 2010 NBCC and 2015 NBCC, significant ground motion data have become available. The availability of more data has led to a number of changes in the 2015 NBCC. The design spectral accelerations currently provided in the 2015 NBCC have been specified for periods of 0.2, 0.5, 1.0, 2.0, 5.0, and 10.0 s. The design spectral accelerations is given by $S(T)=F(T)S_a(T)$ for the given site, where F(T) is the site factor corresponding to period of T (s). The site factors currently used in the 2015 NBCC code are also provided as a function of V_{s30} for periods of 0.2, 0.5, 1, 2, 5 and 10 s. In the current 2015 NBCC, as in the 2010 NBCC, site classification is based on V_{s30}, and the site class C is taken as the reference site condition.

The NBCC 2015 amplification factors are derived primarily from statistical analysis of strong motions data recorded at WNA sites, not based on ground motions observed at highly variable site conditions in Montreal, where strong ground motion recordings are seldom available. Furthermore, the ground motions data used in the 2015 NBCC also include the observed data used in the NBCC 2010. The ground motion data used in the 2010 NBCC were primarily obtained from the Loma Prieta earthquake with an epicenter in the Santa Cruz Mountains, about 90 km from the San Francisco Bay region. The site conditions in San Francisco Bay correspond to soft clay sites. The 1-D ground response analyses were performed for V_s-depth profiles typical of sites along the shorelines of San Francisco Bay. The soil deposits considered for the 1-D study were to a maximum depth of 218 m. In contrast, clay sites in Montreal are about 1 m to 33 m deep, much shallower compared to the Bay area. In addition, the shear wave velocity for bedrock in the island of Montreal varies over a wide range of 1000 m/s to 4000 m/s (Rosset et al., 2014). For these reasons, this study investigates the site factors for site conditions, bedrock shear wave velocities and earthquake ground motions for Montreal conditions to validate the appropriateness of the NBCC site factors. Instead of using the GMPEs, the use of 1-D ground response method for a site-specific evaluation of site effects conceptually allows the stratigraphy of a site to be taken into consideration.

This study uses the newly acquired shear wave velocity profiles (Rosset et al., 2014) for evaluating the site factors for Montreal through the 1-D ground response study. The major reason for performing the 1-D ground response is to incorporate the improvement in the knowledge of the V_s-depth relations for soil deposits in Montreal. A second reason for performing the 1-D site response analysis is to determine whether or not the 2015 NBCC provisions provide the site factors for Montreal to an adequate level. The objectives of the thesis are the following:

- Determine the 2010 NBCC seismic site classifications for the Island of Montreal by using a limited number of seismic measurements of shear-wave velocities and fundamental frequencies,
- Propose and apply a methodology for the probabilistic microzonation of Montreal,

- Use the probabilities of site classification to develop maps for the 2010 NBCC site factors F_a and F_v,
- Propose new foundation factors F(0.2 s), F(0.5 s) and F(1.0 s) as a function of V_{s30} and compare them with published results for sites similar to the Island of Montreal.

1.2 Organization of this Thesis

Chapter 1 introduces the issues and objectives of the thesis. This chapter also presents the structure of the thesis, and the main original contributions.

Chapter 2 discusses the literature review on several topics covered in the thesis: the local seismicity and geological conditions, geotechnical properties of the surface deposits, previous seismic microzonations of Montreal, and the estimation of site amplification factors. The Chapter also presents the detail and analysis of the geotechnical data base developed for the purpose of the thesis and includes information that is not included in the articles that form the basis of the following chapters.

Chapter 3 presents the proposed probabilistic method for site classification and for the development of F_a and F_v maps for the Island of Montreal. This chapter describes the following components of the proposed methodology: 1) combining estimates of V_{s30} from various sources, 2) probabilistic microzonation mapping for site classification and for foundation factors (F_a and F_v).

Chapter 4 discusses the estimation of seismic site amplification factors from site response analysis for typical soil profiles in Montreal. This chapter comprises the following sections: 1) the selection of representative ground motions, 2) definition of typical soil profiles for Montreal and 3) the propagation of uncertainty to estimate the mean amplification factors for various soil classifications.

Chapter 5 presents the conclusions, original contributions and recommendations for future research. Chapter 5 is followed by references, appendices A, B, C, D, E and F.

2 Literature review and geotechnical database for Montreal sites

The literature review covers the following topics which are related to the objectives of this research project: 1) local seismicity and geotechnical conditions, (2) surface deposits in Montreal, 3) microzonation based on V_{s30}, 4) ground motion amplifications as a function of site classification.

2.1 Local seismicity and geotechnical condition

Several studies (Adams and Halchuk, 2007; Atkinson and Boore, 1995; Lamontagne et al., 2000) have addressed the seismicity in the proximity of the Island of Montreal. Seismicity studies identify all possible seismic sources as well as their characteristics in terms of recurrence rate of events above a threshold, the distribution of events in magnitude, focal depth and maximum magnitude. The seismicity is analyzed in combination with ground motion prediction equations that describe site effects as a function of epicentral distance and magnitude of earthquakes to produce seismic hazard functions. Adams and Halchuk (2007) present a map of seismic activity for Canada. The paper indicates that Montreal is located in an intraplate region of moderate seismic activity.

Prest and Hode-Keyser (1977) presented a detailed study of the surface geology for the Island of Montreal. The surface deposits of Montreal Island that overlie bedrock formation were derived from much older bedrock formation during a sequence of geological events of the Quaternary period, that is, the last 125,000 years of the earth's history. On Montreal Island, the basement rocks include igneous and metamorphic rock, that is, the Precambrian rocks start about 3500 million ago and end about 600 million years ago (Prest and Hode-Keyser, 1977). The hill of Mont Royal is referred to as a stock of alkaline igneous rock. On Montreal Island, the basement rocks are alkaline igneous rock overlain by sedimentary rocks including sandstone, shale, limestone, and dolomite. The sedimentary rocks are mainly from the Cambrian or Ordovician age, having been formed between about 515 and 440 million years before present (Prest and Hode-Keyser, 1977). Due to successive erosions of sedimentary rocks in the glacial (Wisconsian) age over the last 125,000 to 10,000 years, the surficial deposits of Montreal were formed in chronological sequence of glacial deposition described as Malone Till, Middle Till Complex and Fort Covington Till (Prest and Hode-Keyser, 1977). The oldest soil is termed as

Malone Till and was formed between 70,000 to 55,000 years before present. The Malone till was deposited by the south westward-flowing Malone ice in the St. Lawrence River valley (St. Lawrence Lowland). The Malone till in Montreal is generally stony and has a variable silty and sandy matrix (Prest and Hode-Keyser, 1977). The Middle-Till formation overlies the Malone till and was deposited during the recession of Malone ice as it fluctuated over the Montreal region over 55,000 to 25,000 years before present. The Middle till includes sand and gravel. The sandy and gravelly sediments occur around the hill of Mont Royal, especially on its south western side, whereas sand and gravel are intermixed in the lowland areas. Sand and gravel also occur in the Dorval area. Fort Covington tills overlie the Middle Till. Following the Quaternary recession of the Laurentide Ice Sheet, a climatic change took place that resulted in renewed glacierization during the 25,000 to 12,500 years before present. This glacial event resulted in an extensive Till sheet known as Fort Covington Till formation overlying the Middle Till formation. Fort Covington till formation is much finer and clayey than the Middle Till complex. The Champlain Sea and upper St. Lawrence valleys were again occupied by a succession of glacial lakes about 12,500 years before present (Prest and Hode-Keyser, 1977). The latest Laurentide Ice Sheet receded rapidly as the climate became warmer. The soil deposited by the rapid recession of the Laurentide Ice Sheet is known as Leda clay or marine clay. The Island of Montreal is situated within the lowlands of the contact point between the St. Lawrence River and the Ottawa River. The lowlands which extend from Montreal to Ottawa in Canada contain thick Leda clay.

2.2 Geotechnical properties of the surface deposits in Montreal

The Montreal urban areas are located on an island bordered southward and eastward by the St. Lawrence River and westward by the Des Prairies River. Due to subsequent urbanization, artificial fill has been placed on the low-lying sites across Montreal. In general, fills on the Island of Montreal consist of loose sand, and gravelly sand intermixed with varying amounts of silts, clay, boulders and miscellaneous materials such as brick, ash, rubble, etc. Montreal Island has clay deposits at the periphery of the island along the south, east, and west shoreline, sand deposits in the south central area, and at both tips of the island. The land-use map of Montreal indicate that some strategic areas of the city are within the soft soil zones, in particular, the downtown area and the Port of Montreal (Chouinard et al., 2004).

The effects of local soil site conditions on propagating seismic waves can be evaluated by studying the dynamic properties of subsurface deposits. Strong ground motion data suggests that ground-motions are sensitive to the stiffness of the soils underlying the recording sites (Borcherdt, 1994; Borcherdt and Glassmoyer, 1992). Rosset et al. (2014) discuss the impact on the subsurface geology on site fundamental frequencies and the estimation of V_{s30} for the seismic microzonation of Montreal. Benjumea et al. (2008) obtained shear wave velocity information for deposits in Ottawa and presented microzonation maps based on V_{s30} derived from integrating information from seismic surveys, data on depth to bedrock, location and type of major geological units, in order to correlate the measured V_s values with stratigraphic units. The geological units comprise of post-glacial sediments (fluvial silt, marine clay, and fluvial sand), glacial sediments (till, sand and gravel), Paleozoic rock (limestone, shale) and Precambrian bedrock.

Geotechnical borehole information on the Island of Montreal is used for the investigation of subsurface and 1-D shear wave velocity variation with depths. Shear wave velocity-depth profiles are routinely used as input to 1-D SHAKE analyses (Hunter et al., 2010). For such analyses, velocity-depth profiles from surface to the bedrock should be known. Several representative site profiles are determined in this study using the available borings and in-situ tests for the seismic 1-D ground response analyses of the urban environment. Geotechnical borehole data were obtained for the determination of representative soil profiles of Montreal to understand its stratigraphy. Each borehole is a summary of depth intervals and corresponding soil types such as sand, gravel, clay and silt. Three profiles of soil layers at three sites in Montreal are determined using a set of 150 geotechnical boreholes supplied by the city of Montreal. These sites are Jardin Botanic (marked by line from BG1 to BG2 in Figure 2.1), Street Notre Dame West (marked by a line from ND1 to ND2 in Figure 2.1) and Street Notre Dame East (marked by a line from ND3 to ND4 in Figure 2.1).

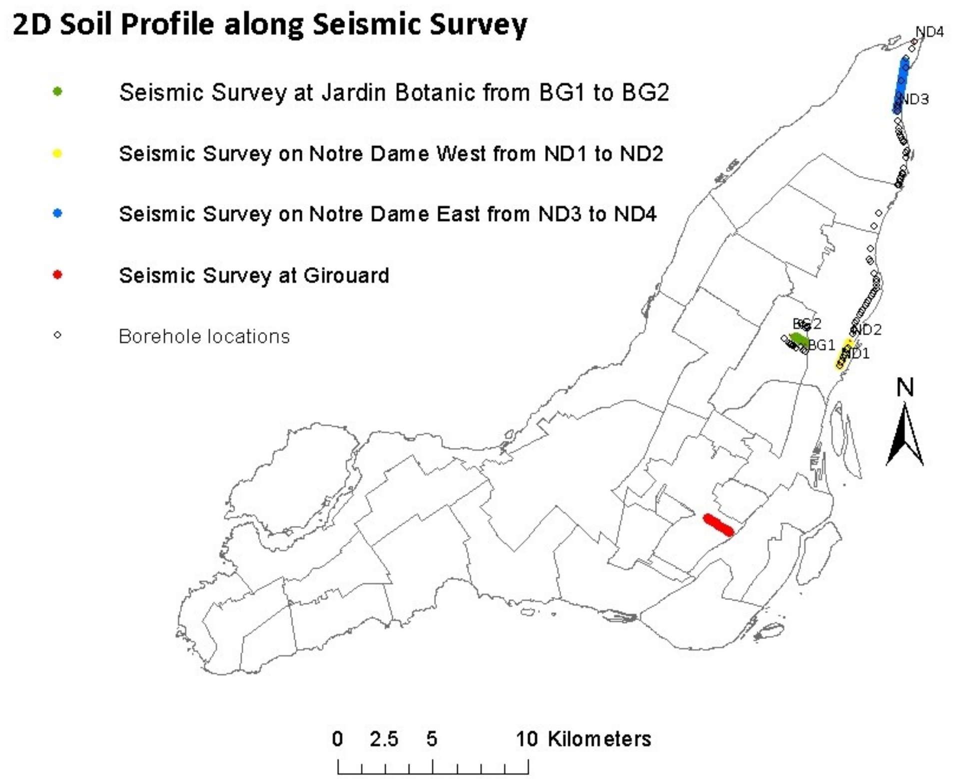

Figure 2.1: A map of the Island of Montreal showing direction lines (in red) for two dimensional soil layering inferred from the geotechnical boreholes underneath the sites of seismic reflection and refraction survey (in yellow).

Presented below in Figures 2.2, 2.3 and 2.4 are examples of two dimensional soil profiles developed in this study using borehole information. The detailed soil profiles for these locations were developed in order to interpret and correlate the results from seismic surveys at these sites.

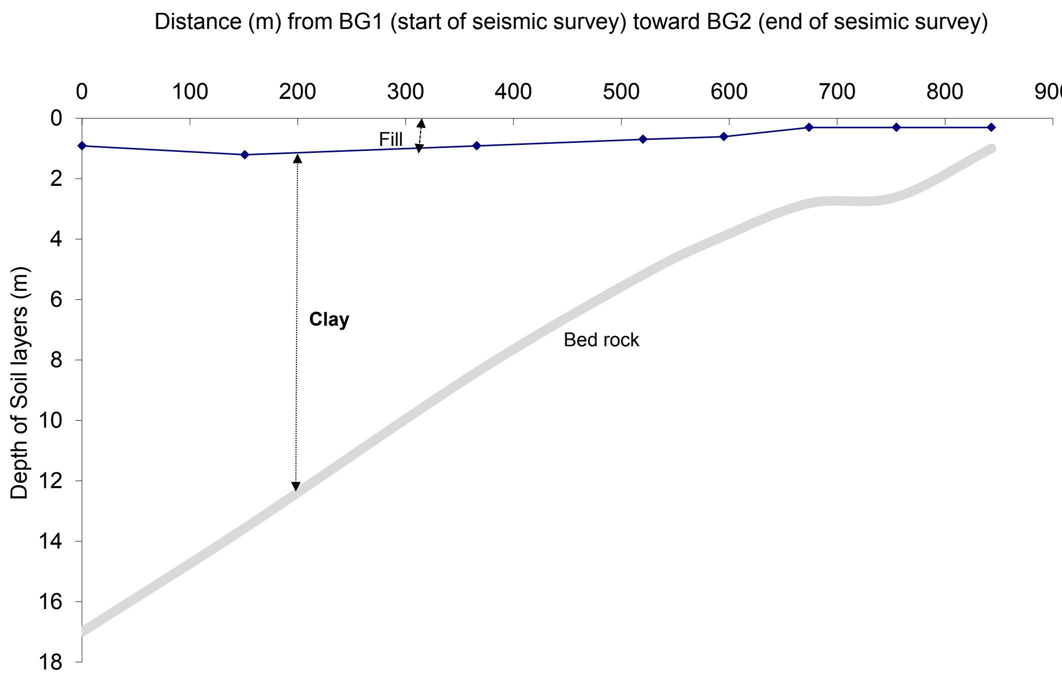

Figure 2.2: Two-dimensional soil profile in proximity to the seismic survey at the Botanical Garden in Montreal.

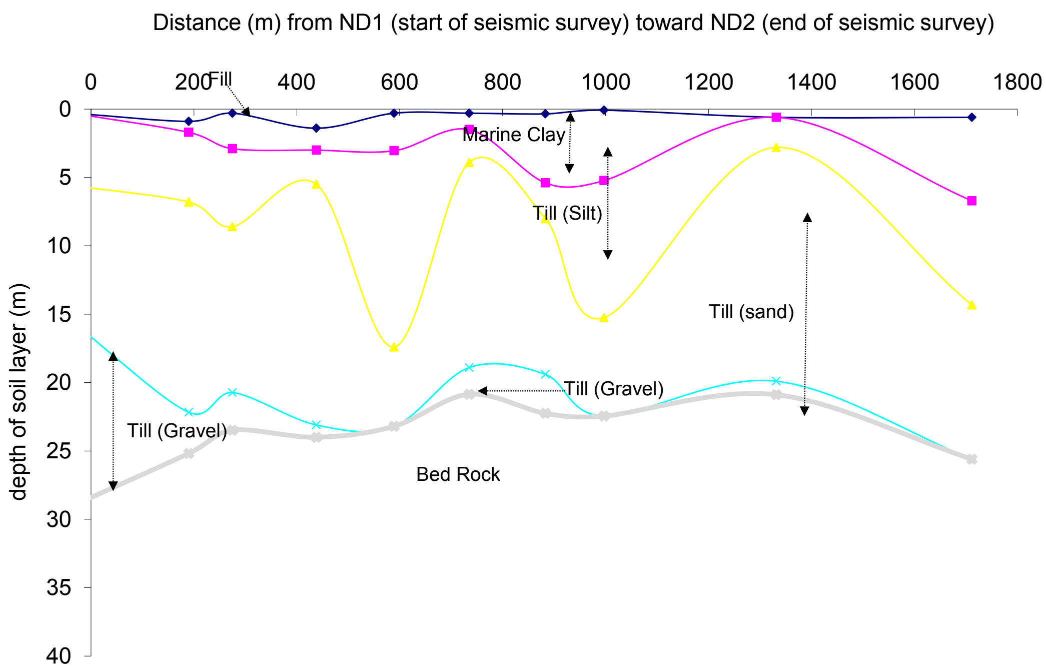

Figure 2.3: Two-dimensional soil profile in the vicinity of the seismic survey along Street Notre Dame West.

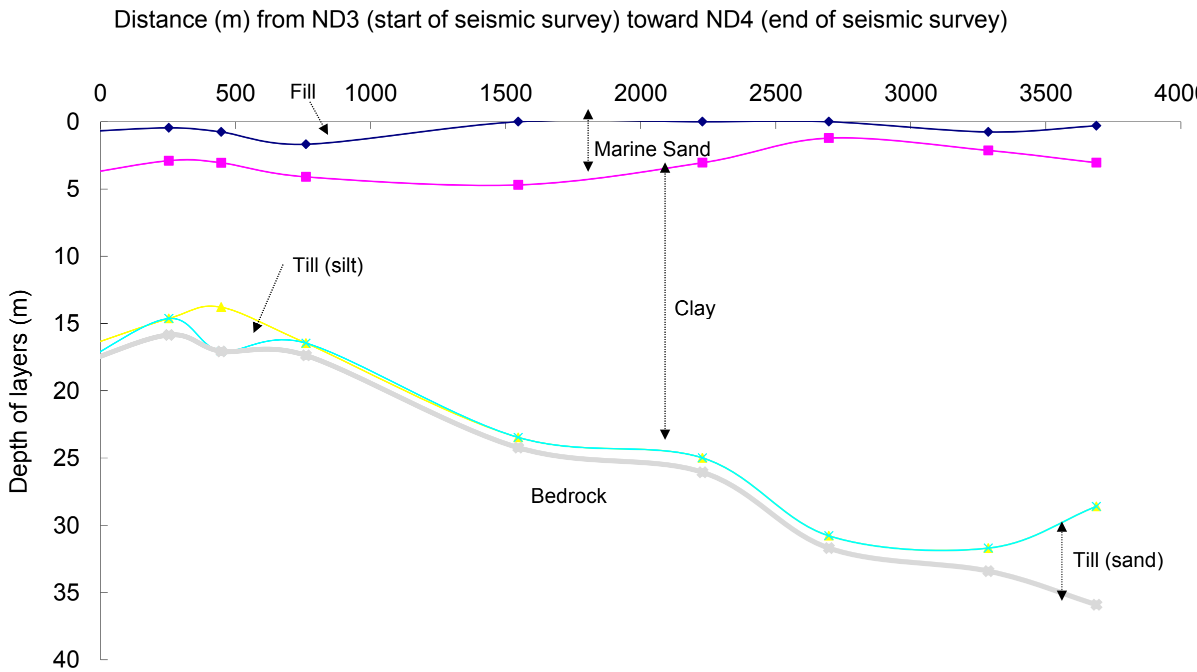

Figure 2.4: Two-dimensional soil profile in the vicinity of the seismic survey along Street Notre Dame East.

Figure 2.2 shows the soil profile obtained for the seismic survey performed at the Jardin Botanique. The site exhibits a clay layer ranging in thickness from 2.5 to 17 m and directly overlying bedrock resulting in a large impedance contrast. The site is located on a plateau inside the island and is characterized by relatively softer clays than those found closer to the shores on the island. One possible explanation for this difference is that the latter clay deposits correspond to stiffer clays that were exposed when the softer clays were eroded by the river.

The soil profile along Street Notre Dame West is shown in Figure 2.3 and exhibits sites where the spatial variability of the soil column is large. In this case, a relatively thin layer of clay (2 to 10 m) sits on top of a thick layer of glacial deposits (sandy and silty tills, and gravel) which produces a weaker impedance contrast. Finally, Figure 2.4 shows the soil profile obtained along Street Notre Dame East. This location is characterized by a thin layer of marine sand (1 m to 5 m thick), followed by a thick (5 to 30 m) layer of clay and small pockets of silt, over a thin layer of glacial sand.

Several Details of the results of surveys performed in Montreal over the last few years can be found in literature (Chouinard and Rosset, 2011; Rosset et al., 2014). Using the results from these surveys, shear wave velocity as a function of depth relations were proposed for clay and sand deposits. Talukder and Chouinard (2016) developed similar relations for silt deposits (Figure 2.5). These relationships are used to estimate the average shear wave velocity to a depth of 30 m (V_{s30}) at sites where borehole data is available. This information is then used to develop regional seismic microzonation maps as described in the following chapters. A review of seismic microzonation procedures (Benjumea et al., 2008; Castellaro and Mulargia, 2009; Chouinard and Rosset, 2011; Cox et al., 2011; Dobry et al., 2000; Hunter et al., 2010; Motazedian et al., 2011; Pitilakis et al., 2013; Wald et al., 2011) is presented next.

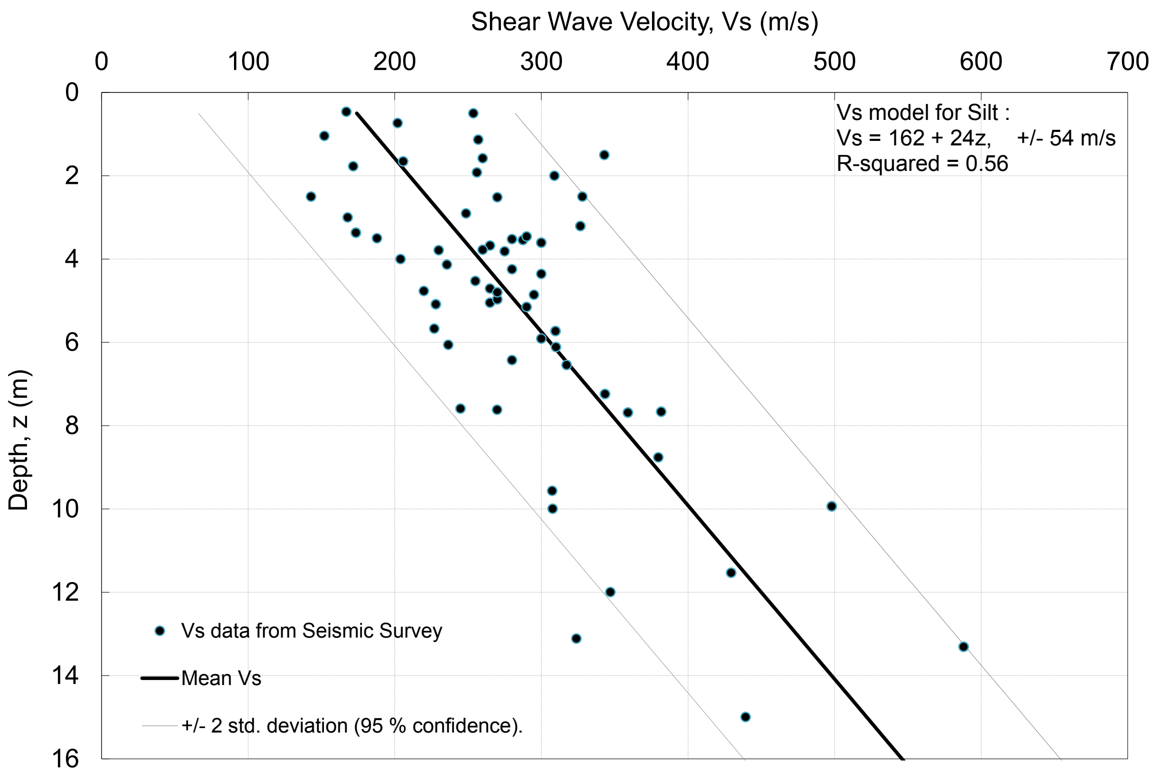

Figure 2.5: Shear wave velocity as a function of soil depth z (m) for silt deposits in Montreal (Talukder and Chouinard, 2016).

2.3 Microzonation of V_{s30} for Seismic Hazard Analysis

Ideally, shear-wave velocity versus depth relations are required for each geologic unit (Holzer et al., 2005; Wills et al., 2000b). A potential limitation of this procedure is the availability of V_{s30} data to properly define the appropriate relations for each geological unit (Wald et al., 2011). In the absence of such data, microzonations can be derived from surface geology maps or in some cases from topographical data (Wald et al. 2011). Thompson et al.

(2007) noted that the V_{s30} maps produced by Holzer et al. (2005) exhibit more spatial variability compared to maps derived exclusively from regional surface geology. The higher degree of variability is attributed to spatial variations in the thickness of geological units which is not considered in surface geology maps. Also, they note that zonation based solely on geologic units may be inaccurate because they can contain sediments with similar shear-wave velocities. To account for the horizontal variability of near surface soil deposits in the San Francisco Bay area, they investigated the horizontal correlation structure of shear-wave velocity across geologic units within a sedimentary basin. Analysis of travel time-weighted average shear wave velocity profiles presented in Thompson et al. (2007) indicates that the spatial correlation distance for the survey area in San Francisco Bay is nearly 4 km. Thompson et al. (2007) reports that for the travel time-weighted shear wave velocity data, the spatial variability of shear wave velocity increases exponentially across geological units as measurement distances increases from 2 m to 4000 m. Above 4000 m, the variance of shear wave velocity is nearly constant. As an alternative to geological units and/or surface geology based mapping of V_{s30}, Wald et al. (2011) proposed a regression model relating V_{s30} to topographical slope for a number of geological units. None of these procedures provide estimates on the uncertainty of V_{s30} determined by using these procedures and their effect on the resulting microzonation maps.

Site classifications which are based on V_{s30} have been adopted by multiple national and international building codes (e.g. NBCC 2015). However, site classifications which are solely based on V_{s30} have some limitations. As an alternative measure, site classifications based on the site fundamental frequency have also been proposed (Hunter et al., 2010; Motazedian et al., 2011; Rosset et al., 2014). Benjumea et al. (2008) presents a case study of a class D site (with V_{s30} = 208 m/s) which is underlain by a 25-m thick post-glacial layer (soft soil) overlying bedrock. The authors noted that if the post-glacial sediments at the site were only a few meters thicker, the site would be classified as NEHRP E. This indicates that the criterion of NEHRP average shear wave velocity for the top 30 m of the soil/rock column for site classification mapping may not provide an adequate description of sites for a region of interest. If soil profiles of depths of d meters do not reach depths of 30 m, travel time-weighted shear wave velocity over the depth of d meter may be estimated instead by the NEHRP V_{s30} (Thomson et al. 2007).

Pitilakis et al. (2013) proposed an alternative soil classification (A, B, C, D, E and X) as a function of the average shear wave velocity of the entire soil/rock column from the surface to the bedrock, the site fundamental period (0.2 s to 3.0 s), the depth to bedrock, the soil type (clay, sand, silt, etc.), undrained shear strength and SPT values. Among the six site classes, A, B, C and D are divided into sub-classes. The site categories correspond approximately to sub-class A1 (V_s>1500 m/s, T0 < 0.2 s), sub-class A2 (V_s> 800 m/s, T0 < 0.2 s) sub-class B1 ($V_{s,av}$ = 400 – 800 m/s, T_0< 0.5 s, N_{SPT} > 50, S_u > 200 kPa), sub-class B2 ($V_{s,av}$ = 400 – 800 m/s, T_0< 0.8 s, N_{SPT} > 50, S_u > 200 kPa), sub-class C1 ($V_{s,av}$ = 400 – 800 m/s, T_0 < 1.5 s, N_{SPT} > 50, S_u > 200 kPa), sub-class C2 ($V_{s,av}$ = 200 – 450 m/s, T_0 < 1.5 s, N_{SPT} > 20, S_u > 70 kPa), sub-class C3 ($V_{s,av}$ = 200 – 450 m/s, T_0 < 1.8 s, N_{SPT} > 20, S_u > 70 kPa), sub-class D1 ($V_{s,av}$ < 300 m/s T_0 < 2.0 s, N_{SPT} < 25, S_u < 70 kPa), sub-class D2 ($V_{s,av}$ < 300 m/s, T_0 < 2.0 s, N_{SPT} < 25), sub-class D3 ($V_{s,av}$ =150 – 600 m/s, T_0 < 3.0 s), and sub-class E (V_s,av< 400 m/s, T_0 < 0.70 s). The sixth class soil (X) is a special case that comprises liquefiable soil layers requiring dynamic site response analyses based on measured sheared wave velocity to find ground motion amplification. From the site classification presented in the paper, it is evident that soil column period should be included in seismic site characterization to differentiate one site from another site.

Chouinard and Rosset (2011), and Rosset et al. (2014) provided estimates of the uncertainty associated with estimates of V_{s30} derived from borehole data. Talukder and Chouinard (2016) used this uncertainty to develop probabilistic microzonation maps that show the probability distribution of site classes instead of a single microzonation map. The probabilistic microzonation maps are then used to determine average site specific foundation factors and their standard deviation. The seismic microzonation is used in combination with national design codes to associate foundation factors to modify ground motion parameters that are usually specified for soil class C. Alternatively, the microzonation can be taken a step further and site amplification factors can be derived for the ground motions and the site characteristics that are more specific to a given region. In addition, the seismic microzonation can also address other site related hazards such as liquefaction and slope stability. For the latter purpose, the site characteristics must be considered in conjunction with the seismic hazards that are prevalent for the given region.

In Eastern North America, seismic hazard (PGA) is typically governed by multiple seismic sources and a process of deaggregation is used to identify likely scenarios of earthquakes as a function of magnitude and epicentral distance. The hazard function can be defined for various strong ground motion parameters (Sa, PGA, etc.) and is developed initially for site class

C conditions. The uniform hazard spectra (UHS) of the 2015 NBCC results in a mean peak ground acceleration of 0.375 g for Montreal for firm ground (site class C) at a probability of exceedance of 2% over 50 years This recurrence rate corresponds to a return period of 2475 years. The deaggregation of the peak ground acceleration for Montreal for a probability of 2% in 50 years (Adams and Atkinson, 2003; Halchuk et al., 2007) indicates that the most likely scenario for an earthquake is with a moment magnitude 6 (M6) at an epicentral distance between 10 and 30 km. Analyses by Atkinson (2009) indicated that an M6 event in the 10–30 km distance range matches the short-period region of the UHS, whereas an M7 event at a distance of 15–100 km is a better match to the long-period portion of the UHS. This observation is used in Chapter 4 to define a set of earthquake records to perform non-linear dynamic site response analyses.

Papaspiliou et al. (2012b) discussed the EL and NL analyses of the two sandy sites (with site period of 0.76 s) and the clayey site (with site period of 0.98 s). The authors estimated median surface spectral accelerations for spectral periods of 0.01 s, 0.2 s, 0.8 s, 1.0 s, 1.5 s, and 3.0 s using their GMPE, as well as using the GMPE developed by the earthquake records for the San Andreas fault region in California. Next, the authors performed PSHA using the median surface spectral accelerations estimated from both GMPEs. The author then performed deaggregation for PGA at the 10% probability of exceedance in 50 years level and 2% probability of exceedance in 50 years level. Their deaggregation results show that at a relatively high annual PE levels (10% in 50 years), the hazard at the California site is dominated by the occurrence of a magnitude 7.0–8.0 event, at a distance of 15 km, with ε close to 0.5. However, at 2% PE in 50 years, the hazard is dominated by a similar magnitude–distance event, but a higher ε close to 1.5; indicating much higher ground motion intensity.

Previous editions (i.e. 1985 and 1995) of the NBCC used ground motions defined for a probability of exceedance of 10% in 50 years (i.e. a period of recurrence of 475 years), while newer editions of the years 2005, 2010 and 2015 used ground motions defined for 2 % probability in 50 years. For example, the values of PGA for the firm ground were 0.173 g in 1985 and 1995, 0.43 g in 2005, 0.31g in 2010 and 0.375 g in 2015. This change in ground motions implies that older structures are more vulnerable compared to those designed under the new code.

2.4 Estimating Site Factors from Ground Motion Amplification

Peak surface accelerations are often computed from seismic response analyses of the 1-D soil columns excited by rock motions due to lack of strong motion data. Results of the 1-D simulation are used to derive empirical relations in most regions as exemplified by the numerous publications that use this approach. In the following, studies that have been performed for locations in Eastern Canada are reviewed as well as some case studies for amplification factors for a variety of locations. The objective of this review is to describe the techniques used for modelling soils (equivalent versus non-linear analysis) and to obtain a representative set of records to perform the analysis.

The peak ground accelerations at bedrock level are often amplified when seismic waves travel through soft soils. For this reason, it is important to estimate the site effect factors for different site conditions (Finn and Wightman, 2003; Humar et al., 2010). Borcherdt (1994) proposed amplification factors which are dependent on the frequency content and peak amplitude of the rock motions (0.1 to 0. 4 g). and proposed a set of short period (in the range of 0.1-0.5 s) factors F_a and long period (0.4 to 2 s) factors F_V. Borcherdt (1994) estimated the site factors for a reference rock condition corresponding to V_{s30} of 1050 m/s. The values for these factors were proposed for rock PGA of 0.1 g using the Loma Prieta strong motion data. For higher PGA levels (0.2, 0.3 and 0.4 g), the site factors were obtained by performing 1-D ground response analyses (Seed et al. (1994). For rock accelerations of the order of 0.05 g to 0.10 g, the corresponding ground surface accelerations are 1.5 to 4 times greater than the rock accelerations. The amplification decreases for higher rock accelerations, and becomes approximately equal to 1 for rock PGA of 0.4 g. A tendency for deamplification for even higher rock accelerations is also observed from the results of their study.

Cao et al. (1992) conducted the 1-D seismic response analysis for the site of Port Alfred, Saguenay in Quebec. The depth of the soil profile at the site was 30 m. The profile consisted of clay soil with V_s increasing from surface (V_s=150 m/s) to bottom (V_s=250 m/s) of the profile. The V_{s30} value of the site was 213 m/s. The clay profile overlay the rock. For the 1-D analysis, the authors obtained shear modulus reduction and damping curves by performing cyclic triaxial test and resonant column test on soil samples collected from different depths ranging from 3 m to 25 m. The mean V_s values for Montreal clay range between 150 m/s (at the surface) and 300 m/s (at a depth of 33 m).

Perret et al. (2013) performed 1-D ground response analyses for fourteen soil profiles that are typical for the St-Lawrence River basin. The soil profiles were assumed to be underlain by a bedrock half-space with a shear wave velocity of 2500 m/s, an average value typical of most rocks in Eastern Canada. For the soil profiles, depths to bedrock ranged from 20 m to about 125 m. The shear wave velocity profiles for sand and clay soil were estimated from seismic surveys. For the till deposits (overlying bedrock), the shear wave velocities were of 350 m/s to 550 m/s. One-dimensional dynamic response analyses were performed with SHAKE91 with the equivalent linear method of analysis in the frequency domain. The variation of soil shear modulus and soil damping ratio with shear strain were modeled by the shear modulus reduction and damping ratio curves from Electric Power Research Institute (EPRI, 1993). From the ground response analyses, the authors obtained stress reduction factor r_d as a function of depth for ground motions with magnitudes of 5.5 (synthetic earthquake), 5.9 (Saguenay earthquake), 6.5 (synthetic earthquake), 6.8 (Nahanni earthquake) and 7.5 (synthetic earthquake). The stress reduction model proposed in this paper is an input to the liquefaction susceptibility assessment model derived by Seed and Idriss (Seed and Idriss, 1971).

Nastev et al. (2008) performed seismic site response analyses using a similar approach to determine mean spectral (5% damping) amplifications for periods of 0.01 s, 0.1 s, 0.2 s, 0.5 s, 1.0 s, and 2.0 s. The mean spectral amplifications were predicted for five representative soil profiles corresponding to 10 m, 20 m, 30 m, 50 m and 80 m depths observed in the Quebec city area in the St. Lawrence low-land. In the soil profiles, sedimentary bedrock (shale and sandstone) underlay glacial tills, which were overlain by sands and silty clay. The average shear wave velocities of the soil columns were in the range of 190–291 m/s in the class D. For sand and clay soils, the authors used normalized strain dependent modulus decay and damping curves developed by Zhang et al. (Zhang et al., 2005). The authors approximated the modulus decay and damping curves for glacial tills as that of clay soils since the tills were composed of fine grained particles. Seismic input motions at the bedrock were computed by the authors to fit the 5% damped acceleration response spectra curve for class B soil in Quebec city, and the input motions were scaled to 0.01 g, 0.05 g, 0.1 g, 0.2 g, 0.3 g, 0.4 g, 0.5 g, 0.75 g, and 1.0 g. The highest amplifications in the range of 1–6 were observed for low shaking intensities of 0.01–0.1 g, and periods between 0.1–0.5 s. Two relatively shallow profiles (depths of 10 to 20 m) with corresponding short predominant periods (0.21 s and 0.38 s) showed the highest spectral amplifications in the range of short periods of 0.01–0.2 s, whereas three relatively deep profiles of depths of 30 m, 50 m and 80 m with corresponding long predominant periods (0.66 s, 0.88 s and 1.14 s) experienced the highest spectral amplifications in longer period range (1.0–2.0 s).

Stewart et al. (2008) compared several softwares to perform Equivalent Linear (EL) and Non-Linear (NL) analyses of the 1-D ground response. The EL methods require fewer input parameters: elastic shear modulus (directly proportional to the square of shear wave velocity), unit weight, viscous damping, modulus reduction and damping curves while the NL methods require calibrating the mathematical model for soil stiffness degradation with increasing strain, material damping at large strain and viscous damping at small strain (Stewart et al., 2008). For the NL approach to soil response analysis, Papaspiliou et al. (2012a) used a significant number of parameters for the modified hyperbolic stress-strain curve to approximate the hysteretic behaviour during the loading and unloading cycles of ground motions, so that the cyclic nonlinear model of the soil stress-strain matches the measured shear modulus reduction curve used in the EL method. The NL methods require more computation time than the EL methods since the soil stress-strain models developed for the NL methods are usually solved with time domain finite element analysis which requires faster computers. The procedure to obtain the material properties for the EL method is also well established and can be easily obtained from literature. In contrast, the number of input parameters for the NL methods varies widely with the variation in the soil stress-strain models requiring expensive laboratory and field tests. For reducing the computational time and the need for doing tests, one may consider the EL analysis in the Frequency domain.

Regional seismic site effect studies require a great number of site response analyses. In this case, one may prefer the EL method to the NL method to save computational time. Ansal et al. (2010) performed site response study for typical soil profiles in an urban area in Istanbul using 1-D equivalent linear analyses with SHAKE91 to develop microzonation maps based on peak surface acceleration. Depth of soil profiles varied between 80 and 180 m. Upper layers consisted mainly of clay followed by sand, gravel, till and rock. The V_s for clay ranges from 100 m/s to 300 m/, and for sand from 200 to 450 m/s. Twenty-four real acceleration time histories compatible with the UHS were selected from the PEER strong motion data base. Selected acceleration time histories were scaled to the PGAs estimated from the seismic hazard analysis for site specific conditions. Site response analyses performed for the area provided microzonation map showing local site effects in terms of variation of peak ground accelerations. Significant variations in the resulting PGAs were seen across the investigated area and they were in the range of 0.1 to 1.1 g.

Andrus et al. (2006) compiled the V_s-depth data in and around Charleston (South Carolina) to perform site response analysis using DEEPSOIL (Hashash and Park, 2001) with the equivalent linear (EL) option. The authors assumed soil profiles consisting of 0.0-30 m of soil deposits with V_s values of 110 m/s to 190 m/s. The top 0-30 m thick layer was underlain by 30-35 m thick soils with a constant V_s of 435 m/s. For the depths between 55 m and 100 m, the Vs values were in the range of 533-663 m/s. Next, a deep deposit was assumed to extend from depths between 100 m and 808 m. For the depths between 100 m and 808 m, the V_s profile was assumed to increase from 800 m/s at 100 m to 920 m/s at 808 m. This deep soil profile was placed on top of the rock with a V_s of 3500 m/s. Synthetic motions were computed for a magnitude of 6.4 for rock conditions in Charleston and scaled to 0.1 g. Synthetic motions were also computed for magnitude of 7.1 and scaled to 0.3 g. Computed peak surface accelerations for each layer did not exceed 0.31 g in any of the models. Calculated peak surface accelerations for the soil profiles shaken by the magnitude 7 motion were 0.8 to 1.0 times the input peak rock acceleration scaled to 0.3 g, indicating de-amplifications of ground motions. For the soil profiles shaken by the motions from the magnitude 6.4 earthquake, peak surface accelerations were 1 to 1.5 times the input peak rock acceleration scaled to 0.1 g, indicating amplification for all soil profiles. Computed maximum shear strains for each layer were less than 1.8%. Andrus et al. (2006) noted that the equivalent linear formulation was considered adequate because the ground surface in Charleston is fairly flat, and the computed ground accelerations and shear strains computed in most of the models are approximately of 0.4 g and 2%, respectively. The authors observed that the ratio of peak surface acceleration to peak rock acceleration is generally greater for sites having stiffer profiles (i.e., mean V_s of 190 m/sec) compared to softer profiles (i.e., mean V_s of 110 m/sec).

It is also important to be aware of the differences in the results computed by the EL and NL methods. Papaspiliou et al. (2012a) reported on the problem of convergence as a limitation of the equivalent linear method when using rock motions of high intensity. They noted that the convergence problem can be related to the shear modulus reduction curve. For the high intensity records, the computed effective strain from the EL method is relatively large and as a result, there is a large difference between the initially assigned shear strain and the predicted effective strain after the first iteration. If the shear modulus degradation curve is relatively steep, at every iterative step a small change in strain can lead to a relatively large change in the shear modulus and thus the large initial difference is carried through subsequent iterations. Furthermore, the authors also noted that at relatively high strains the stiffness may still be degrading quite rapidly, while the damping fast approaches a higher level of a constant value, leading to an even larger effective strain. Increasing the number of iterations only leads to the estimation of unnaturally inflated strains that are simply the result of the inability of the algorithm to converge faster.

Unlike the EL method in which the material damping ratio (viscous damping ratio) for soil layers is obtained from damping versus strain curve, the NL method requires one to obtain the viscous damping at a small shear strain level (less than 0.0001 %) corresponding to any given excitation frequency in each soil layer or element. Papaspiliou et al. (2012a) used the full Rayleigh's (mass and stiffness proportional) damping formulation with the target damping ratio set to 0.5 % equal to the small-strain material damping. For assigning the damping ratios to different periods of vibrations of a soil element, two target periods were set equal to the predominant site period (first mode), and one-fifth of the predominant site period (3rd mode). Between the two target frequencies, the damping ratio for any other excitation frequencies is slightly less than the target damping ratio while for frequencies outside of this range larger damping ratios are obtained. The authors performed site response analyses using simplified (only stiffness proportional) and full Rayleigh's damping formulation. The authors noticed from the computed response spectra for surface ground motion for periods up to about 0.2 s to 0.3 s (i.e., in the high-frequency range) that the simplified formulation of Rayleigh's damping leads to lower spectral accelerations than the case when the full formulation is used. This investigation makes one aware of potential differences in the spectral amplifications when adopting the damping formulations available in the NL methods.

Soil type (clay, silt, sand, and gravel) can impact the amplifications computed from the EL and NL methods. Papaspiliou et al. (2012b) discussed the EL and NL analyses of one sandy site (with site period of 0.76 s) and one clayey site (with site period of 0.98 s). Papaspiliou et al. (2012b) noted that the two investigated sites, one sandy and one clayey, have almost identical value of V_{s30}. For this reason, one may predict equal amplifications for both sites which are classified based on V_{s30} alone. For both clayey and sandy sites, Papaspiliou et al. (2012b) computed amplification factors as a function of the rock spectral acceleration for different periods. However, the results from the site response analyses show that the site effects at both sites are strongly different. Papaspiliou et al. (2012b) observed that the differences between the equivalent linear and nonlinear analyses were considerably smaller in the case of the clayey site than the case of sandy site in California.

The level of input rock motions can significantly impact the ground motions amplifications. From the results of the EL site response of the sandy site, Papaspiliou et al. (2012b) developed plots of median site amplification factors as a function of spectral accelerations and periods of a SDOF system (Papaspiliou et al., 2012b). From these plots, the authors observed that the amplifications were nearly constant for the rock spectral accelerations ranging between 0.01 to 0.1 g at all periods of SDOF. However, there was an upward shift of the amplification functions at longer structural periods (greater than 0.8 s) for the records with higher rock spectral accelerations of 0.2 to 1.0 g.

Site period can significantly impact the ground motion amplifications when the input rock motions vary widely in the range of 0.01 g to 1 g. Papaspiliou et al. (2012b) referred to the sandy site with predominant period of 0.76 s. Referring to the plots of median site amplification factors as a function of spectral accelerations and periods, the authors noted that the period of peak amplification elongates from 0.76 s to 0.9 s for the sandy site, as shaking intensity increases above a shaking level of 0.2 g. The authors explain that elongated site period caused the sandy site to be in resonance with the rock motions that resulted in higher amplifications for the rock spectral accelerations in the range of 0.2 g to 1 g. As for the clayey site with period of 0.98 s, the authors conducted a set of 1-D analyses for input rock motions of intensities less than 0.2 g. From the results of the study for the clayey site, the authors noted that there were pronounced amplifications in the computed response spectra for periods near 1.0 s where resonance occurs at the periods close to the site period of 0.98 s. The authors explained that the clayey soils exhibit slower stiffness degradation, compared to that of sandy sites, and the behaviour of the clayey soil is less nonlinear.

For deriving the ground motion amplification factors from ground response analysis, Rodriguez-Marek et al. (2001) proposed geotechnical site classification using data concerning site periods, V_s of soil overlying bedrock, and depth to bedrock. The site classification is shown in Table 2.1

Table 2.1: Geotechnical site categories proposed by Rodriguez-Marek et al. (2001).

Site	Description	Approximate Site period	Soil Vs and Depth to bedrock
A	Hard rock	≤ 0.1 s	Crystalline Bedrock; Vs ≥ 1500 m/s
B	Competent Bedrock	≤ 0.2 s	Vs ≥ 600 m/s or < 6 m of soil. Most "unweathered" California Rock
C1	Weathered Rock	≤ 0.4 s	Vs ≈ 300 m/s increasing to > 600 m/s, weathering zone > 6 m and < 30 m
C2	Shallow Stiff Soil	≤ 0.5 s	Soil depth > 6 m and < 30 m
C3	Intermediate Depth Stiff Soil	≤ 0.8 s	Soil depth > 30 m and < 60 m
D1	Deep Stiff Holocene Soil	≤ 1.4 s	Depth > 60 m and < 200 m
D2	Deep Stiff Pleistocene Soil	≤ 1.4 s	Depth > 60 m and < 200 m
D3	Very Deep Stiff Soil	≤ 2.0 s	Depth > 200 m
E1	Medium Thickness Soft clay	≤ 0.7 s	Thickness of soft clay layer 3-12 m
E2	Deep Soft Clay	≤ 1.4 s	Thickness of soft clay layer > 12 m
F	Potentially Liquefiable Sand		Holocene loose sand with high water table (zw ≤ 6 m)

It is of paramount importance that one considers investigating major source of uncertainties in the estimation of NEHRP amplification factors when computing the seismic site response of soil columns. Papaspiliou et al. (2012b) presented the comparison of the NEHRP amplification factors to the computed site-specific spectral amplifications for periods of 0.2 s and 1 s. It was seen in the comparison that the NEHRP factor for T= 0.2 s predicts their results well, but the NEHRP factor for T=1.0 s underestimates their results for clayey soil, and overestimates their amplifications for sandy sites. The two examined soil profiles are assigned almost identical V_{s30} value. The clayey profile has a V_{s30} of 284 m/s, and the sandy profile has a V_{s30} of 280 m/s. Based on the results of site response analyses, the authors developed regression model to estimate surface spectral acceleration from the information of median rock spectral acceleration derived from suitable ground motion prediction equations. The authors also proposed the standard error of the estimation resulting from the regression. The paper noted that major source of uncertainties in the estimation of surface spectral accelerations arise from ground-motion variability, shear-wave velocity profile, and dynamic soil properties.

Banab et al. (2013) performed Finite Element analyses for the site response of the Heritage Park site in Ottawa. The soil profile consists of 81 m thick Leda clay with V_s = 210 ±

10 m/s and density ρ = 1700 kg/m^3, 10 m of glacial till with V_s = 580 ± 174 m/s and ρ= 1800 kg/m^3, and bedrock with V_s = 2700 ± 680 m/s and ρ = 2500 kg/m^3. Soil shear modulus reduction and damping were modeled using the functions of Seed and Sun (1989). The site was subjected to seven synthetic time histories, matching the 2005 NBCC specified uniform hazard spectra for a probability of 2% in 50 years. The ground motion amplification factor was defined as the ratio of the Fourier spectra of the ground response acceleration to that of the input ground motion at site fundamental frequency. Computed amplification factors at the site fundamental frequencies were shown as a function of ground shaking intensity with PGA from 0.023 g to 0.35 g for impedance contrast ratios 4, 8, 12 and 23.4 (Figure 12, Banab et al., 2012). The amplification curves show that increasing level of shaking can decrease ground motion amplification due to soil nonlinearity. It is noted from the amplification curves that, by increasing the PGA from 0.023 g to 0.35 g, the amplification factor for the contrast ratio of 23.4 decreased gradually from 11.5 at PGA=0.023 g to 7 at PGA=0.35 g. It is interesting to note from the amplification curve that, the highest amplification factor was of 11.5 at a PGA of 0.023 g, corresponding to the impedance contrast ratio was of 23.4. In contrast, the lowest amplification factor was 7, and it was observed at the PGA of 0.023 g when he contrast ratio was 4. Thus, a sharp fall in the amplification factor was observed when the impedance contrast ratio was decreased from 23.4 to 4.

Kishida et al. (2009) performed the 1-D equivalent linear site response analyses for the Sacramento-San Joaquin Delta in California, which is underlain by sensitive organic soils (or peat). The V_s profiles of the site indicate that it is class D according to NEHRP. The peat deposits were underlain by deposits of clay and sand. The peat deposits had shear wave velocities between 40 to 110 m/s. Shear wave velocities for the interlayered clay and sand deposits ranged from 140 to 290 m/s. Class D outcrop motions were used at the base of the upper 30 m profile. A total of 264 ground motions were selected from the class D category in the PEER-NGA data base with magnitudes from 4.3 to 7.9 and epicentral distances from 1.1 km to 296 km, and peak ground accelerations of 0.04 to 1.8 g. It is noted from the amplification factor curves (Figure 6a, Kishida et al., 2009) that the amplification factors decreased with increasing PGA, and the maximum amplification factor on PGA was 3. However, deamplifications (amplification factor less than 1) for the PGA levels between 0.01 g and 1.8 g were also noticed in the results of some site response analyses.

Kamai et al. (2013) defined reference rock outcrop motion using point source earthquakes with magnitudes 5.0, 6.0 and 7.0. The value of V_{s30} of the reference rock site condition is 1170 m/s. Reference rock motions were used as input motions for the 1-D linear equivalent analysis. An RVT (Random Vibration Technology) approach is used for rock motions which were defined with a power spectral density from point-source models instead of time histories. For the simulation runs of cohesionless (gravelly sands, low plasticity silts or sandy clays) soils, the shear modulus and damping curves assigned to the EPRI and Peninsular range soils were used, while, for the simulation runs with the cohesive soil profiles, the shear modulus and hysteretic damping curves assigned to the Imperial Valley and Young Bay Mud soils (e.g. clay soil with plasticity Index = 30 %) were used. The 1-D simulations were carried out for soils with 9 to 305 m thickness. For sandy and clayey soil profiles, the site response was conducted for three magnitudes: M5.0, M6.0, M7.0 and for 11 different PGA values of the outcrop rock motion: 0.01 g, 0.050 g, 0.10 g, 0.20 g, 0.30 g, 0.40 g, 0.50 g, 0.75 g, 1.0 g, 1.25 g, 1.5 g. For each 1-D simulation, the ground motion amplification on rock was computed with respect to V_{S30}=1170 m/sec, and the amplification factors were shown as the ratio of spectral acceleration values from ground motion on soil for periods 0.01, 0.2, 1, 2, 3, and 5 s to the corresponding spectral values of ground motion on rock.

Hines et al. (2011) considers that a ground motion is acceptable if it matches at least one UHS point very closely and does not vary from any other UHS point by more than a factor of approximately 2.0. For seismic site response analyses for the Boston area, 14 sets of records were selected from a set of 293 records in the NUREG database that are applicable to ENA. The target Peak ground acceleration (PGA) was 0.149 g, and the records were selected if the PGA of one of the orthogonal horizontal components fell between 0.075 and 0.30 g. The records corresponded to the earthquakes with magnitudes between 5 and 7.5, and epicentral distances between 22 km and 100 km. The ground motions were applied to three soil profiles with V_{s30} ranging from 213 to 323 m/s using the equivalent linear method. Depths of subsurface profiles ranged from 22 m to 42 m and site fundamental frequencies ranged from 0.34 to 0.76 s. The results of their analyses indicated that the ground motions were amplified.

The deaggregation of regional seismic hazard provides us with the magnitude-distance pairs making the largest contribution to the regional seismic hazard. Hashash et al. (2013) computed spectral acceleration values for periods in the range of 0.01 s to 10 s using GMPEs based on smaller magnitude data in the Central Eastern United States, as well as GMPEs based on strong motions in the Western United States, in order to perform probabilistic seismic hazard analyses for New Madrid Seismic Zone (NMSZ) in the Central-Eastern North American region. The paper presented seismic hazard curves for PGA, as well as for spectral periods: 0.2 s, 1.0 s and 3.0 s, in order to define the probabilities of the ground motion levels appropriate for the region of interest. Afterwards, for NMSZ, the authors determined a site specific UHS for return period of 2475 years. For periods less than 0.2 s, spectral acceleration values of the UHS were significantly higher than the values computed for longer periods. Next, the authors conducted magnitude-distance deaggregation for a return period of 2475 years for ground motion levels corresponding to T=0.2 s and T=1.0 s. The authors noticed that for T=0.2 s, the ground motion level is dominated by M=5 to 6.5 earthquakes at distances (R) of 0 to 30 km, while for a longer period of T=1.0 s, the hazard is mainly from M=7 to 8 earthquakes at distances of 180 to 300 km. The authors collected representative natural and synthetic ground motions time histories for the controlling earthquake of M=6 at 15 km based on deaggregation results.

Hashash et al. (2013) idealized the surficial soil of the Mississippi Embayment site to a representative one-dimensional (1-D) soil column, where the upper 10 m thick surficial soil (with water content in the range of 20 to 60 %) consisted of alluvial sand, alluvial clay (with PI<20), and alluvial silt. The upper alluvial soils were underlain by glacial sand with 25 m in thickness. The soil profile exhibited shear wave velocity increasing gradually from about 60 m/s at the surface to 300 m/s at rock. The SPT blow count (N-values) of the soil profiles ranged from 1 to 40. The alluvium site was underlain by weathered and unweathered dolomite and limestone. The upper portion of the bedrock exhibited V_s values of 490-1460 m/s, while the V_s values in the unweathered bedrock ranged from about 1830 m/s to 2740 m/s. The authors performed seismic response prediction for the soil column using equivalent linear (EL) and nonlinear (NL) methods. Ground motions were selected from a database of recorded or simulated time histories representative of earthquake magnitudes of 6 at 15 km and 7.5 at 200 km based on deaggregation of site-specific spectral accelerations computed at periods of T=0.2 s and T=1.0 s corresponding to a 2475 year return period. The response spectra obtained from the EL and NL analyses showed that the spectral accelerations at the ground surface computed by the EL approach were greater than those generated by the NL approach at periods between 0.1 s and 1 s. The maximum amplification was 6 at a period of 0.2 s.

Hashash and Moon (2011) used the one-dimensional EL approach to compute NEHRP site factors F_a and F_v for site classes C, D and E for various soil column thickness of 30 m, 100 m, 200 m, 300 m, 500 m, and 1000 m encountered in the deep soil deposits in the upland and lowland Mississippi Embayment (ME) in the Central and Eastern United States. The synthetic ground motion time series for NEHRP site-class A (hard rock) were generated for the seismic faults and source characteristics expected in the upland and lowland of the ME. These hard rock motions were transformed into rock motions of the NEHRP B/C boundary condition (at V_{s30}=760 m/s) using the transfer functions of Hashash and Moon, 2011). The rock motions were computed for large magnitude earthquakes of M>7.5 and source-to-site distances of 1, 10, 30, 70, 100, and 200 km. The V_{s30} of class D sites in the upland and ME were estimated to be of 275 m/s and 234 m/s, respectively. The V_{s30} of class C sites in upland and lowland ME were estimated to be 534 m/s and 482 m/s, respectively. The shear wave velocity at the bottom of the soil columns was assumed to be of 3000 m/s, which is comparable to the bedrock shear wave velocity in Montreal, which varies from 1000 m/s to 4000 m/s with a mean of 2350 m/s (Rosset et al. 2014). Hashash and Moon (2011) presented relations of F_a versus PGA and F_v versus PGA for depths of 30 m, 100 m, 200 m, 300 m, 500 m and 1000 m. For the class C profile with thickness of 30 m in the uplands, the computed Fa decreased from 1.6 to 1.54 as the PGA intensified from 0.1 g to 0.5 g. In addition, the computed Fv slightly decreased from 1.42 to 1.34 as the PGA rose from 0.1 g to 0.5 g. As for the class D profile with the same thickness of 30 m in the upland, the calculated F_a values declined from 1.65 to 0.97 as the PGA escalated from 0.1 g to 0.5 g, whereas the computed F_v plummeted from 2.2 at PGA=0.10 g to 1.34 at PGA=0.5 g. Hashash and Moon (2011) notes that the nonlinearity in the site coefficients Fa and Fv for site classes C, D, and E increases as the soil becomes softer.

Aboye et al. (2015) updated NEHRP F_a and F_v factors for deposits with V_s profiles that extends to soft rock (V_s = 700 m/s) half-space typical of Charleston area. F_a and F_v factors were obtained from the results of 1-D equivalent linear total stress ground response analyses for the V_s profiles of Charleston, South Carolina. The 1-D V_s profile reached soft rock at a depth of 137 m. The hard rock sites in South Carolina consist of 250 m of weathered hard rock (V_s = 2500 m/s), and this weathered hard rock layer is underlain by unweathered hard rock of V_s = 3500 m/s. At 0 m to 10 m of the V_s -depth profile, the V_s value is 190 m/s, while at 10 to 80 m, the V_s values were in the range of 400 m/s to 530 m/s. For depths of 80 m to 137 m, the mean V_s value was of

700 m/s. The authors used shear modulus versus strain, and damping ratio versus strain curves for deposits with effective confining stresses of 220 kPa (depth of 24 m), and 1400 kPa (depth of 137 m). The authors used G/G_{max} = 1 and damping ratio =0.5% for all strain values for modeling the dynamic properties of the half-space. The authors performed deaggregation of the hazards with 10%/50 years and 2%/50 years of probability of exceedance, and obtained estimates of earthquake magnitude and source-to-site distances. The authors used synthetic motions generated from soft rock (V_{s30}=700 m/s) conditions for M = 7.2 to 7.4 and R = 6 m to 36 km. The authors scaled the motions for the 1-D analyses to six PGA levels: 0.05 g, 0.1 g, 0.2 g, 0.3 g, 0.4 g and 0.5 g, and applied them to the soft-rock half space located at 137 m below the surface. The authors noted that the scaling of ground motions breaks the direct relation between the motions and their probability of exceedance, but does not bring additional bias to the computed response. The authors compared the computed F_a and F_v values with the NEHRP F_a and F_v. The results indicate that F_a values were in general agreement with the NEHRP F_a values except for the class D site, where the computed median F_a values were higher than the NEHRP F_a values. A similar trend was seen in the comparison between the computed F_v and the NEHRP F_v values. The computed median F_v values for the class D site were higher than the NEHRP F_v values, but the computed F_v values for the class C site were smaller than the NEHRP F_v values.

In the recent past, the amplification of peak ground acceleration has been studied using the equivalent nonlinear approach for the region of Eastern Canada (Chouinard and Rosset, 2007; Quinn et al., 2012). Quinn et al. (2012) modeled the soft clay of the St. Lawrence basin using shear wave velocity profiles and conducted one-dimensional dynamic modeling of site response using simulated earthquake acceleration time histories of both long period (magnitude of 7 and source to site distance of 70 km) and short period (magnitude of 6 and source to site distance of 30 km) earthquakes applicable for the region of Eastern Canada. The authors estimated the variation of amplification on peak ground acceleration with thickness of clay deposits in the St. Lawrence basin. It can be noted from Quinn et al. (2012) that as the depths of soil thickness increased from 5 m to 60 m, the computed amplification on peak ground acceleration propagating from bedrock to ground surface decreased from a factor of 2.5 to 1.45 for the input ground motion generated from an earthquake with magnitude 7 occurring at a distance of 70 km from the site. Nevertheless, the variation of the amplification factor was not a uniform function of depth. For example, the amplification factor was 2.5, 2.05, 2.2, 2, 1.9, 1.95, 1.5, and 1.45 for clay profiles with depths of 5 m, 13 m, 19 m, 21 m, 25 m, 30 m, 40 m and 60 m, respectively. Similarly, a non-uniform trend in the variation of amplification factors was seen when the input ground motions were calculated from another earthquake with magnitude 6 occurring at a distance of 30 km from the site. It is noted from Quinn et al. (2012) that the variation of the amplification on peak ground acceleration is not a uniform function of depth to bedrock, but rather has peaks at specific depths and the trends are different for different frequency and amplitude content of the input ground motion as well as the resonant characteristics of the soil column.

Geotechnical borehole information may not always contain the layer of rock with $V_s >$ 700 m/s. Zhai (2008) performed 1-D dynamic response analysis of a marine site in Marina Del Rey, California, where the information on depth to bedrock was not available. Due to unavailability of depth to bedrock information, the author assumed a firm ground condition at a depth of about 31 m below the ground surface. Shear wave velocity of the layer below the depth of 100 m was 310 m/s.

In case, natural ground motions records are not available to perform dynamic ground response analysis, synthetic input ground motions can be matched to site-specific uniform hazard spectra. Zhai (2008) performed dynamic response of the marine site in Marina Del Ray of California, which was at a distance of 15 km from the Hollywood fault. The author used the attenuations relations adopted by the California Geological Survey to obtain the peak horizontal ground acceleration of 0.42 g for firm ground condition conditions. A number of response spectra (5 % structural damping ratio) were computed from the time histories of natural earthquake records and matched with the target uniform hazard spectra (10 % in 50 year) for firm ground conditions. Next, spectrally matched time histories of ground input motions were generated. The subsurface soil of the site consisted of 3 m to 5 m fill underlain by 5 m to 8 m of clay. Below the clay layer was about 6 m to 10 m of loose to medium dense silty sand. Below the liquefiable silty sand layer, a dense gravelly sand layer was present. Below the dense gravelly sand layer, a firm ground condition was assumed. The soil profile described in the above was modeled as a single column for the one-dimensional equivalent linear (EL) and nonlinear (NL) effective stress analyses. The spectrally matched outcropping input motions were applied at the base of the 1-D model. The dynamic properties of the soil column were modeled by the strain compatible shear modulus degradation curve and damping ratio curve for the EL procedure. The author used the Mohr-coulomb soil plasticity model for the NL procedure. For the nonlinear dynamic analyses, the author defined the Rayleigh damping parameters (α and β) using the site fundamental frequency of 0.59 s (based on average shear wave velocity) and a target damping ratio of 0.5 %. Zhai (2008) compared the computed surface response spectra from the equivalent linear runs with those computed from the nonlinear effective stress based runs. The author noted that the peak surface accelerations (corresponding to a period of 0.01 s) from the nonlinear runs were about one-half of that generated by the equivalent linear runs. Similar to the difference in the results from the EL and NL procedures reported in Hashash et al. (2013), Zhai (2008) also noted that the surface spectral values for the periods between 0.5 s and 1.5 s, computed from the EL method were much higher than those computed from the NL approach. The difference between the two approaches is significant between periods of 0.5 s and 1.5 s. Nevertheless, for periods ranging from 1.5 s to 4.0 s, the two approaches generated almost similar surface spectral acceleration values.

For investigating the reason, why higher amplifications were obtained from the EL method relative to the NL method, Zhai (2008) computed the shear strain for the liquefied silty sand layer from the NL effective stress approach. The computed shear strain from the NL method was 1 %, while, it reached only 0.2 % in the simulation of the EL approach. The author notes that the equivalent linear approach uses the averaged linear elastic properties (i.e. secant modulus) for the entire duration of ground input motions, which results in less cyclic degradation of soil stiffness and causes higher responses of the soil columns.

In particular, geotechnical engineers have expressed concerns about the impact of increasing ground motions on the potential for liquefaction (Finn and Adrian, 2003). Adams and Halchuk (2007) discuss the implication of higher ground motions on the liquefaction potential as defined by Seed and Idriss (Seed and Idriss, 1971). The authors report that the liquefaction design PGA for a site class F in Montreal is 0.30 g at 10% in the 50 year probability level for the 1995 NBCC, while it is 0.50 g at the 2% in 50 year probability level for the 2005 NBCC. The net result is an increase of about 67% in design PGA for liquefaction assessment. Adams and Halchuk (2007) notes that the liquefaction design PGA of 1-in-2475 year return period might be replaced by the PGA of 1-in-1500 year return period. The authors suggested that the liquefaction design PGA value should be 0.7 times the PGA suggested in the NBCC 2005 (1-in-2475 year

PGA) for Western Canada, and 0.6 times the PGA suggested in the NBCC 2005 (1-in-2475 year PGA) for Eastern Canada.

The conventional ground motion prediction equations provide estimates of the rock and firm ground motions for the PSHA. For estimating soil site design motions for the assessment of liquefaction, the rock motion are modified with soil/rock site factors determined from ground response analysis. Goulet and Stewart (2009) used a nonlinear site factor to modify the peak horizontal accelerations determined from GMPEs for the reference rock site condition taken as V_{s30} = 1100 m/s to estimate peak horizontal accelerations for soil site conditions. The nonlinear site factor is a function of V_{s30}. For an annual probability of exceedance of 0.0021, the authors deterministically determined PGA=0.29 g from GMPE for the rock site condition (V_{s30} = 1100 m/s) in Southern California. By using the nonlinear site factor function, the authors obtained the site factors as 1.17 and 1.13 for other site conditions with V_{s30} = 250 m/s and V_{s30} = 180 m/s, respectively

2.5 Conclusion

Montreal is vulnerable to seismic events because of its population growth coupled with non-upgraded old buildings on thick clay and sand deposits making earthquakes a potentially significant natural hazard. The earthquake risk in Montreal is high due to the urban growth on soft soils capable of amplifying the ground motions. For this reason, the 2015 National Building Code of Canada provides new site factors at periods T=0.2 s, 0.5 s, 1.0 s, 2 s, 5 s and 10 s. For each structural period, the 2015 NBCC specifies the site factors for 5 site classes: A, B, C, D and E. These site classes are determined according to the measured average shear wave velocity of a site from surface to a depth of 30 m known as V_{s30}. Site classification methods proposed for Montreal over the last decade until 2014 have provided 3 different site classification maps using the V_{s30} values estimated from 3 different types of geotechnical information: total thickness of soil up to bedrock, detailed stratigraphy, and site fundamental frequencies. In addition, the existing maps characterize a site in terms of a single site category A, B, C, or D.

Alternative microzonation maps may be developed by deriving a new method for probabilistically updating the V_{s30} values estimated from the aforementioned 3 different sources. Such a probabilistic method may be used to provide a probability of site classification instead of a single site category. Such probabilistic method may also be used for integrating the updated

V_{s30} values from the aforementioned 3 different sources to improve the spatial resolution in comparison to the previous microzonation maps. Once the site class probability maps are developed, uncertainties in the NBCC site factors for sites in Montreal may be quantified from the probabilities of site classes.

The current seismic site factors for different site classes (NBCC, 2015) are based on earthquakes that have occurred at Western American site. Nevertheless, the code site factors do not include site effects in the Montreal area. Research on seismic soil response for sites in Montreal has been conducted over the last decade and provided the PGA amplification (for period T=0.01 s) maps for Montreal on a local scale by using V_s profiles not measured in Montreal. Nevertheless, the existing maps do not provide amplification factors for short and long spectral periods. Since new V_s database is available from seismic surveys, further research may be conducted using the improved knowledge of the V_s-depth relations to determine whether the 2015 NBCC provisions provide the short and long period site factors for Montreal to an adequate level. Site amplifications are calculated in practice by the 1-D seismic ground response analysis. For the ground response modeling, both simulated and measured ground motions can be used. Selected ground motions may be compared with the 2% in 50 year UHS points specified for Montreal to confirm the low and high frequency content of earthquakes with the spectral acceleration values of the UHS at short and long periods. Published shear modulus reduction and damping curves may be used to develop dynamic properties as input to the 1-D analysis, as dynamic tests on in-situ samples in Montreal are not available at present. The 1-D ground response using the EL method can provide an independent check of site factors published in the 2015 NBCC.

3 Probabilistic Methods for the Estimation of Seismic F_a and F_v Maps - Application to Montreal

Manuscript information: The article presented in Chapter 3 is published and available in the paginated issue of Bulletin of Earthquake Engineering, year 2016, volume 14 (No. 2), pp. 345–372, DOI 10.1007/s10518-015-9832-0. The details of the article are: titled 'Probabilistic Methods for the Estimation of Seismic Fa and Fv Maps--Application to Montreal', co-authored by Mohammad Kamruzzaman Talukder and Luc Chouinard. The authors are from McGill University. Mohammad Kamruzzaman Talukder conducted the research under the supervision of Luc Chouinard. Mohammad Kamruzzaman Talukder is the primary author, and Luc Chouinard is the 2nd author.

Abstract

In most national building codes, site classification is based on the V_{s30} parameter, the average shear wave velocity for the first 30 m of soil below the surface, and defines amplification factors (e.g. F_a and F_v) to be applied to ground motions for a reference condition. Seismic microzonation mapping is usually achieved by combining information from various sources, each with varying degrees of uncertainties. A preliminary microzonation can be derived from surface geology or surface elevation maps, while a more detailed and accurate map is usually based on extensive seismic surveys. A procedure is proposed that progressively allows the integration of information from various sources and to estimate the degree of uncertainty on the microzonation. This allows planners to determine where microzonation maps require further investigations given current or future urban development plans. The proposed procedure uses conditional second moment estimation and provides the best linear unbiased estimates of V_{s30} and its uncertainty. Next, these estimates are used to derive soil classification probability maps and to compute the expected values and variance of soil amplification factors F_a ad F_v to be used in probabilistic seismic risk analyses. The proposed procedure is demonstrated for the seismic microzonation of the island of Montreal.

3.1 Introduction

Seismic microzonations are derived by integrating information from several sources and usually consist in providing a map showing boundaries between soil classes. An example of soil classification is shown in Table 3.1 for the National Building Code of Canada (NBCC 2010). Soils are classified in 6 classes as a function of a set of geotechnical properties. The criteria that is used in this application is V_{S30}, the average shear wave velocity over the first 30 meters down from the soil surface.

Table 3.1 Seismic Site Classification in the National Building Code of Canada (NBCC, 2010).

Site Class	Soil Profile Name	Average Properties in Top 30 m as per Appendix A		
		Average Shear Wave Velocity, $\overline{V}_s$ (m/s)	Average Standard Penetration Resistance, $\overline{N}_{60}$	Soil Undrained Shear Strength, S_u
A	Hard rock	$\overline{V}_s > 1500$	Not Applicable	Not Applicable
B	Rock	$760 < \overline{V}_s < 1500$	Not Applicable	Not Applicable
C	Very dense soil and soft rock	$360 < \overline{V}_s < 760$	$\overline{N}_{60} > 50$	$S_u > 100$ kPa
D	Stiff Soil	$180 < \overline{V}_s < 360$	$15 \le \overline{N}_{60} \le 50$	50 kPa $\le S_u \le$ 100 kPa
E	Soft Soil	$\overline{V}_s < 180$	$\overline{N}_{60} < 15$	$S_u < 50$ kPa
		Any profile with more than 3 m of soil with the following characteristics: • Plasticity index: $PI > 20$ • Moisture content: $w \ge 40\%$, and • Undrained shear strength: $S_u < 25$ kPa		
F	(1)Others	Site specific evaluation required		

Notes:

(1) Other soils include:

(a) liquefiable soil, quick and highly sensitive clays, collapsible and weakly cemented soils, and other soils susceptible to failure or collapse under seismic loading,

(b) peat and/or highly organic clays greater than 3 m in thickness,

(c) highly plastic clays ($PI > 20$) more than 8 m in thickness, and

(d) soft to medium stiff clays more than 30 m in thickness.

A microzonation map is usually developed by estimating the mean value of V_{s30} at sites where data is available and by interpolating on a regular grid by using interpolation techniques ranging from linear distance-based interpolation to Krigging (ESRI, 2010). From this map, boundaries are defined for the various soil classes following the ranges defined in Table 3.1. The resulting maps are very dependent on the method of interpolation and on the number of sites where V_{s30} data is available. Information on soil classes is in turn used to assign the amplification and deamplification foundation factors for short structural periods (F_a for T = 0.1-0.5 s, Table 3.2) and long structural periods (F_v for T=0.5-1.5 s, Table 3.3).

Table 3.2: Values of F_a as a function of site class, and spectral acceleration at structural period of T=0.2 s, $Sa_{0.2}$ in the NBCC 2010.

Site Class	$Sa_{0.2}$				
	≤ 0.25 g	0.50 g	0.75 g	1.00 g	≥ 1.25 g
A	0.70	0.70	0.80	0.80	0.80
B	0.80	0.80	0.90	1.00	1.00
C	1.00	1.00	1.00	1.00	1.00
D	1.30	1.20	1.10	1.10	1.00
E	2.10	1.40	1.10	0.90	0.90
F	—[a]	—[a]	—[a]	—[a]	—[a]
Note: Use straight-line interpolation for intermediate values of $Sa_{0.2}$. [a]Site-specific geotechnical investigation and dynamic site response analyses should be performed.					

Table 3.3: Values of F_v as a function of site class, and spectral acceleration at structural period of T=1.0 s, $Sa_{1.0}$ in the NBCC 2010.

Site Class	$Sa_{1.0}$				
	≤ 0.10 g	0.20 g	0.30 g	0.40 g	≥ 0.50 g
A	0.50	0.50	0.50	0.60	0.60
B	0.60	0.70	0.70	0.80	0.80
C	1.00	1.00	1.00	1.00	1.00
D	1.40	1.30	1.20	1.10	1.10
E	2.10	2.00	1.90	1.70	1.70
F	—[a]	—[a]	—[a]	—[a]	—[a]
Note: Use straight-line interpolation for intermediate values of $Sa_{1.0}$. [a]Site-specific geotechnical investigation and dynamic site response analyses should be performed.					

Rosset et al. (2014) propose a seismic site class microzonation map of Montreal based on estimates of V_{s30}. Four different V_{s30} prediction models were used for this purpose: 1) a prediction model based on the site fundamental frequency (F_0), 2) a model based on the thickness of glacial and post-glacial deposits (single layer model, SL), 3) a 4-layer model based on detailed borehole data on multiple soil layers (multi-layer model, ML), and 4) data from site-specific seismic surveys. An ad-hoc procedure is used to select site specific best estimates for V_{S30} and to perform interpolation to obtain the site classifications. A site class microzonation for the region of Ottawa was proposed (Motazedian et al., 2011) in terms of site classes A through E. The authors showed that classes D and E are commonly associated with thick post-glacial Champlain Sea sediments; in contrast, classes A and B are associated with rock outcrop or areas of thin soil over rock.

The purpose of this article is to propose a formal probabilistic procedure for developing microzonations based on estimates of V_{s30} from various sources. Another feature of the proposed procedure is to estimate the uncertainty of the estimates of V_{s30} in assigning soil classes and the corresponding foundation factors. In the following sections, a method is proposed to estimate the mean and variance on V_{s30} at a site when estimates from various sources are available. This is followed by a new procedure to perform spatial mapping of V_{s30} that accounts for its mean and standard deviation. Microzonation is presented in terms of maps for the probability of each soil class instead of the current procedure which consists of assigning a single class to each site. The probabilistic site class maps can then used to derive maps for the expected value and the coefficient of variation of the foundation factors. The resulting maps can also be used in reliability analyses to account for the uncertainty on the foundation factors and to target regions where additional seismic surveys can be performed to reduce the level of uncertainty.

3.2 Geological setting of Montreal

Basement rocks in Montreal include igneous and metamorphic rock from the Precambrian (3500 to 600 million years BP) category reported by Prest and Hode-Keyser (1977) . These basement rocks are overlaid by sedimentary rocks (sandstone, shale, limestone, and dolomite) mainly from the Cambrian or Ordovician age (515 to 440 million years BP). Glacial till deposits are associated with 3 glacial episodes during the Wisconsian age (125000 to 10000 years BP): Malone Till, Middle Till Complex and Fort Covington Till (Prest and Hode-

Keyser, 1977). The Malone Till was formed between 70000 to 55000 BP by the south westward-flowing Malone ice in the St. Lawrence River valley. The Malone till is generally stony and has a variable silty and sandy matrix. The Middle-till formation overlies the Malone till and was deposited during the recession of Malone ice as it fluctuated over the Montreal region (55000 to 25000 years BP). The Middle till includes sand and gravel around the hill of Mont Royal, especially on its south western side in lowland areas. Overlying the Middle Till, the Fort Covington Till was formed during the Quaternary recession of the Laurentide Ice Sheet (25000 to 12500 years BP). The Fort Covington Till is much finer and clayey than the Middle till. The Champlain and upper St. Lawrence valleys were covered by a succession of glacial lakes from about 12500 BP. The soil deposited by the rapid recession of the Laurentide ice is known as Leda Clay or Marine Clay. Figure 3.1 shows the surface geology map of Montreal. A detailed discussion on the geotechnical properties of the sedimentary deposits are provided by Prest and Hode-Keyser (1977).

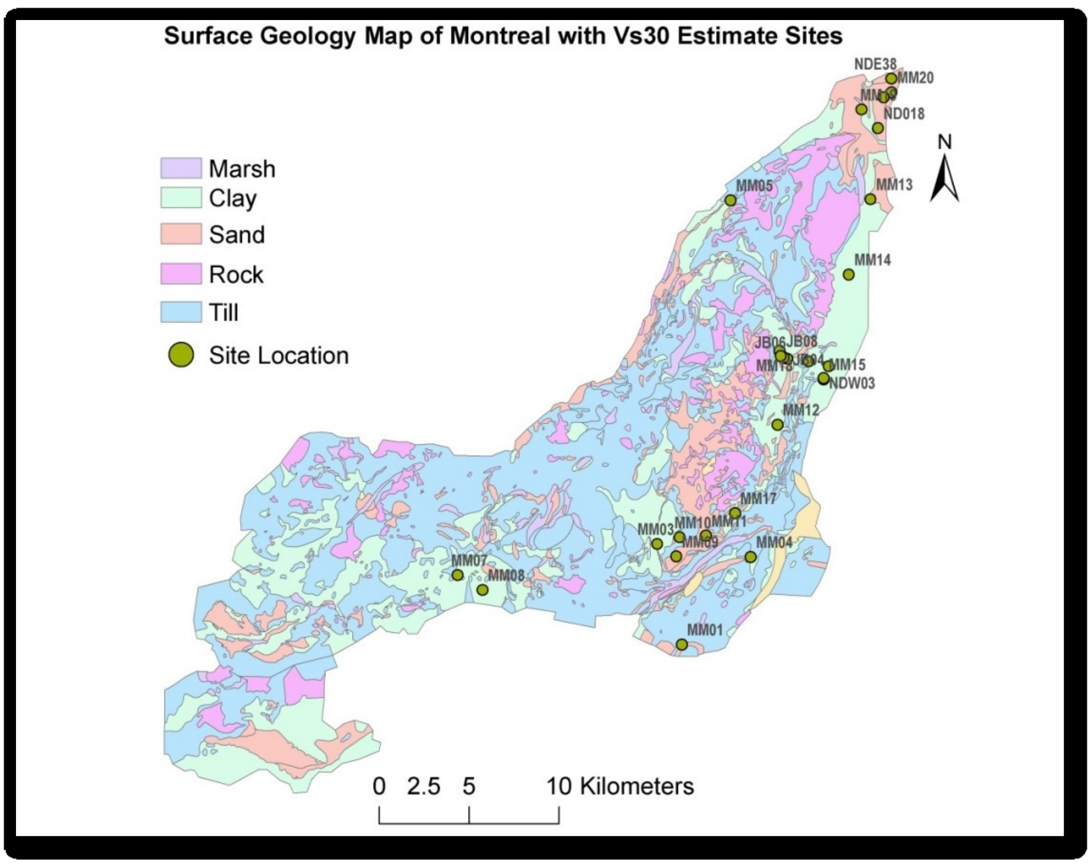

Figure 3.1: Surface Geology map of Montreal with the location of 26 sites for the analyses of V_{s30}.

3.3 Geotechnical and Geophysical Data for V_{s30} Microzonation of Montreal

Ansal et al. (2010) indicate that microzonation studies should be carried out based on integrating data from geological, geotechnical and geophysical site investigations. In the case of Montreal, the data sets consist of depth to bedrock data at 26,000 locations, borehole profiles at 2000 locations, fundamental frequency estimates from ambient noise measurements at 1,600 locations and seismic survey data at 41 locations and along 7.5 km of survey lines (Figure 3.2).

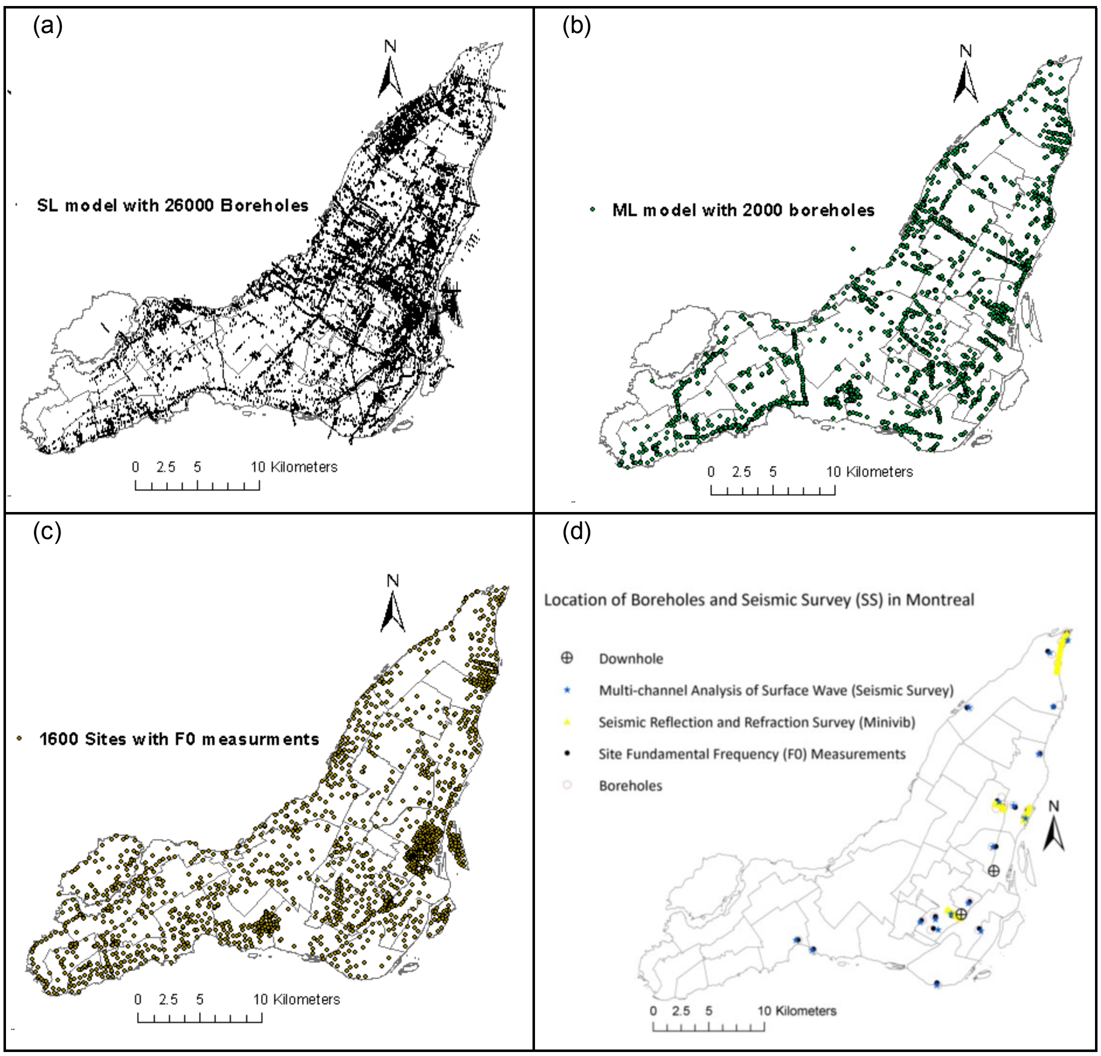

Figure 3.2: Summary of data available for microzonation, (a) Depth to bedrock, (b) Detailed borehole, (c) Fundamental frequency from ambient-noise data and (d) Seismic surveys.

Chouinard and Rosset (2011) propose a relation for the average shear wave velocity as a function of depth of soft sediments as well as distributions for the shear wave velocity as a function of depth for clay and sand deposits for sites in Montreal. For tills, Rosset et al. (2014) suggested average V_s = 565 m/s with a standard deviation of 261 m/s. Rosset et al. (2014) applied the shear wave velocity versus depth relations proposed by Chouinard and Rosset (2011) to the 4-layer model (ML model) for estimating the V_{s30} at sites where detailed borehole information is known.

In this study, a total of 26 sites with V_s measurements from multiple sources (indicated in Figure 3.1) are selected to develop the proposed V_{s30} microzonation procedure. Available borehole information indicates that five of the 26 sites are predominantly silt and clay, 13 have alternating layers of sand and clay, 3 are predominantly clay and 3 predominantly sand. Using the information on multiple soil layers at the 26 sites and the mean V_s-depth relations suggested by Chouinard and Rosset (2011), this study predicted V_s profiles for the 26 sites. Figure 3.3a compares the predicted V_s profiles (in black line) with the V_s profiles (in grey line) obtained from the seismic survey. The predicted V_s profiles shown in Figure 3.3a are used in this study for estimating the V_{s30} information from the ML model proposed by Rosset et al. (2014).

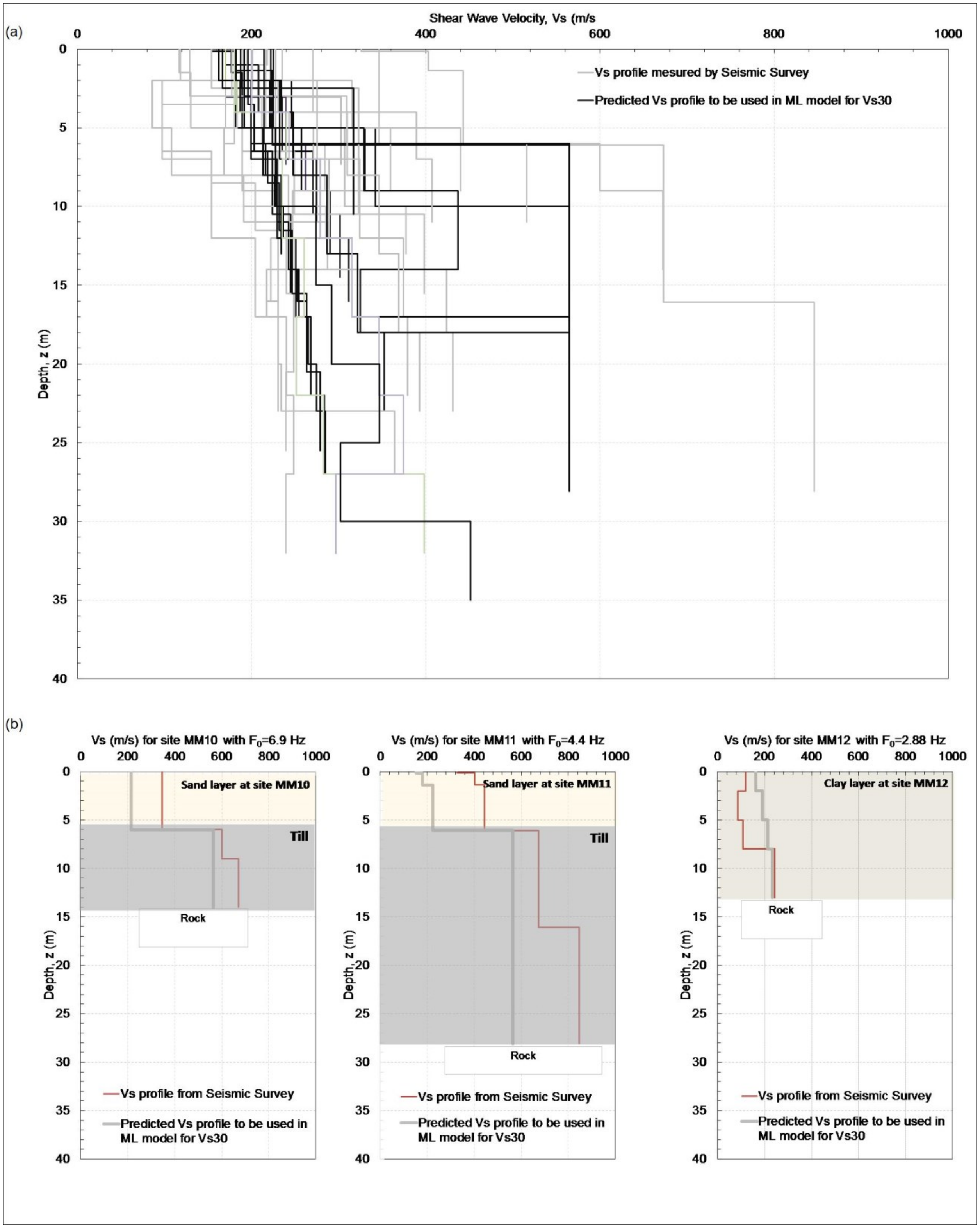

Figure 3.3: (a) Shear wave velocity profiles at the 26 sites (located in Figure 3.1) for the microzonation study, (b) Shear wave velocity profiles at sites: MM10, MM11, and MM12.

Figure 3.3b compares the predicted V_s profiles (in black line) to the V_s profiles (in grey line) obtained from the seismic survey for three sites: MM10, MM11, and MM12; where differences can be seen between the predicted V_s profiles and the V_s profiles obtained from the seismic survey.

3.4 Combining Estimates of V_{s30} from Various Sources

The surface geology map of Montreal was used to derive the first seismic microzonation map of Montreal. The map was defined by assigning Modified Mercalli Intensities (MMI) to each zone as a function of the type of surface deposits. Higher intensity zones correspond mainly to surface deposits of sand and clay and are located primarily along the south-east shore, the south central section, and several areas in the south-west section of the island. Preliminary seismic microzonation maps can also be derived by correlating geological units and/or surface geology to regional data on V_{s30} (Ansal et al., 2010; Holzer et al., 2005; Wills and Clahan, 2006; Wills et al., 2000a; Wills and Silva, 1998). Typically, a representative shear-wave velocity is determined from shear wave velocity profiles for each geologic unit (Holzer et al., 2005, Wills et al., 2000). A potential limitation of this procedure is the availability of V_{s30} data to properly define profiles for all geological units (Wald et al., 2011). Thompson et al. (2007) noted that V_{s30} maps produced by Holzer et al. (2005) exhibit more V_{s30} spatial variability compared to maps derived exclusively from regional surface geology. They attribute the higher variability to variations in the thickness of geological units which is not considered in surface geology maps. Also, they note that zonation based on geologic units may be inaccurate because they can contain sediments with similar shear-wave velocities. To account for the horizontal variability of near surface soil deposits, they investigated the horizontal correlation structure of shear-wave velocity across geologic units within a sedimentary basin. As an alternative to geological units and/or surface geology based mapping of V_{s30}, Wald et al. (2011) proposed a regression model relating V_{s30} to topographical slope for a number of geological units. However, none of these procedures provide estimates on the uncertainty of V_{s30} and its effect on zonation mapping, nor do they propose procedures to develop maps based on combining V_{s30} estimates from multiple sources. In this study, these issues are addressed as well as the treatment of potential biases and uncertainties in the estimates of V_{s30}.

The process of developing seismic microzonation maps is often incremental and maps are progressively updated in time as additional data or information is obtained. The first level of improvement of maps based on surface geology is to include borehole data (Cox et al., 2011). Typical information obtained from boreholes is depth to bedrock, soil layering (soil type and thickness) and the standard penetration index. However, not all boreholes provide the full spectrum of data. Typically, a large proportion of boreholes provide reliable data only on depth to bedrock (Figure 3.2a) and a smaller fraction provide reliable information on soil layering or the standard penetration index (Figure 3.2b). In either case, the information provided by the boreholes can be combined with V_s profiles from seismic survey data to derive depth-velocity relations from which V_{s30} estimates can be obtained. An example of regional depth-velocity relations are those derived for Montreal and Ottawa (Chouinard and Rosset, 2011; Hunter and Crow, 2012). For Montreal, depth-velocity relations are derived for post-glacial, clay and sand deposits, while probability distribution functions are proposed for shear wave velocities of glacial tills and bedrock. The depth-velocity relation for post-glacial deposits is used at borehole sites with data on depth to bedrock (Single-layer model, SL) to obtain estimates of the mean value and variance of V_{s30}.

$$
\begin{aligned}
Vs30_{SL} &= \frac{30}{\dfrac{z_{soil}}{V_{av}} + \dfrac{30 - z_{soil}}{Vs_{rock}}} \\
\sigma^2_{V_{s30,SL}} &= \left(\frac{30 z_{soil}}{V_{av}^2} \sigma^2_{av} + \frac{30(30 - z_{soil})}{Vs^2_{rock}} \sigma^2_{Vs_{rock}} \right) \times \left(\frac{z_{soil}}{V_{av}} + \frac{30 - z_{soil}}{Vs_{rock}} \right)^{-2}
\end{aligned}
\qquad 3.1
$$

where, $V_{av} = 170 + 29z^{0.5} \pm 50\ (m/s)$ is the depth-velocity relation for post-glacial deposits (Chouinard and Rosset, 2011), $V_{s,\ rock}$ is the shear wave velocity of bedrock and z_{soil} is depth to bedrock (m). Estimates of V_{s30} and of the coefficient of variation are shown in Figure 3.4 for the single layer model.

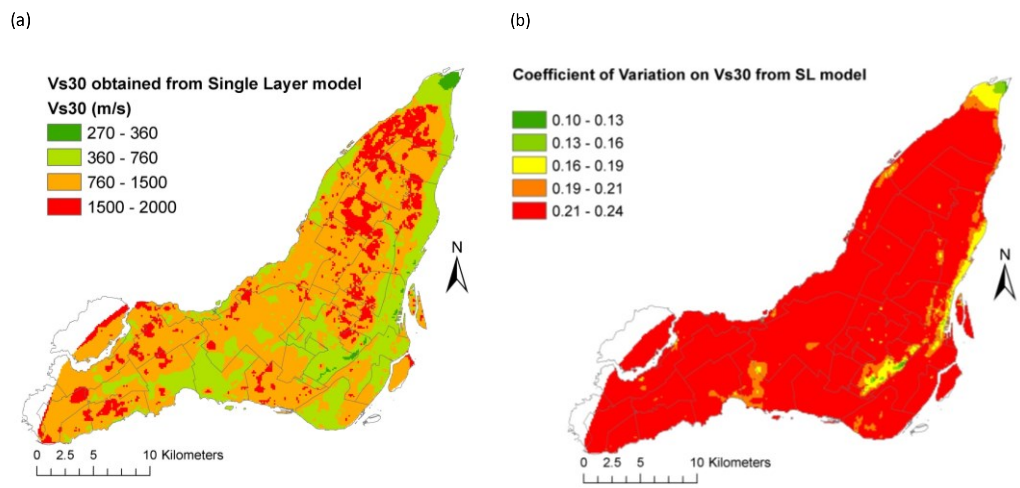

Figure 3.4: a) Estimates of V_{s30}; and b) Coefficient of Variation for the single layer model.

At sites where detailed information on multiple soil profiles is available, a multi-layer model (ML) is used. Five types of soil are considered: backfill, sand, clay, silt and till. Depth-velocity curves are used for sand, clay and silt. Average shear wave velocities for backfill, till and bedrock are set equal to 150 m/s, 565 m/s and 2350 m/s respectively based on field data (Rosset et al., 2014). The resulting multi-layer (ML) soil model for V_{s30} is:

$$Vs30_{ML} = \frac{30}{\frac{z_{backfill}}{Vs_{backfill}} + \frac{z_{clay}}{Vs_{clay}} + \frac{z_{sand}}{Vs_{sand}} + \frac{z_{silt}}{Vs_{silt}} + \frac{z_{till}}{Vs_{till}} + \frac{30 - \left(z_{backfill} + z_{clay} + z_{sand} + z_{silt} + z_{till}\right)}{Vs_{rock}}}$$

3.2

$$\sigma^2_{V_{s30,ML}} = \left(\sum_{i=1}^{4} \frac{30 z_i}{Vs_i^2} \sigma^2_{Vs_i} + \frac{30\left(30 - \sum_{i=1}^{4} z_i\right)}{Vs^2_{rock}} \sigma^2_{Vs_{rock}} \right) \times \left(\sum_{i=1}^{4} \frac{z_i}{Vs_i} + \frac{30 - \sum_{i=1}^{4} z_i}{Vs_{rock}} \right)^{-2}$$

where,

$$Vs_{sand} = 145 + 37z^{0.57} \pm 54\ (\text{m/s})$$
$$Vs_{silt} = 162 + 24z \pm 54\ (\text{m/s})$$
$$Vs_{clay} = 121 + 41z^{0.43} \pm 43\ (\text{m/s})$$

Estimates of V_{s30} and of the coefficient of variation are shown in Figure 3.5 for the multi-layer model.

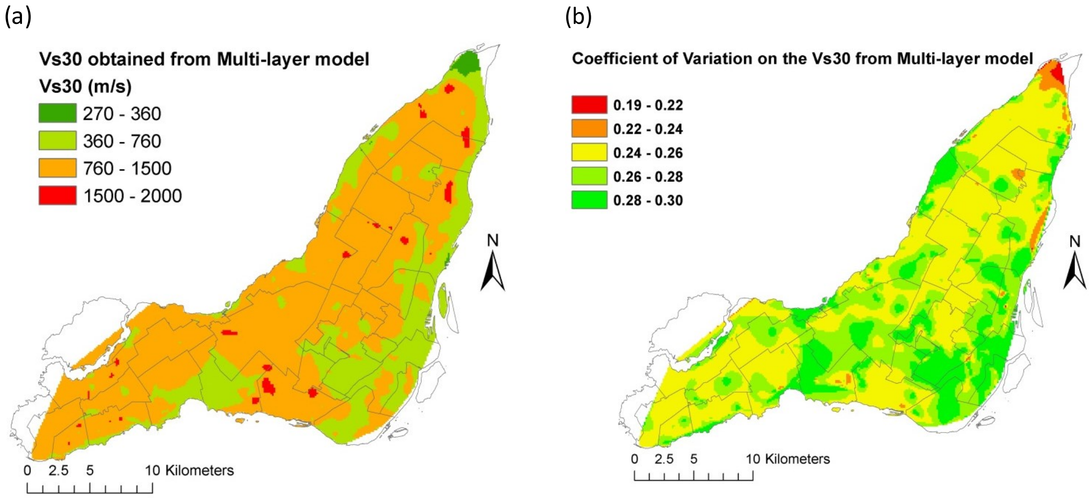

Figure 3.5: a) Estimates of V_{s30} and b) Coefficient of Variation of V_{s30} for the Multi-layer model.

Chouinard and Rosset (2011) also propose a relationship between site fundamental frequency F_0 and V_{s30} for sites where the fundamental frequency is below 10Hz:

$$Vs30_{F_0} = 177 + 44.7 \cdot F_0 \pm 89 \,(\text{m/s}) \qquad 3.3$$

Equations 3.1, 3.2 and 3.3 provide alternative estimates for V_{s30} as a function of the information available at a site when seismic survey data is not available. In the case of Montreal, these other sources of information are very important since seismic surveys were performed at a limited number of sites (Figure 3.2d) while depth to bedrock is available at 26,000 locations, soil layering at 2000 locations and fundamental frequency at 1600 locations. A seismic microzonation based on V_{s30} derived from depth to bedrock alone (Equation 3.1) offers a high degree of spatial resolution (Figure 3.3) but may be spatially biased and have large uncertainties since there is no information on soil types. A seismic microzonation based on V_{s30} derived from multiple soil layers (Equation 3.2) is more precise at borehole locations but has higher uncertainties and potential biases at sites that require interpolation (Figure 3.5). Finally, sites where fundamental frequencies have been measured provide V_{s30} estimates (Equation 3.3) correlated to the dynamic properties of the site but potential biases and uncertainties may again be introduced at interpolation sites. The objectives of the proposed procedure are to objectively use all sources of data in deriving a seismic microzonation map based on V_{s30} in order to retain a high degree of spatial resolution and decrease the uncertainty and biases at interpolation sites. The procedure is based on the principles of the conditional second moment analysis for random vectors (Ditlevsen and Madsen, 1996). Given two random vectors $\underline{X}_1$ and $\underline{X}_2$, characterized by the following partitioned mean vector and covariance matrix,

$$\begin{bmatrix} \underline{X}_1 \\ \underline{X}_2 \end{bmatrix} \sim \begin{bmatrix} \underline{\mu}_1 \\ \underline{\mu}_2 \end{bmatrix}, \begin{bmatrix} \Sigma_{11} & \Sigma_{12} \\ \Sigma_{21} & \Sigma_{22} \end{bmatrix} \tag{3.4}$$

Updates to the mean and covariance matrix of the random vector $\underline{X}_1$ are obtained given a vector of observations $\underline{x}_2$ of the random vector $\underline{X}_2$ as,

$$\begin{aligned} \underline{\mu}_{1|2} &= \underline{\mu}_1 + \Sigma_{12}\Sigma_{22}^{-1}\left(\underline{x}_2 - \underline{\mu}_2\right) \\ \Sigma_{1|2} &= \Sigma_{11} - \Sigma_{12}\Sigma_{22}^{-1}\Sigma_{21}^{T} \end{aligned} \tag{3.5}$$

In this application, $\underline{X}_1$ corresponds to V_{s30} estimates obtained from a compilation of seismic survey data for alluvial deposit sites for a region based only on surface geology information, while $\underline{X}_2$ corresponds to V_{s30} estimates using additional sources of information such as site-specific seismic surveys, depth to bedrock (single layer model), borehole data (multi-layer model), or the fundamental frequency (F_0 model).

The application of this procedure requires the estimation of the mean value vectors and covariance matrices for each type of V_{s30} estimate. This is achieved by analyzing data at sites where the various types of information are simultaneously available. For the island of Montreal, the sites (26 in total) where these conditions are met are shown in Figure 3.1. Given site specific information, estimates of V_{s30} were obtained from: 1) the seismic survey $(Vs30_{SS})$, the one layer model $(Vs30_{SL})$ in Equation 3.1, the multi-layer model ($Vs30_{ML}$) in Equation 3.2, and the F_0 model $(Vs30_{F_0})$ in Equation 3.3 at each of the 26 sites. Figure 3.6 compares the predictions from the 3 models to the velocities derived from the seismic survey (assumed to be the most precise). In these figures, the diagonal line corresponds to a perfect prediction and the vertical or horizontal grids correspond to the NBCC (2010) soil categories. The red markers correspond to estimates obtained from the models while the blue markers are updated estimates to be discussed in the next section. In the case of the single layer model in Figure 3.6a, the initial model (surface geology based SL model) tends to overestimate velocities for deep alluvial sites (class D) and many class D sites are labeled as class C. On the other hand, class C and B sites appear on average to be correctly identified. This comparison shows that although the single-layer model tends to overestimate V_{s30} for deep alluvial sites (greater than 20 m), but the variance is much smaller (Equation 3.6), because deposits tend to be more homogeneous. For shallow sites (smaller than 20 m), the single layer model slightly overestimates V_{S30} and the variance in velocities is large (Equation 3.6) for site classes C and B (smaller than 20 m) due to the large variety of types of soils and the greater influence from the shear wave velocity of till and rock. For these reasons, the mean value vectors and covariance matrices were estimated for 2 ranges of depth to bedrock (less than 20 m and more than 20 m).

3.6
$$\begin{bmatrix} Vs30_{SS} \\ Vs30_{SL} \end{bmatrix} \sim \begin{bmatrix} m_{SS} \\ m_{SL} \end{bmatrix}, \begin{bmatrix} \sigma_{SS}^2 & \rho_{SS,SL}\sigma_{SS}\sigma_{SL} \\ \rho_{SS,SL}\sigma_{SS}\sigma_{SL} & \sigma_{SL}^2 \end{bmatrix}$$
$$\begin{bmatrix} Vs30_{SS} \\ Vs30_{SL} \end{bmatrix} \sim \begin{bmatrix} 554 \\ 595 \end{bmatrix}, \begin{bmatrix} (192)^2 & (0.71)(192)(153) \\ (0.71)(192)(153) & (153)^2 \end{bmatrix} \qquad 3.5\,\mathrm{m} \le z \le 20\,\mathrm{m}$$
$$\begin{bmatrix} Vs30_{SS} \\ Vs30_{SL} \end{bmatrix} \sim \begin{bmatrix} 295 \\ 355 \end{bmatrix}, \begin{bmatrix} (87)^2 & (0.76)(87)(40) \\ (0.76)(87)(40) & (40)^2 \end{bmatrix} \qquad 20\,\mathrm{m} \le z \le 35\,\mathrm{m}$$

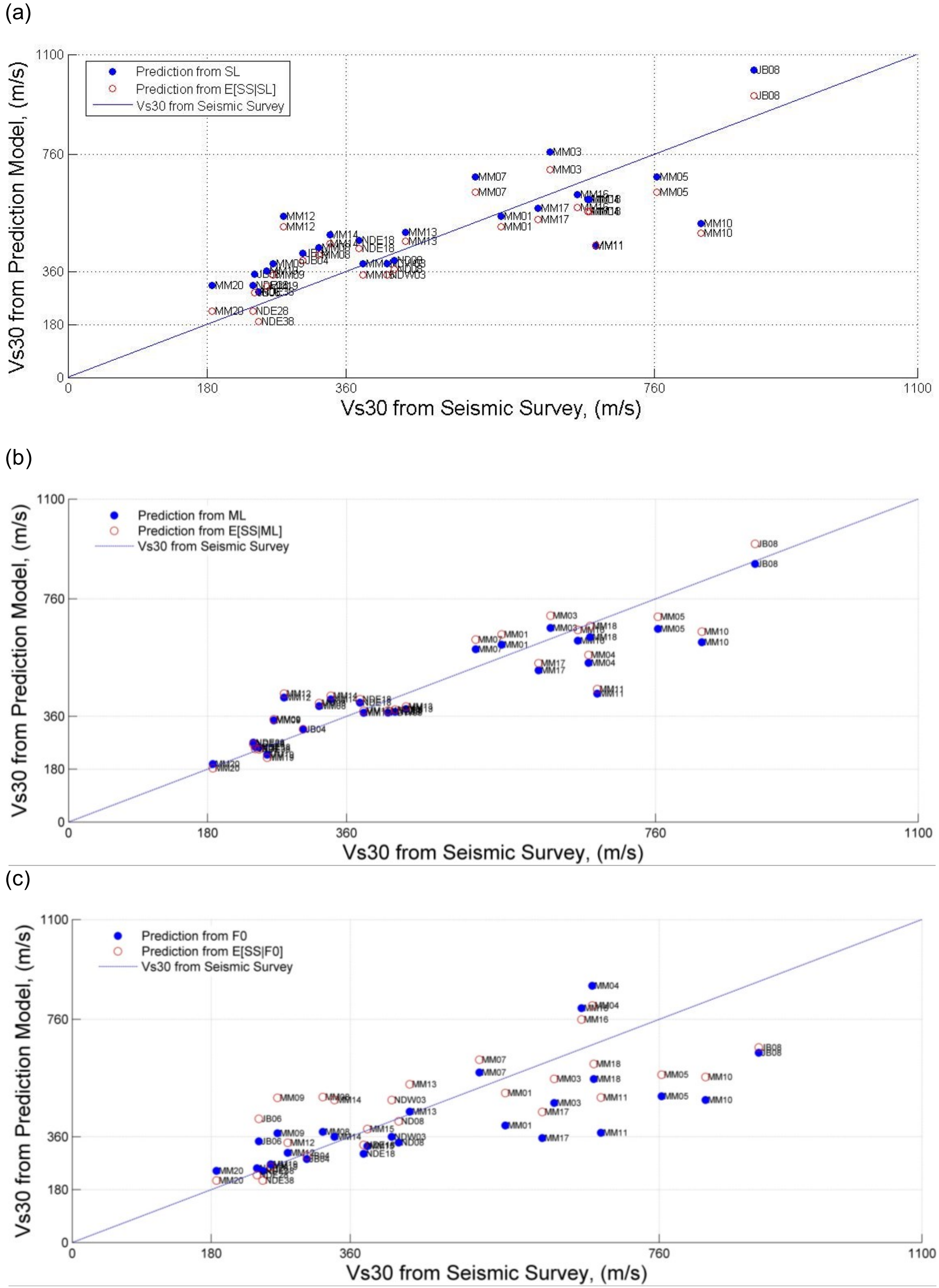

Figure 3.6: Comparing V_{s30} estimates from the seismic survey ($Vs30_{SS}$) with the V_{s30} estimates from SL, ML and F_0 models before and after updating.

For the multi-layer model in Figure 3.6b, a single grouping of sites is considered since the data indicates a linear relation over the full range of depths and the variance is also fairly constant as a function of depth. In this case, predictions are in good agreement with measurements on average when comparing mean values as well as from the high correlation coefficient as in Equation 3.7.

$$\begin{bmatrix} Vs30_{SS} \\ Vs30_{ML} \end{bmatrix} \sim \begin{bmatrix} m_{SS} \\ m_{ML} \end{bmatrix}, \begin{bmatrix} \sigma_{SS}^2 & \rho_{SS,ML}\sigma_{SS}\sigma_{ML} \\ \rho_{SS,SL}\sigma_{SS}\sigma_{ML} & \sigma_{ML}^2 \end{bmatrix}$$

$$\begin{bmatrix} Vs30_{SS} \\ Vs30_{ML} \end{bmatrix} \sim \begin{bmatrix} 469 \\ 453 \end{bmatrix}, \begin{bmatrix} (205)^2 & (0.91)(205)(166) \\ (0.91)(205)(166) & (166)^2 \end{bmatrix} \qquad 3.5\,\text{m} \le z \le 35\,\text{m} \tag{3.7}$$

For V_{s30} predictions based on the site fundamental frequency (Figure 3.6c), the data set is partitioned in two for sites with frequencies below 4 Hz and for sites with frequencies above 4 Hz as shown in Equation 3.8. This division corresponds to sites that have softer or denser soils and is done to satisfy the requirements of conditional second moment analysis for a linear relation and constant variance. For the first range of frequencies, there is good agreement on average as evidenced by the mean values; however, the model underestimates the uncertainty because of the mixture of sites that comprises both sand and clay deposits.

$$\begin{bmatrix} Vs30_{SS} \\ Vs30_{F_0} \end{bmatrix} \sim \begin{bmatrix} m_{SS} \\ m_{F_0} \end{bmatrix}, \begin{bmatrix} \sigma_{SS}^2 & \rho_{SS,F_0}\sigma_{SS}\sigma_{F_0} \\ \rho_{SS,F_0}\sigma_{SS}\sigma_{F_0} & \sigma_{F_0}^2 \end{bmatrix}$$

$$\begin{bmatrix} Vs30_{SS} \\ Vs30_{F_0} \end{bmatrix} \sim \begin{bmatrix} 322 \\ 297 \end{bmatrix}, \begin{bmatrix} (119)^2 & (0.73)(119)(42) \\ (0.73)(119)(42) & (42)^2 \end{bmatrix} \qquad 1.5\,\text{Hz} \le F_0 \le 4\,\text{Hz} \tag{3.8}$$

$$\begin{bmatrix} Vs30_{SS} \\ Vs30_{F_0} \end{bmatrix} \sim \begin{bmatrix} 577 \\ 507 \end{bmatrix}, \begin{bmatrix} (188)^2 & (0.53)(188)(160) \\ (0.53)(188)(160) & (160)^2 \end{bmatrix} \qquad 4\,\text{Hz} \le F_0 \le 16\,\text{Hz}$$

The statistics (Equation 3.6 to 3.8) indicate the characteristics of estimates of V_{s30} from the various sources as well as their degree of correlation. In general, estimates derived from surface geology map have more uncertainty and show better correlation with estimates derived from other sources for deep soft soil deposits. The updating procedures (Equation 3.4 and Equation 3.5) are applied to the 26 sites to demonstrate the effect of the procedure (Figures 3.7 and 3.8). The effects of updating relative to the initial estimates are shown in Figure 3.7 for the individual models, while the effect of updating for the three models are compared in Figure 3.8. Conditional second moment analysis (Equation 3.4 and Equation 3.5) is used to update estimates based on site specific information. In the absence of site-specific data, the regional average V_{s30}

and standard deviation are assigned to a site as a function of the surface geology classification. If depth to bedrock (or to top of till) is known, this information is used to calculate $Vs30_{SL}$. Typically, a large number of boreholes is available in urban areas and corresponds with the location of the built environment. In Montreal, over 26,000 such boreholes are used to define depth to bedrock (Figure 3.2), and this information is used to estimate $Vs30_{SL}$ values from Equation 3.1. The $Vs30_{SL}$ model allows for a very detailed representation of the spatial variation of V_{s30}; however, the level of uncertainty is expected to be large given the lack of detailed information on stratigraphy. Estimates are more accurate for boreholes with detailed information on stratigraphy using $Vs30_{ML}$. In Montreal, 2000 boreholes (Figure 3.2) provide such information. Finally, 1600 sites with measurements of ambient noise (Figure 3.2) were analyzed with the HVSR method (Castellaro and Mulargia, 2009) to obtain the site fundamental frequencies (F_0). Estimates of $Vs30_{F0}$ are obtained with equation 3.3 and are considered accurate for site frequencies below 10 Hz. Using these results, updates for the expected value and the variance of V_{s30} as a function of the information available at a site are shown in Table 3.4 and are compared in Figure 3.7.

Table 3.4: Expected estimates of $Vs30_{SS}$ and its conditional variance based on single layer model, multi-layer and F_0 models of V_{s30}.

Information	Equation for Expected $Vs30_{SS}$ (m/s) and conditional variance $(m/s)^2$ of $Vs30_{SS}$ (m/s)	Expected $Vs30_{SS}$ (m/s) and conditional variance $(m/s)^2$ of $Vs30_{SS}$ (m/s)
Sites with only depth to bedrock (3.5 to 20 m)	$E[SS\,\|\,SL] = \mu_{SS} + \rho_{SS,SL}\dfrac{\sigma_{SS}}{\sigma_{SL}}(Vs30_{SL} - \mu_{SL})$	$E[SS\,\|\,SL] = 554 + 0.71\dfrac{192}{153}(Vs30_{SL} - 595)$ (m/s)
	$\Sigma_{SS\|SL} = \sigma^2_{SS}(1 - \rho^2_{SS,SL})$	$\Sigma_{SS\|SL} = 192^2(1 - 0.71^2) = 18280.86$ $(m/s)^2$
Sites with only depth to bedrock (20 to 35 m)	$E[SS\,\|\,SL] = \mu_{SS} + \rho_{SSSL}\dfrac{\sigma_{SS}}{\sigma_{SL}}(Vs30_{SL} - \mu_{SL})$	$E[SS\,\|\,SL] = 295 + 0.76\dfrac{87}{40}(Vs30_{SL} - 355)$ (m/s)
	$\Sigma_{SS\|SL} = \sigma^2_{SS}(1 - \rho^2_{SS,SL})$	$\Sigma_{SS\|SL} = 87^2(1 - 0.76^2) = 3124.07$ $(m/s)^2$
Sites with detailed stratigraphy (3.5 to 35 m)	$E[SS\,\|\,ML] = \mu_{SS} + \rho_{SSML}\dfrac{\sigma_{SS}}{\sigma_{ML}}(Vs30_{ML} - \mu_{ML})$	$E[SS\,\|\,ML] = 469 + 0.91\dfrac{205}{166}(Vs30_{ML} - 453)$ (m/s)
	$\Sigma_{SS\|ML} = \sigma^2_{SS}(1 - \rho^2_{SS,ML})$	$\Sigma_{SS\|ML} = 205^2(1 - 0.91^2) = 7224.098$ $(m/s)^2$
Sites with Fundamental Frequency (1.5 to 4 Hz)	$E[SS\,\|\,F_0] = \mu_{SS} + \rho_{SS,F_0}\dfrac{\sigma_{SS}}{\sigma_{F_0}}(Vs30_{F_0} - \mu_{F_0})$	$E[SS\,\|\,F_0] = 322 + 0.73\dfrac{119}{42}(Vs30_{F_0} - 297)$ (m/s)
	$\Sigma_{SS\|F_0} = \sigma^2_{SS}(1 - \rho^2_{SS,F_0})$	$\Sigma_{SS\|F_0} = 119^2(1 - 0.73^2) = 6614.603$ $(m/s)^2$
Sites with Fundamental Frequency (4 to 16 Hz)	$E[SS\,\|\,F_0] = \mu_{SS} + \rho_{SS,F_0}\dfrac{\sigma_{SS}}{\sigma_{F_0}}(Vs30_{F_0} - \mu_{F_0})$	$E[SS\,\|\,F_0] = 577 + 0.53\dfrac{188}{160}(Vs30_{F_0} - 507)$ (m/s)
	$\Sigma_{SS\|F_0} = \sigma^2_{SS}(1 - \rho^2_{SS,F_0})$	$\Sigma_{SS\|F_0} = 188^2(1 - 0.53^2) = 25415.87$ $(m/s)^2$

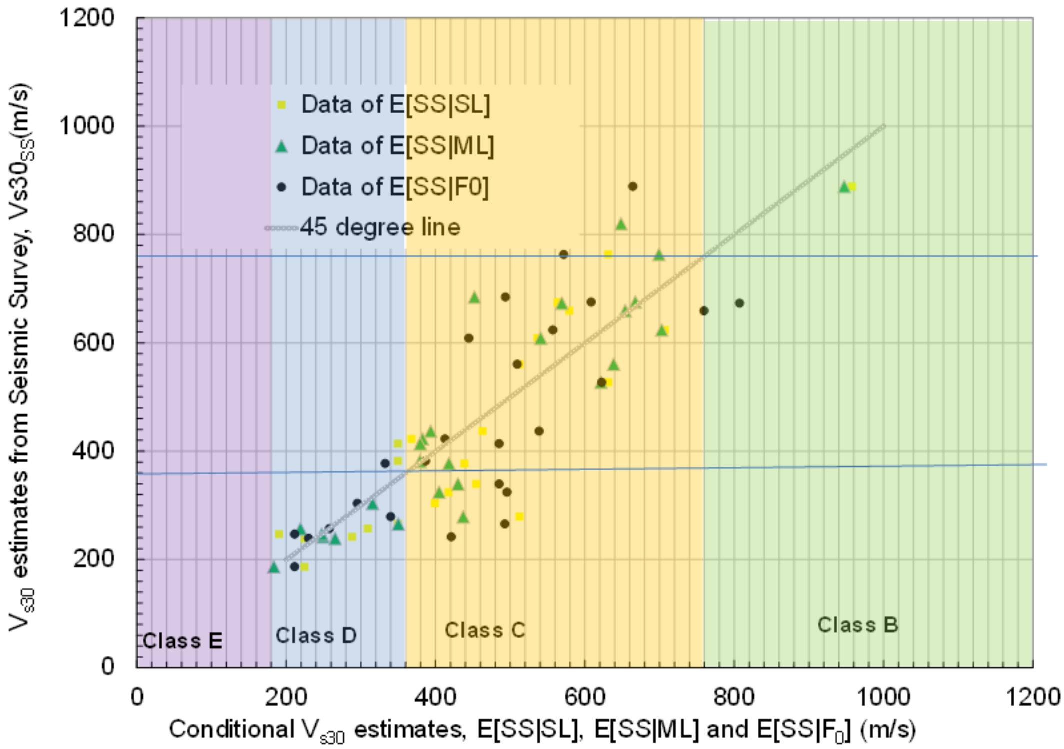

Figure 3.7: Comparison between the data of $Vs30_{SS}$ and conditional V_{s30} estimates of E[SS|SL], E[SS|ML] , and E[SS|F_0] at the 26 sites where site fundamental frequencies are between 1.5-16 Hz.

3.5 Accuracy of Predicted V_{s30} Estimates obtained from SL, ML and F_0 models

The accuracy of the proposed method is evaluated by comparing the performance of the initial models ($Vs30_{SL}, Vs30_{ML}$, and $Vs30_{F_0}$) to the updated estimates of V_{s30} ($E[SS \mid SL]$, $E[SS \mid ML]$ and $E[SS \mid F_0]$) at the 26 sites. Improvements are measured in terms of reductions in the bias of predictions and in the variance of predictions. The overall performance is assessed through the mean squared error (Table 3.5). The errors of predictions are defined as,

$$
\begin{aligned}
e_i &= \hat{V}_{s30i} - V_{s30i} \\
\bar{e} &= \frac{1}{n}\sum_{i=1}^{n}(e_i)
\end{aligned}
\tag{3.9}
$$

where, V_{s30} is the true value assumed to correspond to estimates obtained from seismic surveys and $\hat{V}_{s30}$ is obtained from one of the prediction model (SL, ML or F_0).

The bias ($\overline{e}$), or systematic error is defined as the average of the errors of prediction (Equation 3.9), and the variance and means squared error (MSE) of the residuals,

$$3.10 \qquad \sigma_e^2 = \frac{1}{n}\sum_{i=1}^{n}(e_i - \overline{e})^2$$

$$3.11 \qquad MSE = \overline{e}^2 + \sigma_e^2$$

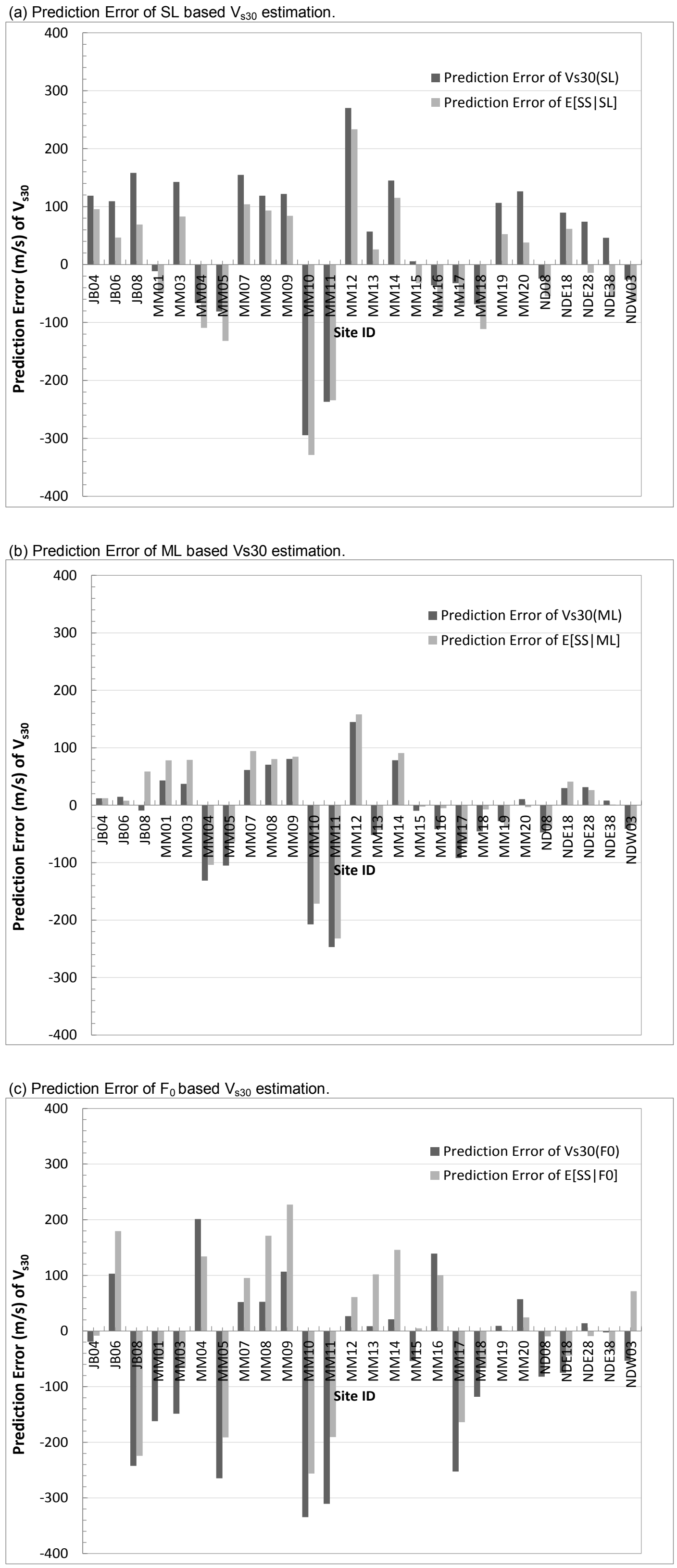

Figure 3.8: Prediction Error of V_{s30} estimates from SL, ML and F_0 models at 26 sites.

The prediction error on estimates of V_{s30} for the updated SL, ML, and F_0 models have been computed using Equation 3.9 through 3.11, and are presented in Figure 3.8 and Table 3.5. These results indicate a significant reduction in the bias and mean squared error (variance + bias^2) of predictions for the various options of prediction. Table 3.5 indicates that the single layer model is more accurate for deep sites than for shallow sites and has a positive bias in both cases. The higher variance for shallow sites is attributed to a greater diversity of soil types, in particular tills, while most of the sites with deeper alluviums are associated with deposits dominated by clay and sand.

Figure 3.8 also shows large prediction errors with the ML and F_0 models for the sites MM10, MM11 and MM12. Figure 3.3b shows the V_s profiles for these sites and shows that sites MM10 and MM11 are comprised of sand and tills (8 to 22 m thick), while site MM12, consists mainly of clay. At sites MM10 and MM11, an average velocity of 565 m/s was assumed for thick till layers for predicting the V_s profiles in the ML model. However, the V_s profiles obtained from the seismic survey ($Vs30_{SS}$ model) have much higher V_s for till layers in the range of 600 to 840 m/s (Figure 3.3b) resulting in higher $Vs30_{SS}$ values compared to the $Vs30_{ML}$ values as shown in Figure 3.6b. This discrepancy is due to the difficulty in identifying the three types of Till (Malone Till, Middle Till Complex and Fort Covington Till) on the basis of borehole data alone. For site MM12, the prediction error (Figure 3.8b) is due to overestimation of the V_s profile for the clay layer by the ML models as compared to the V_s profile determined from the seismic survey (Figure 3.3b). Similarly, the prediction errors from the $Vs30_{F_0}$ models (Figure 3.8c) for sites MM10 and MM11 show large under predictions. This may be due to the presence of a soft sand layer overlying thick layer of till which influences the estimation of F_0 which is not consistent with the other sites used to derive the prediction model for V_{s30}.

The updating procedure eliminates the bias and reduces the variance which also reduces the MSE. The multilayer model has the lowest bias and slightly underestimates the velocities. The updating procedure eliminates the bias and slightly reduces the variance indicating that the initial model is accurate. Finally, the predictions based on the fundamental frequency of the site have negative bias for both ranges of frequencies. The bias and variance are higher for high frequencies (shallow sites) since the initial model was derived mainly from data for deeper sites (0 to 10 Hz). For both ranges of frequencies, the updated model improves significantly the predictions.

Table 3.5: Comparing the performance of the initial models (SL, ML and F_0) to the updated estimates of V_{s30} for the 26 sites.

Model	Bias (m/s)	Variance (m/s)^2	MSE (m/s)^2
SL (3.5 m to 30 m)	42	$(132)^2$	$(139)^2$
Updated SL (3.5 m to 20 m)	0	$(131)^2$	$(131)^2$
SL (20 m to 35 m)	60	$(58)^2$	$(85)^2$
Updated SL (20 m to 35 m)	0	$(53)^2$	$(53)^2$
ML (3.5 m to 35 m)	-17	$(86)^2$	$(87)^2$
Updated ML (3.5 m to 35 m)	0	$(84)^2$	$(84)^2$
F_0 (1.5 Hz to 4 Hz)	-25	$(89)^2$	$(93)^2$
Updated F_0 (1.5 Hz to 4 Hz)	0	$(78)^2$	$(78)^2$
F_0 (4 Hz to 16 Hz)	-70	$(170)^2$	$(184)^2$
Updated F_0 (4 Hz to 16 Hz)	0	$(154)^2$	$(154)^2$

3.6 Combining V_{s30} from ML and F_0 models to update V_{s30}

In some instances, estimates of V_{s30} can be obtained by combining several models ($Vs30_{SL}$, $Vs30_{ML}$ and $Vs30_{F_0}$) at a single site. The case when depth to bedrock (for $Vs30_{SL}$), and detailed borehole data (for $Vs30_{ML}$) are available is not considered. The other two potential cases are when the fundamental frequency at a site is available as well as information on either depth to bedrock or soil layering. Only, the case for combining estimates from the fundamental frequency ($Vs30_{F_0}$) with detailed borehole data ($Vs30_{ML}$) is presented here since this corresponds to the data available for the island of Montreal. Updating based on information from these sources is performed by using the following equations for the expected value and variance respectively,

$$3.12 \qquad E\left[SS \middle| \begin{pmatrix} ML \\ F_0 \end{pmatrix}\right] = \mu_{SS} + \Sigma_{SS,\begin{pmatrix} ML \\ F_0 \end{pmatrix}} \left(\Sigma_{\begin{pmatrix} ML \\ F_0 \end{pmatrix}} \right)^{-1} \left[\begin{pmatrix} Vs30_{ML} \\ Vs30_{F_0} \end{pmatrix} - \begin{pmatrix} \mu_{ML} \\ \mu_{F_0} \end{pmatrix} \right]$$

$$3.13 \qquad \Sigma_{SS,\begin{pmatrix} ML \\ F_0 \end{pmatrix}} = \left[\left(\rho_{SS,ML} \cdot \sigma_{SS} \cdot \sigma_{ML} \right) \quad \left(\rho_{SS,F_0} \cdot \sigma_{SS} \cdot \sigma_{F_0} \right) \right]$$

The covariance Matrix of the estimates of $Vs30_{ML}$ with $Vs30_{F_0}$ is:

$$3.14 \quad \Sigma_{\begin{bmatrix} ML \\ F_0 \end{bmatrix}} = \begin{bmatrix} \sigma^2_{ML} & (\rho_{ML,F_0}\sigma_{ML}\sigma_{F_0}) \\ (\rho_{ML,F_0}\sigma_{ML}\sigma_{Fo}) & \sigma^2_{F_0} \end{bmatrix}$$

and the conditional variance is

$$3.15 \quad \Sigma_{SS\left|\begin{pmatrix} ML \\ F_0 \end{pmatrix}\right.} = \Sigma_{SS,SS} - \Sigma_{SS,\begin{pmatrix} ML \\ F_0 \end{pmatrix}} \left(\Sigma_{\begin{bmatrix} ML \\ F_0 \end{bmatrix}}\right)^{-1} \left(\Sigma_{SS,\begin{pmatrix} ML \\ F_0 \end{pmatrix}}\right)^{T}$$

Table 3.6 and 3.7 show the covariance matrices used or updating the mean values and variances for the ML-F_0 model.

Table 3.6 Covariance matrices for updating $Vs30_{SS}$ when both the information of $Vs30_{ML}$ and $Vs30_{F0}$ are available at a site.

Information	Numerical Values of covariance $(m/s)^2$
Sites with Fundamental Frequency (1.5 to 4 Hz)	$\Sigma_{SS,\begin{pmatrix} ML \\ F_0 \end{pmatrix}} = [(0.88 \cdot 119 \cdot 99) \quad (0.73 \cdot 119 \cdot 42)]$
	$\Sigma_{\begin{bmatrix} ML \\ F_0 \end{bmatrix}} = \begin{bmatrix} (99^2) & (0.72 \cdot 99 \cdot 42) \\ (0.72 \cdot 99 \cdot 42) & (42^2) \end{bmatrix}$
	$\sigma^2_{ss} = 119^2$
Sites with Fundamental Frequency (4 to 16 Hz)	$\Sigma_{SS,\begin{pmatrix} ML \\ F_0 \end{pmatrix}} = [(0.84 \cdot 188 \cdot 148) \quad (0.54 \cdot 188 \cdot 160)]$
	$\Sigma_{\begin{bmatrix} ML \\ F_0 \end{bmatrix}} = \begin{bmatrix} (148^2) & (0.53 \cdot 148 \cdot 160) \\ (0.53 \cdot 148 \cdot 160) & (160^2) \end{bmatrix}$
	$\sigma^2_{ss} = 188^2$

The updated variances obtained for this model are shown in Table 3.7.

Table 3.7: Conditional variance on the expected estimates of $Vs30_{SS}$ given $Vs30_{ML}$ and $Vs30_{F0}$ are available at a site.

Information	Symbol of Conditional Variance	Numeric value $(m/s)^2$
Site Fundamental Frequency (1.5 - 4 Hz)	$\Sigma_{ss\mid\binom{ML}{F_0}}$	$(54)^2$
Site Fundamental Frequency (4 - 16 Hz)	$\Sigma_{ss\mid\binom{ML}{F_0}}$	$(100)^2$

The prediction errors on the estimates of V_{s30} for the updated ML, F_0 and ML-F_0 models have been compared in Figure 3.9. It shows that the updating procedure with detailed borehole and fundamental frequency data (ML-F_0 model) does not improve predictions relative to the case with borehole data only. Figure 3.9 also indicates that predictions of V_{s30} based only on F_0 have larger prediction errors. However, at sites where no other information is available, predictions based on F_0 provide useful information on V_{s30} and on dynamic soil properties that are relevant to the seismic performance of structures. The next section describes how the bias corrected estimates of V_{s30} from the various sources are combined to develop the overall seismic microzonation map.

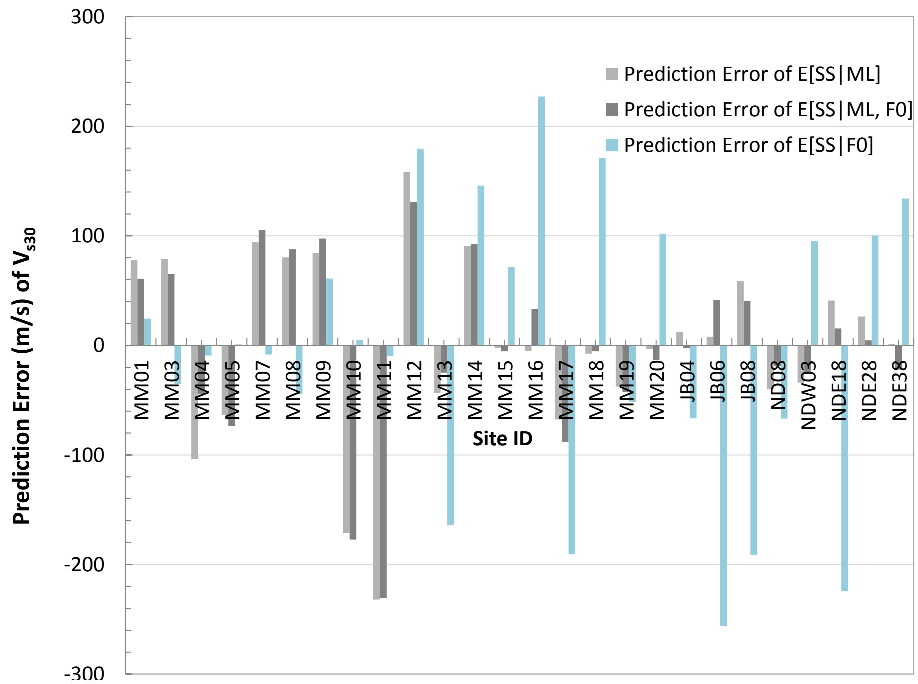

Figure 3.9: Error prediction of $Vs30_{SS}$ when updated by the V_{s30} estimates from solely ML and combined estimates from ML and F_0.

3.7 Probabilistic Microzonation Mapping

Table 3.1 shows the seismic site classification of the NBCC (2010) as a function of site characteristics and in particular as a function of V_{s30}. As shown in the previous section, estimates of V_{s30} can have varying levels of uncertainty as a function of the type on information available at a site. This uncertainty is generally not considered in developing seismic microzonation maps and mapping is based only on the expected value of V_{s30}.

In this study, updated values of V_{s30} were found to be well represented by the normal distribution which allows for a probabilistic assessment of site classification (Figure 3.10). The first distribution (in red line) represents the case where only surface geology data is available at a site which corresponds to an estimate with large uncertainty. The second distribution (in blue line) indicates the effect of the updating procedure when detailed borehole data is available at the site (ML model). In this case, the updating procedure has reduced the average value for the estimate of V_{s30} as well as the variance. The normal distribution can then be used to obtain estimates for the probability of each category of site classification. In this example, site classification based only on the average value would result in the same site classification (C). When accounting for uncertainty, the site classification initially becomes (P[B] = 0.2, P[C] = 0.5, P[D] = 0.2 and P[E] = 0.1) while it becomes (P[B] = 0.15 and P[C] = 0.85) after updating.

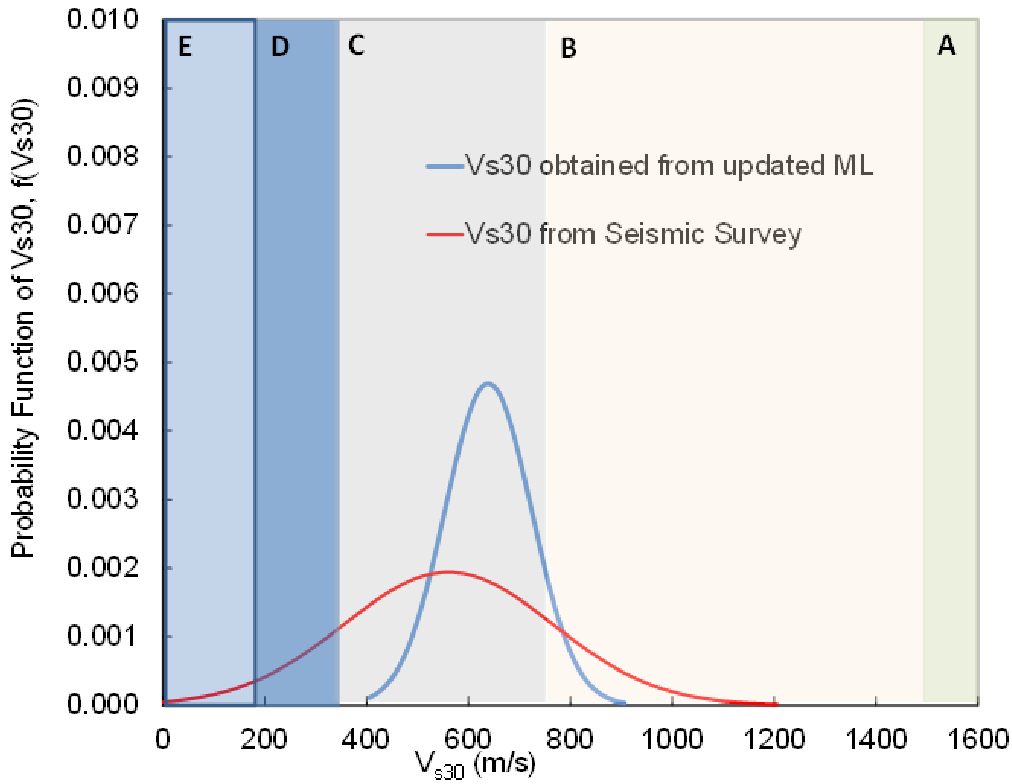

Figure 3.10: Probability Distribution Function of V_{s30} before and after updating with soil classification.

The procedure is applied in Montreal to update V_{s30} as a function of the information available at each site. Figure 3.11 shows the probability distribution of site classification based on the updating procedure based only on depth to bedrock (SL model). In this case, a very detailed map is obtained due to the large number of boreholes down to bedrock (over 26000) and shows that site class C is predominantly associated with sites in the periphery and south of the island. One interesting feature is the spatial and sudden changes in soil classification due to corresponding rapid changes in the thickness of soil deposits which would not be captured by interpolation techniques using a limited number of high quality boreholes. This is illustrated by the soil classification obtained when updating V_{s30} solely on the basis of high quality borehole data with detailed soil layering information (Figure 3.12). In this case, data is available at a reduced (~2000) number of sites and provides more accurate estimates at the location of the boreholes; however, the interpolation between sites cannot account for rapid changes in soft soil deposit thickness. In particular, since no detailed data is available in the zone previously identified as potential class D sites, the zonation fails at identifying these zones. Using the map based on depth to bedrock and the map on surface geology as guides, targeted surveys using ambient noise measurements were used to investigate potential locations with deep soft sediments. A total of 1600 measurements were performed over a period of few years. Figure 3.13 illustrates the microzonation maps derived from the data on site fundamental frequency and demonstrates the efficiency of this procedure in identifying zones with soils of class D with greater accuracy. In this case, these locations are at the periphery of the island and at sites of ancient lakes or marshes. Figure 3.14 shows the microzonation obtained for a subset of sites where both data on natural frequency of the site and detailed borehole data (ML model) are available. For these sites, the uncertainty is reduced and provides higher probabilities of single class membership and illustrates the benefits of characterizing sites with several parameters.

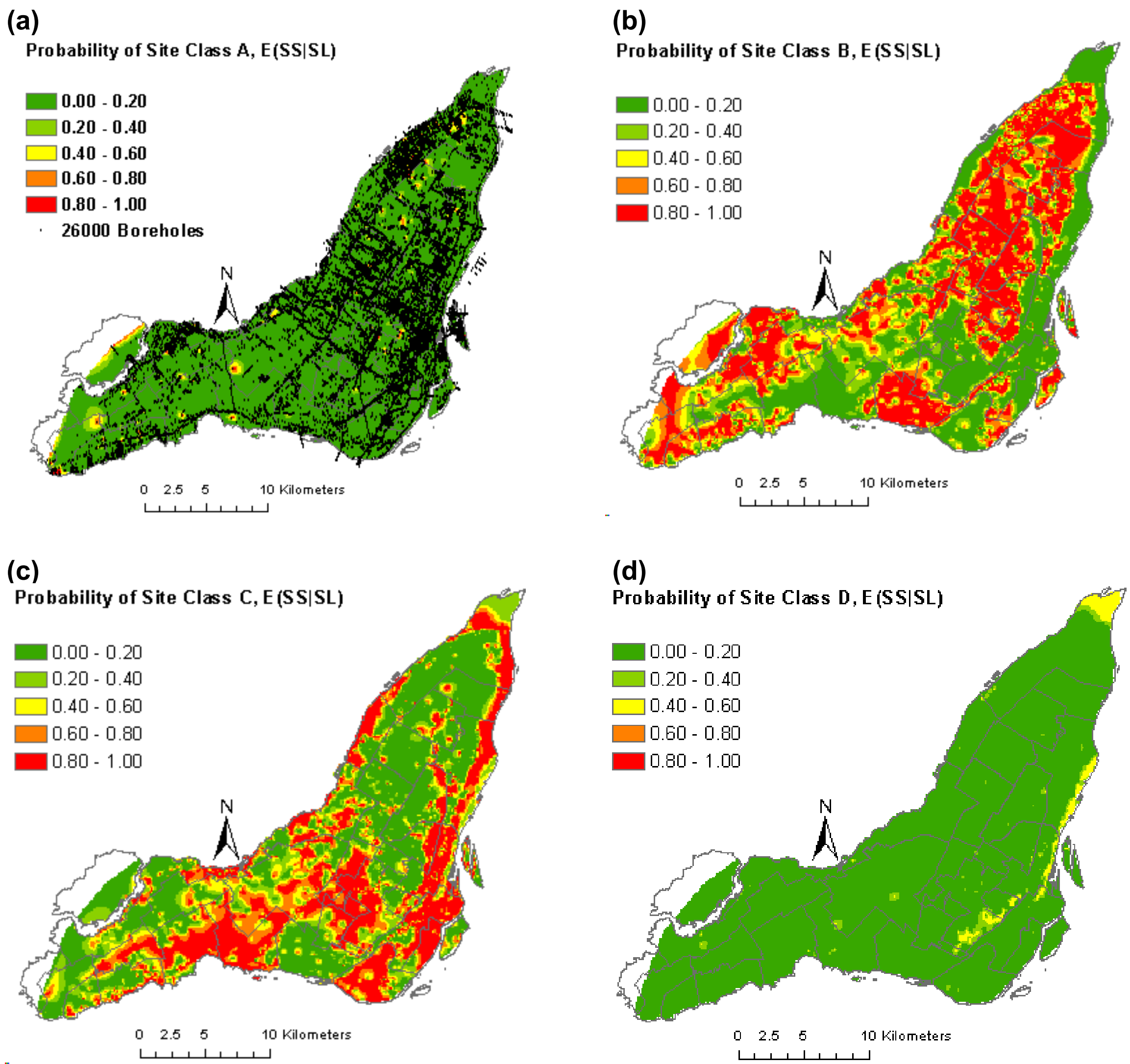

Figure 3.11: The maps for the probability of soil site classes: A, B, C and D using the proposed updating procedure at sites with data on depth to bedrock.

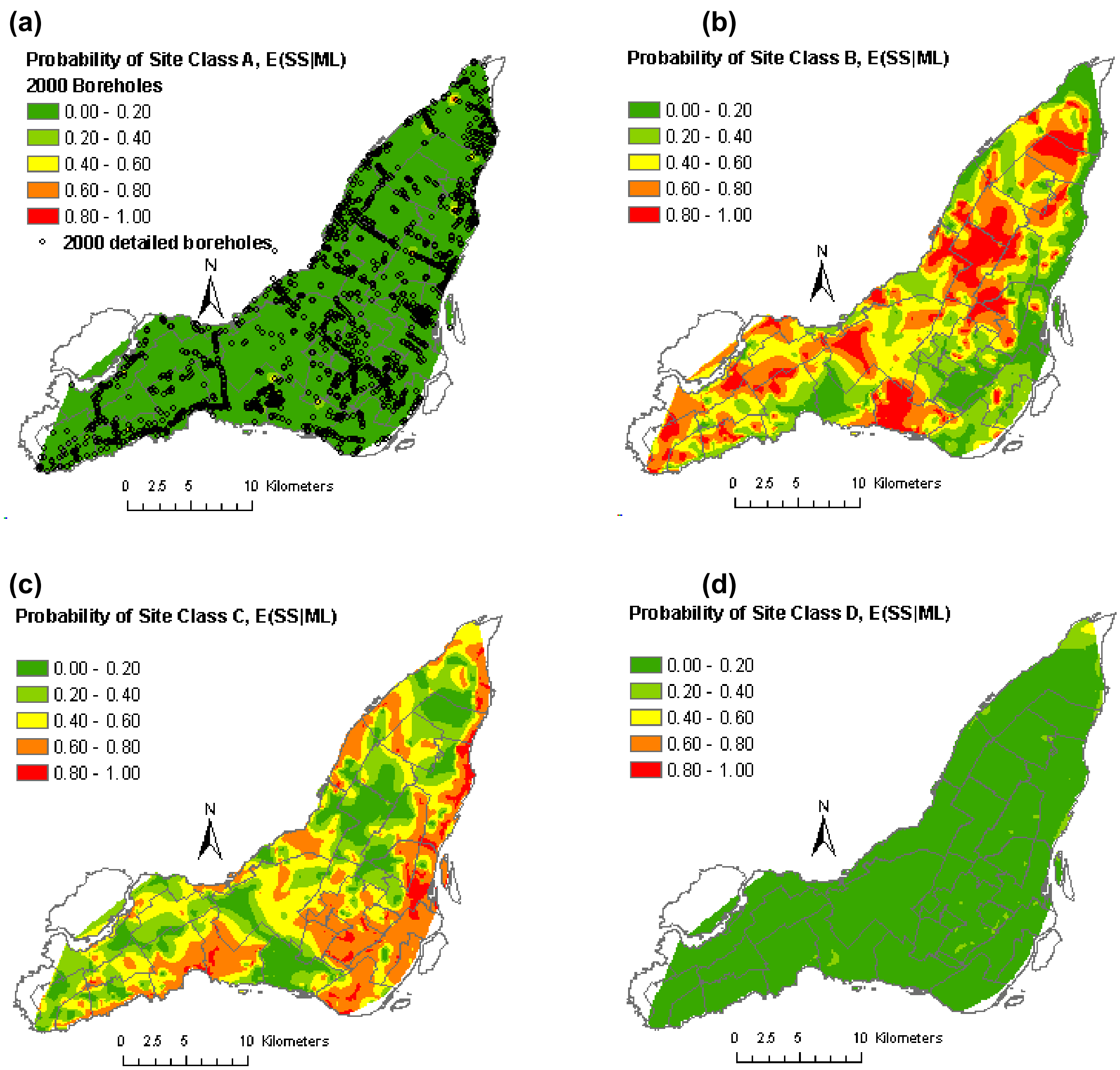

Figure 3.12: The maps for the probability of soil site classes: A, B, C and D using the proposed updating procedure at sites with detailed borehole data.

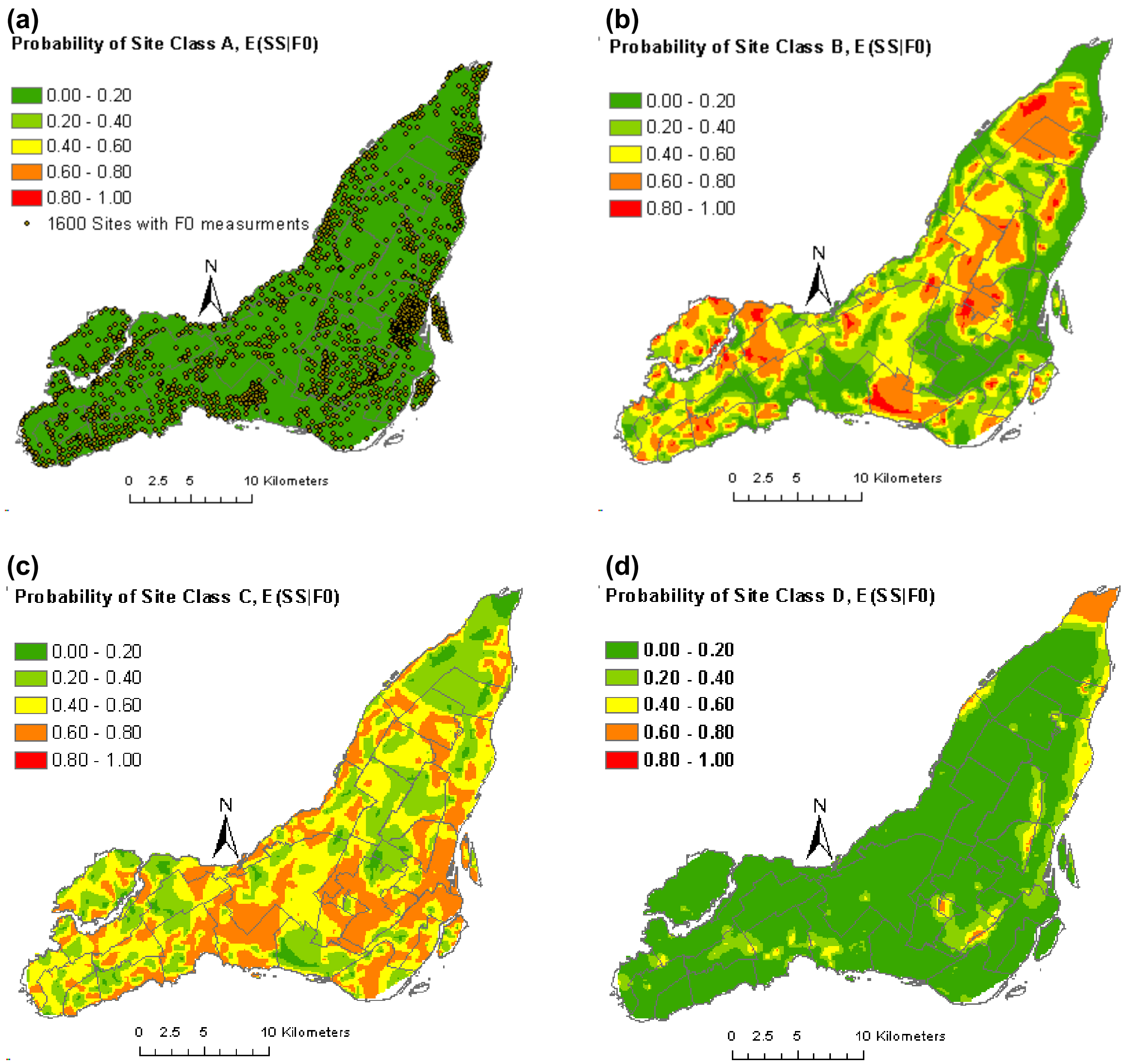

Figure 3.13: The maps for the probability of soil site classes: A, B, C and D using the proposed updating procedure at sites with data on site fundamental frequency.

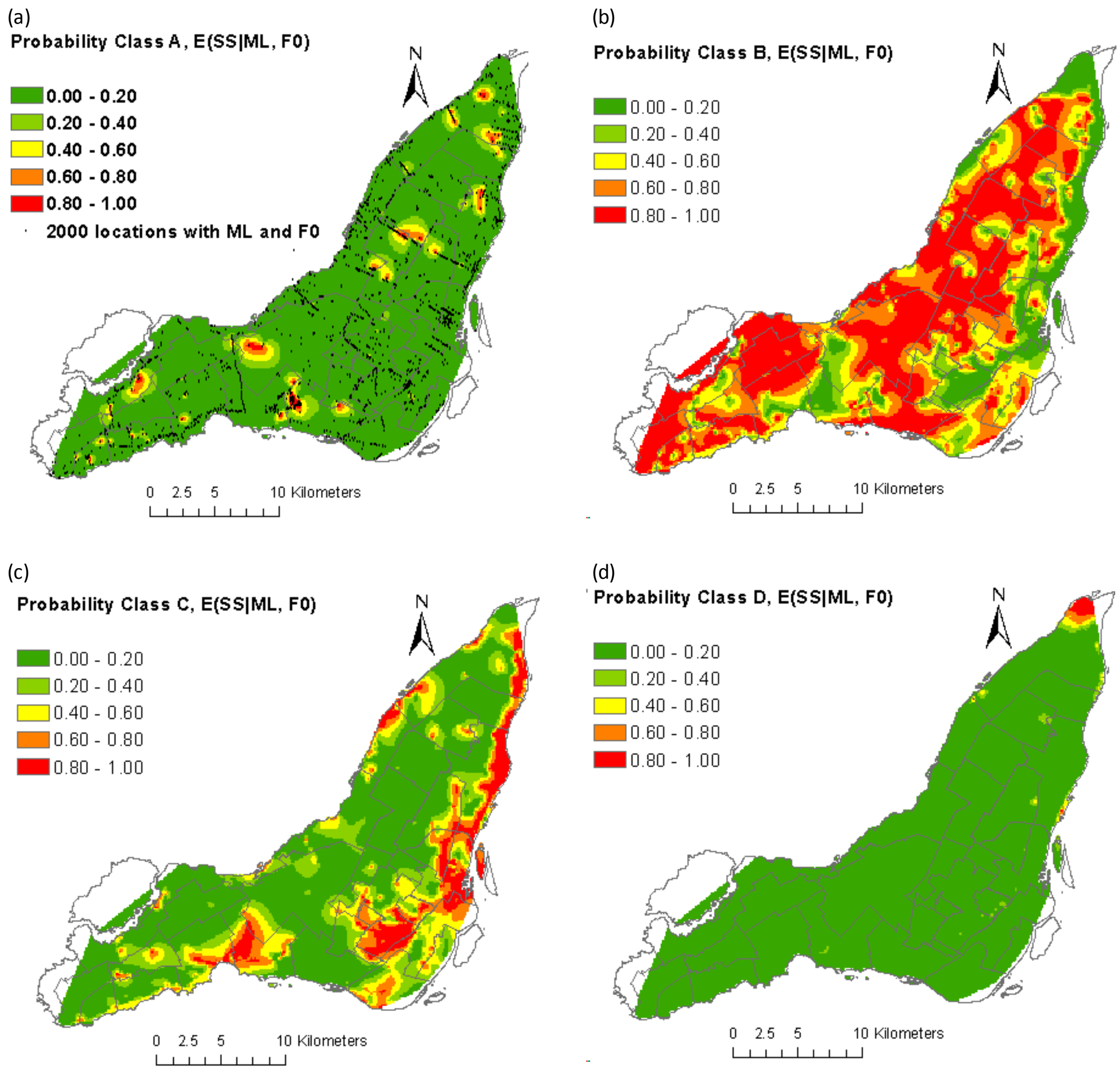

Figure 3.14: The maps for the probability of soil site classes: A, B, C and D using the proposed updating procedure at sites where both site fundamental frequency and detailed borehole data are available.

3.8 Site Class Probability Maps proposed for the island of Montreal

The final map is compiled by combining the information from all these maps for a subset of data points consisting of 13000 boreholes to bedrock, 1600 sites with F_0, and 400 boreholes with detailed borehole data on ML information as well as data derived from seismic surveys (Figure 3.15). Analysis of V_{s30} data following the methodology of Thompson et al. (2007) indicates that the spatial correlation distance for Montreal is most significant below 300 m. Consequently, a distance of 300 m is used to define the spatial resolution of the map. First, V_{s30} data derived from seismic surveys is assigned to the map (~ 26 sites). Next, estimates of V_{s30} at sites derived by considering simultaneously detailed borehole, and fundamental frequency were added to the map. Sites that are closer than 300 m from sites where seismic surveys were performed are not considered since they have higher residual bias and variance compared to the latter. Next, sites where V_{s30} is derived from fundamental frequency measurements are considered. As in the previous case, sites that are located within 300 m of sites previously incorporated on the map are ignored since they have higher residual bias and variance. Next, sites where V_{s30} is derived from detailed borehole data are considered. Again, the same rule is used and only sites that are not within 300 m of one of the previous sites included in the map are considered. Finally, sites where V_{s30} is derived solely on the basis of depth to bedrock are considered and included in the map if no other site has been previously entered within 300 m of a site.

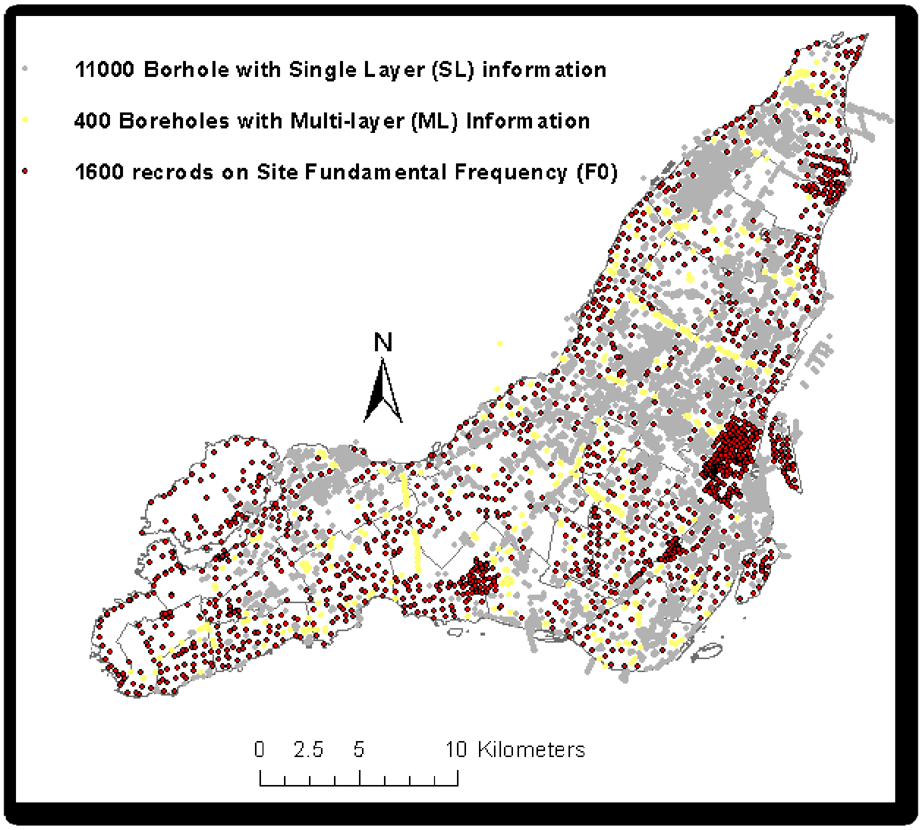

Figure 3.15: Map of the island of Montreal showing the sites where single Layer, multi-Layer and F_0 information is used for the combined microzonation map.

The combined data on V_{s30} is used to derive the site class probabilities -- P(A), P(B), P(C) and P(D), and shown in Figure 3.16. In addition to these classes, the probability of site class E, P(E) is shown in Figure 3.17. For all these maps, interpolation between sites is performed with the Natural Neighborhood Method (Hunter et al., 2010).

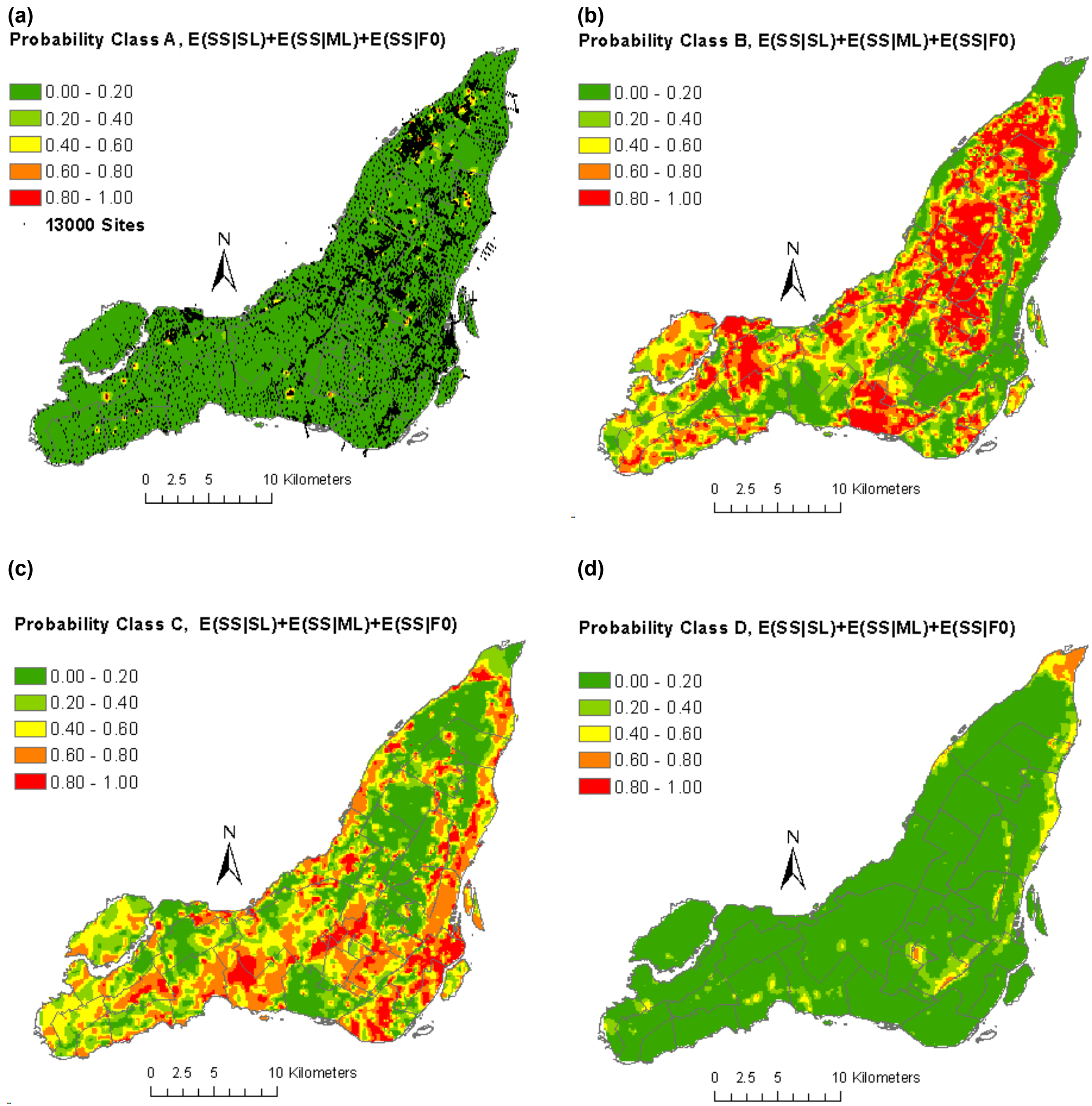

Figure 3.16: Microzonation maps derived from the combined model for site classes A, B, C and D.

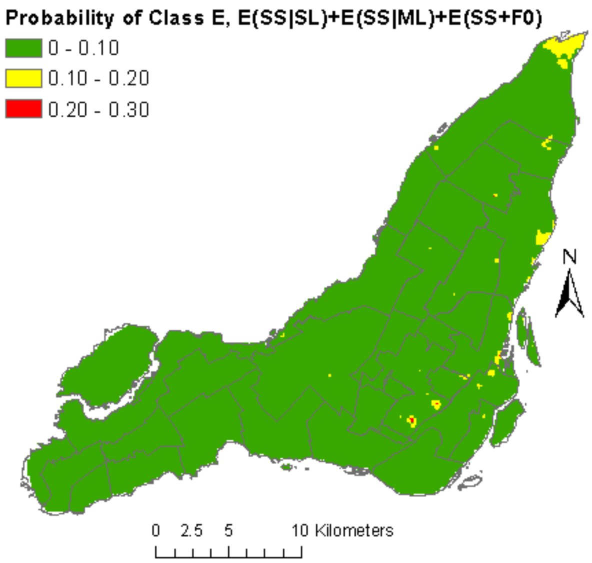

Figure 3.17: Microzonation maps of the combined model for site class E.

3.9 Maps on F_a and F_v based Microzonation

In the previous section, a procedure was described to estimate the probability of soil site classification A, B, C, D and E suggested in the 2010 NBCC. The 2010 NBCC uses this classification to assign foundation factors (F_a and F_v) to ground motion parameters at long (T=1.0 s) and short structural periods (T=0.20 s) respectively. Table 3.8 summarizes the specific values of the coefficients of F_a and F_v applicable to Montreal.

Table 3.8 Short period (F_a) and long period (F_v) seismic design coefficients for Montreal (NBCC 2010).

Seismic Site Classes	F_a for $S_a = 0.64$ g at $T = 0.2$ s	F_v for $S_a = 0.14$ g at $T = 1.0$ s
A	0.76	0.50
B	0.86	0.60
C	1.0	1.0
D	1.14	1.36
E	1.23	2.06

The probabilities of site classification are used to obtain estimates of the expected site factors and their standard deviation as below.

3.16 $$E[F_a] = P(A)F_a^A + P(B)F_a^B + P(C)F_a^C + P(D)F_a^D + P(E)F_a^E$$

3.17 $$E[F_v] = P(A)F_v^A + P(B)F_v^B + P(C)F_v^C + P(D)F_v^D + P(E)F_v^E$$

3.18 $$\sigma[F_a] = \sqrt{(F_a^A - E[F_a])^2 P(A) + (F_a^B - E[F_a])^2 P(B) + (F_a^C - E[F_a])^2 P(C) + (F_a^D - E[F_a])^2 P(D) + (F_a^E - E[F_a])^2 P(E)}$$

3.19 $$\sigma[F_v] = \sqrt{(F_v^A - E[F_v])^2 P(A) + (F_v^B - E[F_v])^2 P(B) + (F_v^C - E[F_v])^2 P(C) + (F_v^D - E[F_v])^2 P(D) + (F_v^E - E[F_v])^2 P(E)}$$

Figure 3.18 shows the expected values and coefficients of variation for F_a and F_v. For short period structures, zones in red show areas where amplifications are expected and zones in yellow and green where deamplifications are expected. In general, zones where the amplifications have the largest uncertainty are illustrated by the higher coefficients of variation associated with these zones. The foundation factors for long period structures show a much greater level of spatial variation and a higher level of uncertainty as well.

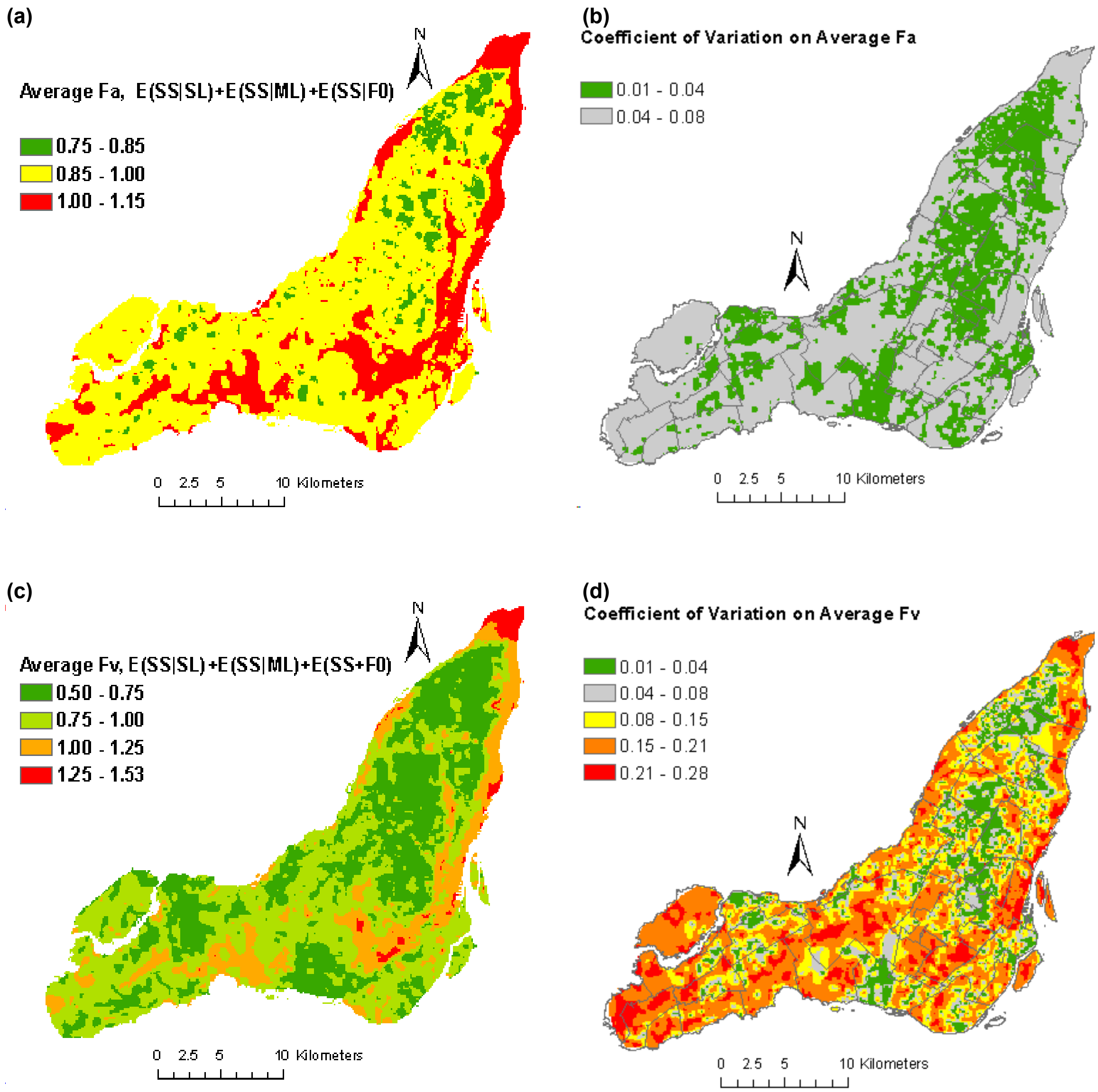

Figure 3.18: Maps of Montreal showing the seismic design coefficients for short (F_a) and long (F_v) structural periods. (a) Average F_a, (b) Coefficient of variation of F_a, (c) average F_v, (d) Coefficient of variation of F_v.

3.10 Qualitative Evaluation of Microzonation Maps

The proposed probabilistic site classification is compared qualitatively to the surface geology map of Montreal (Figure 3.1) for evaluation purposes (Ansal et al., 2009; Kilic et al., 2006). Figure 3.1 shows that the vast majority of the central part of the Island of Montreal is covered with stiff soil, till or hard rock. Clays is found mainly along the south, south-east and eastern borders of the island of Montreal. In the south-west of the island, there are also sand deposits at the surface, stretching from the edge of the Island to deep inside the island. Surficial sand deposits exist along the northern shoreline as well as at northern tip of the island. The proposed final microzonation map presented in Figures 3.16 and 3.17 show that, there is 60 to 100% of probability of occurrence of site class A (Figure 3.16a) at places in Montreal where surface soil is hard rock. The contour map of probability of class B site shown in Figure 3.16(b) corresponds to areas where glacial tills are present. Sites where the surficial soil deposits are clays or sands have 60 to100 % probabilities of being identified as site class C (Figure 3.16c). Finally, the deepest and softest deposits on the eastern shore of the island as well as at the northern and south western tips of the island have 60 to 80% probabilities of being identified as class D (Figure 3.16d) and 10 to 20% probabilities of being identified as class E (Figure 3.17).

3.11 Discussion and Conclusions

A comparison of the surface geology map (Figure 1) and the final microzonation (Figures 16 and 17) indicates that zones identified as class A sites with high probability show a good correspondence with locations identified as hard rock but is spatially limited to fewer locations. Locations with high probability of site class B show the highest correspondence with locations identified as either soft-rock (V_s = 700 m/s) or glacial till. Locations with high probability of soil class C show the highest correspondence with locations identified as either clay or sand along the edges of the island, a plateau in the central area of the island, and locations corresponding to ancient rivers, lakes and marshes. The softest and deepest soil deposits are located on the lowest lying areas of the island with a high probability of type D soil classification.

The procedure that is presented provides a framework for sequentially updating seismic microzonation maps as more data is obtained as a function of time. In this process, information from various sources can be considered and integrated to obtain the most precise map possible. The application of the procedure requires that V_{s30} data can be derived at a number of sites using alternate sources of data. In this application, V_{s30} estimates were derived at a number of sites using seismic data, surface geology information, depth to bedrock, detailed borehole profiles, and site fundamental frequency. The conditional second moment analysis is used for updating initial estimates of V_{s30} at a site when multiple sources of information are available. The conditional second moment estimator reduces the bias inherent in each estimation procedure as well as the variance of estimates. Updated estimates from each source are then combined sequentially to form a single map starting from the most precise sources of estimates for V_{s30}. The map provides site information on the expected value and variance of V_{s30}. A microzonation based on the probability of site classification is developed as an alternative to a single characterization per site. The latter is finally used to develop a microzonation map for the expected value and standard deviation of foundation factors F_a and F_v (Figure 3.18).

The maps for probabilistic seismic site classification and the foundation factors proposed in this study can be used by emergency management agencies in Montreal to better understand and communicate the level of uncertainty associated with the microzonation and its impact on risks. These microzonation maps can be used to target regions where the information of the maps may be further improved and to provide designers and emergency management personnel with a means of propagating uncertainty on foundation factors in performance based design. Areas with high uncertainty and high potential risks due to the built environment, this information can be used to target these regions for more detailed and precise surveys, perhaps with seismic measurements. The latter are expensive to perform and this procedure offers a rational procedure for identifying regions require this higher level of accuracy.

4 Seismic Site Amplification Factors from Site Response Analysis for Typical Soil Profiles in Montreal

Abstract

The site amplification factors of F(0.2 s), F(0.50 s) and F(1.0 s) in the NBCC (2015) are dependent on soil site classes A, B, C, D and E. These factors were derived from a combination of field data on ground motions recorded during earthquakes and equivalent linear and nonlinear site response analyses and are meant to be representative of a wide variety of soil profiles and ground motions across Canada. For sites located in Eastern North America, very few strong ground motion records are available in order to determine empirically the aforementioned site factors as a function of the mean shear wave velocity of the top 30 m soil, V_{s30}. Recently, the NGA-East project compiled data and performed equivalent linear dynamic analyses of one-dimensional soil columns in order to update these factors. Using a similar approach, database for soil profiles at 12 sites in Montreal are analyzed with the equivalent linear 1-D ground response method for natural and synthetic rock input motions scaled to 0.1 to 0.5 g. Since in the island of Montreal, bedrock depths are generally shallower than 30 m, this study investigates the influence of bedrock shear wave velocities on the site factors. Analyses indicate that bedrock is highly variable in Montreal. In order to better characterize the variability in bedrock, data on the shear wave velocities of bedrock are correlated to the Rock Quality Designation (RQD) (which ranges between 1 and 5). To account for bedrock variability, the site factors are computed for RQDs of 1, 3 and 5. The results are used to propose new relations for site amplification factors as a function of V_{s30} and the fundamental site period. The resulting site factors are compared to those of NBCC 2015. The amplification factor of peak ground acceleration on rock F(0.01 s), which is commonly used as an input in models for liquefaction potential assessment, is also evaluated and compared to the amplification factors in literature. The results of the study indicate that the current 2015 NBCC site factors underestimate amplifications for the sites typical of Montreal. The results also indicate that there are large uncertainties associated with these parameters due to variability in soil profiles, soil properties and input seismic ground motions. Average and confidence intervals for the mean and for predictions of amplifications are calculated for each site class to quantify this uncertainty, and to determine the contributions from each source of uncertainty. Since design standards often standardize amplifications relative to site class C (V_{s30} = 360 - 760 m/s), mean amplification factors and confidence intervals are also calculated for

normalized values. The latter are calculated by accounting for the correlation between site amplifications for given ground motions. The confidence intervals on the mean value provide a measure of the uncertainty on design values while the prediction intervals provide information on the variability expected for each individual event.

4.1 Introduction

The region of Montreal has a significant urban seismic risk, estimated to be the 2nd largest in Canada (Lamontagne, 2009); however, very few strong motion events have been recorded, which would provide insight on site response and structural performance. One of the most significant recent event is the 1988 Saguenay earthquake (M 5.7) which had its epicenter in the Charlevoix seismic zone, approximately 350 km north of the city. Interestingly, some structural damage was observed at Montreal East city hall, which is located on a deep soft clay deposit that greatly amplified the ground motions (Mitchell et al., 1990). Multiple similar soft soil zones are found in the downtown area and along the south east shore of the island (Rosset and Chouinard, 2009) which have the potential for severe damage in the event of a major earthquake in the vicinity of Montreal. A concern is that site effects that are currently used in design codes may not reflect the amplification to be expected for site conditions and ground motions that are typical to eastern Canada as well as the uncertainty associated with these factors. Given the lack of historical data, an approach based on simulation of ground motions is favored to investigate site effects.

The equivalent linear 1-D ground response analysis method is often used to estimate site effects and provides the site specific acceleration response spectrum of a single degree of freedom system for a given rock motion. Rosset and Chouinard (2009) present 1-D dynamic response analyses for typical soil profiles for rock motions scaled to 0.16 g using the equivalent linear model of SHAKE2000 and develop an empirical relation between amplification of rock motions and site periods. In this study, results from the most recent seismic surveys are used to characterize shear wave velocity profiles for soil classes B, C and D for a wider range of ground motions and to estimate site amplification factors from the 1-D ground response analysis using Strata (Kottke and Rathje, 2010). For this purpose, the site amplification factor for a given period is defined as the ratio of the spectral acceleration computed at the ground surface to the spectral acceleration at the rock interface. The site amplification factors of the 2015 NBCC are specified for NEHRP-defined site classes (A, B, C D and E) as a function of structural periods and are mainly derived from 1994 NEHRP specifications (Atkinson, 2008; Choi and Stewart, 2005).

The 1994 NEHRP site factors are based on the work of Borcherdt (1994), Seed et al. (1994) and Dobry et al. (1994). Borcherdt (1994) proposed empirical correlations for amplification factors (F_a for site periods between 0.1 and 0.5 s and F_v for site periods between 0.4 and 2.0 s) for soft soil sites in the San Francisco Bay area using strong motion data from the Loma Prieta earthquake for rock motions of 0.1 g. Dobry et al. (1994) proposed amplification factors derived from numerical 1-D simulations (with SHAKE) for 15 m to 30 m thick clay deposits (plasticity index of 50 and V_s in the range from 60 to 150 m/s) for a set of 20 strong ground motions (rock) motions from the 1989 Lomaprieta earthquake were scaled to 0.1 g. Bedrock with a shear wave velocity of 1200 m/s was assumed beneath the clay. For 4 out of the 20 ground motions used in the SHAKE runs, deamplifications were observed. Borcherdt (1994) notes that typical soils exhibit nonlinear behaviour at large shear strains which increase damping and reduce the shear modulus, which increase the fundamental period of the soil. It is also noted that nonlinearity increases impedance ratios since the shear modulus of layers in a nonlinear state is reduced relative to the shear modulus in the linear state, which can increase amplification ratios. However, effects due to higher damping at large strains dominate which reduces amplifications. Nonlinear effects are more significant for softer soil deposits and high frequency input ground motions. Consequently, nonlinearity effects are more important for F_a than F_v. Dobry et al. (1994) proposed F_v values of 3.3 for periods in the range of 0.4 s to 2 s, and F_a values of 1.7 for periods of 0.1 s to 0.5 s. Finn and Wightman (2003) discussed an empirical relation for F_a and F_v: $F_a = \left(V_{ref} / \overline{V}_{30}\right)^{m_a}$ and $F_v = \left(V_{ref} / \overline{V}_{30}\right)^{m_v}$, where V_{ref} =1050 m/s, is the mean shear wave velocity for the reference ground condition (class B soil), and $\overline{V}_{30}$ is the mean shear wave velocity to a depth of 30 m at the site. Values of exponents m_a and m_v were proposed for PGA ranging from 0.10 g to 0.4 g. Values of exponent m_a were 0.35, 0.25, 0.1, and -0.05 for PGA values of 0.1, 0.2, 0.3, and 0.4 g, respectively. Values of exponent m_v were 0.65, 0.60, 0.53, and 0.45 for PGA values of 0.1, 0.2, 0.3, and 0.4 g, respectively. It can be noted from Finn and Wightman (2003) that the expressions are for average amplifications and that the residuals have large standard deviations.

Hashash and Moon (2011) estimated amplification factors for class D sites (V_{s30} in the range of 275-314 m/s) of the Upland Mississippi embayment by performing 1-D dynamic ground response analyses using DEEPSOIL. Hashash and Moon first obtained artificial ground motions for hard rock (V_s=3000 m/s of class A sites). The hard rock motions were then converted to NEHRP ground motions at the site class boundary of B/C and matched the B/C boundary ground motions with the spectral ordinates of the UHS. The matched ground motions were used to perform the 1-D Equivalent linear site response analyses and to estimate F_a and F_v factors for class C and class D sites for ground motions of PGA from 0.1 g to 0.5 g.

Aboye et al. (2015, 2013) conducted 1-D site response analyses to derive site amplification factors for a single site with a 137 m thick soil profile near Charleston, South Carolina. These include amplification factors for peak ground accelerations on rock (F_{PGA}) at 0.01 s spectral period and F_a and F_v factors for class B, C, D and E sites for PGA levels from 0.03 g to 0.5 g. For the 1-D model for site response analyses, the V_s profile of the 137 m deep deposit rests on top of soft-rock half-space (V_s=700 m/s). The synthetic motions are applied at the surface of the soft-rock half-space. The authors use two different models of rock profiles to generate rock outcropping motions for South Carolina. The first rock model consisted of 700—1000 m of a thick outcropping soft-rock layer over hard rock of V_s=2500 m/s. The second rock model consists of 250 m of a weathered hard-rock half-space layer (V_s=2500 m/s) which is underlain by an unweathered hard-rock half-space with V_s=3500 m/s (Aboye et al. 2015). A total of 24 Synthetic soft rock input motions were generated for events with *M* of 7.2-7.4 and *R* of 6-36 km. The median F_a values are slightly higher than the NEHRP F_a values for both class C and D sites, while the median F_v values were less than the NEHRP values for Class C sites and significantly higher than the NEHRP values for Class D sites.

Shallow deposits (< 30 m) are more common in Montreal. Similar types of deposits are also common in Korea. Kim and Yoon (2006) investigate the dynamic response of soil profiles in Korea for shallow sites (< 30 m) and for rock motions of 0.11 g, 0.15 g and 0.22 g. The shallow profiles overlie bedrock with V_s values of 650-1750 m/s. Amplification factors were proposed as a function of V_{s30}, or site period. A site classification based on site periods was also proposed as follows: A T_0<0.1 s, B: 0.1 s<T_0<0.3 s, C: 0.3 s<T_0<0.5 s, and D: T_0> 0.5 s, which exhibits less variability than a classification based on V_{s30}. The authors noted that the site factors F_a and F_v as a function of V_{s30} are higher than NEHRP values.

Soft soil deposits in Montreal consist mainly of Leda clay, sand, silt and gravel and range in thickness from, 1 m to 33m. Leda clay is prevalent at most sites in the St-Lawrence River

Valley. Banab et al. (2013) perform 2D FEM dynamic response analyses for a site in Ottawa with a 81 m layer of soil. The soil profile comprises clay layer (81 m in thickness with constant V_s=210 m/s), a till layer (10 m in thickness with constant V_s=580 m/s) and hard bedrock (V_s= 2700 m/s). Ground motions recorded on rock were used as input motions and were scaled in relation to PGA from 0.02 g to 0.35 g. Amplifications were obtained as the ratio of the Fourier spectral value for the site to the Fourier spectral value for a reference site (at a rock station in Ottawa). Amplification is alternatively defined as the spectral ratio of the acceleration response of a SDOF at the surface to the acceleration response at bedrock. These latter amplifications provide a smoother representation of the site response than the Fourier spectra. Soil amplification factors from the Fourier spectrum of soil response at the fundamental frequency are also presented as a function of the soil/bedrock impedance contrast ratio and the PGA of the input rock motions. Soil amplifications are shown to increase with impedance contrast ratio for a given PGA_{rock}, and to decrease with increasing PGA_{rock} due to nonlinearity effects.

In Montreal, the shear wave velocity of bedrock is highly variable from 1000 m/s to 4000 m/s, whereas the V_s profiles of the soft soil deposits vary between 150 m/s and 450 m/s (Rosset et al. 2014). The high impedance contrast between surface deposits and bedrock can produce larger amplifications than those specified in the NBCC 2015 and NBCC 2010. For this reason, 1-D EL analyses are performed to determine if site factors rom the NBCC are appropriate for the site conditions and seismic setting in Montreal. Amplifications are also estimated as a function of site fundamental period as an alternative to V_{s30} for site classification.

In summary, the main objectives of this project are to compute the amplification factors at T=0.01, 0.2, 0.5 and 1 s for peak ground acceleration on rock as a function of V_{s30} (or fundamental period) and PGA for class C and D sites that are typical to Montreal. The factors from this study are then compared to factors proposed in NBCC 2015, and for other Eastern North American and Korean sites.

Multiple 1-D equivalent linear ground response analyses were performed to investigate the influence of ground motions, nonlinear dynamic soil properties, V_s profiles and impedance contrast on the site factors and their variability. The results of the analyses are summarized to evaluate the variability of site factors as a function of PGA for investigating three different cases: a) due to the uncertainty on both V_s profile and nonlinear dynamic soil properties for site classes C and D, b) due to the uncertainty only on V_s profile for site classes C and D, c) due to the uncertainty only on nonlinear dynamic soil properties for site classes C and D. A total of 216000 simulations are performed for each case using 5 PGA levels, 3 Rock Quality Designation, 2 values of V_s for each rock quality designation index, 12 site profiles, and 30 sets of randomized nonlinear dynamic soil properties, and 20 ground motions,

4.2 Methodology of Equivalent Linear 1-D Analysis

Equivalent Linear (EL) 1-D modeling of site response approximate the nonlinear cyclic response of soil through the use of a degradation curve for the shear modulus and a damping ratio curve (Cao et al., 1992; Darendeli, 2001; EPRI, 1993; Rasmussen, 2012; Seed and Idriss, 1970; Seed et al., 1986; Sun et al., 1988). Seismic ground motion propagating through soft soil deposits generates shear waves and Raleigh waves in the subsurface zones of the earth. In practice, shear wave propagation from the bedrock to the ground surface is approximated as one-dimensional (1-D) vertically propagating waves from the underlying rock formation.

The solution of the 1-D shear wave equation is performed in the frequency domain where the bedrock (input) motions are represented in the frequency domain with the Fast Fourier Transform (FFT). A transfer function is used to relate input bedrock motions to ground surface (output) motions. The transfer function is a function of soil thickness, shear wave velocity V_s, damping ratio and shear wave frequency. In the equivalent linear approach, the soil is treated as a linear viscous Kelvin-Voigt material. However, the behavior of the soil under cyclic (seismic) loading is nonlinear (Kramer, 1996). Nonlinear behavior of soil is accounted for by the use of strain-dependent stiffness and damping parameters. The stiffness of the soil is usually characterized by the maximum shear modulus G_{max} ($G_{max} = \rho V_s^2$, where, ρ=density of soil, V_s= velocity of shear wave) mobilized at low strain (less than 10^{-4} %) and a modulus reduction curve which shows how the shear modulus of soil decreases with increasing strain. The damping behavior of soil is represented by the damping ratio, which increases with increasing amplitude of cyclic strain. The cyclic shear stress and strains measured by laboratory tests (Seed and Idriss, 1970; Sun et al., 1988) are used to represent the shear modulus reduction curve and hysteretic damping. The secant shear modulus (G) normalized by the maximum shear modulus decreases with increasing cyclic shear strain of soil under cyclic loading (Seed and Idriss, 1970).

For layered soil deposits, the first step in the equivalent linear 1-D approach is to set initial estimates for the modulus and damping for each layer. Next, the transfer function between bedrock and each layer for all major frequencies of the rock motion are computed. Using the product of the Fourier spectra of the bedrock accelerograms and transfer function at various frequencies of the motions, an updated Fourier response spectra is computed for each layer. Next, using the inverse fast Fourier technique; acceleration, displacement and shear strain time histories are computed for each layer. After the shear strain time histories are obtained for a layer, an estimate of an effective shear strain (65% of peak strain) is determined for the layer. Next, for each layer, the modulus reduction and damping curves are then used to obtain the updated values of shear modulus (G) and damping ratio compatible with the current effective strain. Subsequent iterations continue with the updated values until convergence is achieved for the strain levels between two consecutive runs (Kramer, 1996).

In this study, it is assumed that the soil layer at each site is underlain by elastic rock. The 1-D EL method is extensively used in the literature (Aboye et al., 2015; Chouinard and Rosset, 2007; Chouinard et al., 2004; Papaspiliou et al., 2012b; Rosset and Chouinard, 2009) for estimating site fundamental frequencies in the microzonation of seismic hazard. The prediction of site fundamental frequencies reported by Chouinard and Rosset (2007) and Rosset and Chouinard (2009) compared well with field measurements of site fundamental frequencies. The 1-D Equivalent linear analysis in the frequency domain is used in this study to carry out parametric studies on the effect of ground motion characteristics, dynamic soil properties and impedance contrast ratio for typical soil profiles.

4.3 Selection of Rock Motions for Equivalent Linear 1-D Dynamic Analysis

The region of Montreal is located near the Western Quebec and St. Lawrence Valley seismic zones (Boyer, 1985). Several procedures are available for selecting records that are appropriate for a given location by comparing the spectrum of the event to the target design spectrum. Bommer and Acevedo (2004) selected ground motions records by calculating the average root-mean square deviations between the spectrums,

$$D_{RMS} = \frac{1}{n}\sqrt{\sum_{i=1}^{n}\left(\frac{SA_0(T_i)}{PGA_0} - \frac{SA_s(T_i)}{PGA_s}\right)^2} \quad (4.1)$$

where n is the number of periods at which the spectral shape is specified, $SA_0(T_i)$ is the spectral acceleration from the record at period T_i, $SA_s(T_i)$ is the target spectral acceleration at the same period; PGA_0 and PGA_s are the peak ground acceleration of the record and the zero-period anchor point of the target spectrum, respectively. The smaller the value of D_{RMS} is, the closer the match is between the spectrum of the record and the target spectrum. Bommer and Acevedo (2004) suggest that four parameters should be considered when selecting ground motions from the ground motion record database. These are in order of precedence: 1) earthquake magnitude, 2) source-site distance, 3) site classification for the recording station, and 4) rupture mechanisms. The authors investigated the influence of increases in magnitude from 5.5 to 7 and distance from 5 km to 50 km on spectral shapes. They observed that the spectral shape is less sensitive to distance than to magnitude. The authors propose that in making selections of real records, the search window should be as narrow as possible in terms of magnitude, and it can be widened by extending the range of distances for capturing the required number of real records. Bommer and Acevedo (2004) show that when spectral ordinates are normalized relative to the spectral ordinate at a period of 0.2 s for rock motions, the spectral amplification ratio do not change significantly with increasing distances. The authors recommend that if there are insufficient real records providing a reasonable match to the design scenario in terms of magnitude and distance in the site class, records can be considered from sites that are within one site class (NEHRP or EC8) either side of the classification of the site under consideration. If the site of interest is characterized as hard rock, it is preferable to exclude the soft soil recordings. The authors note that there are no significant differences between the ground motions from normal and strike-slip faulting earthquakes but the ground motions from reverse faulting can have larger amplitudes.

Finally, it is recommended that at least 7 records should be selected and used to obtain the average response from the site response analysis. It is also noted from Bommer and Acevedo (2004) that it is preferable to use a large number of real records without making adjustments to their spectral shape for fitting them to a target spectrum.

Rathje et al. (2010) note that there are no standard procedures for selecting acceleration-time histories to fit a target response spectrum. The authors propose a procedure that selects and scales the acceleration-time histories to minimize the root-mean-square error (RMSE) in log space between the target spectra and the median response spectra of the scaled suite of motions. The procedure includes a scaling method that not only minimizes RMSE but also minimize the standard deviation of the suite of input motions by using scaling factors. The RMSE represents the average percent difference between the target spectrum and the median spectra of the scaled input ground motions. The authors selected three sets of input motions with 5, 10 and 20 ground motions, respectively. The selected motions came from earthquake magnitudes between 6.2 and 6.9, and distances between 5 and 40 km. The authors note that the 20-motions suite provide better fit to the target spectrum across the periods considered than the 5-motions suite because of the difficultly in controlling the standard deviation with only five motions. When the number of motions in the suite is increased from 5 to 20, the RMSE is reduced from 0.06 to 0.03 for average fit within 5–10% off the target spectrum.

Bommer and Acevedo (2004) review the literature on scaling of ground motions, and note that the scaling factor is normally less than 4, and exceptionally up to 6. Scaling of the PGA of input-acceleration time histories may be avoided by selecting ground motion records which can fit directly to a target spectrum. Hines et al. (2011) select a set of 14 ground motion records for rock site conditions for the seismic response analysis of deposits in the Boston area. The ground motions were selected from the set of 293 ground motions of the U.S. Nuclear Regulatory Commission for ENA. The records were selected if the PGA of one of the orthogonal horizontal components was between 0.075 and 0.30 g (for a target PGA of 0.149 g) with earthquake magnitude between 5 and 7.5, with source-site distance R in the range of 19 to 104 km and a frequency content similar to that of the UHS. The selected motions fell mostly within 0.5 to 2 times the UHS spectral ordinates at most spectral periods.

Nastev et al. (2008) selected two different sets of accelerograms recorded for seismic site response analysis for Quebec City with PGA from 0.10 to 0.20 g. One set consisted of 10 real accelerograms, whereas the other set contained 10 synthetic accelerograms. In order to achieve a wide variation of PGA levels of the input motions, the target spectrum was scaled to 0.01, 0.05, 0.10, 0.20, 0.30, 0.40, 0.50, 0.75 and 1.0 g. The time histories of the two sets of accelerograms were also scaled at the same rate to closely match the design spectrum for Quebec City sites in class B over a wide range of periods from 0.01 to 1.0 s.

The deaggregation of seismic hazards (PGA) for a probability of exceedance of 2% in 50 years for Montreal indicates that the events that contribute the most are those with a moment magnitude of M=6 with epicentral distances in the range of 10 and 30 km, and moment magnitudes of M=7 with epicentral distances in the range of 15 to 100 km (Halchuk et al., 2007). Atkinson (2009) developed synthetic accelerograms (www.seismotoolbox.ca) for Montreal for NEHRP class A (V_{s30} > 1500 m/s, hard rock site). The synthetic records are available for a range of earthquake magnitudes and distances that contribute the most to the seismic hazards at the 2 % in 50 years level: M6 at 10 to 15 km (M6 set 1), and 20-30 km (M6 set 2), M7 at 15 to 25 km (M7 set 1), and 50 to 100 km (M7 set 2).

Aboye et al. (2015) performed a comprehensive study of site effects for Charleston (SC). They obtained estimates of magnitudes and source-site distances from the USGS Interactive Deaggregation application for Charleston. The events that dominated the seismic hazard for Charleston have moment magnitude M of 7.2-7.4 and epicentral distances R of 6-36 km. A total of 24 synthetic acceleration time histories for the NEHRP B-C boundary condition (V_{s30} of 760 m/s) representing 12 different sites and 2 different levels of exceedance probabilities (10% and 2% in 50 years) of the seismic hazard were selected. The range of PGA_{B-C} corresponding to 10% probability of exceedance in 50 years were of 0.11-0.18 g and 0.40-0.77 g for 2% probability of exceedance in 50 years. In order to compare the calculated site factors with those of NEHRP, the records were scaled to 0.05, 0.1, 0.2, 0.3, 0.4, and 0.5 g to compute site effects as a function of $PGA_{B,C}$. For analyses involving the V_s profiles extending to hard rock, 24 synthetic records for hard rock condition were selected

4.4 Selection of ground motion records for Montreal

In this study, a set of 15 natural rock input motions (Figure 4.1) is selected from the databases of the Pacific Earthquake Engineering Research Center (PEER), the Engineering Strong-Motion database (Luzi et al., 2016) from the European Project NERA, and the Center for Engineering Strong Motion (https://www.strongmotioncenter.org/) and 5 synthetic ground motions (Figure 4.2) from Atkinson (2009) that provide a good fit to short periods of the UHS, which are important for amplification at sites of shallow deposits. The ground motion search method employed at PEER database (http://ngawest2.berkeley.edu/site) is based on Equation 4.1. The characteristics of the selected 20 ground motions are presented in Table 4.1.

As it can be seen in Table 4.1, the natural ground motions that are selected cover a range of predominant periods from 0.1 to 1.5 s. The suite of ground motions has a high energy content at smaller periods (Figures 4.1 and 4.2) which is characteristic for ENA and important for the shallow sites with fundamental frequency between 3 and 20 Hz which are prevalent in Montreal.

The ground motions are selected to match the 2% in 50 years spectrum for Montreal for moment magnitudes between 4.5 and 7.5 and epicentral distances from 10 to 170 km on strike-slip and normal faults recorded at class B and A sites (Figures 4.1 and 4.2). The accelerograms are selected to ensure an approximate match to the UHS PGA of 0.25 g, and an overall match with the shape of the UHS for periods in the range from 0.1 s to 2 s.

Table 4.1: Characteristics of ground input motions used for the equivalent 1-D analysis for soils in Montreal.

Input Motion	Year	Earthquake Mechannism	Site Class	PGA (g)	Moment Magnitude	Epicentral Distance (km)
Kocaeli-Turkey1999-M7.51-R11 km	1999	Strike-slip	B	0.260	7.51	11
Lipari-Italy2010-M4.7-R12 km	2010	Strike-slip	B	0.320	4.7	12
Tottori-Japan2000-M6.61-R-15 km	2000	Strike-slip	B	0.130	6.61	15
Morgan Hil-Gilroy-M6.19-R15 km	1984	Strike-slip	A	0.100	6.19	15
Basilicata-Italy1998-M5.6-R18 km	1998	Normal Faulting	B	0.160	5.6	18
Southern Iran1990-M6.2-R18 km	1990	Strike-slip	B	0.160	6.2	18
Greece	1990	Normal Faulting	B	0.120	5.9	19
Synthetic19-Atkinson (2009)-M6-R27 km	N/A	Strike-slip	A	0.330	6	27
Irpinia-Italy1980-M6.9-R28 km	1980	Normal Faulting	B	0.080	6.9	28
Saguenay (Chicoutimi-North)	1988	Strike-slip	A	0.130	5.7	30
Synthetic9-Atkinson (2009)-M7-R45 km	N/A	Strike-slip	A	0.280	7	45
Synthetic14-Atkinson (2009)-M7-R51 km	N/A	Strike-slip	A	0.210	7	51
Presbytere, Martinique 2007-M7.4-R69 km	2007	Normal Faulting	B	0.160	7.4	69
Saguenay (St-Andrea)	1988	Strike-slip	A	0.160	5.7	70
Synthetic27-Atkinson (2009)-M7-R70 km	N/A	Strike-slip	A	0.120	7	70
Western Iran1990-M7.4-R85 km	1990	Strike-slip	B	0.130	7.4	85
La Malbaie, Saguenay	1988	Strike-slip	A	0.170	5.7	95
Synthetic44-Atkinson (2009)-M7-R99 km	N/A	Strike-slip	A	0.133	7	99
Guadeloupe 2007-M7.4-R144 km	2007	Normal Faulting	B	0.080	7.4	144
Goudeloupe, France	2007	Strike-slip	B	0.110	7.4	167

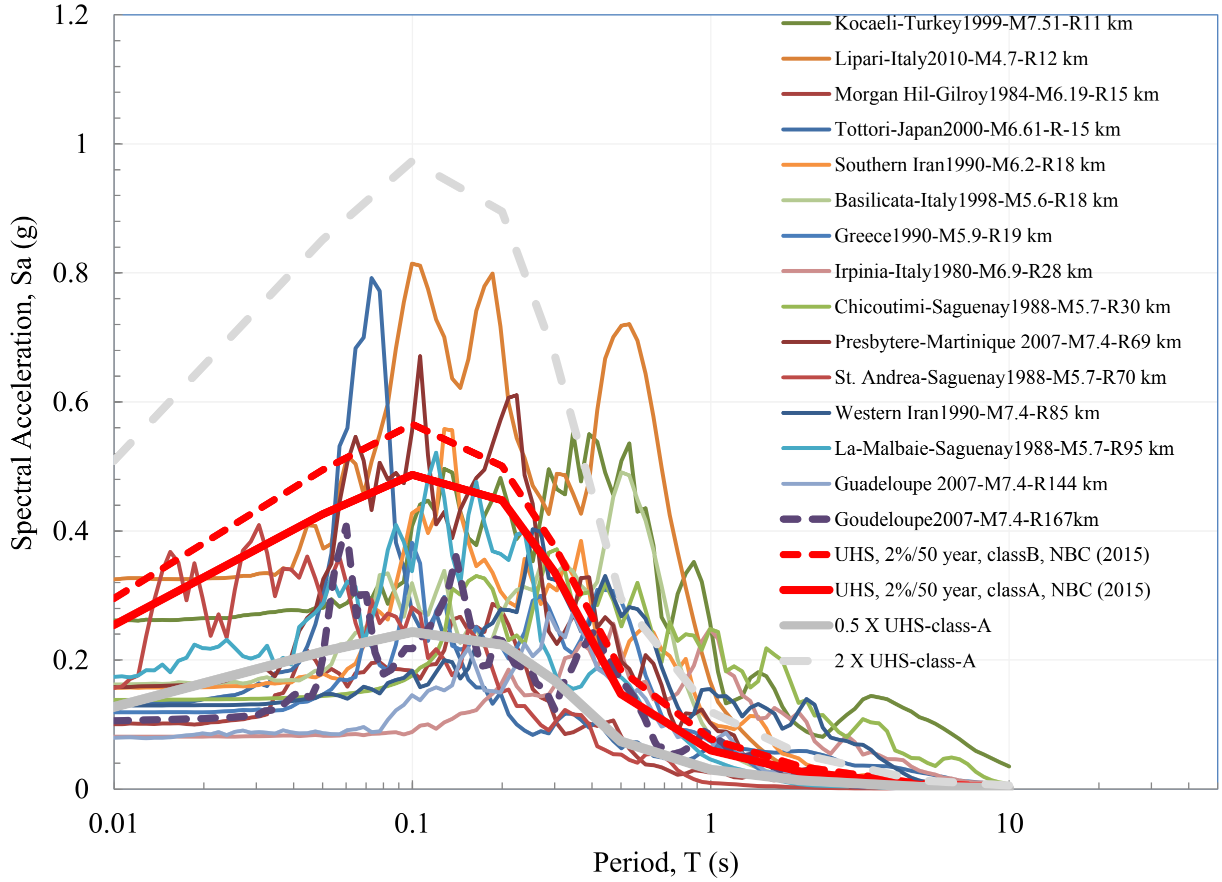

Figure 4.1: Response spectra (damping ratio of 5%) of natural accelerograms recorded on rock (Class B, NBC 2015) and hard rock sites (class A, NBCC 2015.

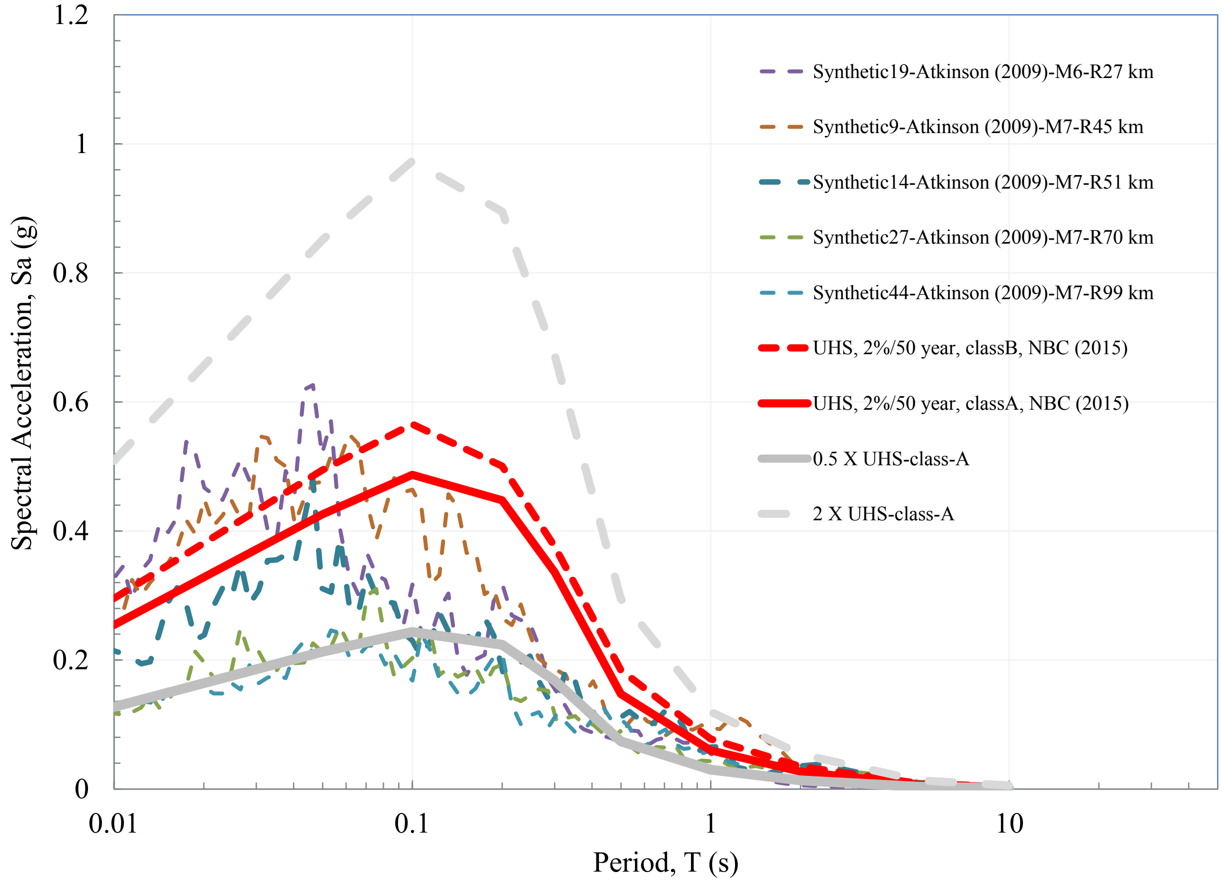

Figure 4.2: Response spectra (damping ratio of 5%) of synthetic (simulated) accelerograms for site class A -- hard rock condition (Atkinson, 2009).

In this study, the site factors are computed relative to ground motions on rock obtained at class A and B sites. In contrast, the 2015 NBCC site factors are provided in reference to ground motions for sites with V_{s30} of 760 m/s corresponding to the boundary between soil classes C and B.

4.5 Randomization of V_s profiles obtained from Seismic Surveys

The analysis of site factors requires that all sources of uncertainties are considered in the analysis. Among these, the variability in soil profiles for each soil class is an important element. In this study, the variability in soil profiles is considered by randomizing V_s profiles as input to the 1-D ground response analysis (Aboye et al., 2015; Kamai et al., 2014; Rathje et al., 2010). Aboye et al. (2015) used the 1-D equivalent linear approach to evaluate the ground response of Charleston area in South Carolina. They presented 28 V_s profiles (Aboye et al., 2015) with depths of 137 m for accounting for the variations of V_s profiles in the Charleston area, and they considered the profiles to be in the range of likely variations in the Charleston area. Their study included 12 V_s profiles corresponding to class E, 13 profiles corresponding to class D, and 3 profiles corresponding to class C. It can be noted from Aboye et al., the reference V_s profiles used for the 1-D EL analyses are the same for all three site class E, site class D, and site class C.

Aboye et al. (2015) define a reference profile for the Charleston (SC) region which is defined as the median profile from 12 sites and V_s is assumed to follow a lognormal distribution. Variability is considered by defining parallel profiles defined for ±1, 2 and 3 standard deviations from the $\ln(V_s)$ reference profile and ignoring correlations as a function of depth for each soil class.

Silva et al. (1996) proposed a stochastic model for the variation of shear wave velocity with depth for the purpose of calculating amplification factors for generic soil sites. The model was calibrated by using data from 557 measured Vs profiles. The V_s values at a given depth are assumed to be lognormally distributed and correlations are developed for $\ln(V_s)$ as a function the relative depth of layers. The authors propose a model for the interlayer correlation coefficient as a function of depth (h) and layer thickness (t). The soil column is divided in layers and the shear wave velocity for the layer is normalized such that,

$$4.2 \qquad Z_i = \frac{\ln(V_i) - \ln\left(V_{median}(h_i)\right)}{\sigma_{\ln V}}$$

where, V_i is the shear-wave velocity of the i^{th} layer, $V_{median}(h_i)$ is the median shear-wave velocity at mid-depth of the layer, and $\sigma_{\ln V}$ is the standard deviation of $ln(V)$, and variable Z_i is the normalized quantity for a given soil class. The normalized values Z_i are correlated with the layer above (i-1) using the following first order auto-regressive relation:

$$4.3 \qquad Z_i = \rho \cdot Z_{i-1} \pm \varepsilon_i \cdot \sqrt{1-\rho^2} \qquad i > 1$$

where ε_i is a normal random variable with zero mean and unit standard deviation; and ρ is the interlayer correlation coefficient which is a function of depth h and thickness t of the layers.

$$4.4 \qquad \rho(h,t) = [1-\rho(h)]\rho_t(t) + \rho(h)$$

where $\rho(h)$ is a depth dependent interlayer correlation coefficient, and $\rho_t(t)$ is a thickness dependent correlation coefficient, which is higher at shallow depths.

$$4.5 \qquad \begin{aligned} \rho(h) &= \rho_{200}\left(\frac{h}{200}\right)^{b} && h \le 200 \text{ m} \\ \rho(h) &= \rho_{200} && h > 200 \text{ m} \end{aligned}$$

$$4.6 \qquad \rho_t(t) = \rho_0 \exp\left(\frac{-t}{\Delta}\right)$$

where ρ_{200} is the correlation coefficient at 200 m depth, ρ_0 is the correlation coefficient at the surface and Δ is a parameter for the correlation with depth. Silva et al. (1996) estimated these parameters for each soil class (Table 4.2).

Table 4.2: Parameters for Silva et al. (1996) model for V_s profile randomization.

Parameters	V_{s30}			
	(B) >760 m/s	(C) 360-750 m/s	(D) 180-360 m/s	(E) <180 m/s
$\sigma_{\ln Vs}$	0.36	0.27	0.31	0.37
ρ_{200}	0.42	1	0.98	0.5
ρ_0	0.95	0.97	0.99	0
Δ	3.4	3.8	3.9	5
b	0.063	0.293	0.344	0.744

Silva et al. (1996) define $median\ V_s\ (\pm\sigma_{\ln Vs})$ profiles for each soil category for sites in California. The correlation functions are considered to be valid for other locations and have been used by Hashash and Moon (2011), Kamai et al. (2014), Rathje et al. (2010) for randomizing soil profiles for the Eastern and Central United States

As noted by Rathje et al. (2010) a model with constant interlayer correlation corresponds to the case $b = \rho_0 = 0.0$. Since the V_s profiles for Montreal are shallower than 30 m, a constant interlayer correlation as a function of depth is selected setting two of the model parameters b, and ρ_0 equal to zero. The information required to develop randomized shear-wave velocity profiles is then reduced to the baseline shear-wave velocity profiles, the standard deviation of the natural log of the shear-wave velocity, and the interlayer correlation model parameter ρ_{200}, The software STRATA (http://nees.org/resources/strata) is used in this study to randomly generate soil profiles suing this methodology.

4.6 V_s profiles for Montreal

The surface geology of Montreal is an interlayered deposit with clay, silt and dense sand overlying till or rock and is the result of several alternating periods of glaciation followed by the emergence of the Champlain Sea and channeling by the St. Lawrence River and its tributaries (Prest and Hode-Keyser, 1977). In this study, equivalent linear 1-D analyses of ground response are performed for a set of 12 sites representative of soil classes C and D (Figures 4.3).

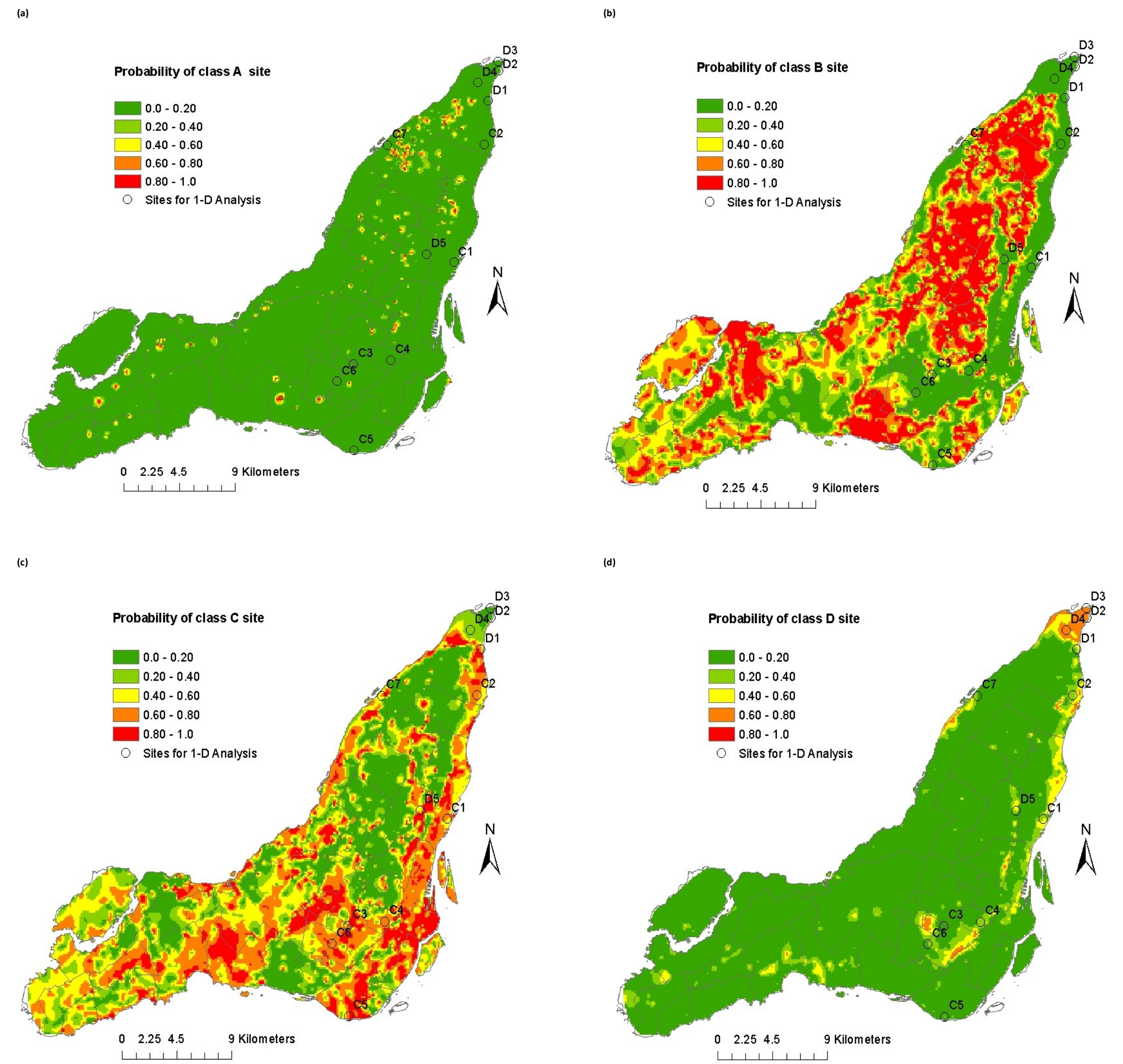

Figure 4.3: Locations of 12 representative sites are shown on the probabilistic microzonation map derived from the method proposed by Talukder and Chouinard (2016) for site classes: A, B, C and D.

The selected sites are representative of the variability in the stratigraphy and depth to bedrock for each site class (Figure 4.3). Figures 4.5 and 4.6 show the measured V_s profiles for the sites in soil classes D and C, respectively. A comparison of velocity profiles to the stratigraphy of each site (Figure 4.4) shows that V_s is more variable in surface layers (0 to 10 m) compared to deeper layers (10 to 35 m). This variation is attributed to the heterogeneity of soil deposits in the upper 10 m and more homogeneous deposits (mainly clay) below 10 m. Figures

4.5 and 4.6 show that the median Vs profiles for Montreal are significantly different of those of Silva et al. (1996) below 5 m depth.

Bedrock in Montreal consists mainly of Ordovician Limestone, Dolomite, Shale and Cambrian sandstone and can vary widely in quality (Prest and Hode-Keyser, 1977). Bauer (2007) notes that average V_s for shale and limestone are 967 and 2900 m/s, respectively. As a result, average bedrock shear wave velocities can vary between 967 m/s and 2900 m/s (Bauer, 2007).

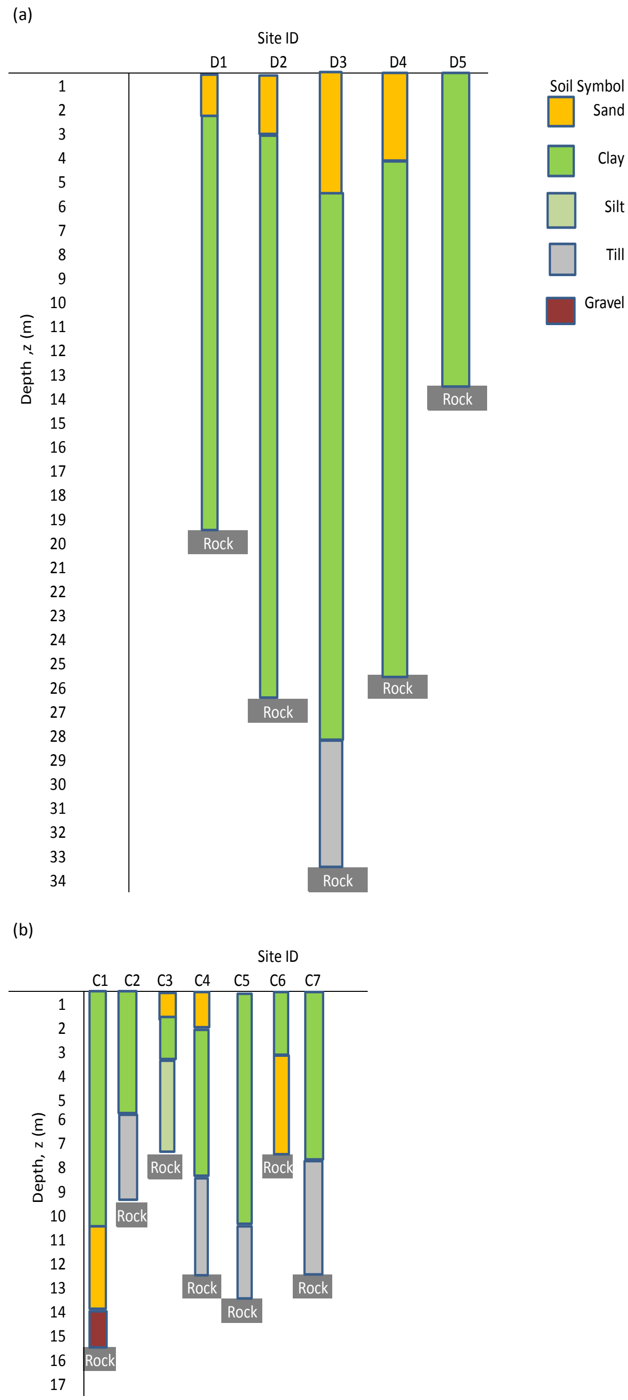

Figure 4.4: Borehole diagram for the selected (a) class D sites, and (b) class C sites.

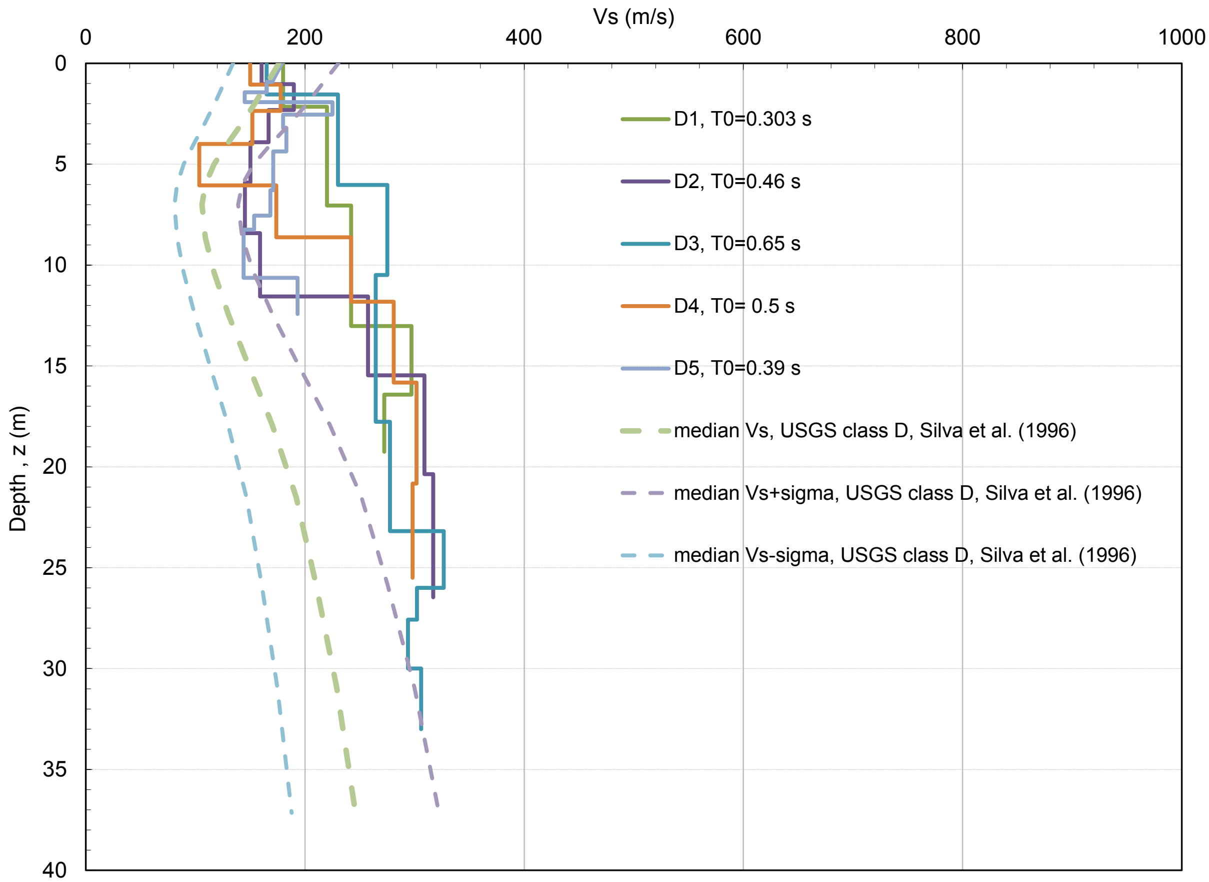

Figure 4.5: V_s profiles for selected class D sites in Montreal compared with the median V_s Profiles of Silva et al. (1996) with site periods between 0.303 s and 0.65 s estimated from ambient noise measurements.

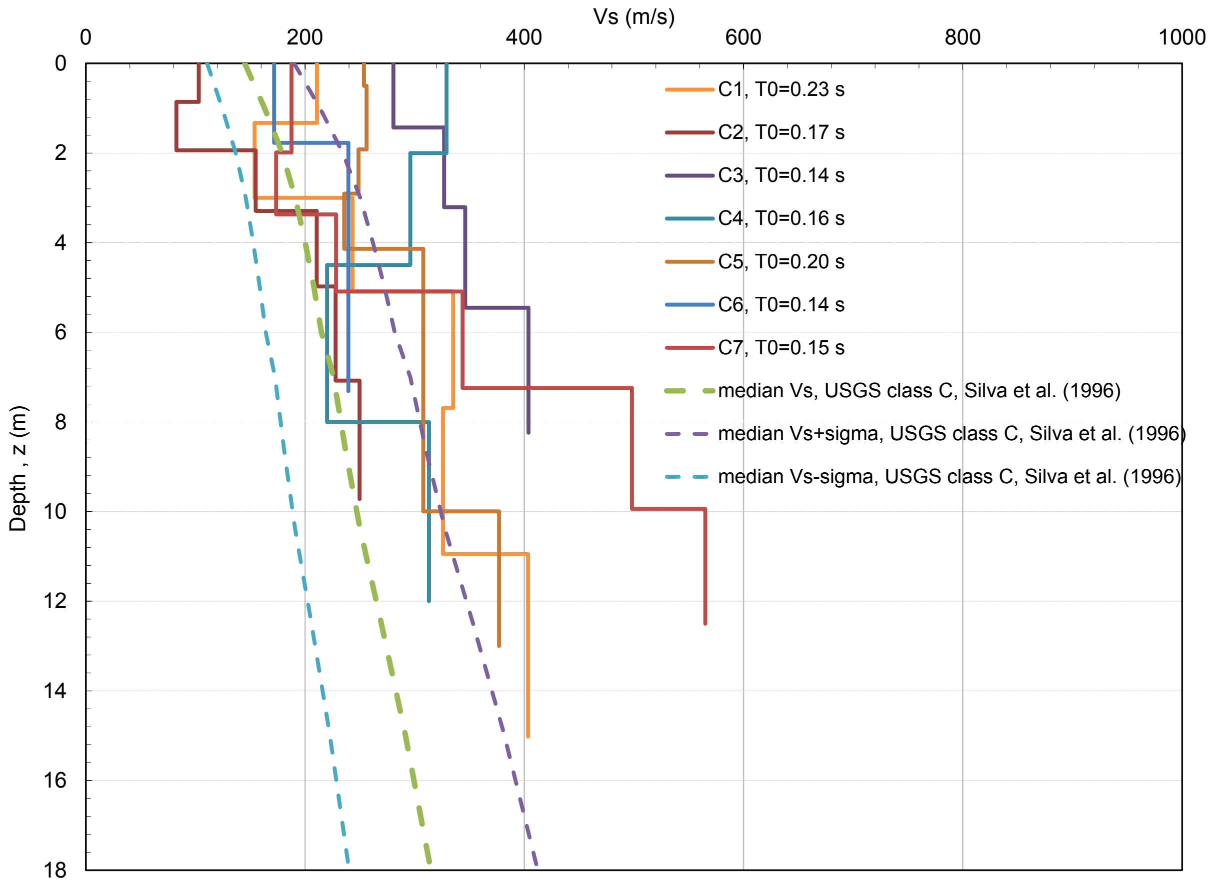

Figure 4.6: V_s profiles for selected class C sites in Montreal compared with the median V_s Profiles of Silva et al. (1996) with site periods between 0.14 s and 0.23 s estimated by the ambient measurements).

4.7 Literature on nonlinear dynamic properties

For the purpose of the equivalent site response analysis, the shear modulus reduction and damping ratio (%) curves must be specified for clay, sand, silt and till. The modulus reduction and damping curves for clay, sand, silt and till used in this study are shown in Figures 4.7 to 4.10. Table 4.3 lists the literature that is the source of the curves for nonlinear dynamic properties.

Table 4.3: Studies on soil dynamic properties for 1-D site response analyses.

Soil Type	**Shear Modulus reduction curve and Damping ratio curve**
Clay	Rasmussen (2012), Sun et al. (1988), EPRI (1993), Darendeli (2001)
Silt	Sun et al. (1988)
Sand	Seed and Idriss (1970), Darendeli (2001), EPRI (1993)
Till and Gravel	Seed et al. (1986), EPRI (1993)

Rasmussen (2012) performed strain controlled Direct Cyclic Simple Shear Tests (DCSS) for shear strains in the range of 0.1 % to 1% and resonant column tests (for shear strain of 0.001 to 0.1 %) on Leda clay samples from Ottawa to determine the shear modulus reduction and damping ratio at various shear strain amplitudes (Figure 4.7). The percentage of clay-sized (less than 0.002 mm) particles was between 56 and 84 % and had a PI of 37 %. The samples were retrieved from depths of 4 m to 16 m corresponding to in-situ effective vertical stresses in the range of 39 to 103 kPa. The strain amplitude in the conventional resonant column test was measured at the resonant frequency (33.5 Hz) and the DCSS tests were performed at a much lower frequency (1 Hz) keeping the specimens under 100 kPa effective confining pressure. Both the RC and DCSS test were performed for 10 cycles of shear stress. Additionally, strain-controlled DCSS tests were performed by Rasmussen at varying frequencies (0.1, 1, 5 and 10 Hz) and strain amplitudes (0.1-1 %) at the in situ overburden stress of each sample in order to determine the effect of these parameters on cyclic behavior.

Darendeli (2001) collected soil samples from different sites in Northern California, Southern California, South Carolina and Taiwan. The predominant types of soils were clay, clean sand (FC<12 %), sand with FC >12%, and silty sand. The recovered samples were from a depth range of 3 to 263 m. Resonant Column and Cyclic Torsional Shear tests were performed on the samples for a range of loading frequencies and number of cycles. The test results were used to derive normalized shear modulus reduction G/G_{max} and damping ratio (D %) curves. Results indicate that the normalized G/G max curves for clay are not very sensitive to the loading frequency and number of cycles and that soil physical properties (e.g. Plasticity Index and soil type) and mean effective confining pressure are more important.

For comparing the normalized shear modulus reduction and damping curves from Darendeli (2001) with the normalized shear modulus and damping ratio curves from Rasmussen (2012), the curve from Darendeli are selected based on N=10 cycles, a loading frequency of f=1 Hz, and an over consolidation ratio (OCR) of 1. For Montreal soils, an OCR value of 1 is assumed since soils are generally slightly overconsolidated. Figure 4.7 compares G/G_{max} reduction and damping ratios curves for clay soil available in the literature.

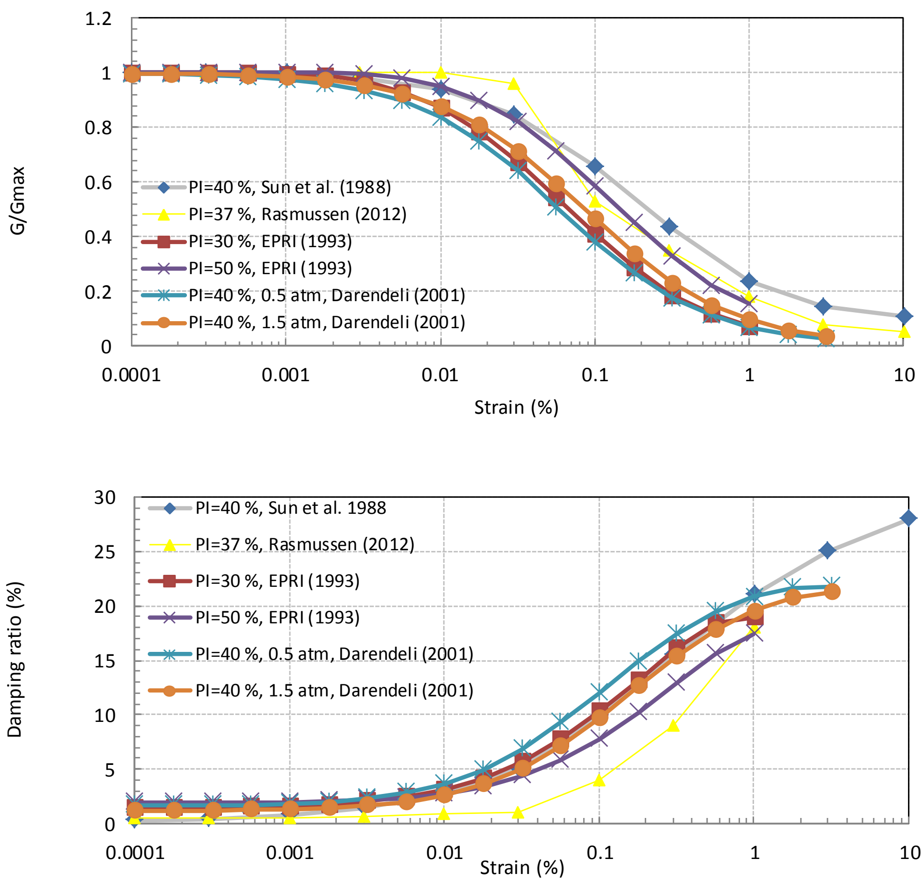

Figure 4.7: Curves showing variation of shear modulus degradation and damping ratio with strain in clay.

The mean plasticity index for clay and silt for Montreal sites is estimated at 38% with a standard deviation of 14 %, based on borehole data from 11 different sites. Since the plasticity index of Montreal clay is comparable with that of clay samples reported in Rasmussen (2012), the dynamic soil properties for clay are adopted from the test results of Rasmussen. Relations for shear modulus reduction and damping ratio with strain for silt that have been proposed by Sun et al. (1988) are used in this study (Figure 4.8). Sun et al. (1988) presented test data on the shear modulus and damping ratios for cohesive soils: clay, silty clay, and clayey silt. The plasticity index values of the cohesive soils were in the range of 40 to 80 %. However, the plasticity index for cohesive soils in Montreal can widely vary since it has an average value of 38% with a standard deviation of 14%. Sun et al. (1988) developed the relations for the shear modulus reduction and damping ratios as a function of shear strain (Figure 4.8) by using the test data on the plasticity index of the cohesive soils.

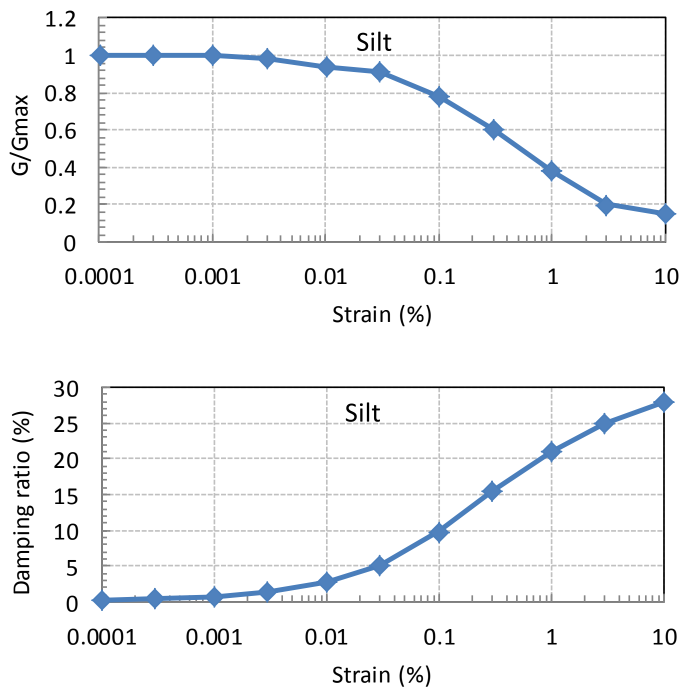

Figure 4.8: Curves showing variation of shear modulus and damping ratio with strain in silt (Sun et al. 1988).

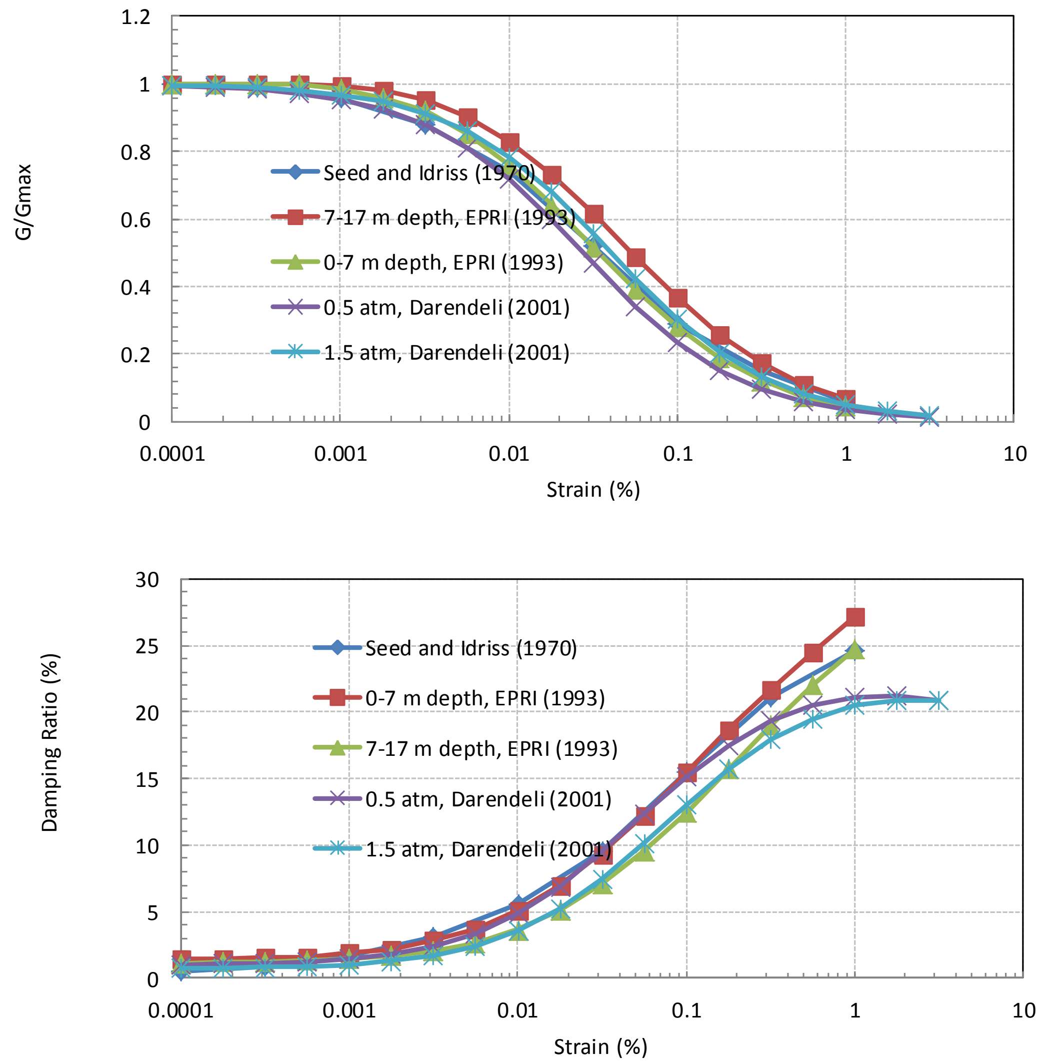

Figure 4.9: Curves showing variation of Shear modulus and damping ratio with strain in sand.

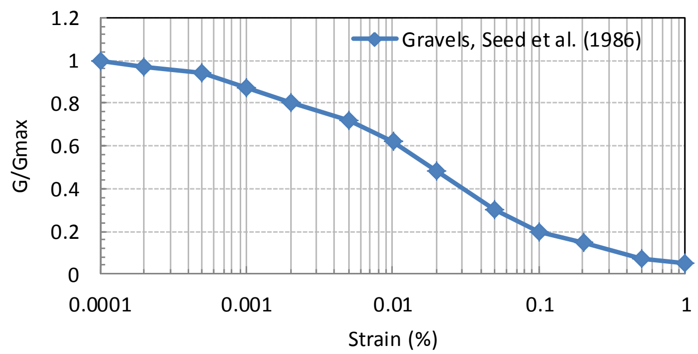

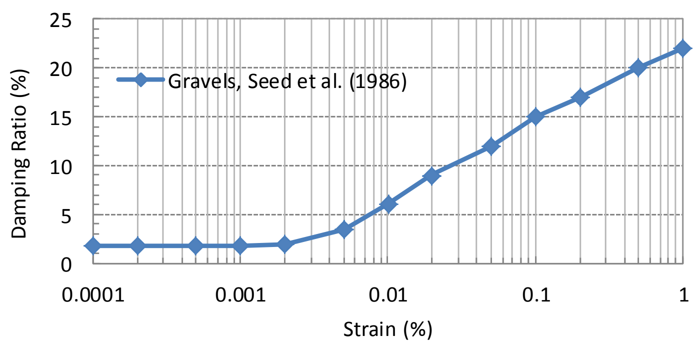

Figure 4.10: Shear Modulus reduction and damping ratio curves for Gravels (Seed et al., 1986).

Seed and Idriss (1970) propose relationships for the shear modulus reduction versus shear strain for sand samples of different relative densities (30 to 90%). The tests procedures included forced vibrations involving resonant frequencies of samples, cyclic triaxial compression, cyclic shear test, and cyclic torsional shear tests. Average curves are proposed corresponding to a relative density of 60% and suggest that the average normalized curves provide a reasonable estimate for many practical purposes. Relationships are also proposed for the damping ratio with shear strain as a function of effective vertical stresses in the range of 450 to 8500 psf. The authors noted that the average relationships, corresponding to an effective stress of 3000 psf provides sufficient accuracy for many practical purposes.

The Electric Power Research Institute (EPRI, 1993) conducted dynamic laboratory testing of undisturbed soil samples collected from 5 geotechnical sites (Treasure Island, Gilroy, Oakland Outer Harbor, San Francisco Airport, and Lotung in Taiwan). The samples were tested in the soil dynamics laboratory at University of Texas at Austin using the Laboratory Cyclic Triaxial with excitation frequencies in the range of 0.5 to 4 Hz and Resonance Cyclic Torsional Shearing (RCTS) equipment with excitation frequencies in the range of 20 to 100 Hz. The samples predominantly consisted of clay, silty sand, sand, and gravel collected from depths of 3 to 150 m under confining pressures between 0.3 and 8.7 atm. The sand and gravel samples were collected from the site of Gilroy-2 in California. The test samples were collected from Pleistocene Alluvium deposits encountered at depths of 10 to 20 m and 40 to 65 m which contain sands and gravels. Clay samples were taken from Pleistocene lake deposits while sand samples were collected from Pleistocene alluvium deposits. Results of laboratory tests indicated that the mean Seed and Idriss (Seed and Idriss, 1970) modulus and material damping ratio curves can fit the sand data very well. Figure 4.9 shows the resulting guideline relations for sand (EPRI, 1993); Park and Hashash (2005) used the EPRI guideline curves for sand at depths from 0.0 to10 m and from 10-20 m for their study of site effects for the Mississippi Embayment in the Eastern United States.

Seed et al. (1986) analyzed the dynamic properties of undrained gravelly soils using samples at depths from 150 ft to 255 ft from Caracas, Washington and South California. The specific gravity of the samples ranged from 2.65 to 2.95. The specimens were isotropically consolidated at a mean effective confining stress of 100 kPa before performing cyclic undrained tests. Each specimen was then subjected to small axial strains on the order of ±0.0003% over six cycles without drainage. For each loading cycle during the cyclic undrained triaxial tests, hysteretic stress-strain loops were determined. Shear modulus and damping characteristics of soils were then determined form the stress-strain relationships. The equivalent damping ratios at shear strains γ was determined from the area inside the hysteretic loop. Figure 4.10 shows the normalized shear modulus versus strain and damping ratios versus strain curves for gravelly soils at $D_r = 80\%$. These curves are used in this study for Tills in Montreal.

As presented in Figures 4.7-4.10, differences in G/G_{max} reduction and damping ratio curves for clay and sand are similar at small strain level (less than 10^{-4} %) regardless of depth. At intermediate levels of strain (from 10^{-3} to 10^{-1} % strain) and for large strain levels (greater than 10^{-1} %), differences in the curves for clay and sand become significant.

4.8 Randomization of G/G_{max} and damping ratios curves

Given the uncertainty associated with the specification of dynamic properties to each soil type, a randomization procedure is used to account for the latter in the site response analyses. In the case of the normalized modulus reduction curve, the uncertainty is maximum for the position of the curve in the middle range of values since the curve tends to asymptotic values at both extreme ends. Darendeli (2001) proposes values for the standard deviation on nonlinear properties (i.e. G/G_{max} and damping ratio) and assumes that they follow a normal distribution (Figure 4.11).

$$\sigma_{G/G_{\max}} = 0.015 + 0.16 \cdot \sqrt{0.25 - (G/G_{\max} - 0.5)^2}$$

4.7

$$\sigma_{D\%} = 0.0067 + 0.78 \cdot \sqrt{D(\%)}$$

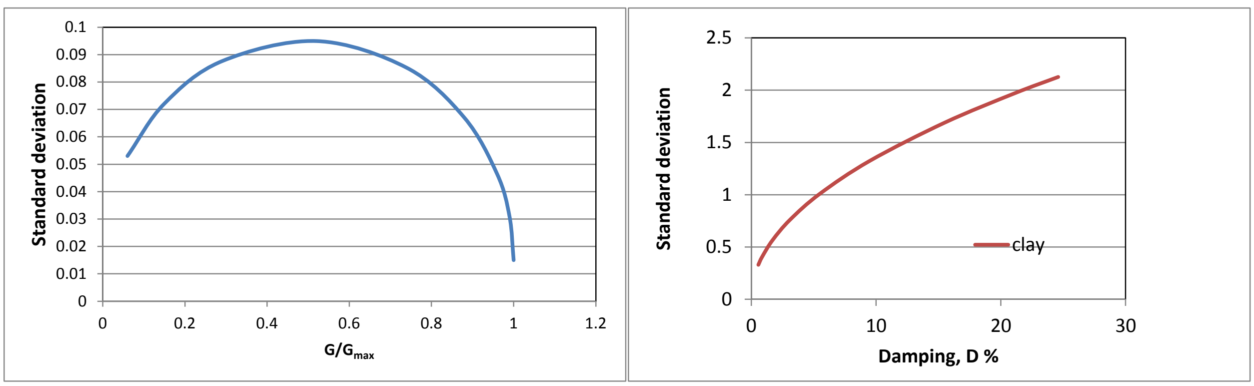

Figure 4.11: The standard deviation of nonlinear properties (G/G_{max} and Damping) predicted from Darendeli (2001) models.

As it can be seen in Figure 4.11, the model for the standard deviation of G/G_{max} results in small standard deviation when G/G_{max} is close to 1 or 0 and relatively large standard deviation when G/G_{max} is equal to 0.5. The standard deviation on damping ratio (D, %) increases with increasing damping ratios.

The nonlinear properties G/G_{max} and damping ratios are considered to be negatively correlated. To generate correlated G/G_{max} and D curves from baseline (mean) curves, the following expressions are used for each shear strain level:

$$\begin{bmatrix} G/G_{max}(\gamma) \\ D(\gamma) \end{bmatrix} = \begin{bmatrix} \sigma_{G/G_{max}} & 0 \\ \rho_{G/G_{max},D} & \sigma_{G/G_{max}}\sqrt{1-\left(\rho_{G/G_{max},D}\right)^2} \end{bmatrix} \begin{Bmatrix} \varepsilon_1 \\ \varepsilon_2 \end{Bmatrix} + \begin{Bmatrix} m_{G/G_{max}(\gamma)} \\ m_{D(\gamma)} \end{Bmatrix} \quad (4.8)$$

where ε_1 and ε_2 are uncorrelated random variables with zero. Using a correlation coefficient of $\rho_{G/G_{max},D} = -0.5$, the nonlinear properties of clay (Rasmussen, 2012) and the standard deviation model of Darendeli (2001), a set of 30 random G/G_{max} versus strain curves for clay are generated (Figure 4.12a), and compared to curves from literature. Similar random curves are obtained for sand (PI=0) sand, silt and gravel using the same methodology (Figures 4.12b, 4.12c, and 4.12d, respectively). Note that the correlation coefficient $\rho_{G/G_{max},D}$ is negative since the normalized shear modulus reduction curves decreases as the damping ratio (D %) increases with strain.

Figures 4.13a, 4.13b, 4.13c and 4.13d, illustrate the set of 30 randomized damping ratio curves for clay, sand, silt and gravel, respectively. It can be noted that because of the negative correlation between G/G_{max} and the Damping ratio, high shear modulus reduction are associated with low damping ratios. Darendeli (2001) updated the dynamic test results obtained by EPRI (1993) by adding to it the test results for sites in South Carolina. For this reason, the nonlinear dynamic property curves from Darendeli (2001) for sand are selected in this study for the 1-D site response analyses.

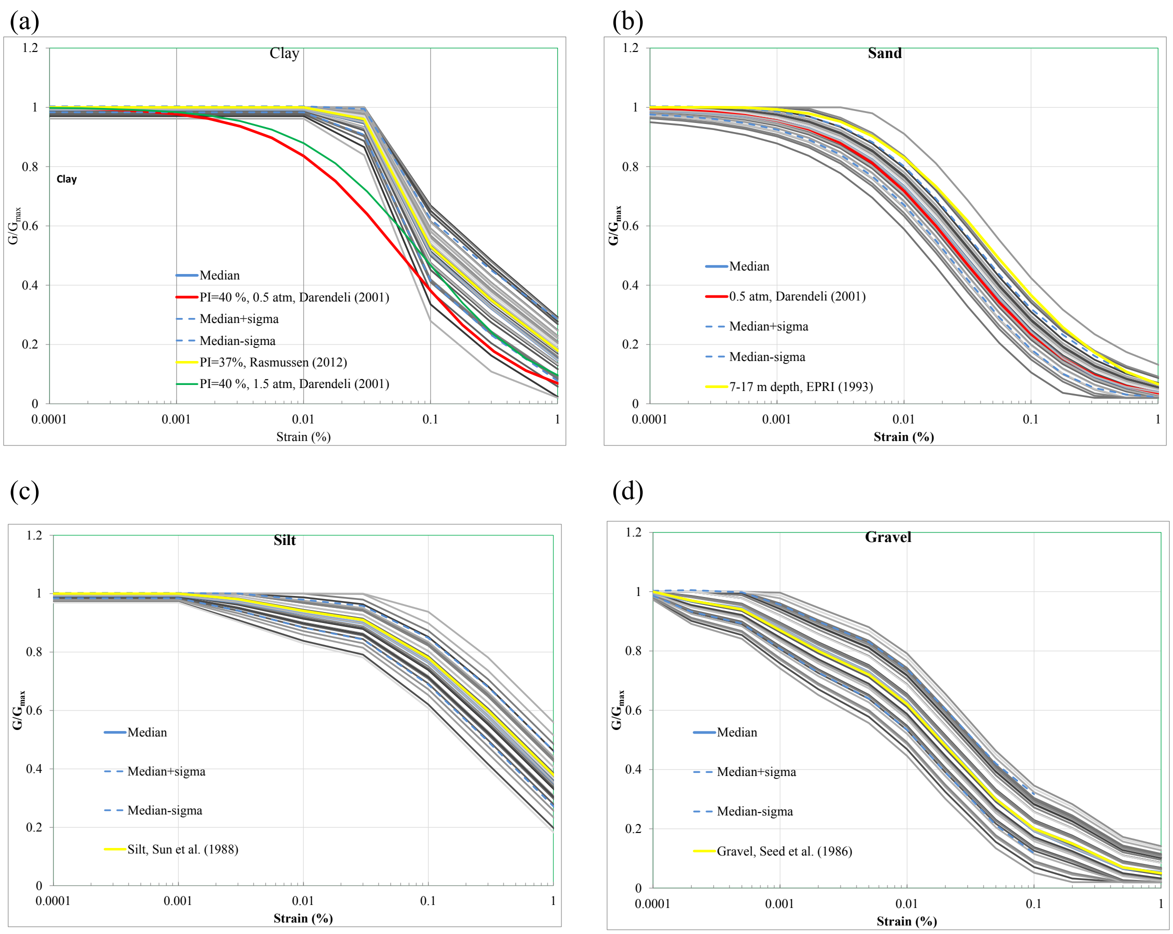

Figure 4.12: Thirty randomized G/G_{max} and Strain (%) curves for clay, sand, silt and gravel.

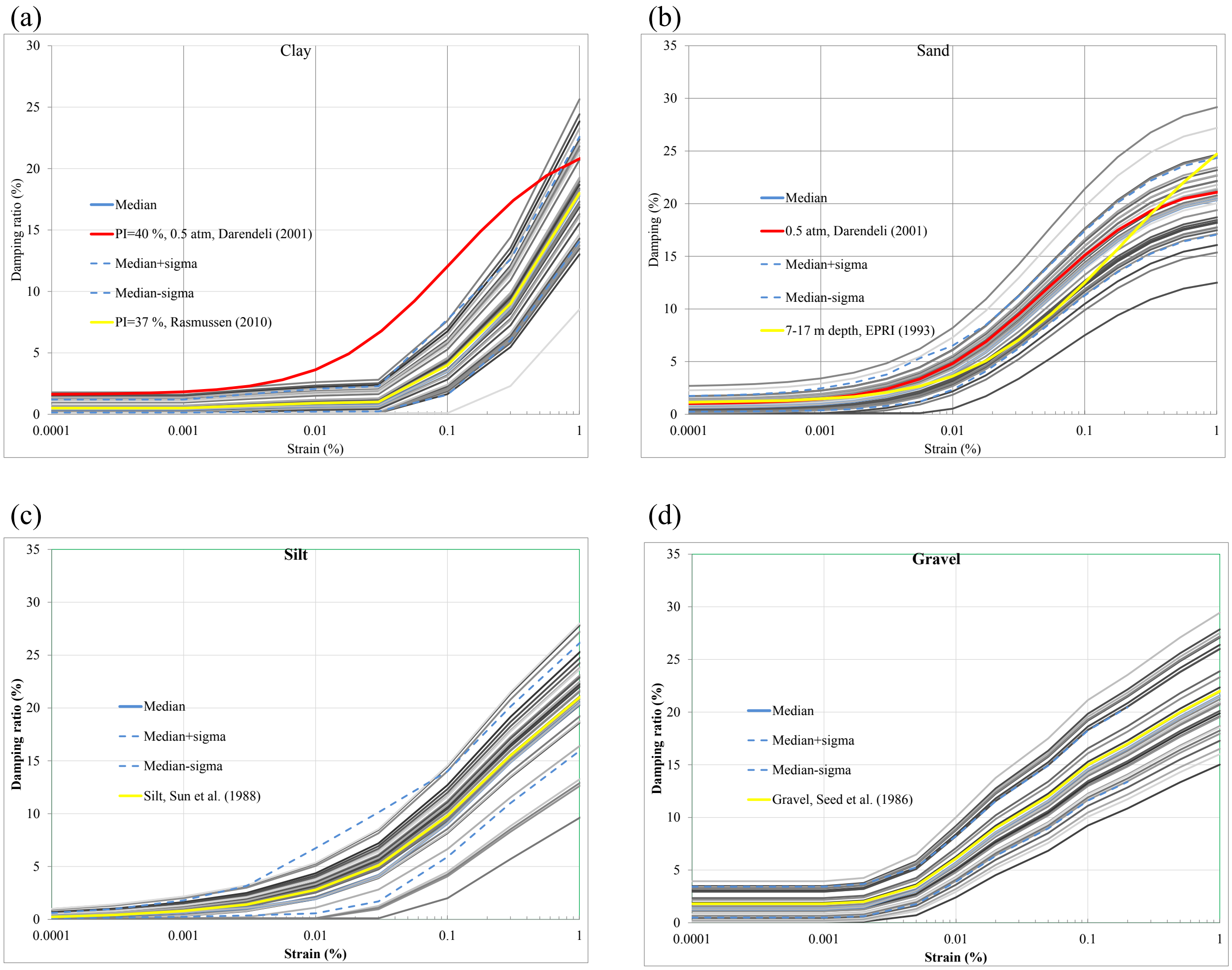

Figure 4.13: Thirty random Damping Ratio versus Strain (%) curves for clay, sand, silt and gravels.

4.9 Relationship between bedrock V_s versus Rock quality designation for Montreal

Shear wave velocity of bedrock in Montreal is highly dependent on RQD (Deere and Deere, 1988). Data on the shear wave velocity at various sites where the RQD was also available shows a strong correlation between the two measures (Figure 4.14). RQD is usually expressed as a quantity that varies between 0 and 100% and is calculated as the percentage of intact rock over a length of 2m. For our analysis purposes, the RQD is expressed on a scale from 1through 5 corresponding to categories of RQD in 20% increments.

$$Vs_{rock} = 816.12 + 422 \cdot F; \qquad \sigma = 322\, m/s \quad \mathrm{R}^2 = 0.72 \tag{4.9}$$

The information on RQD at a site can be used to greatly reduce the uncertainty on shear wave velocities. For example, previous studies when this information was not considered used a pooled estimate for the average velocity of 2300 m/s and its standard deviation of 590 m/s (Rosset et al. 2014). At sites where RQD is available, the standard deviation on the shear wave velocity is reduced to 322 m/s. This information is used to obtain more precise and unbiased estimates of site amplifications at these sites given the strong influence of the impedance ratio. Consequently, site amplification factors are obtained in the following sections for cases when there is for RQDs of 1, 3 and 5.

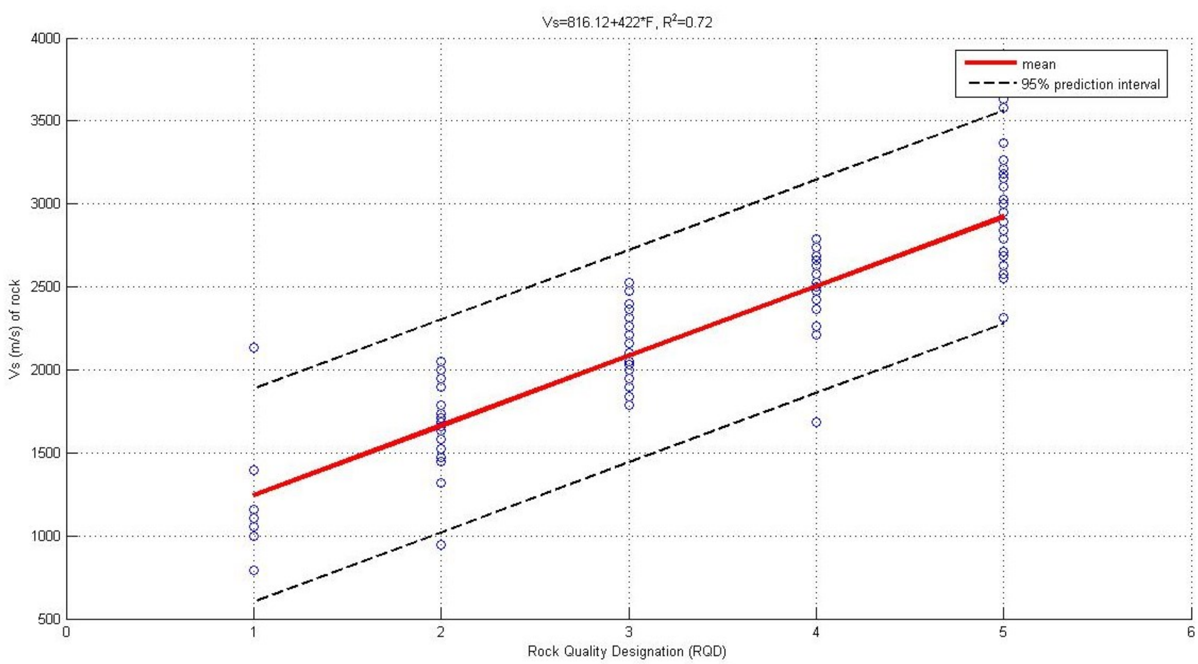

Figure 4.14: Variation of bedrock V_s (m/s) with rock quality designation (RQD)

4.10 Influence of uncertainty in V_s profiles on site amplification

Silva et al. (1996) analyzed the within-class variability of shear wave velocities for each soil class for sites in California and showed that $\sigma_{\ln Vs}$ can vary between 0.27 and 0.37 (Table 4.2). These values were obtained from a compilation of data from 787 sites in California, which may explain the large values for uncertainty assigned to each class. The analysis over a much smaller region, such as the island of Montreal, is expected to exhibit less variability within each soil class. The data compiled by Rosset et al. (2014) comprises data collected from seismic surveys at 30 sites that are with either predominantly Leda clay or sand.

Rathje et al. (2010) performed 1-D EL simulations to analyze the effect of profile variability on soil amplifications by performing parametric analyses where $\sigma_{\ln Vs}$ was varied between 0.10 and 0.40, and recommended a value of 0.20. In the following, the effect of $\sigma_{\ln Vs}$ on the amplification for sites in Montreal with soil thickness of 15 and 30 m is investigated by conducting the 1-D site response analyses with 4 different values of $\sigma_{\ln Vs}$ (0.1 , 0.2, 0.3 and 0.4). The range of 15 to 30 m in depth corresponds to the deepest and most critical deposits in Montreal for soil classes C and D, respectively. Figures 4.15 and 4.16 show the resulting random profiles for sites C1 and D3, respectively, with the methodology of Silva et al. (1996).

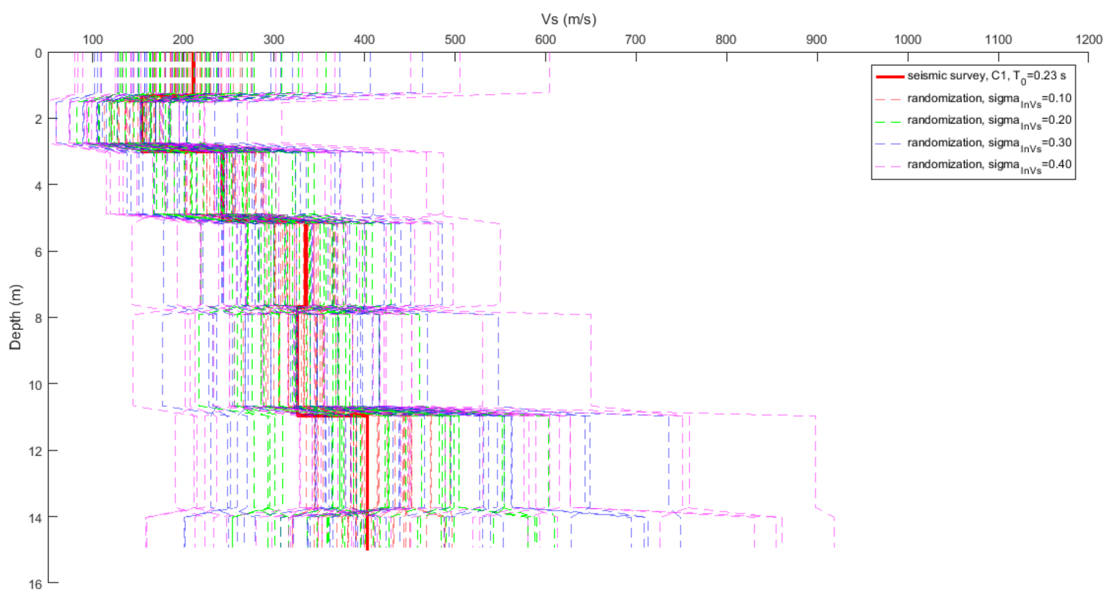

Figure 4.15: Random V_s profiles using profile C1 as baseline as a function of $\sigma_{\ln(Vs)}$.

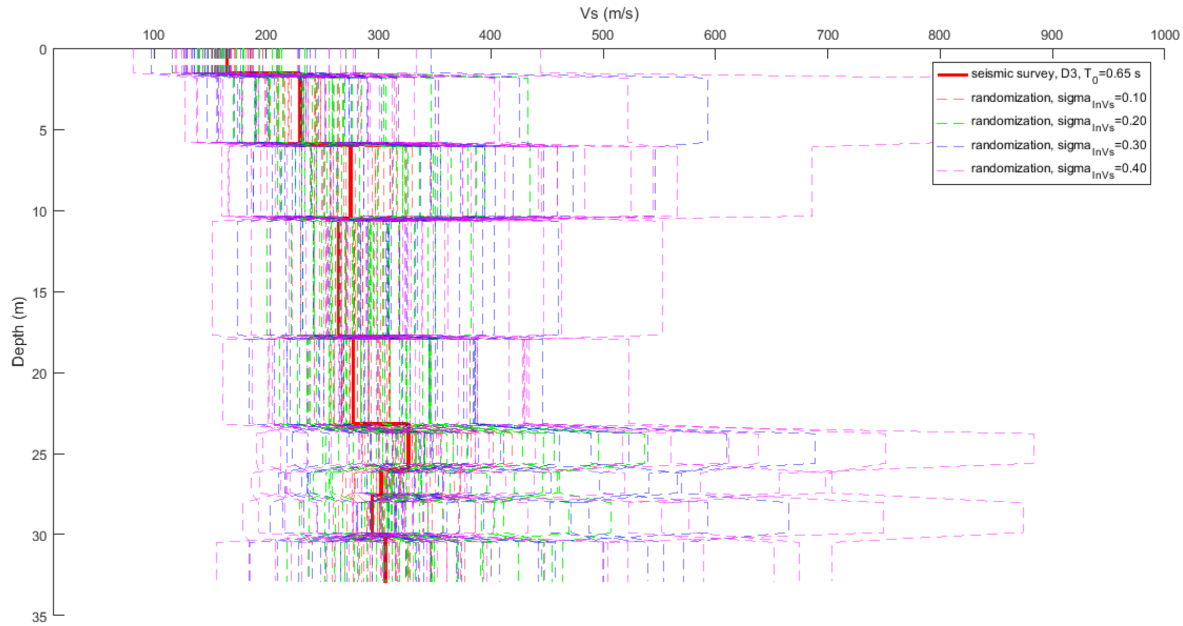

Figure 4.16: Random V_s profiles using profile D3 as baseline as a function of $\sigma_{\ln(Vs)}$.

Since larger amplifications are expected for larger impedance contrasts, the parametric investigation on $\sigma_{\ln Vs}$ is performed only for bedrock with a RQD of 5 for a set of 20 ground motions scaled to in the range of 0.1 to 0.5 g. Each Vs profile is associated with specific G/G_{max} and Damping ratio curves that are related to the stiffness of the soil layers. For example, the stiffest Vs profile is associated with the highest G/G_{max} curve and the lowest damping ratio curve.

Results for site C1 show the effect of $\sigma_{\ln Vs}$ on the mean amplification and on the standard deviation of the amplification as a function of the ground motion period (Figure 4.17). The mean amplification has a peak corresponding to the natural frequency of the randomized soil profiles which gets slightly wider for larger $\sigma_{\ln Vs}$. The mean amplification is also slightly reduced with increasing $\sigma_{\ln Vs}$ due to a decrease in the degree of impedance contrast. The effect of $\sigma_{\ln Vs}$ is also smaller with increasing amplitude of ground motions due to non-linear effects. The standard deviation for amplifications as a function of ground motion period is largest for periods near the natural period of the soil deposit. The effect of $\sigma_{\ln Vs}$ on the standard deviation of amplifications seems minimal suggesting that most of the variability is due mainly to either ground motions or non-linear soil properties. Finally, the standard deviations of amplifications decrease with the magnitude of the ground motions due to non-linear effects (Figures 4.17). Results for site D3 show similar tendencies (Figure 4.18). In Figure 4.17, the curves for mean AF versus T demonstrate the effect of $\sigma_{\ln Vs}$ on the mean amplification factor for site C1. In Figure 4.18, the curves for mean AF versus T demonstrate the effect of $\sigma_{\ln Vs}$ on the mean amplification factor for site D3.

As expected, the AF for site C1 are larger than those for D3 due to the larger velocity contrast at soil-rock interface. The effect of $\sigma_{\ln Vs}$ is to increase the variability in the AF; however, the average AF is reduced with an increase in $\sigma_{\ln Vs}$.

Table 4.4: Mean Amplification factors computed for the randomized V_s profiles.

Site ID	PGA	Vs profile	σ_{lnVs}	mean AF at T=0.01 s
C1	0.1			
		Randomized profiles	0.1	2.88
		Randomized profiles	0.2	2.77
		Randomized profiles	0.3	2.65
		Randomized profiles	0.4	2.53
	0.3			
		Randomized profiles	0.1	2.07
		Randomized profiles	0.2	1.98
		Randomized profiles	0.3	1.91
		Randomized profiles	0.4	1.85
	0.5			
		Randomized profiles	0.1	1.78
		Randomized profiles	0.2	1.74
		Randomized profiles	0.3	1.67
		Randomized profiles	0.4	1.61
D3	0.1			
		Randomized profiles	0.1	1.76
		Randomized profiles	0.2	1.75
		Randomized profiles	0.3	1.70
		Randomized profiles	0.4	1.65
	0.3			
		Randomized profiles	0.1	1.12
		Randomized profiles	0.2	1.10
		Randomized profiles	0.3	1.07
		Randomized profiles	0.4	1.04
	0.5			
		Randomized profiles	0.1	0.86
		Randomized profiles	0.2	0.89
		Randomized profiles	0.3	0.94
		Randomized profiles	0.4	0.94

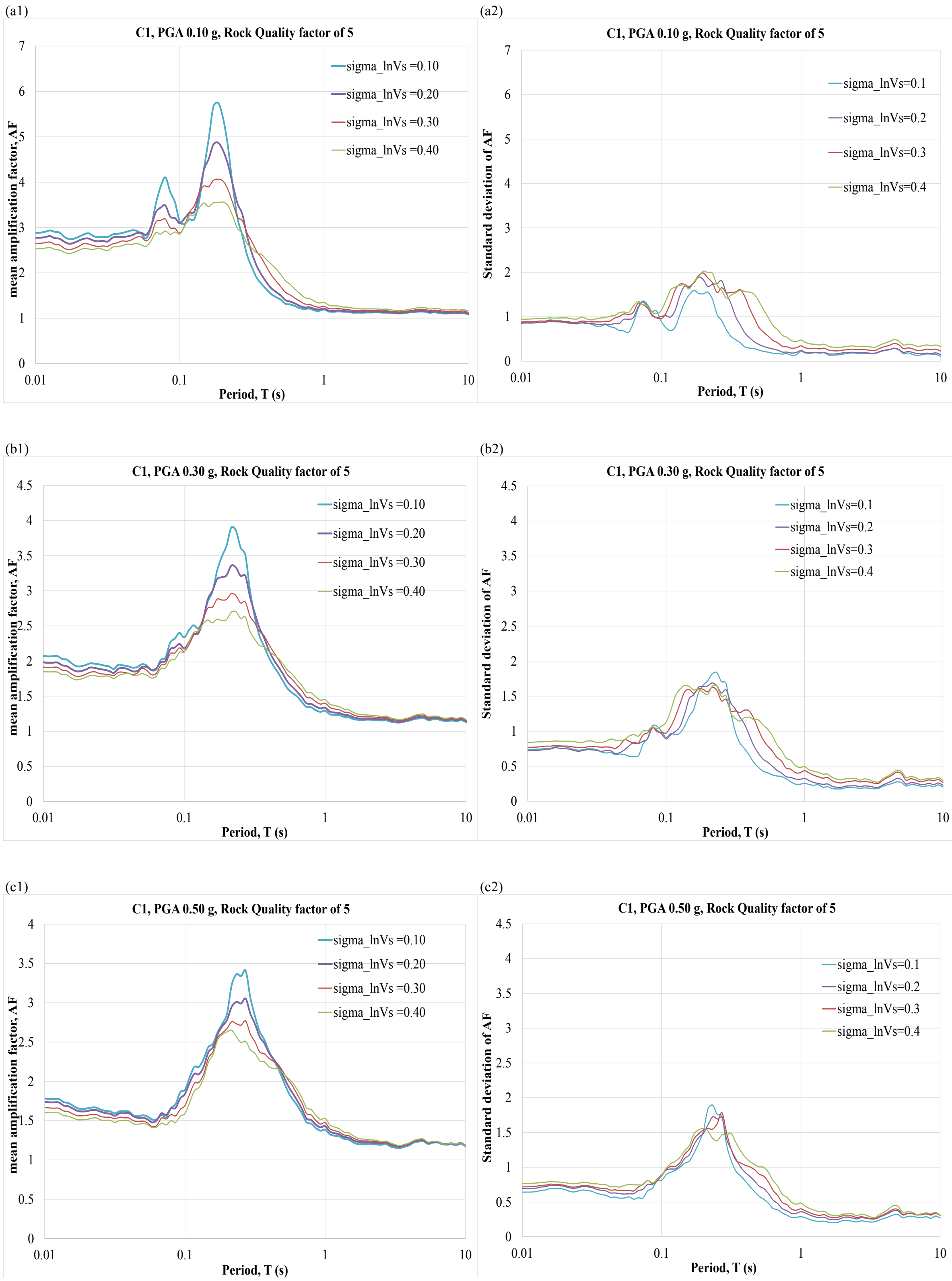

Figure 4.17: Change in the mean amplification factor computed for different levels of shear wave velocity profile randomization of the V_s profile measured at site C1.

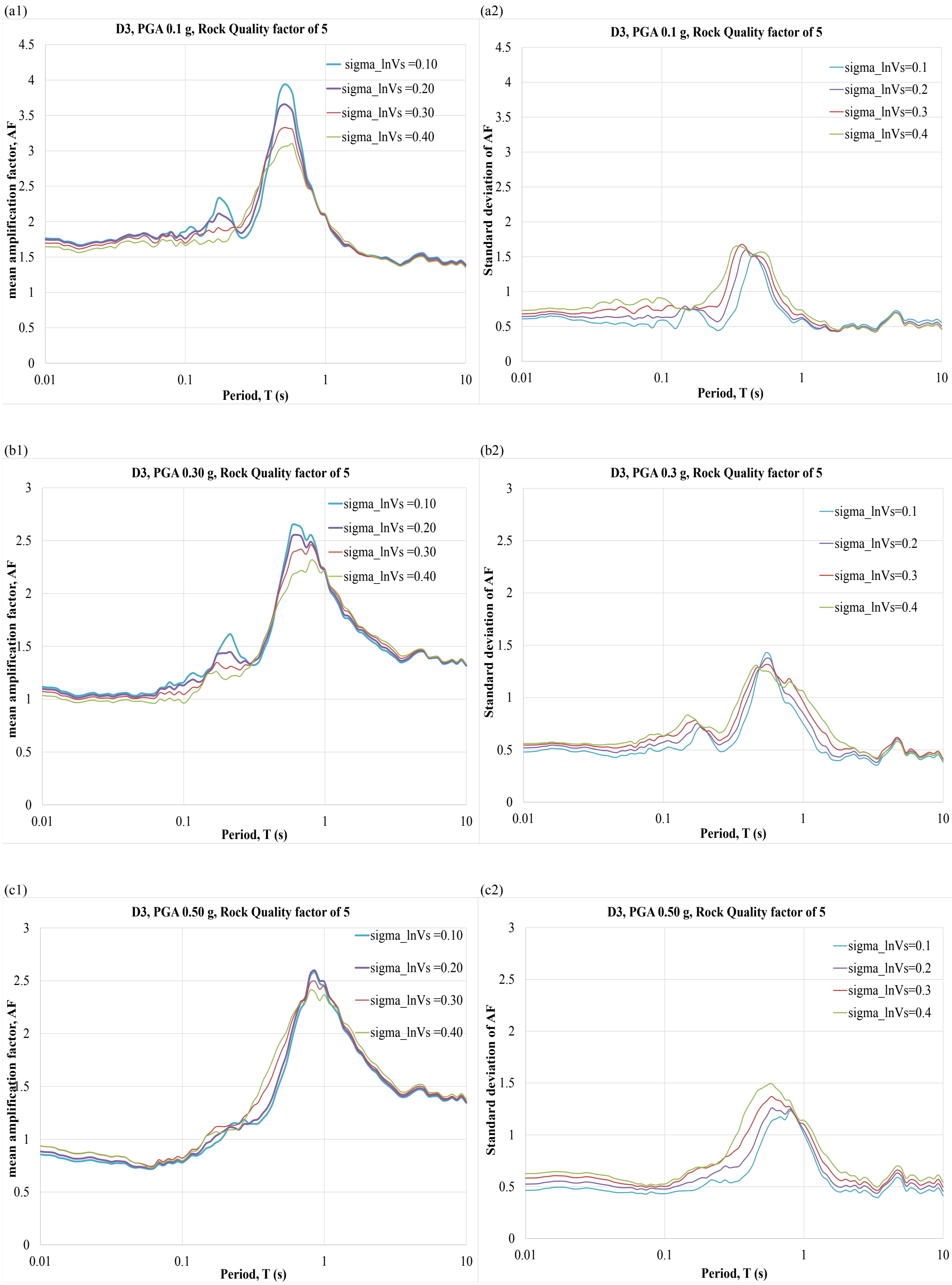

Figure 4.18: Change in the mean amplification factor computed for different levels of shear wave velocity profile randomization of the V_s profile measured at site D3.

4.11 Randomization of V_s profiles for Montreal sites

A total of 30 randomized V_s profiles are generated for each of the selected 12 soil V_s profiles obtained from seismic surveys (Figures 4.5 and 4.6) using a standard deviation of $\sigma_{\ln(Vs)}$ = 0.20 which corresponds to a coefficient of variation of 0.20 (Figures 4.19 to 4.20). The randomization is performed for each profile to account for both the variability of the depth to bedrock and shear wave velocities within each soil class.

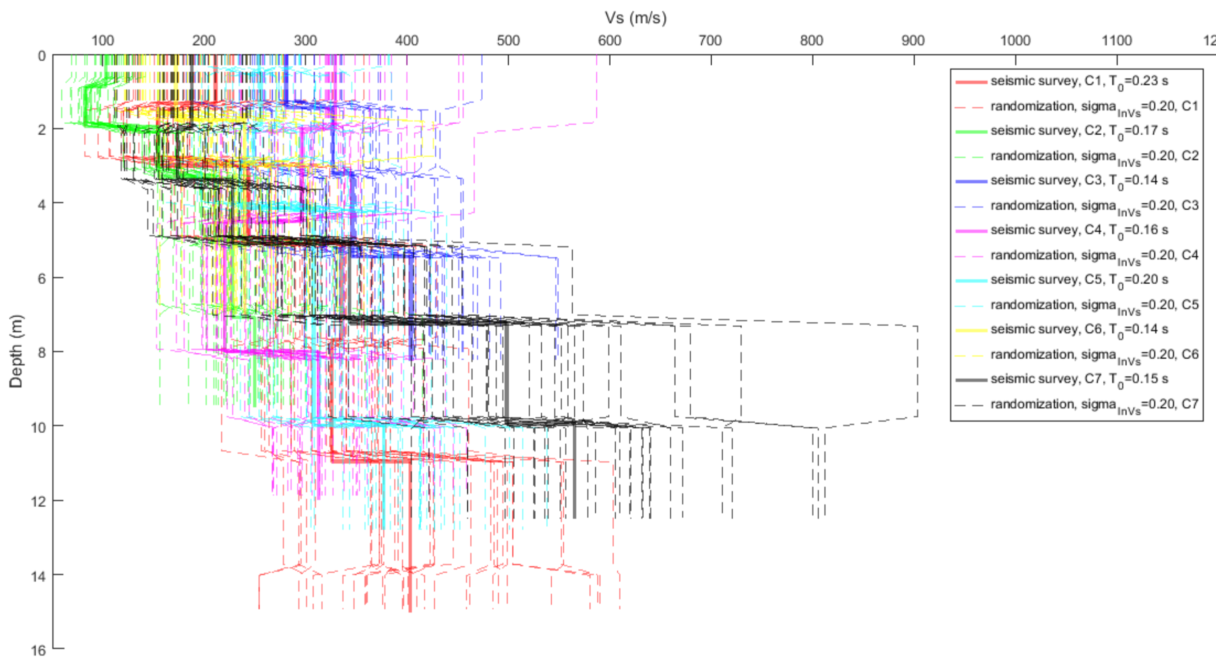

Figure 4.19: Random V_s profiles estimated for the soil profiles at sites: C1 to C7.

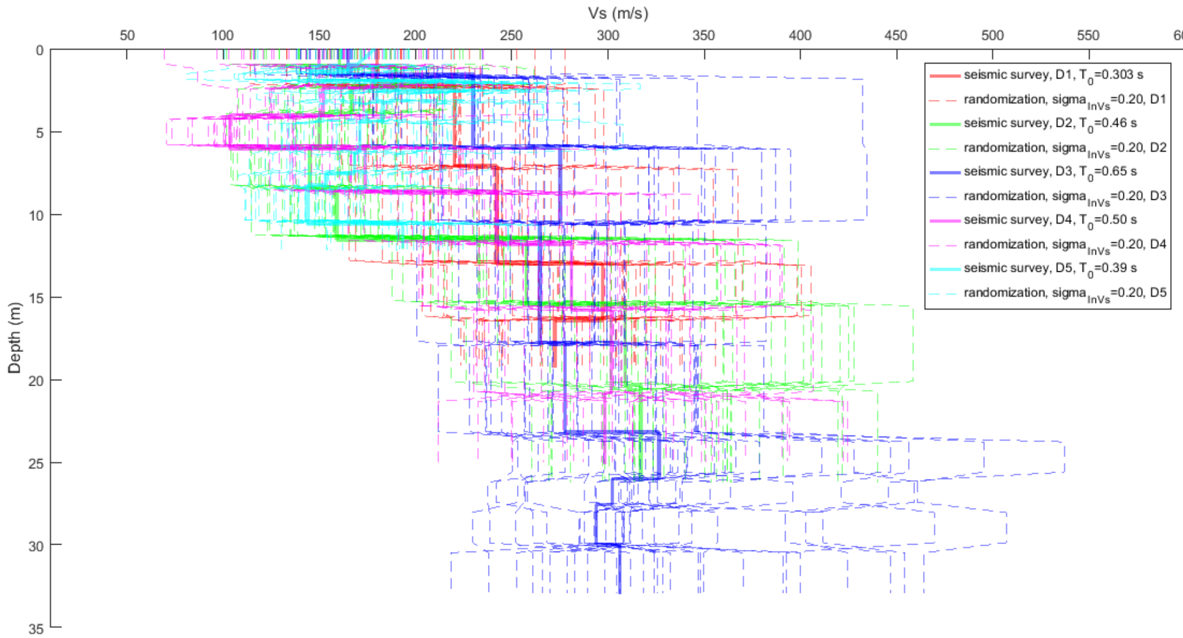

Figure 4.20: Random V_s profiles estimated for the soil profiles at sites: D1 to D5.

4.12 Sensitivity of site factors for spectral periods of 0.01, 0.2, 0.5 and 1.0 s to uncertainty in V_s profiles and nonlinear shear modulus-damping curve

The 1-D ground response of the 12 soil profiles in class C and D with the randomized V_s profiles (Figures 4.16-4.17) are evaluated by the EL procedures using Strata (Kottke and Rathje, 2010) under total stress conditions. The set of 20 rock motions are scaled to 0.1, 0.2, 0.3, 0.4 and 0.5 g. Spectral acceleration response calculations are performed for 5 % damping to be consistent with NBCC (2015).

Since the relationship between rock V_s and the RQD is linear, the site factors are calculated for bedrock V_s corresponding to RQD of 1, 3 and 5 (Figure 4.14). The average of site amplification for each RQD is estimated with the Rosenblueth point estimation procedure (Rosenblueth, 1975, 1981),

$$4.10 \qquad E\left[AF \middle| V_s(RQD), site\right] = 0.5\left\{AF\left(\mu_{V_s|RQD} + \sigma_{V_s|RQD}\right) + AF\left(\mu_{V_s|RQD} - \sigma_{V_s|RQD}\right)\right\}$$

The analyses are performed with 30 randomized profiles for each of the 12 baseline V_s profiles and each of the 3 RQD. Randomly generated sets of G/G_{max} and damping ratio curves for clay, sand, silt and gravels (Figures 4.12-4.13) are used as nonlinear dynamic properties of the 1-D profiles for the EL analyses.

Figures 4.21 to 4.23 show the amplification factors at low periods (T = 0.01 s) as a function of V_{s30} and site fundamental frequency F_0 for different RQDs of 1 to 3 and PGA of 0.1 g. Figures 4.21 to 4.23 show the site factors as a function of V_{s30}, site fundamental frequency, and RQD for PGA for 0.1 g. Figures 7.1 to 7.12 in Appendix A show the site factors as a function of V_{s30}, site fundamental frequency, and RQD for PGA from 0.1 g to 0.5 g. and are compared to site factors from Chouinard and Rosset (2007). It can be noted from Figures 4.21 to 4.23 that confidence intervals are provided for the mean amplification factors as well as for predicted amplification factors. The latter corresponds to the uncertainty expected for single events and highlights the possibility of amplifications significantly larger than mean amplifications specified in design codes for specific earthquakes. The results for low periods show good agreement with the previous study of Rosset and Chouinard (2007). The amplification factors increase as a function of RQD, which corresponds to an increase in the impedance contrast. Non-linear effects are more important for site with low V_{s30} and smaller amplifications can be observed specially for large ground motions and impedance ratios.

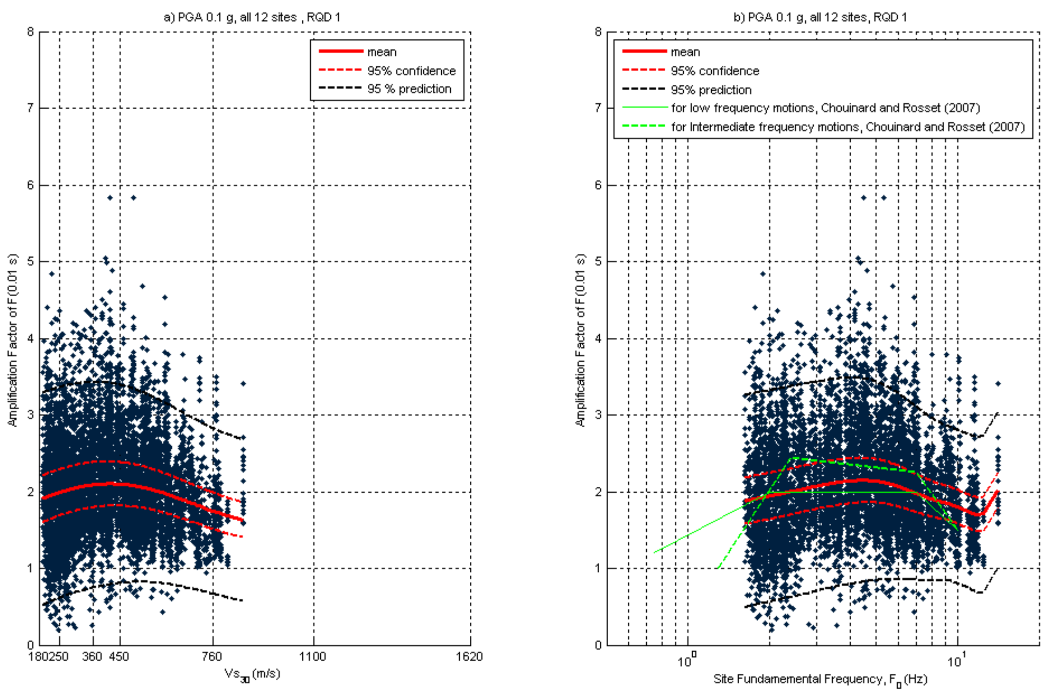

Figure 4.21: RQD of 1 and PGA of 0.1 g: a) relation between F(0.01 s) and Vs_{30}, b) relation between F(0.01 s) and site fundamental frequency F_0 for randomized V_s profiles and randomized nonlinear shear modulus-damping curve.

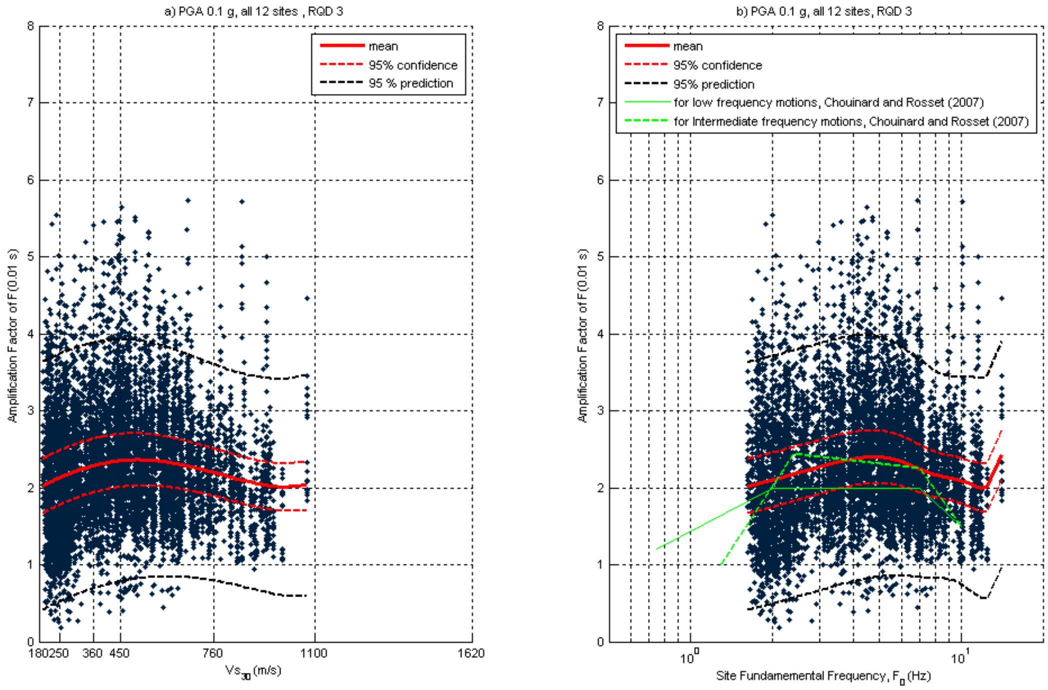

Figure 4.22: RQD of 3 and PGA of 0.1 g: a) relation between F(0.01 s) and Vs_{30}, b) relation between F(0.01 s) and site fundamental frequency F_0 for randomized V_s profiles and randomized nonlinear shear modulus-damping curve.

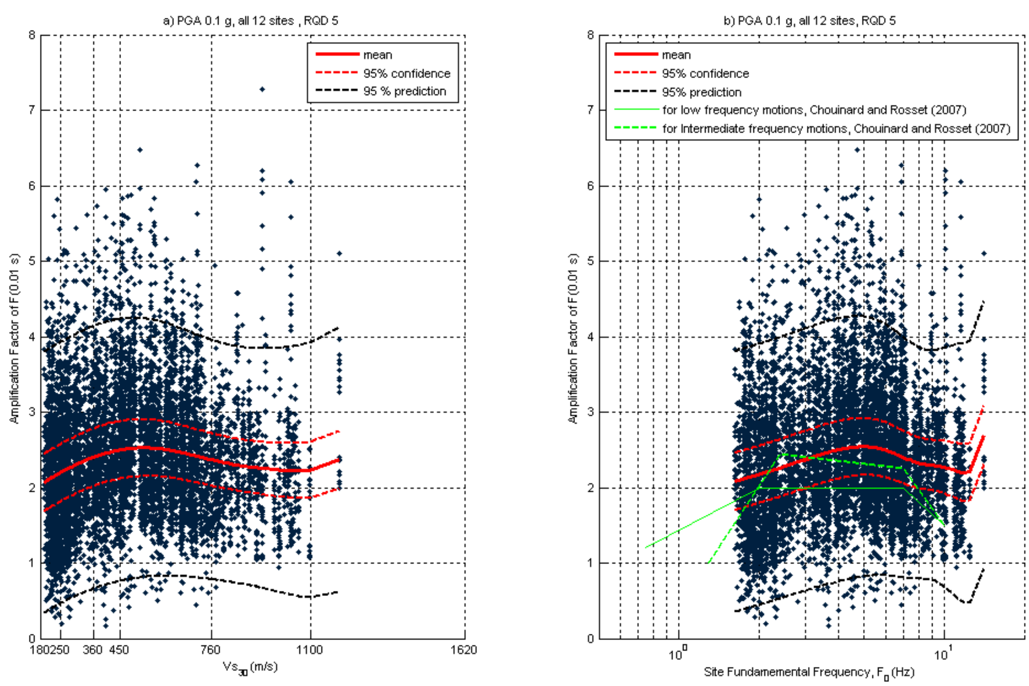

Figure 4.23: RQD 5 and PGA 0.1 g: a) relation between F(0.01 s) and Vs_{30}, b) relation between F(0.01 s) and site fundamental frequency F_0 for randomized V_s profiles and randomized nonlinear shear modulus-damping curve.

Figures 4.24 to 4.28 show the histograms and probability distribution functions for the amplification factor F(0.01 s) for class C and D sites for each RQD for increasing ground motions. These results illustrate the level of variability expected for the amplification factors for each soil class. The RQD has a significant effect on the mean amplification with larger amplifications due to increasing contrast ratios.

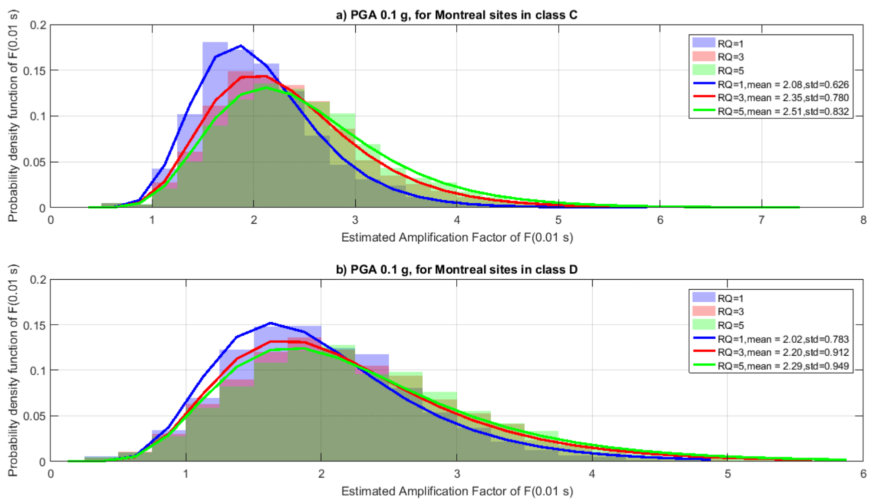

Figure 4.24: Comparison of Histograms, and Probability Density Functions for Amplification factor of F(0.01 s) calculated for RQD=1, 3, 5 with rock motions scaled to 0.1 g for randomized V_s profiles and randomized nonlinear shear modulus-damping curve.

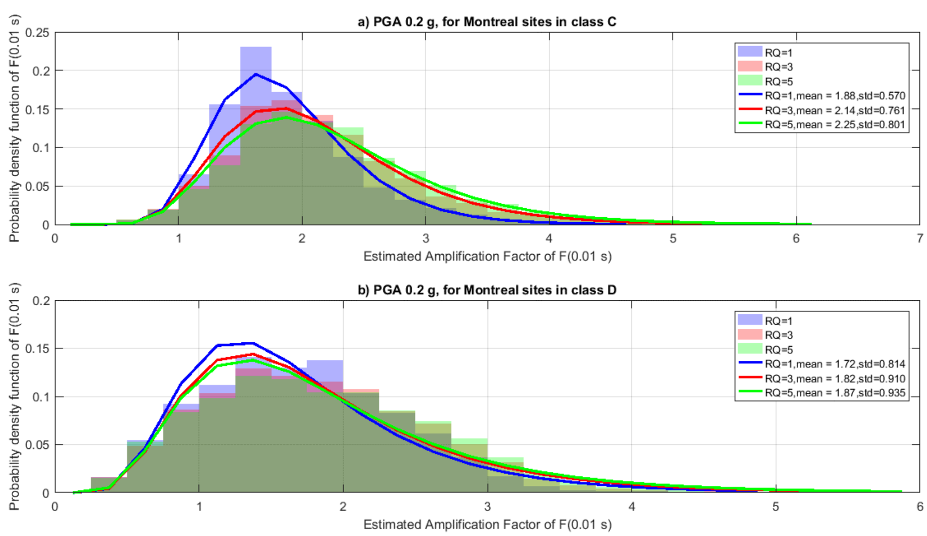

Figure 4.25: Comparison of Histograms, and Probability Density Functions for Amplification factor of F(0.01 s) calculated for RQD=1, 3, 5 with rock motions scaled to 0.2 g for randomized V_s profiles and randomized nonlinear shear modulus-damping curve.

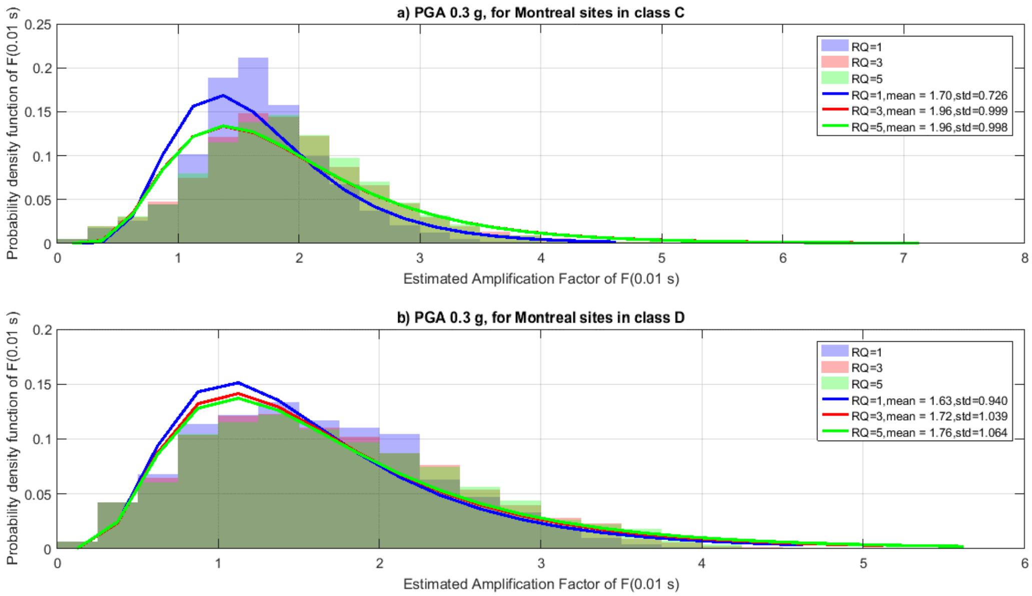

Figure 4.26: Comparison of Histograms, and Probability Density Functions for Amplification factor of F(0.01 s) calculated for RQD=1, 3, 5 with rock motions scaled to 0.3 g for randomized V_s profiles and randomized nonlinear shear modulus-damping curve.

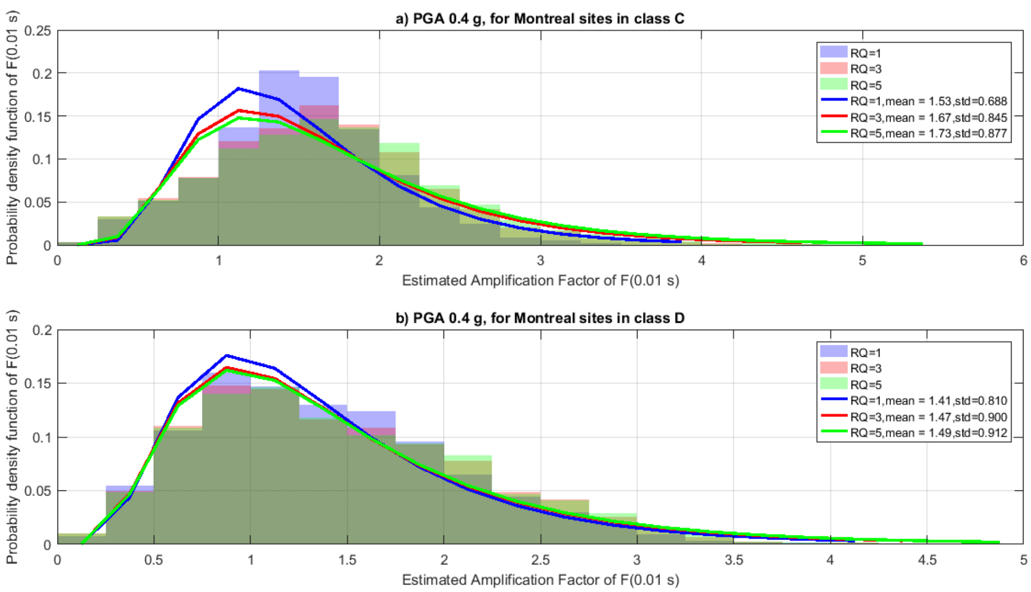

Figure 4.27: Comparison of Histograms, and Probability Density Functions for Amplification factor of F(0.01 s) calculated for RQD=1, 3, 5 with rock motions scaled to 0.40 g for randomized V_s profiles and randomized nonlinear shear modulus-damping curve.

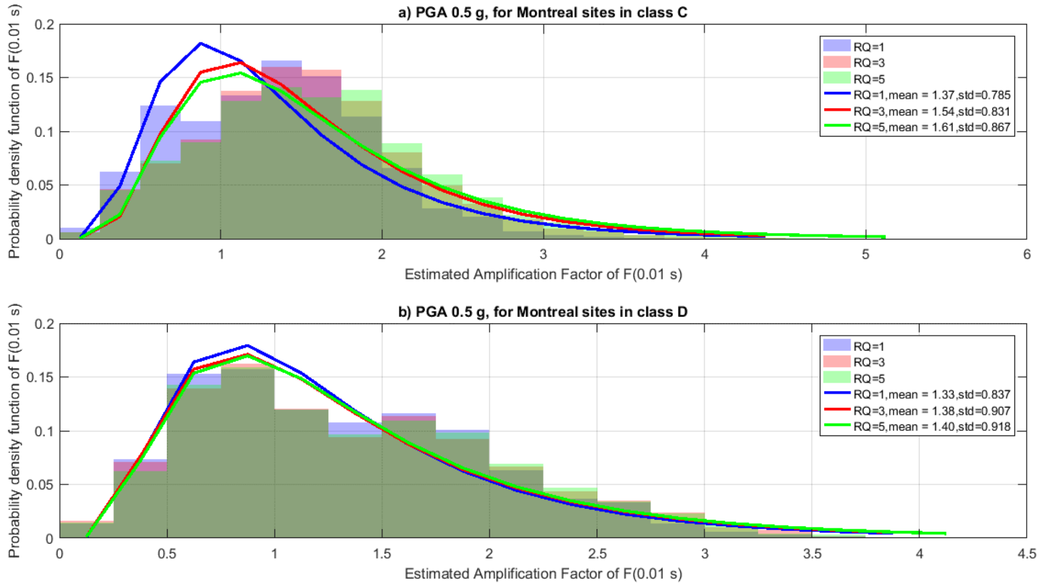

Figure 4.28: Comparison of Histograms, and Probability Density Functions for Amplification factor of F(0.01 s) calculated for RQD=1, 3, 5 with rock motions scaled to 0.50 g for randomized V_s profiles and randomized nonlinear shear modulus-damping curve.

The results shown in Figures 4.29 to 4.31 compare the calculated site factors of F (0.2 s), F(0.5 s) and F(1.0 s) with the published values available in the papers of Kim and Yoon (2006), and the 2015 NBCC for PGA of 0.1 g. It is to be noted from Figures 4.29 to 4.31, that the NBCC site factors for both class C and D site are normalized with the factors for class A and B sites since the calculated site factors are calculated for bedrock with mean V_s values in the range of 1200 to 3000 m/s. In the NBCC, the amplification factors are defined by using amplification at site class C as a reference (F_C = 1). For the purpose of the comparison with simulation results, the NBCC factors are adjusted for rock amplifications as a reference (F_A for RQD of 3 and 5 and F_B for RQD of 1).

Figures 8.1 to 8.12 in Appendix B show the site factors as a function of V_{s30}, , and RQD for PGA from 0.2 g to 0.5 g. and are compared to site factors from Kim and Yoon (2006), and the 2015 NBCC. A primary reason for the difference between the calculated and published values is due to the Rock quality designation (RQD) index.

Figures 4.32 to 4.34 show the amplification factors at short and long periods (T = 0.2 , 0.5 and 1.0 s) as a function of site period of T_0 for different RQD and PGA of 0.1 g. Confidence intervals are provided for the mean amplification factors as well as for predicted amplification factors. Figures 9.1 to 9.12 in Appendix C show the site factors as a function of site period T_0, , and RQD for PGA from 0.2 g to 0.5 g. and are compared to site factors from Kim and Yoon (2006), and the 2015 NBCC. A primary source of differences between site factors is RQD.

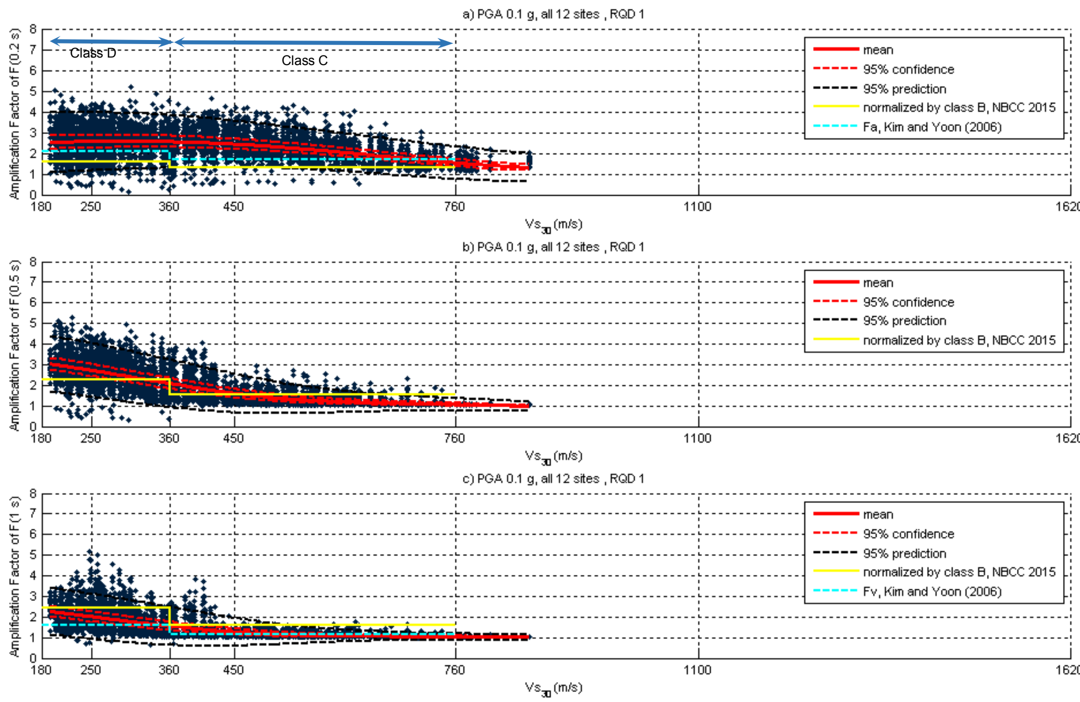

Figure 4.29: RQD 1 and PGA 0.1 g: a) relation between F(0.2 s) and $V_{s\ 30}$, b) relation between F(0.5 s) and V_{s30}, and c) relation between F(1.0 s) and V_{s30} for randomized V_s profiles and randomized nonlinear shear modulus-damping curve.

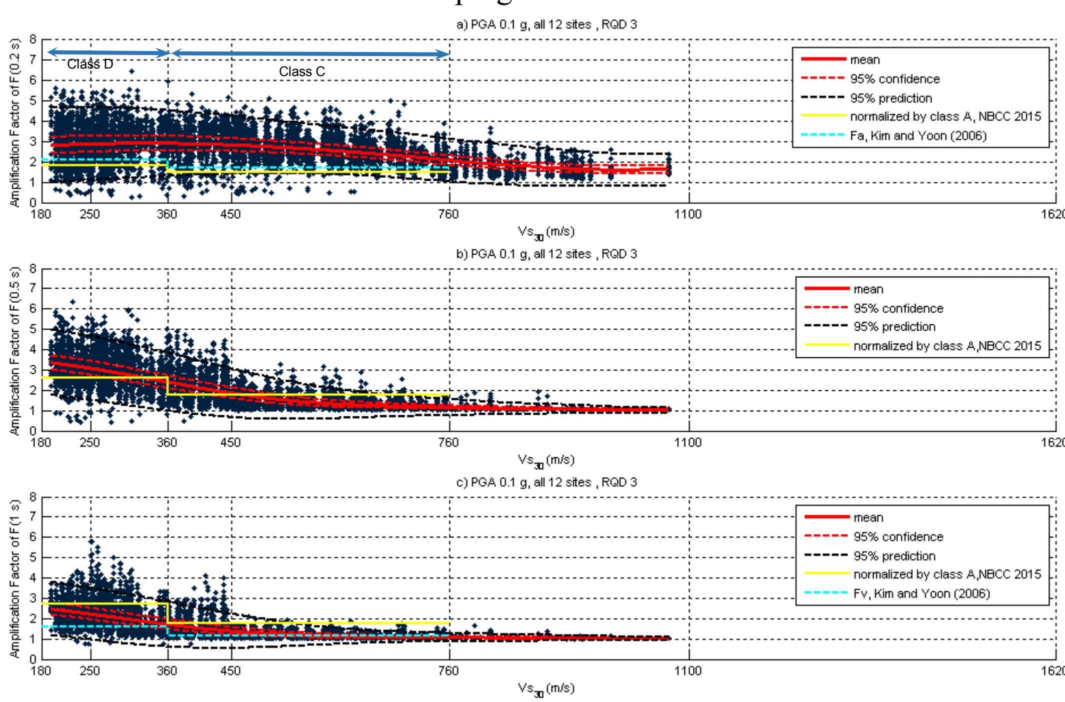

Figure 4.30: RQD 3 and PGA 0.1 g: a) relation between F(0.2 s) and V_{s30}, b) relation between F(0.5 s) and V_{s30}, and c) relation between F(1.0 s) and V_{s30} for randomized V_s profiles and randomized nonlinear shear modulus-damping curve.

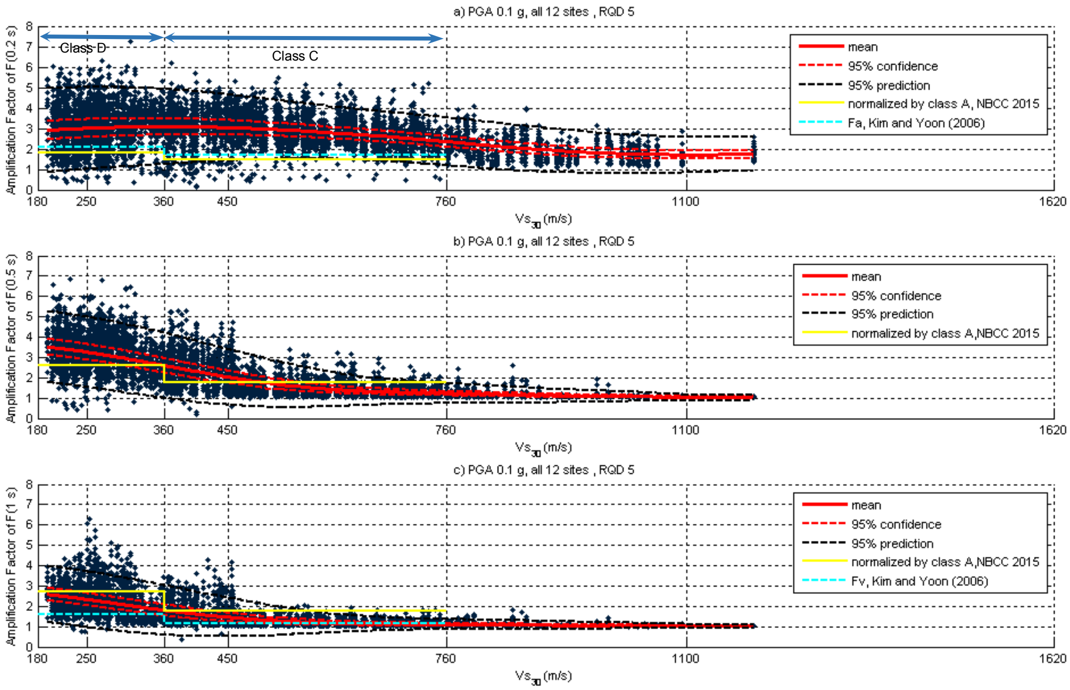

Figure 4.31: RQD of 5 and PGA 0.1 g: a) relation between F(0.2 s) and V_{s30}, b) relation between F(0.5 s) and V_{s30}, and c) relation between F(1.0 s) and V_{s30} for randomized V_s profiles and randomized nonlinear shear modulus-damping curve.

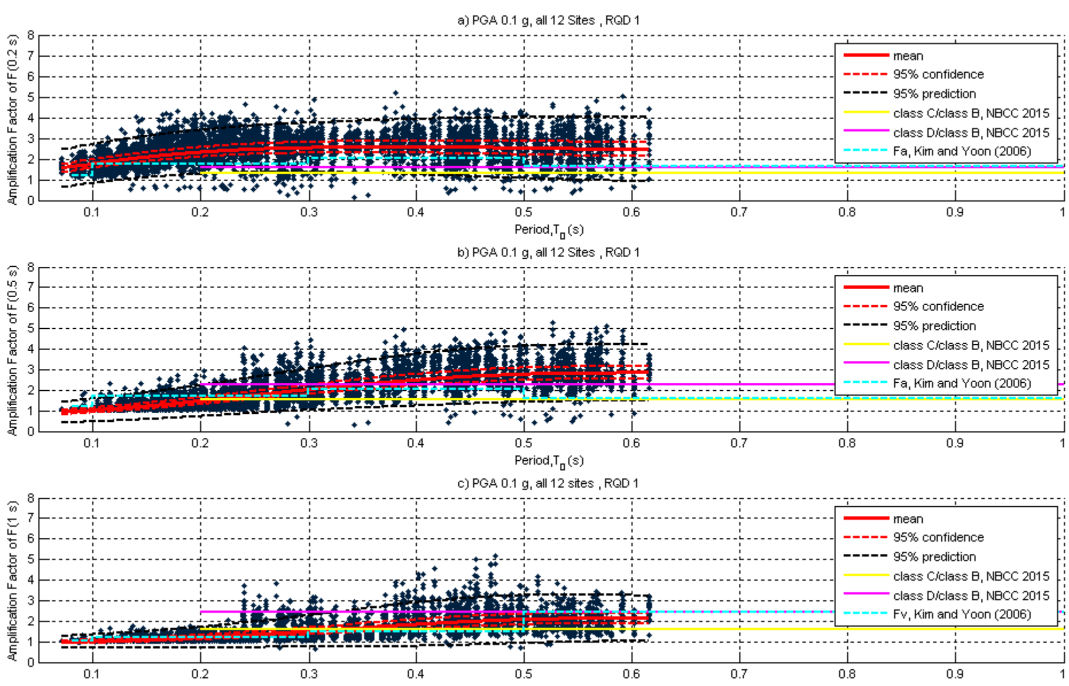

Figure 4.32: RQD of 1 and PGA 0.1 g: a) relation between F(0.2 s) and T_0, b) relation between F(0.5 s) and T_0, and c) relation between F(1.0 s) and T_0 for randomized V_s profiles and randomized nonlinear shear modulus-damping curve.

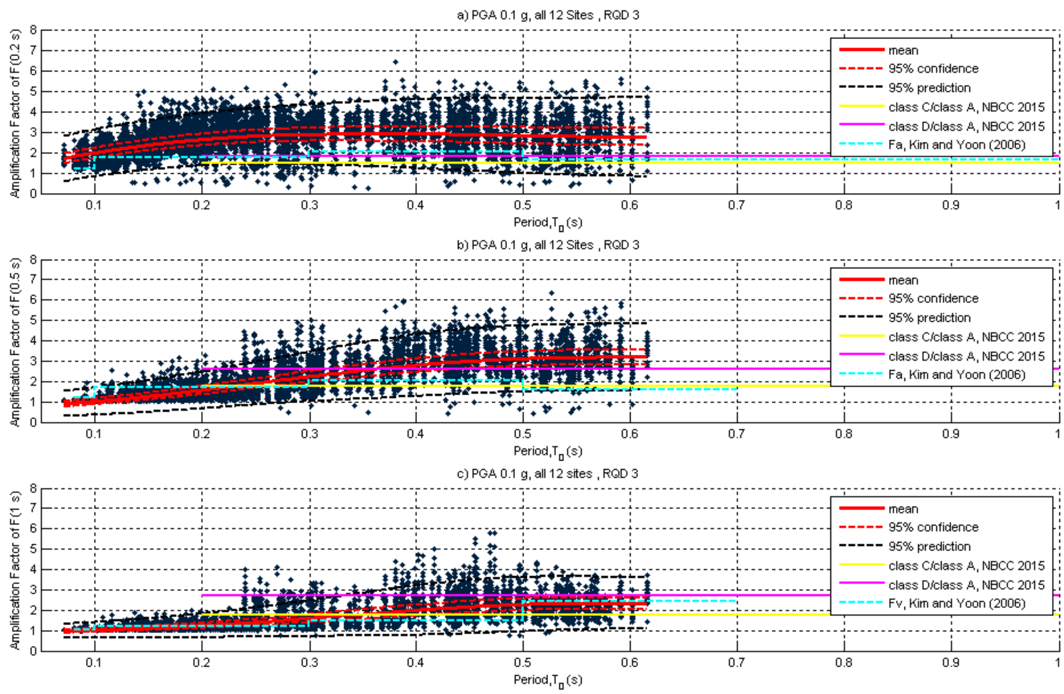

Figure 4.33: RQD of 3 and PGA 0.1 g: a) relation between F(0.2 s) and T_0, b) relation between F(0.5 s) and T_0, and c) relation between F(1.0 s) and T_0 for randomized V_s profiles and randomized nonlinear shear modulus-damping curve.

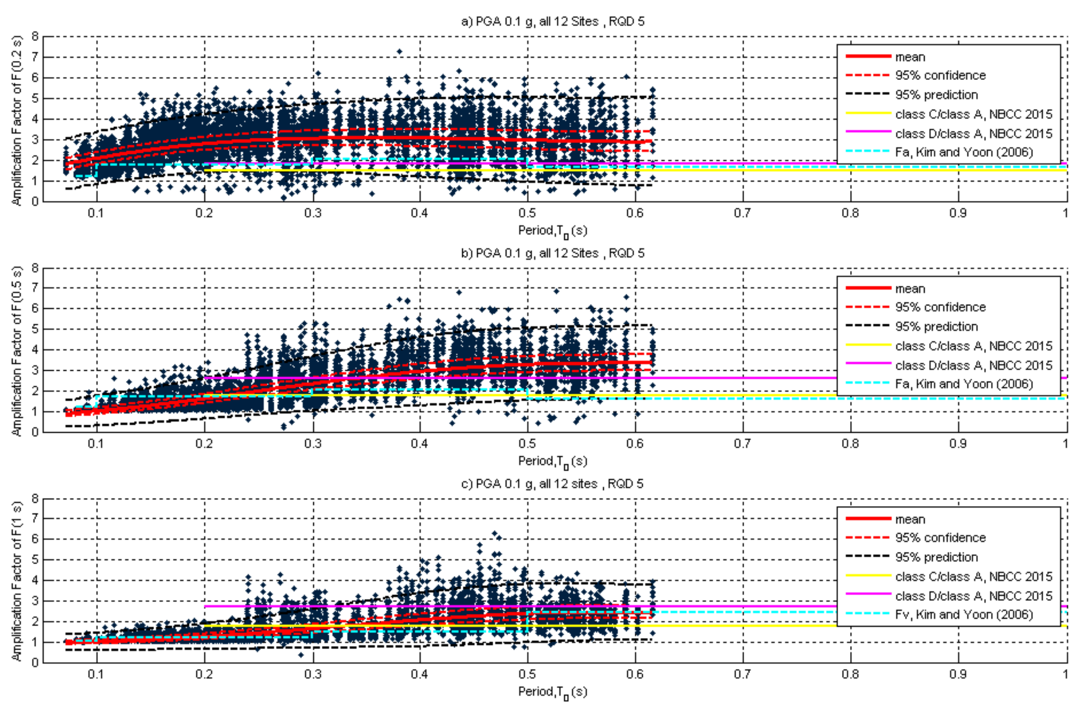

Figure 4.34: RQD 5 and PGA 0.1 g: a) relation between F(0.2 s) and T_0, b) relation between F(0.5 s) and T_0, and c) relation between F(1.0 s) and T_0 for randomized V_s profiles and randomized nonlinear shear modulus-damping curve.

4.13 Variability of Site Factors for Montreal and CENA as a function of PGA

Figures 4.35 compares median site factors (without correlation) F(0.01 s), F(0.2 s), F(0.5 s) and F(1 s) obtained for Montreal to CENA median site factors (Darragh and Silva, 2016) as a function of PGA. The latter are obtained for soil depths of 15 and 30 m and PGA from 0.1 and 0.4 g for class C and D sites overlying bedrock with V_s=2900 m/s which is equivalent to rock with a RQD of 5 in Montreal. The results show good agreement with the results for site class C for low periods.

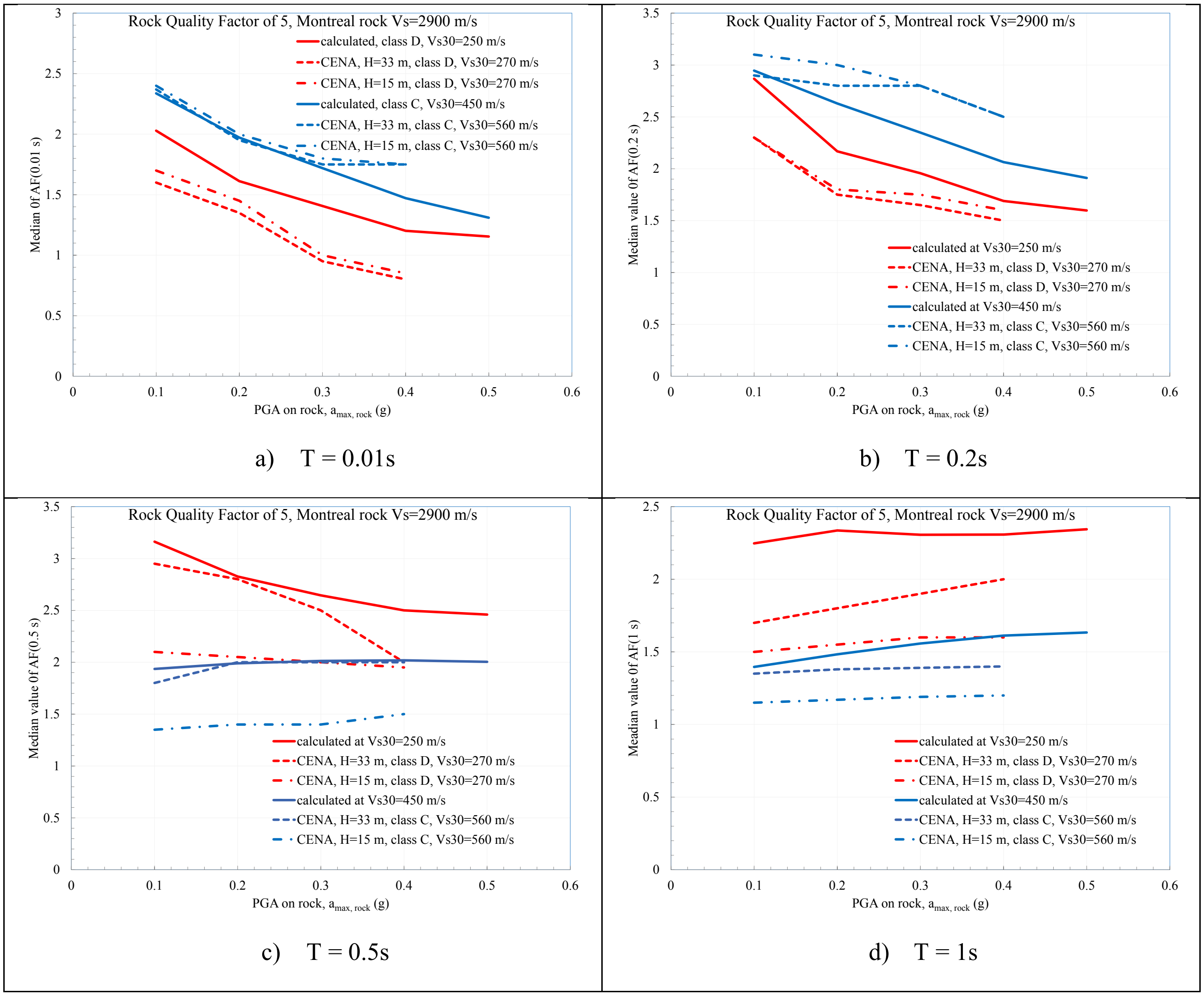

Figure 4.35: Median amplification factors as a function of PGA_{rock} at a) T = 0.01s, b) T = 0.2s, c) T = 0.5s and d) T = 1s.

The agreement is better with CENA estimates for the depth of 30 m for class D site; however, the typical depth for class C sites in Montreal is 15 m. For site class D, amplifications for Montreal sites are higher than those for similar CENA sites and the results are more in agreement for higher periods for depths of 30 m, which are typical for site class D sites in Montreal. Higher amplifications can be explained by the presence of Leda clay which has low damping ratios in comparison to other soft soils.

4.14 Distribution for F_D/F_C

The amplifications corresponding to V_{s30} =250 m/s and 450 m/s are used to define representative values for soil classes D and C respectively (i.e. F_D and F_C). Figures 4.36 to 4.38 show the simulated amplification factors F_D and F_C at periods of 0.2 s, 0.5 s and 1.0 s for randomized V_s profiles and randomized nonlinear shear modulus-damping curve. The amplifications for each soil class are assumed to be lognormally distributed and uncorrelated for all earthquake ground motions.

$$\begin{pmatrix} \ln F_D \\ \ln F_C \end{pmatrix} \sim N\left[\begin{pmatrix} \mu_{\ln F_D} \\ \mu_{\ln F_C} \end{pmatrix}, \begin{pmatrix} \sigma^2_{\ln F_D} & 0 \\ 0 & \sigma^2_{\ln F_C} \end{pmatrix}\right]$$

where

4.11 $$\sigma^2_{\ln F_C} = \ln\left[1+\frac{\sigma^2_{F_c}}{\mu^2_{F_c}}\right]; \quad \mu_{\ln F_c} = \ln\left[\mu_{F_c}\right] - \frac{1}{2}\sigma^2_{\ln F_C}$$

$$\sigma^2_{\ln F_D} = \ln\left[1+\frac{\sigma^2_{F_D}}{\mu^2_{F_D}}\right]; \quad \mu_{\ln F_D} = \ln\left[\mu_{F_D}\right] - \frac{1}{2}\sigma^2_{\ln F_D}$$

The ratio F_D/F_C (as well as F_A/F_C and F_B/F_C) is used in NBCC to normalize the short period and long period site factors (formerly F_a and F_v), which is also lognormally distributed. The values presented in the codes are the ratio for mean values. Alternatively, given that the ratio F_D/F_C is lognormally distributed, its mean value and variance can be derived from the distributions of F_D and F_C,

4.12 $$\mu_{F_D/F_C} = \exp\left(\mu_{\ln F_D} - \mu_{\ln F_C} + 0.5\left\{\sigma^2_{\ln F_D} + \sigma^2_{\ln F_C}\right\}\right)$$

4.13 $$\sigma^2_{F_D/F_C} = \exp\left(2\cdot\left(\mu_{\ln F_D} - \mu_{\ln F_C}\right) + \sigma^2_{\ln F_D} + \sigma^2_{\ln F_C}\right)\cdot\left(\exp\left(\sigma^2_{\ln F_D} + \sigma^2_{\ln F_C}\right) - 1\right)$$

The 95% prediction interval on F_D/F_C is then:

4.14 $$\exp\left[\left(\mu_{\ln F_D} - \mu_{\ln F_C}\right) \pm 1.96 * \sqrt{\left(\sigma^2_{\ln F_C} + \sigma^2_{\ln F_D}\right)}\right]$$

A confidence interval can also be derived for the ratio of the mean values of F_D and F_C which has narrower bounds and is a function of the number of simulations. The latter indicate the level of accuracy on estimates of the mean values for the number of simulations performed.

4.15 Correction for correlation between F_C and F_D due to ground motions using the results of 1-D runs with randomized V_s profiles and randomized dynamics nonlinear property curves.

A feature of amplifications obtained by simulation as opposed to empirical data is that each scaled ground motion record is applied to a set of randomized soil profiles and soil properties. This introduces positive correlation between amplifications obtained for different soil classes that are not present in empirical observations of amplifications. This correlation is a result of using the same input ground motion for each randomized profile.

Correlations between $\ln F_C$ and $\ln F_D$ are obtained for ground motions scaled from 0.1g to 0.5g and for rock quality designations of 1, 3 and 5 for periods of 0.2s, 0.5s and 1s (Figures 4.36 to 4.38 for 0.1g, and Figures 10.1 to 10.12 in Appendix D for other PGA from 0.2 to 0.5 g). The correlations are obtained by performing 1-D simulations for each of the 20 ground motions and the set of randomized site class C and D profiles and calculating the mean amplifications.

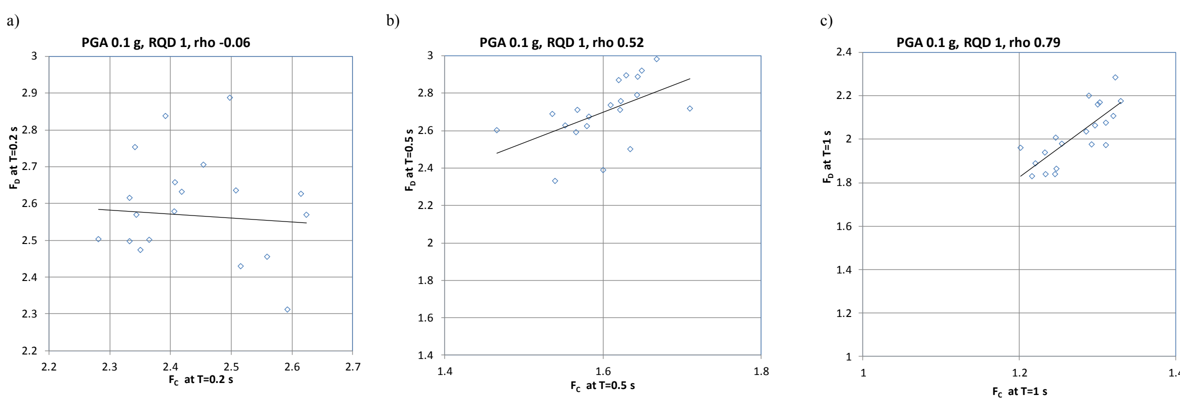

Figure 4.36: Amplification factors and correlation coefficient between site classes C and D for 20 ground records scaled to 0.1g, and Rock Quality Designation of 1 (V_s= 1258 m/s) for randomized V_s profiles and randomized nonlinear shear modulus-damping curve.

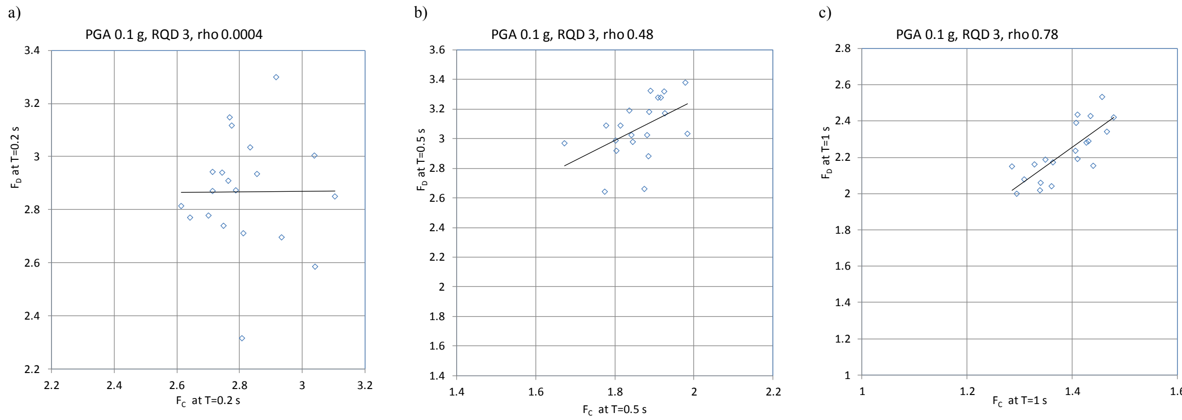

Figure 4.37: Correlation scatter plots for PGA of 0.1 g and RQD of 3 (V_s=2082 m/s) compare F_D and F_C calculated from the ground response to each of the 20 motions for T= 0.2, 0.5 and 1.0 s; for randomized V_s profiles and randomized nonlinear shear modulus-damping curve.

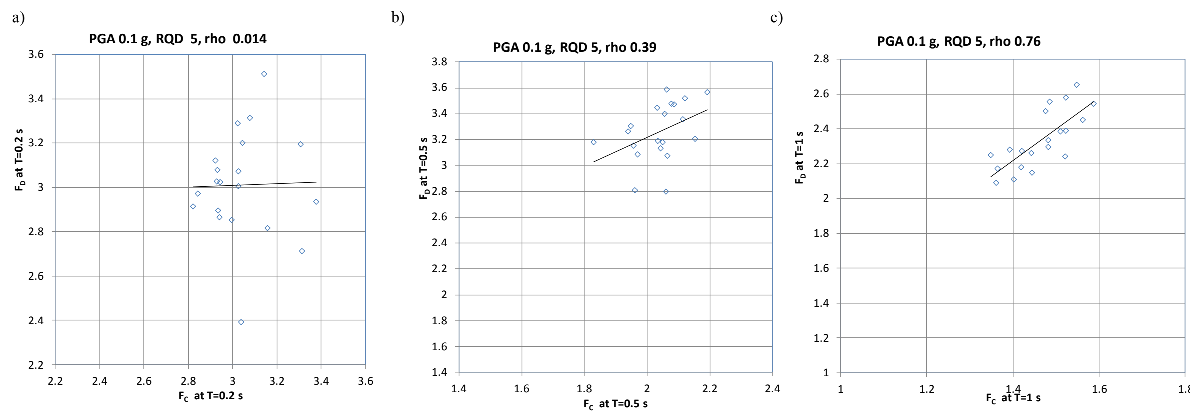

Figure 4.38: Correlation scatter plots for PGA of 0.1 g and RQD of 5 (V_s= 2926 m/s) compare F_D and F_C calculated from the ground response to each of the 20 motions for T= 0.2 , 0.5 and 1.0 s for randomized V_s profiles and randomized nonlinear shear modulus-damping curve.

Figure 4.39 shows the Coefficient of correlation between $\ln F_D$ and $\ln F_C$ as a function of PGA for RQD of 1, 3 and 5. It shows that the correlation coefficients are positive and decrease with increasing PGA values for F_C and F_D obtained for periods of 0.5 s and 1 s. For F_C and F_D obtained for period of 0.2 s, the correlation coefficients increase with increasing PGA values. The correlation for the amplification for soil classes C and D is largest for higher periods due to similarities in soil responses for the two site classes in that range, and decrease with increasing ground motions due to nonlinear effects, decrease with increasing impedance ratios.

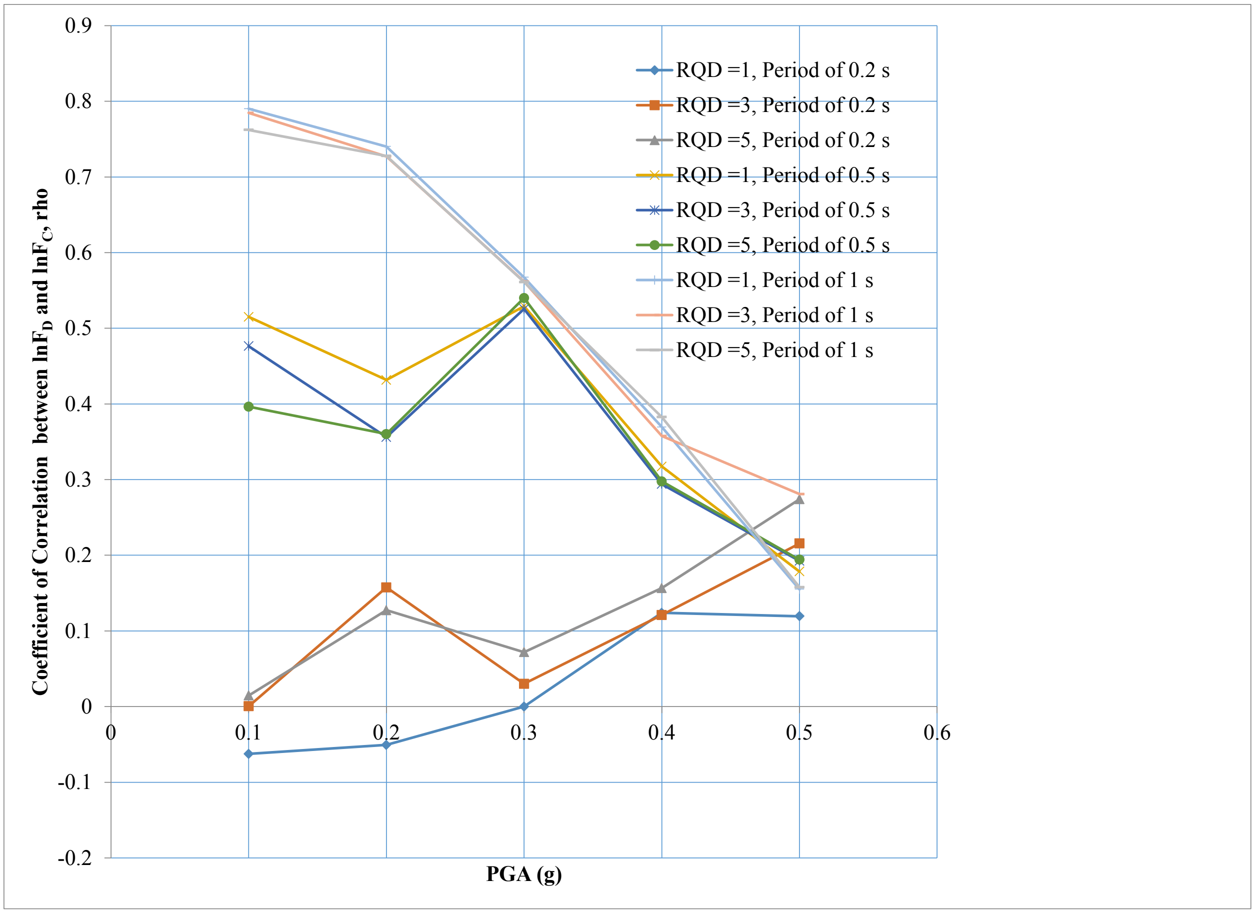

Figure 4.39: Coefficient of correlation between $\ln F_D$ and $\ln F_C$ as a function of PGA, obtained from the 1-D runs with randomized V_s profiles and randomized nonlinear shear modulus-damping curve.

Considering correlations, the mean value and the variance for the amplifications normalized relative to site class are derived as follows,

$$\begin{pmatrix} \ln F_D \\ \ln F_C \end{pmatrix} \sim N\left[\begin{pmatrix} \mu_{\ln F_D} \\ \mu_{\ln F_C} \end{pmatrix}, \quad \begin{pmatrix} \sigma^2_{\ln F_D} & \rho\sigma_{\ln F_C}\sigma_{\ln F_D} \\ \rho\sigma_{\ln F_C}\sigma_{\ln F_D} & \sigma^2_{\ln F_C} \end{pmatrix}\right]$$

4.15 $$\mu_{F_D/F_C} = \exp\left(\mu_{\ln F_D} - \mu_{\ln F_C} + 0.5\left\{\sigma^2_{\ln F_D} - 2\rho\sigma_{\ln F_C}\sigma_{\ln F_D} + \sigma^2_{\ln F_C}\right\}\right)$$

4.16

$$\sigma^2_{F_D/F_C} = \exp\left(2\cdot\left(\mu_{\ln F_D} - \mu_{\ln F_C}\right) + \sigma^2_{\ln F_D} + \sigma^2_{\ln F_C} - 2\rho\sigma_{\ln F_C}\sigma_{\ln F_D}\right)\cdot\left(\exp\left(\sigma^2_{\ln F_D} + \sigma^2_{\ln F_C} - 2\rho\sigma_{\ln F_C}\sigma_{\ln F_D}\right) - 1\right)$$

The 95% prediction interval for $\left(F_D/F_C\right)$ is:

$$4.17 \qquad \exp\left[\left(\mu_{\ln F_D} - \mu_{\ln F_C}\right) \pm 1.96 * \sqrt{\left(\sigma^2_{\ln F_C} + \sigma^2_{\ln F_D} - 2\cdot\rho_{\ln F_D,\,\ln Fc}\cdot\sigma_{\ln F_D}\cdot\sigma_{\ln F_C}\right)}\right]$$

Presented in Figure 4.40 is the site factor $E(F_D/F_C)$ calculated at T=0.2 as a function of PGA. Figures 4.40 also shows the comparison between the calculated site factors and the 2015 NBCC site factors for RQD of 1, 3 and 5.

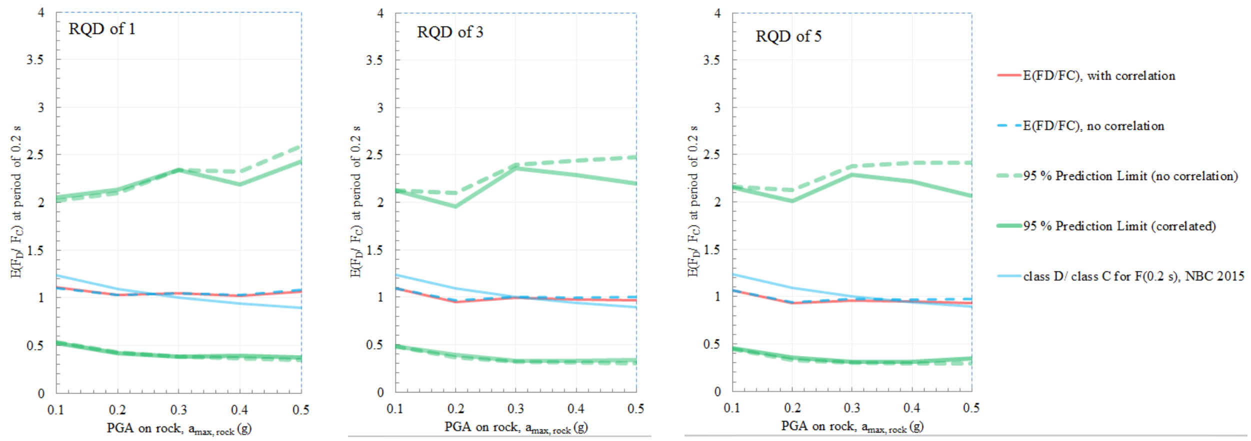

(a) (b) (c)

Figure 4.40: Comparison between the calculated $E(F_D/F_C)$ at T=0.2 s and the NBCC 2015 factor for randomized V_s profiles and randomized nonlinear shear modulus-damping curve.

As it can be seen in Figure 4.40, the site factor of $E(F_D/F_C)$ is presented with 95% prediction interval for showing the uncertainty on the estimate of the mean values for $E(F_D/F_C)$. Presented in Figure 4.41 is the site factor $E(F_D/F_C)$ calculated at T=0.5 as a function of PGA. It shows the comparison between the calculated site factors and the 2015 NBCC site factors for Rock quality designation of 1, 3 and 5

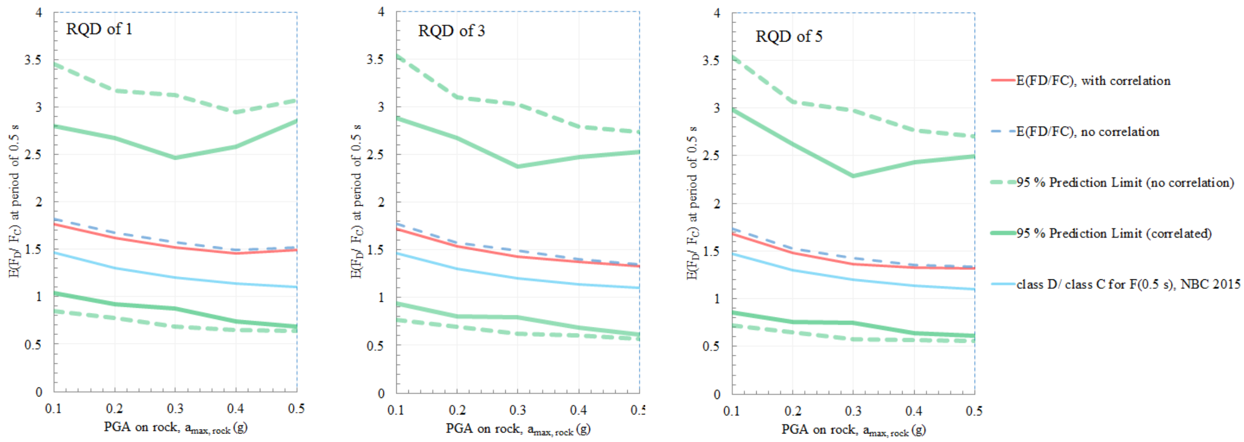

(a) (b) (c)

Figure 4.41: Comparison between the calculated $E(F_D/F_C)$ at T =0.5 s and the NBCC 2015 factor for randomized V_s profiles and randomized nonlinear shear modulus-damping curve.

As it can be seen in Figure 4.41, the site factor of $E(F_D/F_C)$ is presented with the estimate of 95% prediction interval for showing the uncertainty on the estimate of the mean values for $E(F_D/F_C)$. Presented in Figure 4.42 is the site factor $E(F_D/F_C)$ calculated at T=1.0 as a function of PGA. It shows the comparison between the calculated site factors and the 2015 NBCC site factors for Rock quality designation of 1, 3 and 5.

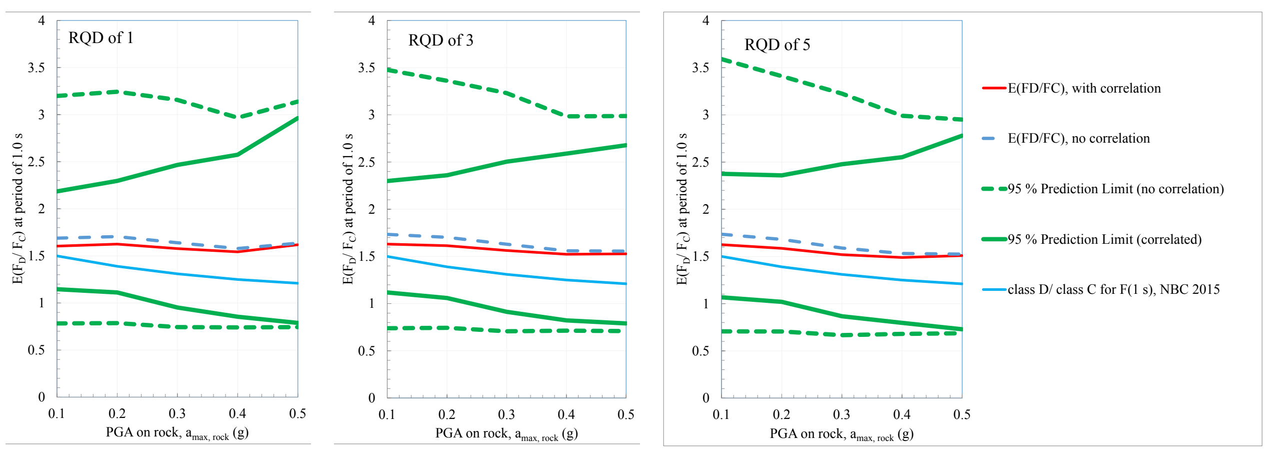

(a) (b) (c)

Figure 4.42: Comparison between the calculated $E(F_D/F_C)$ at T =1.0 s and NBCC 2015 factor for randomized V_s profiles and randomized nonlinear shear modulus-damping curve.

4.16 Uncertainty on site amplification due to randomized V_s profiles and ground motions

Randomized V_s profiles for each soil site class C and D are analyzed by using the same nonlinear dynamic property curves for a set of 20 ground motions scaled from 0.1g to 0.5 g and for rock quality designations of 1, 3 and 5.

Scatter plots showing the correlation between F_C and F_D for PGA 0.1 g to 0.5 g for randomized V_s profiles are shown in Figures 11.1 to11.15 in Appendix E. Next, the correlations between $\ln F_C$ and $\ln F_D$ for randomized V_s profile, and for rock quality designations of 1, 3 and 5 are shown in Figure 4.43. The correlations are obtained in a similar way as in the previous section for ground motions scaled to 0.1, 0.2, 0.3, 0.4 and 0.5 g for periods of 0.2 s, 0.5 s and 1 s (Figure 4.43). The correlations are obtained by performing 1-D simulations for each of the 20 ground motions and calculating the mean amplifications. The correlations show no pattern as a function of PGA and period, are generally small and have little influence on the average and uncertainty of $F_D/\ F_C$. (Figure 4.43).

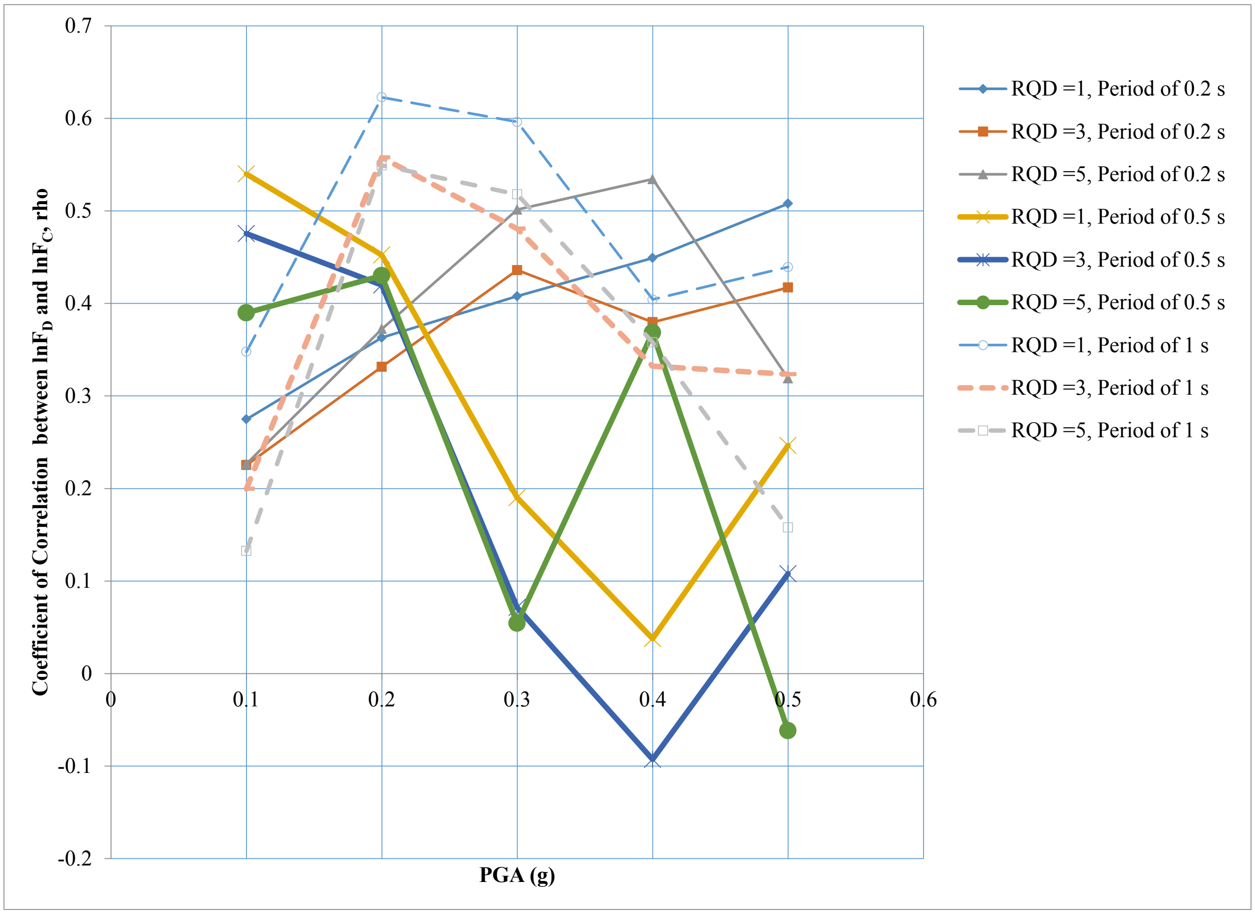

Figure 4.43: Coefficient of correlation between $\ln F_D$ and $\ln F_C$ as a function of PGA for randomized V_s profiles and ground motions.

Figures 4.44 to 4.46 show the comparison between the 2015 NBCC site factor and the calculated $E(F_D/F_C)$ for T=0.2 s, 0.5 s and 1 s respectively for Rock quality designation indexes of 1, 3 and 5. The results show that the uncertainty on non-linear dynamic properties has little influence on the mean value of F_D/F_C and increases slightly the uncertainty on the prediction interval.

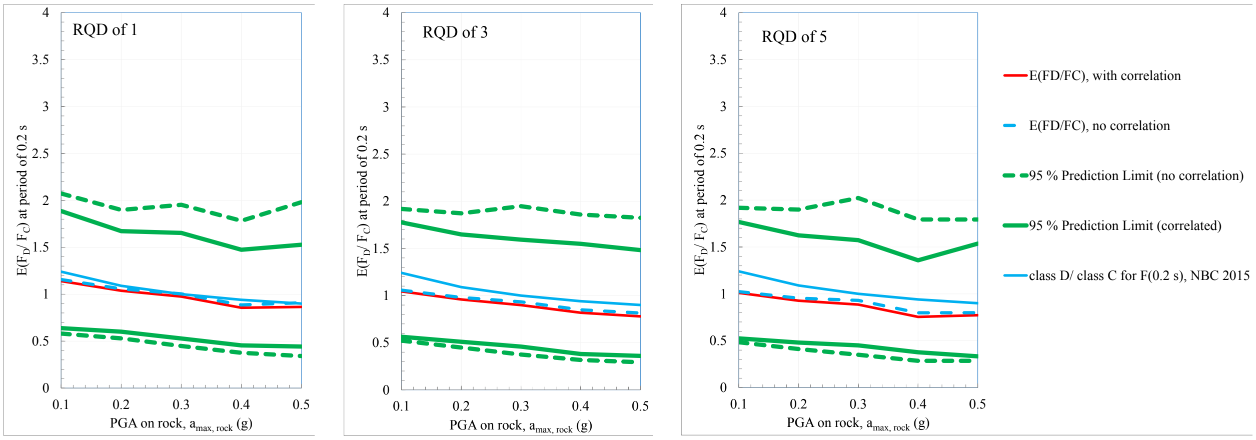

(a) (b) (c)

Figure 4.44: Comparison between $E(F_D/F_C)$ at T=0.2 s and the NBCC 2015 factor due to randomized V_s profiles and ground motions.

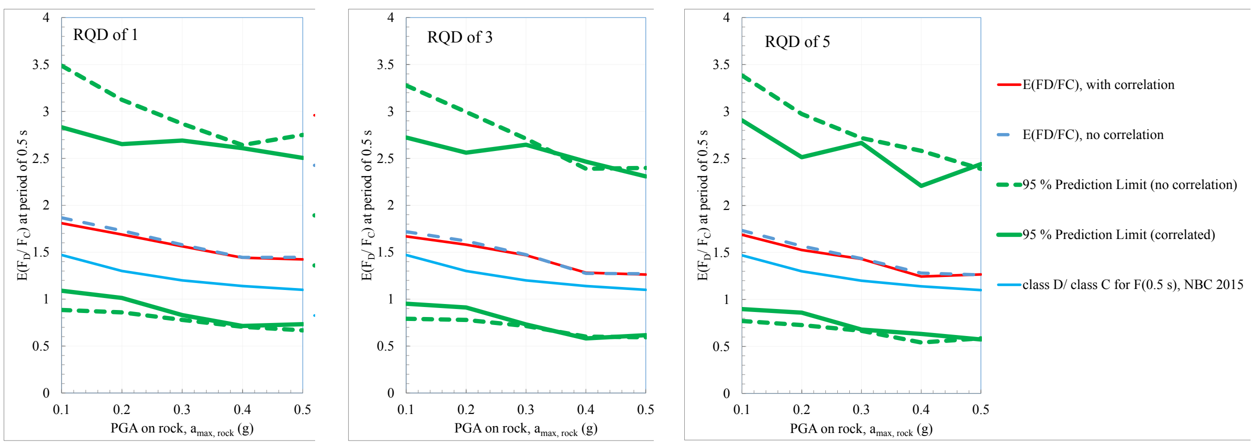

(a) (b) (c)

Figure 4.45: Comparison between $E(F_D/F_C)$ at T=0.5 s and the NBCC 2015 factor due to randomized V_s profiles and ground motions

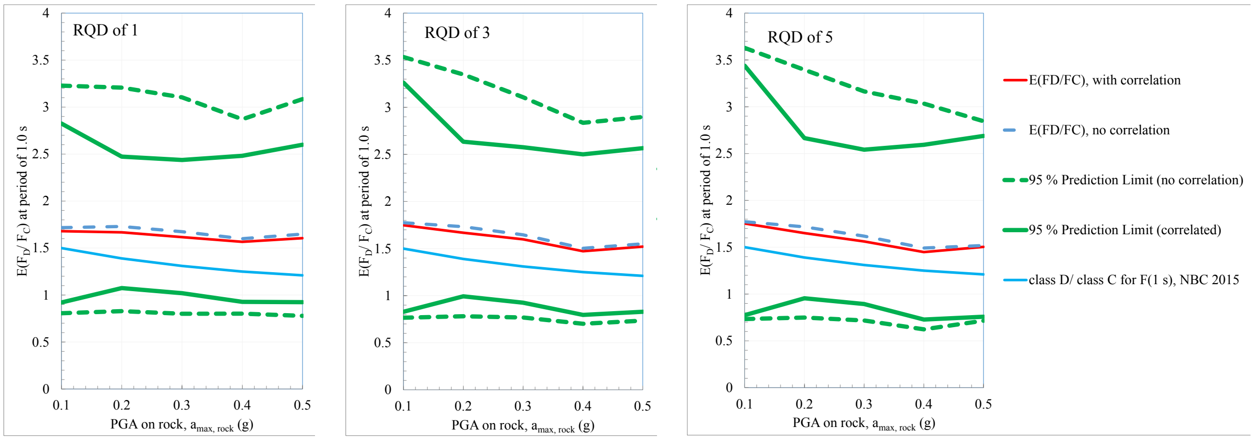

(a) (b) (c)

Figure 4.46: Comparison between $E(F_D/F_C)$ at T=1s and the NBCC 2015 factor due to randomized V_s profiles and ground motions

4.17 Uncertainty on site amplification with ground motions and non-randomized V_s profile

The analyses are performed by analyzing the 5 site class C sites and the 7 site class D sites using best estimates of the V_s profiles without performing V_s profile randomization. Uncertainties in non-linear dynamic properties are considered as well as variability on ground motions (20 records).

Scatter plots showing the correlation between F_C and F_D for PGA 0.1 g to 0.5 g for non-randomized V_s profiles are shown in Figures 12.1 to 12.15 in Appendix F. Next, the correlations between $\ln F_C$ and $\ln F_D$ for non-randomized V_s profile, and for rock quality designations of 1, 3 and 5 are obtained in a similar way as in the previous section for ground motions scaled to 0.1, 0.2, 0.3, 0.4 and 0.5 g for periods of 0.2 s, 0.5 s and 1 s (Figure 4.47). The correlations show no pattern as a function of PGA and period, are generally small and have little influence on the average and uncertainty of $F_D/\ F_C$. The correlations are obtained by performing 1-D simulations for each of the 20 ground motions and calculating the mean amplifications.

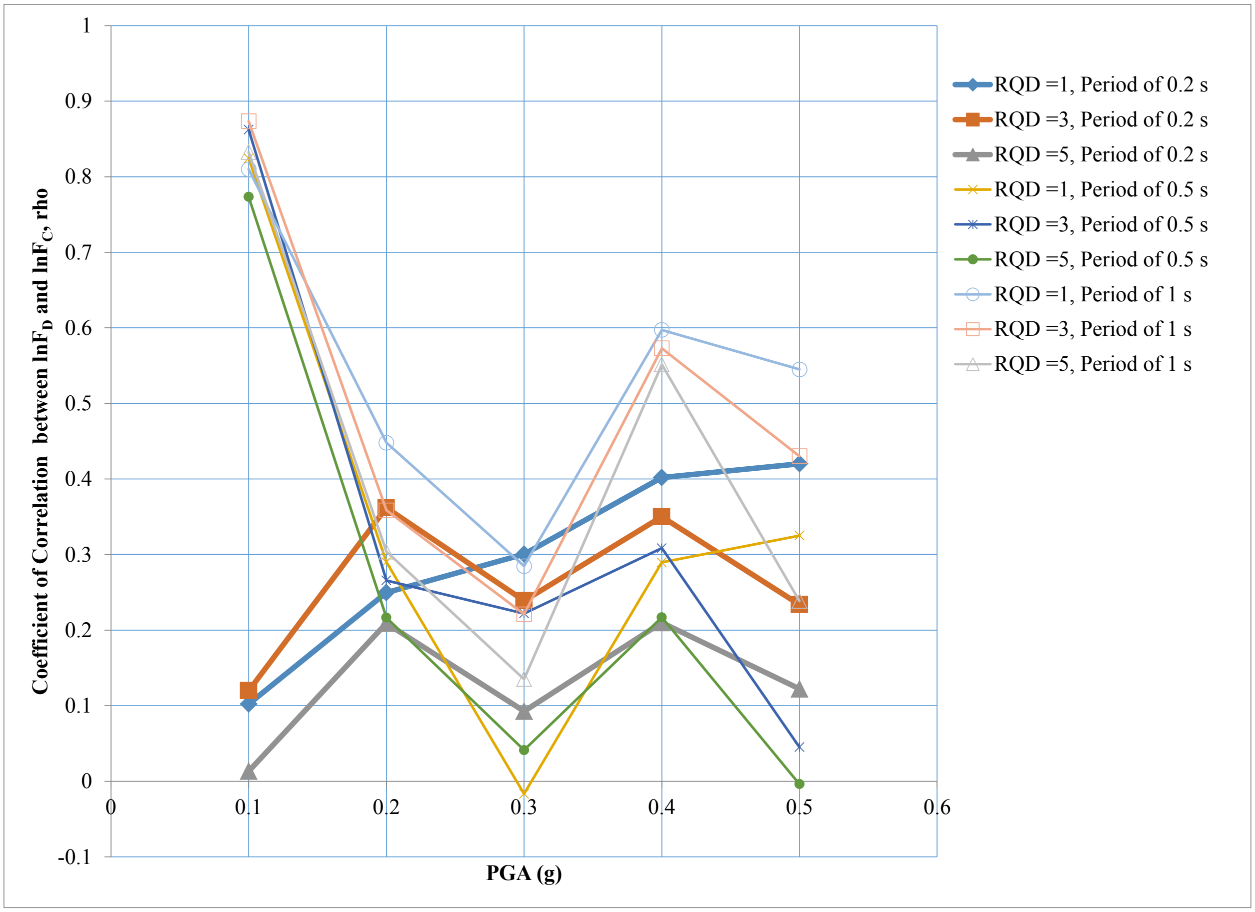

Figure 4.47: Coefficient of correlation between $\ln F_D$ and $\ln F_C$ as a function of PGA for ground motions and non-randomized V_s profiles

Figures 4.48 to 4.50 show the comparison between the 2015 NBCC site factor and the calculated $E(F_D/F_C)$ for T=0.2 s, 0.5s and 1s respectively for RQD of 1, 3 and 5. The results show that the randomization of soil profiles has little influence on the mean value of F_D/F_C and increases only slightly the uncertainty on the prediction interval. These results combined to those of the previous section indicate that most of the uncertainty associated with the amplification factors is due to the uncertainty associated with the ground motions and that a relatively small number of sites that are representative of each soil class is sufficient to estimate the uncertainty on amplifications.

Site factors specified in design codes such as the NBCC are based exclusively on the average of the ratio of amplifications relative to site class C. The results obtained by simulation indicate that the prediction interval associated with amplifications that can be related to single events is quite large and that amplifications much larger than those specified in NBCC can be expected in practice. This observation is consistent with the large uncertainties reported in the literature when analysis amplifications observed empirically.

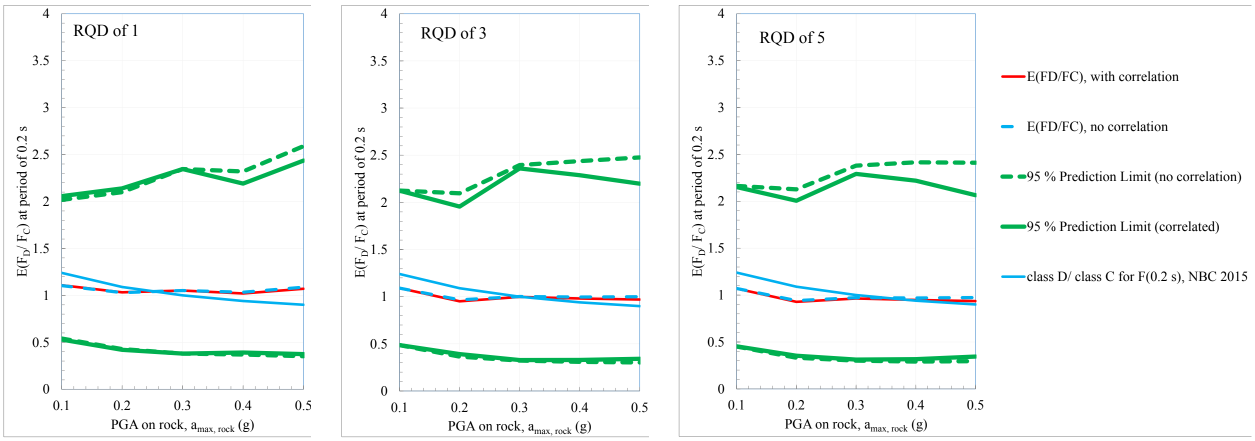

(a) (b) (c)

Figure 4.48: Comparison between $E(F_D/F_C)$ at T=0.2 s and the NBCC 2015 factor as a function of PGA for ground motions and non-randomized V_s profiles.

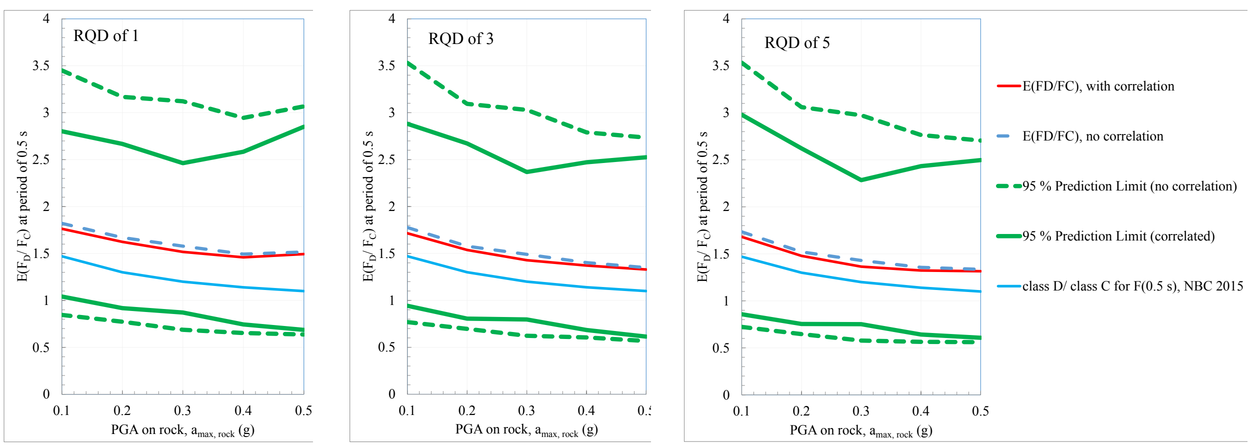

(a) (b) (c)

Figure 4.49: Comparison between $E(F_D/F_C)$ at T=0.5 s and the NBCC 2015 factor as a function of PGA for ground motions and non-randomized V_s profiles.

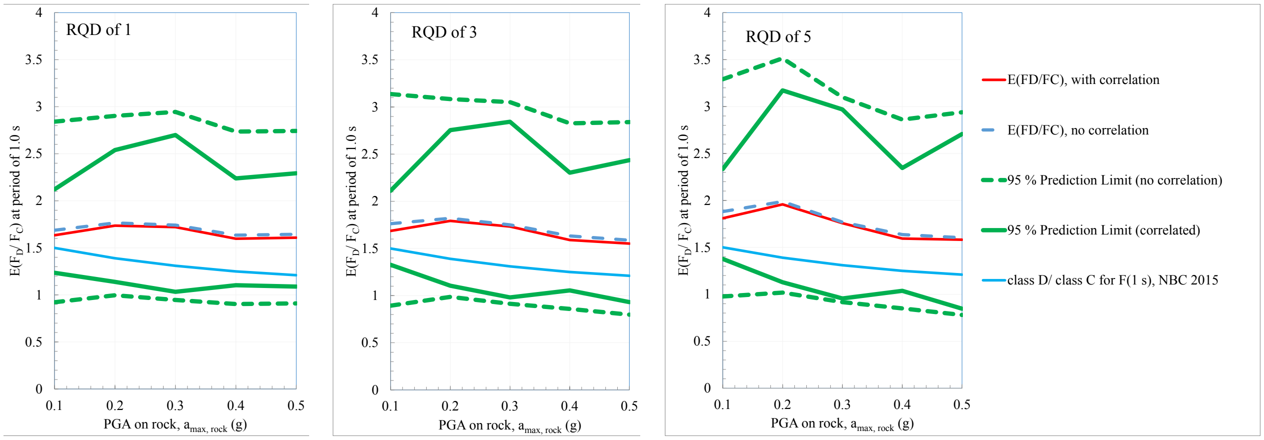

(a) (b) (c)

Figure 4.50: Comparison between $E(F_D/F_C)$ at T=1s and the NBCC 2015 factor as a function of PGA for ground motions and non-randomized V_s profiles.

4.18 Discussion and Conclusion

In this Chapter, a 1D model for the propagation of seismic ground motions to obtain site amplifications that are representative of conditions to be expected for site located in Eastern North America. Previous works by other researchers indicate that site effects can differ greatly for different regions of the world. Site effects that are incorporated in many design codes (e.g. NBCC) were derived from relations that are based mainly from data collected in the seismically active regions of Western North America. It is generally well known that characteristics of ground motions between Eastern and Western North America differ greatly and that the depositional environment for soft sediments differs also. Both effects may contribute to significant differences for sites with similar site classifications based solely on V_{s30}. This is especially true to eastern sites which are characterized by more pronounced impedance contrasts between bedrock and soft sediments and a prevalence of shallow soft soil deposits. This has led to the suggestion by several researchers that a classification based solely on V_{s30} may not be appropriate and may be, at the very least, complemented by other information such as the fundamental frequency of the site.

In this Chapter, numerical simulations were performed for a collection of soil profiles that would be classified as site class C and D using the V_{s30} criterion. Uncertainty in site responses was investigated by randomizing each of the soil profiles, the non-linear dynamic properties and by selecting a set of representative ground motions. Results are summarized such that they can be compared to site factors currently specified in the 2015 NBCC. For this purpose, amplifications were obtained for periods of 0.01s, 0.2s, 0.5 s and 1s and for ground motions scaled at 0.1 g, 0.2 g, 0.3 g, 0.4 g and 0.5 g. The results are presented for site classes based on the V_{s30} classification as well as a function of site fundamental frequency and site period. Data on seismic velocities in bedrock for Montreal indicate a strong correlation between the degree of defects in the rock (measured by the Rock Quality Designation) and shear wave velocity, which affects the impedance contrast. To analyze this effect, results are obtained for the full range of RQD (i.e.: 1, 3 and 5).

The results indicate that average site amplifications based on the V_{s30} classification are underestimated by the 2015 NBCC. This finding is consistent with results obtained for sites along the Eastern United States (e.g. South Carolina) and other regions of the world that exhibit similar characteristics (e.g. South Korea). The results also indicate that there are large uncertainties associated with site amplifications which are also consistent with the degree of uncertainty reported for empirically derived amplifications from seismic observations. These uncertainties are typically neglected when performing seismic hazard analyses which may lead to underestimation of damages.

Average site amplifications for PGA of 0.1 g is used to characterize linear site amplifications. For this level of ground motions, the results indicate that the average amplifications increase with RQD (or the impedance contrast). Another feature of the results is that the average amplifications do not monotonically decrease as a function of V_{s30} and indicate for some class D sites, average amplifications are smaller than for class C sites. Similar results have been reported in the recent literature of NGA-East for simulation results and cannot be disproved on the basis of incomplete and partially documented empirical data. Finally, the presentation of the results as a function of site fundamental frequency instead of V_{s30} can result in higher mean amplifications for some sites given the typical frequency content of ground motions in ENA. The results for ground motions scaled to increasing levels of PGA are presented in Appendix A. The results indicate similar trends as a function of RQD; however, with an increase of PGA, non-linear effects become more important, especially for softer soils, as exemplified by the de-amplifications observed for class D sites.

The amplification factors associated with each soil class spans a range of V_{s30} velocities (180 to 360 m/s for class D and 360 to 760 m/s for class C). This introduces some variability in amplifications which is illustrated by the histograms of Figures 4.24 to 4.28. Lognormal distributions are found to provide a good representation of these distributions and are used to estimate mean amplifications and their standard deviation. As before, results are also shown as a function of RQD to emphasize the effect of the contrast ratio on amplifications. One can note the large uncertainties associated with amplifications, especially when site classes are defined for a range of velocities.

Figures 4.29 to 4.31 compare amplifications as a function of V_{s30} to amplifications of NBCC (2015) and in some cases with mean amplifications from Kim and Yoon (2006) for Korean sites. Results are presented for periods of 0.2 s, 0.5 s and 1 s and for RQD of 1, 3 and 5. Results indicate that NBCC (2015) underestimates mean amplifications and that the best agreement corresponds to a RQD of 1 or lower impedance ratios. This result is consistent with the general observation that impedance ratios are smaller for western sites that form the basis for NBCC (2015). Good agreement is obtained with the results of Kim and Yoon (2006) which also indicate underestimation by NBCC (2015).

Figures 4.32 to 4.34 show the site factors for T = 0.2 s, 0.5 s and 1 s as a function of site period for records scaled at 0.1g for RQD of 1, 3 and 5 respectively. The factors are compared to site factors derived by Kim and Yoon (2006) for South Korea and to NBCC site factors. The site factors increase in general with site period and are larger for high impedance contrasts (RQD = 5). The results show best agreement with Kim and Yoon (2006) for the analyses performed with the lower RQDs of 1 and 3. For comparison purposes, the NBCC 2015 values are normalized relative to site factors for site class B (for RQD of 1) and for class A (for RQD of 3 and 5). Normalized factors are shown for both site classes C and D since there is no direct relation between site class and site fundamental period. In both cases, class C sites have characteristically lower periods than site class D sites. The results indicate good agreement with NBCC values for normalized C site factors at low periods and for normalized D site factors at high periods especially for RQD of 1 and 3. Site factors tend to be significantly higher than NBCC values for higher impedance contrasts (RQD = 5).

Appendix C provides complementary results for ground motion records scaled to 0.2, 0.3, 0.4 and 0.5 g and show similar tendencies but with lower site factors and better agreement with NBCC due to non-linear effects. Table 4.5 lists the major differences between the local geological conditions for site factors obtained from different sources. The table also lists the ground motions used to derive site factors for each source. Major differences are observed in ground motion characteristics between intraplate and plate-boundary locations. For the latter ground motions are dominated by frequency contents between 0.05 and 1.0 s while the former are characterized by frequency contents between 0.01s and 0.3s.

Table 4.5: Differences in geotechnical characteristics between the sites of Montreal and the sites analyzed in different publications.

Codes and literature	**Ground motions**	**Site class of input rock motion**	**Soil deposit thickness (m)**	**Range of site periods (s)**	**Existence of Leda clay (ɣ=16.5 kN/m^3)**
This study	WNA, CENA, Iran, Turkey, Europe, and Japan	A and B	10-33	0.14-0.65	Yes
NBCC 2015	World wide	B/C	6-200	0.4-2.0	No
Kim and Yoon (2006)	WNA, Taiwan, and Japan	A, B, C, and D	5-50	0.07-0.67	No
Darragh and Silva (2016)	CENA	A	8, 15, 30, 62, 153, and 305	-	No

Input ground motions used in EL 1D site response analyses in this study are for records obtained for rock sites corresponding to Class A and B. Results obtained by Kim and Yoon (2006) are obtained for a limited set of records (8), 2 of which are from stations with site class C and D. The small number of records and the selection of some on the records on site class C and D may contribute to their smaller site factors due differences in ground motion characteristics. It can be noted that local geological site conditions such as the bedrock depth and range of site periods observed at Montreal sites are similar to those of Kim and Yoon (2006).

Figure 4.35 compares the results (for RQD 5) with those of Darragh and Silva (2016) for shallow CENA soil class C and D sites (15 m and 30 m). The comparison of the results shows comparable trends for low periods (T= 0.01s and 0.2s): Amplifications for site class C sites are slightly higher than for site class D sites and the effect of deposit thickness appears to have little influence for the range of depths considered. For higher periods (T = 0.5 s and 1 s), site factors for site class D are higher than those for site class C and an increase in the thickness of the deposits increase the magnitude of the site factors. Results for a RQD of 5 were selected for the comparison since the rock velocities for this category is 2900 m/s which is similar to the velocity assumed in the CENA study (3000 m/s). The values of the CENA study are slightly smaller than those obtained with the current study which could be partially explained by the lower degree of damping for Leda clay and differences in shear wave velocity profiles (Figures 4.51 and 4.52). The soil profile for site class D sites in the CENA study is similar to the median profile for sites in Montreal. Conversely, the soil profile for class C sites in the CENA study is stiffer than all of the site C profiles used in this study which explains partially the higher site factors obtained due to a higher impedance ratio.

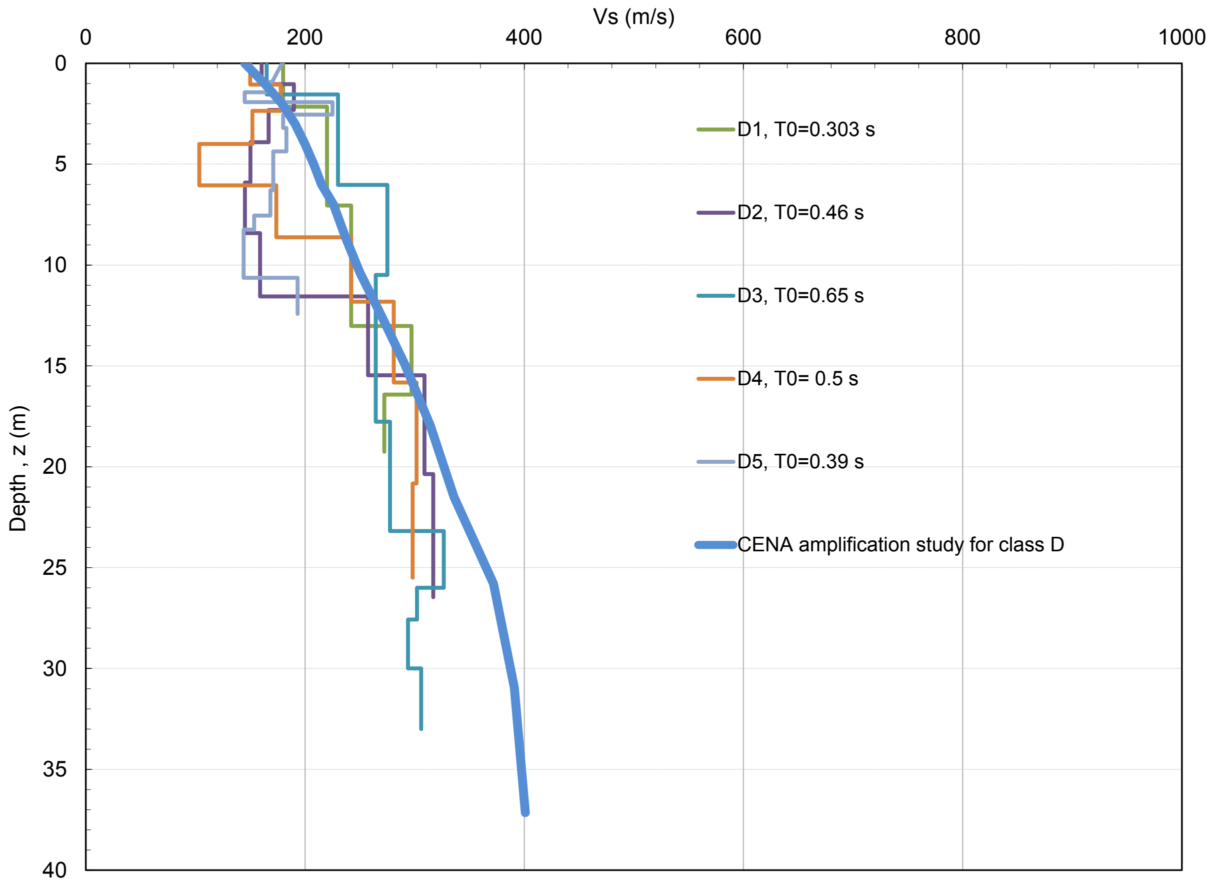

Figure 4.51: V_s profiles in class D sites in Montreal are compared with the V_s profile for the CENA amplification study. The periods of class D sites estimated by ambient noise measurements range from 0.303 s to 0.65 s.

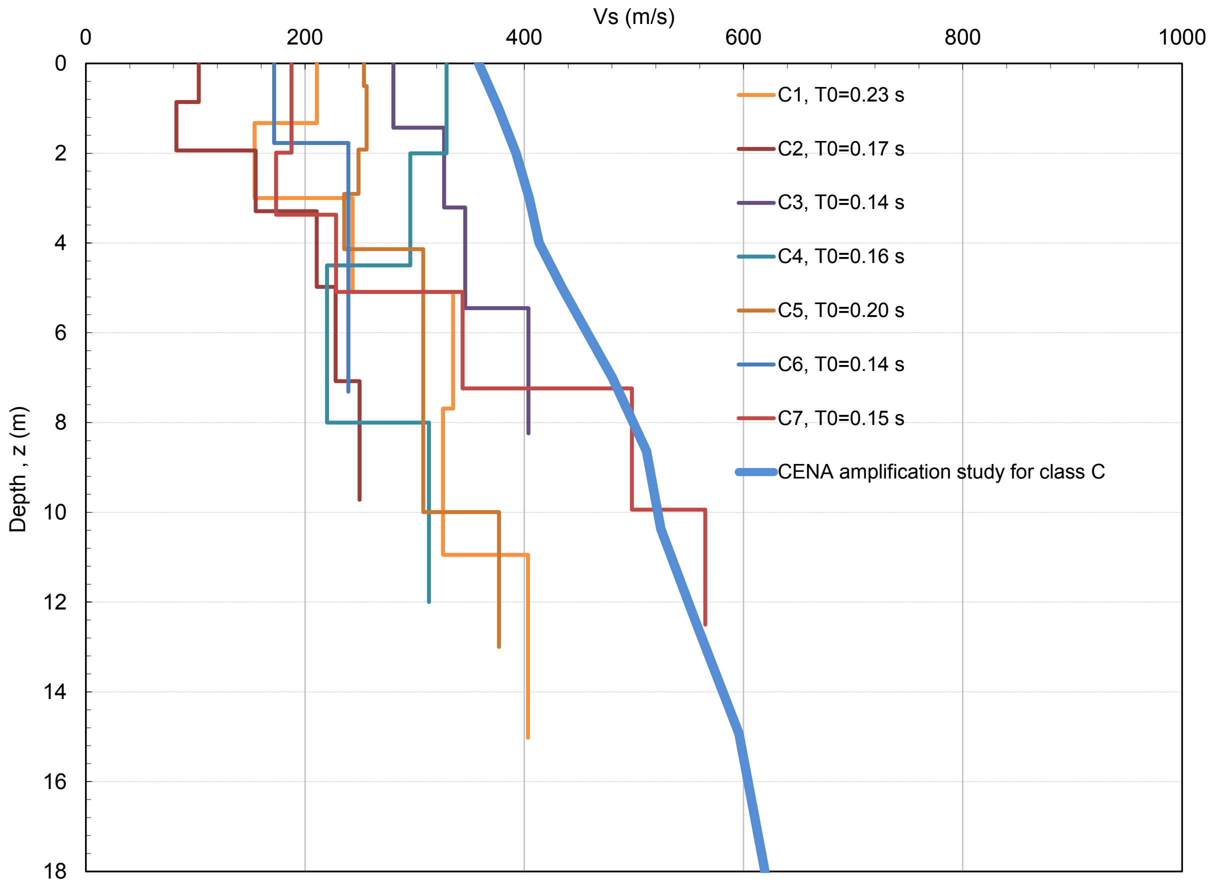

Figure 4.52: V_s profiles in class C sites in Montreal are compared with the V_s profile for the CENA amplification study. The periods of class C sites estimated by ambient noise measurements range from 0.14 s to 0.23 s.

Figures 4.40-50 compare the results of this study to the site factors in NBCC 2015. For the purpose of this comparison, site factors have been normalized relative to the site class C factors. In summary, the results indicate that the normalized factors are similar for low periods (T = 0.2 s) and that the results for this study are significantly larger for higher periods (T = 0.5s and 1s). The results also indicate that due to uncertainties in ground motions, soil profiles and non-linear dynamic properties, the uncertainty on the ratio of F_D/F_C can be large and that a wide range of site amplifications are to be expected for individual earthquake occurrences. Simulations are also performed to investigate the contribution of the various sources of uncertainty on the uncertainty of site factors. The conclusion from these simulations is that most of the uncertainty that is observed is mainly due to the variability of input ground motions. Once a set of representative profiles has been defined, performing additional site randomization profiles contributes marginally to the uncertainty. Similarly, randomization of non-linear soil properties contributes only marginally to the total uncertainty.

The 2015 NBCC site factors are largely derived from analyses performed by Choi and Stewart (2005). The analyses used 1828 recordings from 154 shallow crustal earthquakes and provide factors for NEHRP V_{s30} soil classes inferred from geotechnical data at 209 strong motion stations. Approximately 60 % of the sites have 60 to 200 m deep soil profiles with site periods between 0.80 and 2.0 s, and roughly 32 % of the sites with 6-60 m deep profiles with site periods between 0.40 and 0.80 s. This can be contrasted with the 12 sites considered in this study, 7 of them have 7-15 m soil profiles with site periods between 0.14-0.25 s, and 5 sites have 15-33 m soil profiles with site periods between 0.3-0.65 s. Therefore, the soil profiles in this study are relatively shallow (mostly less than 40 m in thickness) with site periods much shorter than those in Choi and Stewart (2005). Another notable difference is in the composition of the soil profiles, in Choi and Stewart (2005) only 5% of the 209 sites analysed have clay overlying bedrock comparatively to 40% of the sites in this study. Finally, Montreal sites also exhibit large impedance ratios which with the other factors contribute to relative greater site amplifications to those of Choi and Stewart (2005).

Kim and Yoon (2006) derived site factors using 162 site profiles in Korea. A total of 9 accelerograms from earthquakes including the 1979 Elcentro, 1995 Kobe, and 1999 Chi Chi earthquake were used to perform site response analyses. The sites have comparable periods to those of Montreal. Approximately 47 % of the sites analyzed are class C with 5.3 to 50 m soil profiles with site periods in the range of 0.14 to 0.23 s, and 37 % of the sites are class D with 10-47 m soil profiles with site periods between 0.24-0.67 s.

Earthquake ground motion amplifications for shallow bedrock sites which are typical of Montreal are evaluated for shear wave velocity profiles at 12 typical sites. At Montreal sites in class D, thickness of Leda clay is in the range of 20-30 m and the presence of Leda clay overlying hard bedrock (with rock quality designation index of 1 to 5) results in high impedance contrasts. For this reason, it is observed in this study that on average, the computed AF(0.5 s) and AF(1.0 s) for the Montreal sites in class D are greater than those calculated for the class C sites.

A parametric study was performed to analyze the uncertainties in the estimates of the site factors calculated by using different ground motion characteristics, PGA levels, rock quality designation, V_s profiles, and dynamic property curves. The computed F(0.2 s) versus T_0 (s) and also F(1.0 s) versus T_0 (s) functions for shallow deposits of Montreal are compared with the analyses for similar sites in Korea. The computed F(0.2 s) values are slightly greater than the same factor for sites in Korea, and the computed F(1.0 s) is almost the same as the F_v suggested for the Korean sites.

The study shows that ground motions can have a great influence on the correlation between the F_D and F_C calculated at all spectral periods. The correlation between the F_D and F_C calculated at periods of 0.2 s is not the same as those calculated for other periods of 0.5 s or 1.0 s. The correlation coefficients computed for determining the correlation between the $\ln F_D$ and $\ln F_C$ can change to a great extent when the intensity of PGA is increased from 0.1 to 0.5 g; and when the bed rock quality designation is increased from 1 to 5.

For the range of rock PGA of 0.1 to 0.5 g, the existing 2015 NBCC site factors for short as well as long periods are found to be within the 95 % prediction interval calculated for the mean F_D/F_C. The extent of 95 % prediction intervals for the mean F_D/F_C calculated at any periods depend on whether both the V_s profile and nonlinear dynamic properties are varied in the 1-D EL analyses. The calculated 95 % prediction intervals are largest when both the V_s profile and nonlinear dynamic properties are randomized in the 1-D EL analyses; but the prediction intervals are smaller when either the randomized V_s profiles or the randomized nonlinear curves for the dynamic properties are used in the 1-D EL runs. The prediction interval is smallest when the 1-D runs are performed with non-randomized V_s profiles and randomized nonlinear dynamic properties.

The parametric study shows that the impedance contrast between soil and rock interface is a major source of uncertainty in the amplification of the motions recorded on rock. In addition, variation in the frequency content of input rock motions from site to site, V_s profiles, the nonlinear relationship of G/G_{max} versus shear stain, and damping ratio versus shear strains are also important.

5 Conclusion

5.1 Seismic Microzonation of V_{s30}

Seismic microzonation provide essential information for the purpose of performing seismic hazard and seismic risk analyses. These analyses can be used to develop more effective earthquake preparedness strategies and identify optimal seismic mitigation measures. The current procedure for producing a seismic microzonation map is to identify soil site classes (A,B,.C,D and E) that are assigned to locations within a given region. The criteria for delimiting soil classes is set in the NBCC and is mainly based on V_{s30}, the mean shear wave velocity within the first 30 m from the surface.

To develop this map for Montreal, it was necessary to collect data available from various sources and to complement this information by performing multiple site surveys. Many of the latter were performed during the research for this thesis, as well as in collaboration with other researchers,

Current seismic microzonations assign a site class to a given location; however, this assignment may be based on incomplete information which is not acknowledged as a result of the analysis. When performed for a metropolitan area such as Montreal, the compilation of available data indicates that there are large discrepancies in the level of available information as a function of location. These spatial discrepancies can often be attributed to the density of the built environment and the differences in record keeping between boroughs. The sources of data used in this project are: 1) depth to bedrock from boreholes (~ 20,000), 2) stratigraphy from borehole data (~2,000), 3) fundamental periods from ambient noise analysis (~1,600), and 4) seismic surveys. A probabilistic procedure was developed to obtain probabilistic V_{s30} microzonation maps. First, models are developed to estimate V_{s30} as a function of the different sources of information: 1) A single layer model (SL) based only on depth to bedrock, 2) a multilayer model (ML) based only on boreholes with information on stratigraphy, and 3) a site fundamental frequency based model (F_0). Each model provides estimates of the average V_{s30} and its standard deviation at each site where information is available. A conditional second moment analysis is used to update the models and reduce uncertainty when data is available from multiple sources at a given site. The mean and standard deviation on V_{s30} is then used to develop probabilities for each soil class (A, B, C, D and E). The proposed probabilistic maps are an improvement over conventional seismic microzonations since they provide a probability of site classification instead of a single site category and integrate spatial information at a much smaller scale than previous mapping schemes. The probability maps can be readily integrated in seismic hazards and seismic risk analyses and also be used to target spatial areas to perform additional site surveys in order to reduce uncertainty and increase soil class probabilities. Soil classes are used in the NBCC (2010) to assign short period foundation factors (F_a) and long period foundation factor (F_v) to compute design spectral accelerations. The probabilistic site class maps are used to derive maps for the expected value and the coefficient of variation of both foundation factors for their use in seismic hazard and risk analyses.

5.2 Site Factors for Montreal for Seismic Design of Structures

Experience from past strong earthquakes indicates the strong relation between site conditions and damage level. The NBCC (2015) accounts for site effects through site factors as a function of site class. These factors are based mainly from analyses and observations from Western sites and may not reflect conditions that are prevalent in Eastern North America where ground motions are dominated by short period motions, shallow soft soil deposits and strong impedance ratios.

In this study site factors are computed at periods of 0.01 s, 0.2 s, 0.5 s and 1.0 s using typical shear wave velocity profiles for site class C and D in Montreal by performing equivalent linear site response analyses. Depth to bedrock of the selected sites ranges from 7 m to 33 m and cover the typical range of soft soil deposits on the island.

Uncertainties were considered in the analyses by randomizing the soil profiles, the non-linear dynamic properties of soils (clay, silt and till) and by selecting 20 ground motions that are representative of ground motions in Eastern North America. A good relationship was found between the rock quality designation and the rock shear wave velocity and was used to evaluate the effect of rock shear wave velocity on site factors. The analyses were performed for ground motions scales for PGA of 0.1g, 0.2g, 0.3g, 0.4g and 0.5g. The site factors: F(0.01 s), F(0.2 s), F(0.5 s) and F(1.0 s) are presented as a function of V_{s30} and compared to site factors from other regions that have similar ground motions and site characteristics. The results are also presented as a function of site fundamental frequency, which may be better site classification criteria for eastern North America sites. The calculated site factors for T=0.01, 0.2, 0.5 and 1.0 s show good agreement with those obtained for CENA sites. Site factors for this study are slightly higher and can be partially attributed to lower damping associated with Leda clay which is prevalent in Montreal.

The calculated site factors are found to be comparable to those obtained for South Korean sites which have similar site characteristics in terms of thickness of deposits. Good agreement is observed between the site factors F(0.2 s), F(0.5 s) and F(1.0 s) with those of NBCC (2015) for Rock Quality Designation of 1. The site factors are larger than those of NBCC (2015) for RQD of 3 and 5 due to the greater impedance contrast. The F_D/F_C ratio is in good agreement with the NBCC for T=0.2 s for all 3 RQD factors of 1, 3 and 5. As for T=0.5 and 1.0 s, the F_D / F_C ratio is observed to be greater than the NBCC values. Coefficients of correlation between amplifications of lnF_D and lnF_C for T=0.2, 0.5 and 1.0 s are obtained from the 1-D simulations for each of the 20 ground motions. Positive correlations between amplifications of lnF_D and lnF_C are observed. The 95 % prediction intervals on the mean amplifications of F_D/F_C that are calculated with correlation coefficients for PGA of 0.1 to 0.5 g are seen to be smaller than the 95 % prediction intervals calculated without the correlation coefficients. Due to the positive correlations between the mean amplifications, the mean estimate of F_D/F_C is seen slightly smaller than that calculated without the correlations coefficients.

5.3 Original Contributions

This Thesis brings the following original contributions to the advancement of the study of seismic hazards:

- This study first obtains estimates of V_{s30} based on seismic surveys ($Vs30_{SS}$) at 26 sites to obtain estimates of the average and variance of V_{s30} for soft soil deposits in Montreal. The data base is complemented by data on seismic surveys for rock formations in Montreal. Based on the analysis of this data, a relation is proposed between rock shear wave velocity and the rock quality designation (RQD).
- The seismic data is used to develop a depth velocity relation for Montreal which in turn is used to obtain V_{s30} estimates as a function of depth to bedrock. The relation is used to estimate the mean and standard deviation ofV_{s30} ($Vs30_{SL}$) for a compilation of 26000 borehole where only depth to bedrock is known. The estimates are used to develop a first

seismic microzonation map given depth to bedrock providing the probability distribution of soil site classes: A, B, C and D as a function of location (Figure 3.11). A very detailed map is obtained due to the large number of boreholes down to bedrock but with large uncertainties on site classification.

- The seismic data is also used to develop depth-velocity relations for sand, silt, clay and till deposits for Montreal. The relations are used to estimate the mean and standard deviation of V_{s30} ($Vs30_{ML}$) at about 2000 boreholes where stratigraphy down to bedrock is known. The estimates are used to develop a second seismic microzonation map providing the probability distribution of soil site classes: A, B, C, and D as a function of location (Figure 3.12). A less spatially detailed but more precise map is obtained.
- The seismic data is also used to develop a relationship between the fundamental frequency of a site and V_{s30}. Estimates for the mean and standard deviation of $Vs30_{F0}$ are obtained at about 1600 locations where site frequency (F_0) was measured using ambient noise. Measurements were performed at locations where borehole data was available in order to investigate the relation between estimates of V_{s30} using different techniques, but also to cover regions where no data was available. The estimates are used to develop a third seismic microzonation map providing the probability distribution of soil site classes: A, B, C and D as a function of location (Figure 3.13). As before, a less spatially detailed but more precise map is obtained.
- Using the conditional second moment method, a probabilistic procedure (Equations 3.12 to 3.15, Chapter 3) was developed to combine and update estimates when data is obtained from various sources to reduce uncertainty on V_{s30}. Figure 3.14 illustrates the procedure and resulting probabilistic microzonation for sites where both the fundamental frequency and detailed borehole data are available.
- Finally, a microzonation that combines all data from available sources is proposed (Figure 3.16 to 3.17) which comprises data from the 26 locations of seismic surveys, 11000 estimates based on depth to bedrock, 400 based on detailed borehole data, and 1600 estimates based both on borehole data and the fundamental frequency.
- Using the total probability rule and the probabilistic microzonation, a procedure is developed to obtain estimate for the mean and standard deviation of the short and long period foundation design factors F_a and F_v of NBCC 2010.

- The resulting F_a and F_v maps (Figure 3.18) can be used in reliability analyses to account for the uncertainty site class and to target regions in Montreal where additional seismic surveys can be performed to reduce the level of uncertainty.
- Site response analyses were performed using samples of representative soil profiles for site classes C and D in Montreal. Design peak acceleration on soft soil sites in Montreal can be estimated using the proposed relationship for F(0.01 s) versus V_{s30} and F(0.01 s) versus site fundamental frequency F_0 for ground motions scaled to PGA of 0.1, 0.2, 0.3, 0.4 and 0.5 g and for RQD of 1, 3 and 5.
- Site factors are obtained at periods of T=0.2, 0.5 and 1.0 s for class C and D sites as a function V_{s30} for ground motion records scaled for a range of PGA from 0.1 to 0.5 g for Rock Quality Designations of 1 (mean V_s=1258 m/s), 3 (mean V_s=2082 m/s) and 5 (mean V_s= 2926 m/s).
- Values of site factors for T=0.2, 0.5 and 1.0 s sites are proposed as a function of site period for PGA scaled from 0.1 to 0.5 g for Rock Quality Designation of 1 , 3 and 5 .
- The results are also derived as the ratio of (F_D/F_C) for T=0.2, 0.5 and 1.0 s as a function of PGA for RQD of 1, 3 and 5 in a format similar to the one found in the 2015 NBCC.
- The 95 % prediction intervals on the mean amplifications of F_D/F_C are determined using the correlation between $\ln F_D$ and $\ln F_C$ due to ground motions.

5.4 Recommendations for future Research:

The study is based on a limited amount of data and it would be important to continue performing seismic surveys to obtain additional shear wave velocity profiles in the greater Montreal area. There is also a need to obtain more data on dynamic properties of tills and bedrock and information on the location of the different tills, rock types and rock quality.

There are few laboratory test results on the dynamic properties of Leda clay. More tests should be performed to determine its dynamic properties.

The current study did not address the potential for liquefaction of sand deposits. Soil parameters-void ratio, relative density, grain size distribution including hydrometer analysis and SPT values should be obtained for as many sites as possible. Sites located along the shorelines and the north tip of the Island of Montreal should be considered for liquefaction potential analyses.

The results of the simulations indicate that the uncertainties on site amplifications are large and are of the same order of magnitude of those observed empirically. The uncertainties on site factors are not considered in building codes and those that are provided correspond to mean values. It may be important in future studies to investigate the effect of uncertainties in site factors on seismic hazards and seismic risk analyses since fragility functions are not symmetric in relation to mean ground motions. The analysis performed on Fa and Fv could be updated using the new site factors defined through this research.

6 References

Aboye, S. A., Andrus, R. D., Ravichandran, N., Bhuiyan, A. H., and Harman, N. E. (2013). Amplitude- and VS30-based Seismic Site Factor Model for Myrtle Beach, South Carolina. *7th National Seismic Conference on Bridges and Highways, Multidisciplinary*

Aboye, S. A., Andrus, R. D., Ravichandran, N., Bhuiyana, A. H., and Harman, N. (2015). Seismic Site Factors and Design Response Spectra Based on Conditions in Charleston, South Carolina. *Earthquake Specrta, 31*(2), 723-744.

Adams, J., and Atkinson, G. (2003). Development of seismic hazard maps for the proposed 2005 edition of the National Building Code of Canada. *Canadian Journal of Civil Engineering, 30*(Compendex), 255-271.

Adams, J., and Halchuk, S. (2007). A review of NBCC 2005 seismic hazard results for Canada-the interface to the ground and prognosis for urban risk. *Geological Survey of Canada, Natural Resources Canada, 7 Observatory,Geological Survey of Canada, Natural Resources Canada, 7 Observatory*, 837-846.

Andrus, R. D., Fairbanks, C. D., Zhang, J., Camp Iii, W. M., Casey, T. J., Cleary, T. J., and Wright, W. B. (2006). Shear-wave velocity and seismic response of near-surface sediments in Charleston, South Carolina. *Bulletin of the Seismological Society of America, 96*(5), 1897-1914.

Ansal, A., Kurtulus, A., and Tonuk, G. (2010). Seismic microzonation and earthquake damage scenarios for urban areas. *Soil Dynamics and Earthquake Engineering, 30*(11), 1319-1328.

Ansal, A., T¨on¨uk, G. o. e., and Kurtulus, A. (2009). Microzonation for Urban Planning *Earthquakes and Tsunamis, Civil engineering disaster mitigation activities implementing millennium development goals* (Vol. 11, pp. 133-152). Turkey: Springer, ©2009.

Atkinson, G. M. (2008). Ground-motion prediction equations for Eastern North America from a referenced empirical approach: Implications for epistemic uncertainty. *Bulletin of the Seismological Society of America, 98*(Compendex), 1304-1318.

Atkinson, G. M. (2009). Earthquake time histories compatible with the 2005 National building code of Canada uniform hazard spectrum. *Canadian Journal of Civil Engineering, 36*(Compendex), 991-1000.

Atkinson, G. M., and Boore, D. M. (1995). Ground-Motion Relations for Eastern North America. *Bulletin of the Seismological Society of America, 85*(1), 17-30.

Banab, K. K., Kolaj, M., Motazedian, D., Sivathayalan, S., Hunter, J. A., Crow, H. L., Pugin, A. J. M., Brooks, G. R., and Pyne, M. (2013). Seismic Site Response Analysis for Ottawa, Canada: A Comprehensive Study Using Measurements and Numerical Simulations. *Seismological Research Letters, the Seismological Society of America, 86*(460-476).

Bauer, R. A. (2007). Shear Wave Velocity, Geology and Geotechnical Data of Earth Materials in the Central U.S. Urban Hazard Mapping Areas. *Final Technical Report, U.S. Geological Survey, National Earthquake Hazards Reduction Program*.

Benjumea, B., Hunter, J. A., Pullan, S. E., Brooks, G. R., Pyne, M., and Aylsworth, J. M. (2008). Vs30 and Fundamental Site Period Estimates in Soft Sediments of the Ottawa Valley from Near-Surface Geophysical Measurements. *J ENVIRON ENG GEOPHYS, 13*(4), 313-323. doi: 10.2113/jeeg13.4.313

Bommer, J., and Acevedo, A. B. (2004). The use of real earthquake accelerograms as input to dynamic analysis. *Journnla of Earthquake Engineering, 8*(1), 43-91.

Borcherdt, R. D. (1994). Estimates of Site-Dependent Response Spectra for Design (Methodology and Justification). *Earthquake Spectra, 10*(4).

Borcherdt, R. D., and Glassmoyer, G. (1992). On the characteristics of local geology and their influence on ground motions generated by the Loma Prieta earthquake in the San Francisco Bay region, California,. *Bulletin of Seismological Society of America, 82*, 603-641.

Boyer, L. (1985). Geology of Montreal, Province of Quebec, Canada.

Cao, Y. L., Rainer, J. H., and Chidiac, S. E. (1992). Etudes sismiques au poste port-alfred region du saguenay. *National Research Council Canada Report to Hydro-Quebec, 1*, 1-113.

Castellaro, S., and Mulargia, F. (2009). Vs30 Estimates Using Constrained H/V Measurements. *Bulletin of the Seismological Society of America, 99*(2A), 761-773.

Choi, Y., and Stewart, J. P. (2005). Nonlinear Site Amplification as Function of 30 m Shear Wave Velocity. *Earthquake Spectra, 21*(1), 1-30. doi: 10.1193/1.1856535

Chouinard, L., and Rosset, P. (2007). Seismic site effects and seismic risk in the Montreal urban area. The influence of marine clays. *Proceedings of the Ninth Canadian conference on earthquake engineering, Ottawa, Ontario, Canada, 26–29.*

Chouinard, L., and Rosset, P. (2011). Microzonation of Montreal, Variability in Soil Classification. *4th IASPEI / IAEE International Symposium, University of California Santa Barbara*.

Chouinard, L., Rosset, P., Puente, A. D. L., Madriz, R., Mitchell, D., and ADAMS, J. (2004). Seismic hazard analyses for Montreal. *13th World Conference on Earthquake Engineering,Vancouver, B.C., Canada.*(7010).

Cox, B. R., Bachhuber, J., Rathje, E., Wood, C. M., Dulberg, R., Kottke, A., Green, R. A., and Olson, S. M. (2011). Shear wave velocity- and geology-based seismic microzonation of port-au-prince, Haiti. *Earthquake Spectra, 27*(SUPPL. 1), S67-S92. doi: 10.1193/1.3630226

Darendeli, M. B. (2001). Development of a new family of normalized modulus reduction and material damping curves. *Ph.D. Thesis, The University of Texas at Austin*.

Darragh, B., and Silva, W. (2016). Development of Amplification Factors (5% Damped Response Spectra) For NEHRP Categories in CENA. *Conference Call on Seismic Site Amplification in Central and Eastern North America, PEER, Berkeley, Ca*.

Deere, D. E., and Deere, W. D. (1988). The Rock Quality Designation Index in Practice. *Rock Classification Systems for Engineering Purposes, American Society for Testing and Materials, ASTM STP 984*, 91-101.

Ditlevsen, O., and Madsen, H. (1996). Structural Reliability Methods. *John Wiley & Sons, New York*.

Dobry, R., Borcherdt, R. D., Crouse, C. B., Idriss, I. M., Joyner, W. B., Martin, G. R., Power, M. S., Rinne, E. E., and Seed, R. B. (2000). New Site Coefficients and Site Classification System Used in Recent Building Seismic Code Provisions. *Earthquake Spectra, 16*(1), 41-67. doi: 10.1193/1.1586082

Dobry, R., Marti, G. R., Pain, E., and Bhattacharyya, A. (1994). Development of Site-dependent ratios of Elastic Resposne Spectra (RRS).

EPRI, E. P. R. I. (1993). Guidelines for determining design basis ground motions. *Report TR-102293, Palo Alto, CA,, 2*

ESRI. (2010). ArcMap 10.1 *ESRI (Environmental Systems Resource Institute), Redlands, California.*

Finn, W. D. L., and Adrian, W. (2003). Ground motion amplification factors for the proposed 2005 edition of the National Building Code of Canada. *Canadian Journal of Civil Engineering, 30*(2), 272-278.

Finn, W. D. L., and Wightman, A. (2003). Ground motion amplification factors for the proposed 2005 edition of the National Building Code of Canada. *Can. J. Civ. Eng., 30*, 30: 272–278 (2003).

Goulet, C. A., and Stewart, J. P. (2009). Pitfalls of Deterministic Application of Nonlinear Site Factors in Probabilistic Assessment of Ground Motions. *Earthquake Spectra, 25*(3), 541-555. doi: doi:10.1193/1.3159006

Halchuk, S., Adams, J., and Anglin, F. (2007). Revised Deaggregation of Seismic Hazard for Selected Canadian Cities. *Ninth Canadian Conference on Earthquake Engineering and Structural Dynamics, Ottawa, Ontario, Canada*, 420-432.

Hashash, Y., and Moon, S. (2011). Site amplification factors for deep deposits and their application in seismic hazard analysis for Central U.S. *USGS. USGS/NEHRP Grant: G09AP00123: 91 pages*.

Hashash, Y. M. A., Abrahamson, N. A., Olson, S. M., Hague, S., and Kim, B. (2013). Conditional Mean Spectra in Site-Specific Seismic Hazard Evaluation for a Major River Crossing in the Central U.S. *Earthquake Spectra*. doi: 10.1193/033113EQS085M

Hashash, Y. M. A., and Park, D. (2001). Non-linear one-dimensional seismic ground motion propagation in the Mississippi embayment. *Engineering Geology, 62*(2001), 185-206.

Hines, E. M., Baise, L. G., and Swift, S. S. (2011). Ground-Motion Suite Selection for Eastern North America. *Journal of Structural Engineering, ASCE, 137*(3).

Holzer, T. L., C, A. C. P. A., Bennett, M. J., Noce, T. E., and III, J. C. T. (2005). Mapping NEHRP Vs(30) site classes. *Earthquake Spectra, 21*(2), 1-18.

Humar, J., Adams, J., Tremblay, R., Rogers, C. A., and Halchuk, S. (2010). Poposals for the seismic design provisions of the 2010 national building code of canada. *Proceedings of the 9th U.S. National and 10th Canadian Conference on Earthquake Engineering,Toronto, Ontario, Canada*.

Hunter, J. A., and Crow, H. L. (2012). Shear Wave Velocity Measurement Guidelines for Canadian Seismic Site Characterization in Soil and Rock. *Geological Survey of Canada, Open File 7078*. doi: 10.4095/291753

Hunter, J. A., Crow, H. L., Brooks, G. R., Pyne, M., Motazedian, D., Lamontagne, M., Pugin, A. J.-M., Pullan, S. E., Cartwright, T., Douma, M., Burns, R. A., Good, R. L., Kaheshi-Banab, K., Caron, R., Kolaj, M., Folahan, I., Dixon, L., Dion, K., Duxbury, A., Landriault, A., et al. (2010). Seismic site classification and site period mapping in the Ottawa area using geophysical methods. *Geological Survey of Canada, Open File 6273*.

Kamai, R., Abrahamson, N. A., and Silva, W. J. (2013). Nonlinear Horizontal Site Response for the NGA-West2 Project. *Pacific Earthquake Engineering Research Center*(PEER 2013/12).

Kamai, R., Abrahamson, N. A., and Silva, W. J. (2014). Nonlinear Horizontal Site Amplification for Constraining the NGA-West2 GMPEs. *Earthquake Spectra, 30*(3), 1223–1240.

Kilic, H., Ozener, P. T., Ansal, A., Yildirim, M., Ozaydin, K., and Adatepe, S. (2006). Microzonation of Zeytinburnu region with respect to soil amplification: A case study. *Engineering Geology, 86*(4), 238-255.

Kim, D. s., and Yoon, J. K. (2006). Development of new site classification system for the regions of shallow bedrock in Korea. *Journal of Earthquake Engineering, Vol. 10*(No. 03).

Kishida, T., Boulanger, R. W., Abrahamson, N. A., Driller, M. W., and Wehling, T. M. (2009). Site effects for the Sacramento-San Joaquin Delta. *Earthquake Spectra, 25*(2), 301-322. doi: 10.1193/1.3111087

Kottke, A. R., and Rathje, E. M. (2010). Technical Manual for Strata. *PEER 2008/10*.

Kramer, S. L. (1996). *Geotechnical Earthquake Engineering*: Prentice Hall,ISBN-10 0133749436.

Lamontagne, M. (2009). Description and analysis of the earthquake damage in the quebec city region between 1608 and 2008. *Seismological Research Letters, 80*(3), 514-524.

Lamontagne, M., Keating, P., and Toutin, T. (2000). Complex Faulting Confounds Earthquake Research in the Charlevoix Seismic Zone, Quebec. *Transactions, American Geophysical Union, 81*(26).

Luzi, L., Puglia, R., Russo, E., and ORFEUS, W. (2016). Engineering Strong Motion Database, version 1.0. *Istituto Nazionale di Geofisica e Vulcanologia, Observatories & Research Facilities for European Seismology*. doi:10.13127/ESM

Mitchell, D., Tinawi, R., and Law, T. (1990). Damage caused by the November 25, 1988, Saguenay earthquake. *Canadian Journal of Civil Engineering, 17*(3), 338-365.

Motazedian, D., Hunter, J. A., Pugin, A., and Crow, H. (2011). Development of a Vs30 (NEHRP) map for the city of Ottawa, Ontario, Canada. *Canadian geotechnical journal, 48*(3), 458-472. doi: doi:10.1139/T10-081

Nastev, M., Lin, L., Naumoski, N., Perret, D., Parent, M., and Lamarche, L. (2008). Effects of soil behaviour modelling on the seismic response of representative soils in the quebec city region. *Annual Conference of the Canadian Society for Civil Engineering*(36th).

Papaspiliou, M., Kontoe, S., and Bommer, J. J. (2012a). An exploration of incorporating site response into PSHAPart I: Issues related to site response analysis methods. *SDEE Soil Dynamics and Earthquake Engineering, 42*, 302-315.

Papaspiliou, M., Kontoe, S., and Bommer, J. J. (2012b). An exploration of incorporating site response into PSHA-part II: Sensitivity of hazard estimates to site response approaches. *Soil Dynamics and Earthquake Engineering, 42*(0), 316-330.

Park, D., and Hashash, Y. M. A. (2005). Evaluation of seismic site factors in the Mississippi Embayment. I. Estimation of dynamic properties. *Soil Dynamics and Earthquake Engineering, 25*(2), 133-144.

Perret, D., Desgagnés, P., and Pelletier, S. (2013). A critical appraisal of some r_d relationships for liquefaction analyses in Eastern Canada with the simplified procedure. *Conference of GeoMotreal 2013, Monreal, Quebec, Canada.*

Pitilakis, K., Riga, E., and Anastasiadis, A. (2013). New code site classification, amplification factors and normalized response spectra based on a worldwide ground-motion database. *Bulletin of Earthquake Engineering, 11*(4), 925-966.

Prest, V. K., and Hode-Keyser, J. (1977). Geology and engineering characteristics of surficial deposits, Montreal Island and Vicinity, Quebec. *Geological Survey of Canada, Ottawa, Energy, Mines and Resources Canada.*

Quinn, P. E., Diederichs, M. S., Rowe, R. K., and Hutchinson, D. J. (2012). Development of progressive failure in sensitive clay slopes. *Can. Geotech. J., 49*, 782-795.

Rasmussen, K. K. (2012). An investigation of monotonic and cyclic behavior of leda clay. *Master's Thesis,The University of Western Ontario, Canada.*

Rathje, E. M., Kottke, A. R., and Trent, W. L. (2010). Influence of input motion and site property variabilities on seismic site response analysis. *Journal of Geotechnical and Geoenvironmental Engineering, 136*(Compendex), 607-619.

Rodriguez-Marek, A., Bray, J. D., and Abrahamson, N. A. (2001). An empirical geotechnical seismic site response procedure. *Earthquake Spectra* *17*(1), 65–87.

Rosenblueth, E. (1975). Point estimates for probability moment. *Proceedings National Academy of Science, 72*(10), 3812-3814.

Rosenblueth, E. (1981). Two point estimates in probabilities. *Applied Mathematical Modelling, 5*(2), 329-335.

Rosset, P., Bour-Belvaux, M., and Chouinard, L. (2014). Microzonation models for Montreal with respect to V_{s30}. *Bulletin of Earthquake Engineering, 13*, 2225–2239.

Rosset, P., and Chouinard, L. E. (2009). Characterization of site effects in Montreal. *Canada. Nat Hazards, 48*, 295-308.

Seed, H. B., and Idriss, I. M. (1970). Soil moduli and damping factors for dynamic response analyses. *Earthquake Engineering Research, Center, University of California, Berkeley, UCB/EERC-70/10*.

Seed, H. B., and Idriss, I. M. (1971). Simplified procedure for evaluating soil liquefaction potential. *J Soil Mech Found Div, 97*, 1249-1273.

Seed, H. B., Wong, T. R., Idriss, I. M., and Tokimatsu, K. (1986). Moduli and damping factors for dynamic analyses of cohesionless soils. *Journal of Geotechnical Engineering, ASCE, 112*(11), 1016-1032.

Seed, R. B., Dickenson, S. E., and Man Mok, C. (1994). *Site effects on strong shaking and seismic risk: recent developments and their impact on seismic design codes and practice*, Atlanta, GA, USA.

Silva, W. J., Abrahamson, N., Toro, G., and Costantino, C. (1996). Description and validation of the stochastic ground motion model. *Brookhaven National Laboratory, Associated Universities Inc., Upton, New York 11973*.

Stewart, J. P., Kwok, A. O.-L., Hashash, Y. M. A., Matasovic, N., Pyke, R., Wang, Z., and Yang, Z. (2008). Benchmarking of Nonlinear Geotechnical Ground Response Analysis Procedures. *Pacific Earthquake Engineering Research Center, Berkeley.*

Sun, J. I., Golesorkhi, R., and Seed, H. B. (1988). Dynamic Moduli and Damping Ratios For Cohesive Soils. *Earthquake Engineering Research Center, University of California at Berkeley, Report No UCB/EERC-88/15*.

Talukder, M. K., and Chouinard, L. (2016). Probabilistic Methods for the Estimation of Seismic F_a and F_v Maps - Application to Montreal. *Bulletin of Earthquake Engineering, 14*(2), 345-372. doi: 10.1007/s10518-015-9832-0

Thompson, E. M., Baise, L. G., and Kayen, R. E. (2007). Spatial correlation of shear-wave velocity in the San Francisco Bay Area sediments. *Soil Dynamics and Earthquake Engineering, 27*(2), 144-152.

Wald, D. J., McWhirter, L., Thompson, E., and Hering, A. S. (2011). A New Strategy For Developing Vs30 Maps. *4th IASPEI / IAEE International Symposium, University of Santa Barbara, USA: Effects of Surface Geology on Seismic Motion*.

Wills, C. J., and Clahan, K. B. (2006). Developing a Map of Geologically Defined Site-Condition Categories for California. *Bulletin of the Seismological Society of America, 96*(4A), 1483-1501. doi: 10.1785/0120050179

Wills, C. J., Petersen, M., Bryant, W. A., Reichle, M., Saucedo, G. J., Tan, S., Taylor, G., and Treiman, J. (2000a). A site-conditions map for California based on geology and shear-wave velocity. *Bull Seismol Soc Am, 9*(6B), S187–S208.

Wills, C. J., Petersen, M., Bryant, W. A., Reichle, M., Saucedo, G. J., Tan, S., Taylor, G., and Treiman, J. (2000b). A site-conditions map for California based on geology and shear-wave velocity. *Bulletin of the Seismological Society of America, 90*(6B), S187–S208.

Wills, C. J., and Silva, W. (1998). Shear-wave velocity characteristics of geologic units in California. *Earthquake Spectra, 14*(3), 533-556.

Zhai, E. (2008). *Developing site-specific design response spectra for a type F site due to liquefaction.* Paper presented at the Geotechnical Earthquake Engineering and Soil Dynamics IV Congress 2008 - Geotechnical Earthquake Engineering and Soil Dynamics, May 18, 2008 - May 22, 2008, Sacramento, CA, United states.

Zhang, J., Andrus, R. D., and Juang, C. H. (2005). Normalized Shear Modulus and Material Damping Ratio Relationships. *Journal of Geotechnical and Geoenvironmental Engineering, 131*(4), 453-464.

7 Appendix A

Figures for F(0.01 s) as a function of V_{s30} Relation and site fundamental frequencies for PGA 0.2 g to 0.5 g.

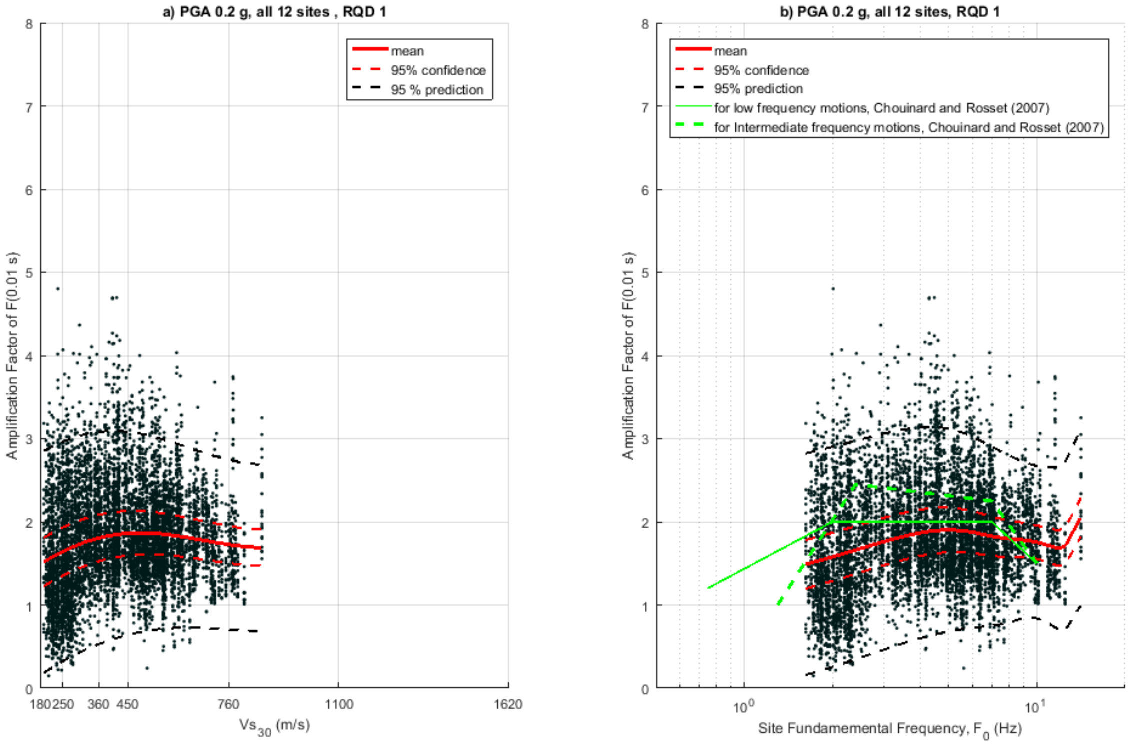

Figure 7.1: RQD 1 and PGA 0.2 g: a) relation between F(0.01 s) and V_{s30}, b) relation between F(0.01 s) and site fundamental frequency F_0 for randomized V_s profiles and randomized nonlinear shear modulus-damping curve.

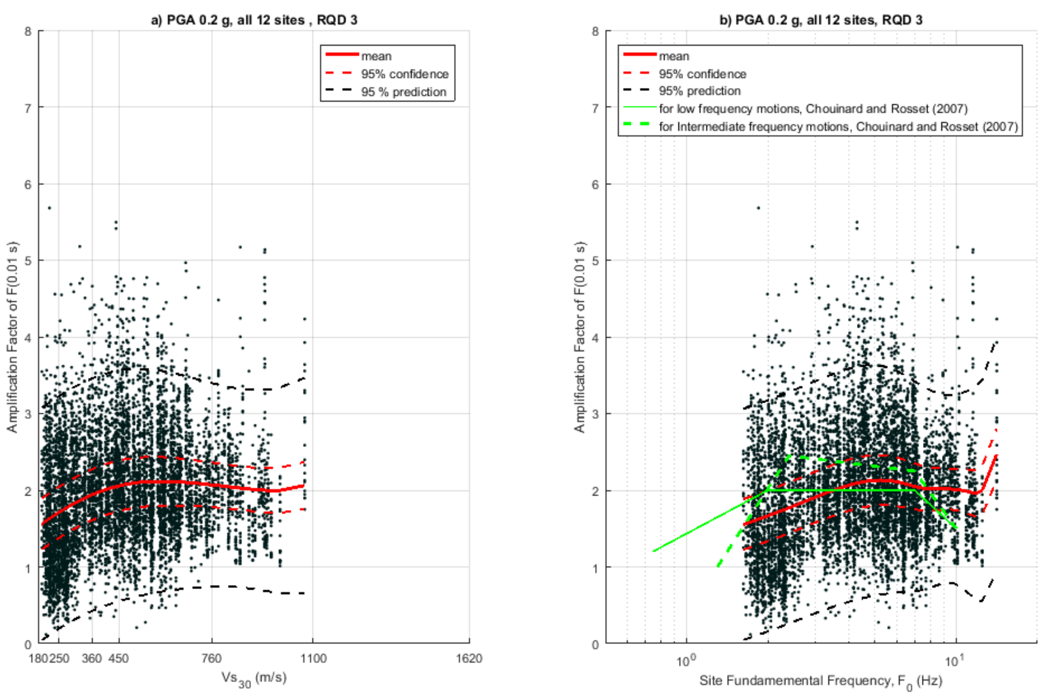

Figure 7.2: RQD 3 and PGA 0.2 g: a) relation between F(0.01 s) and V_{s3}, b) relation between F(0.01 s) and site fundamental frequency F_0 for randomized V_s profiles and randomized nonlinear shear modulus-damping curve.

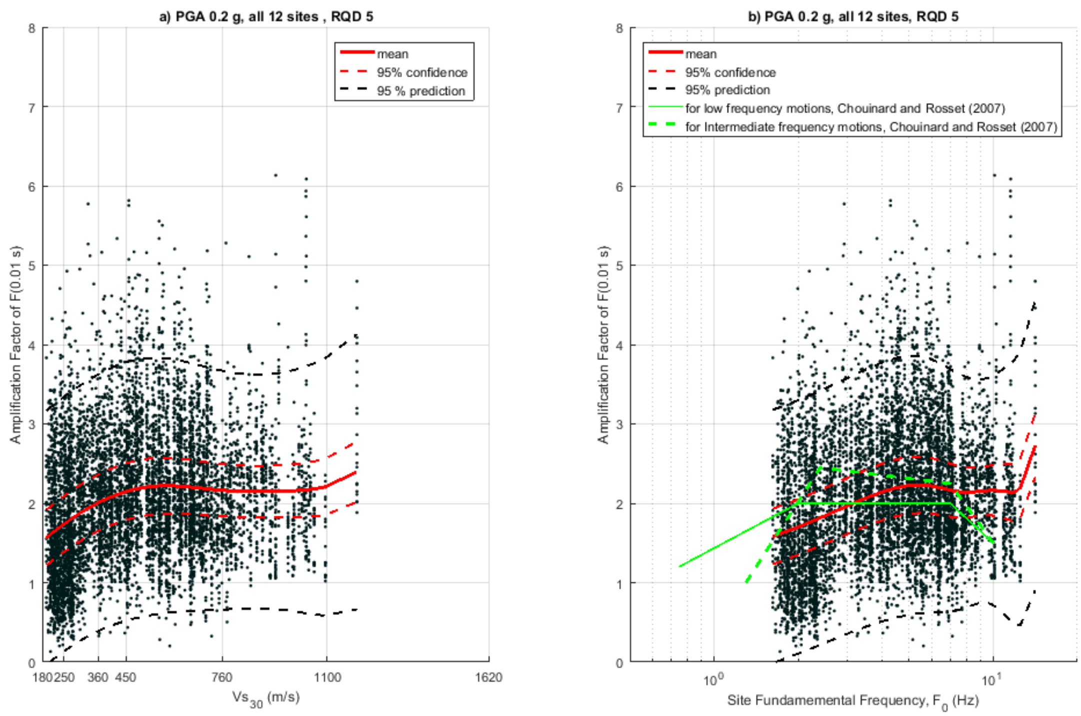

Figure 7.3: RQD 5 and PGA 0.2 g: a) relation between F(0.01 s) and V_{s30}, b) relation between F(0.01 s) and site fundamental frequency F_0 for randomized $V_s$profiles and randomized nonlinear shear modulus-damping curve.

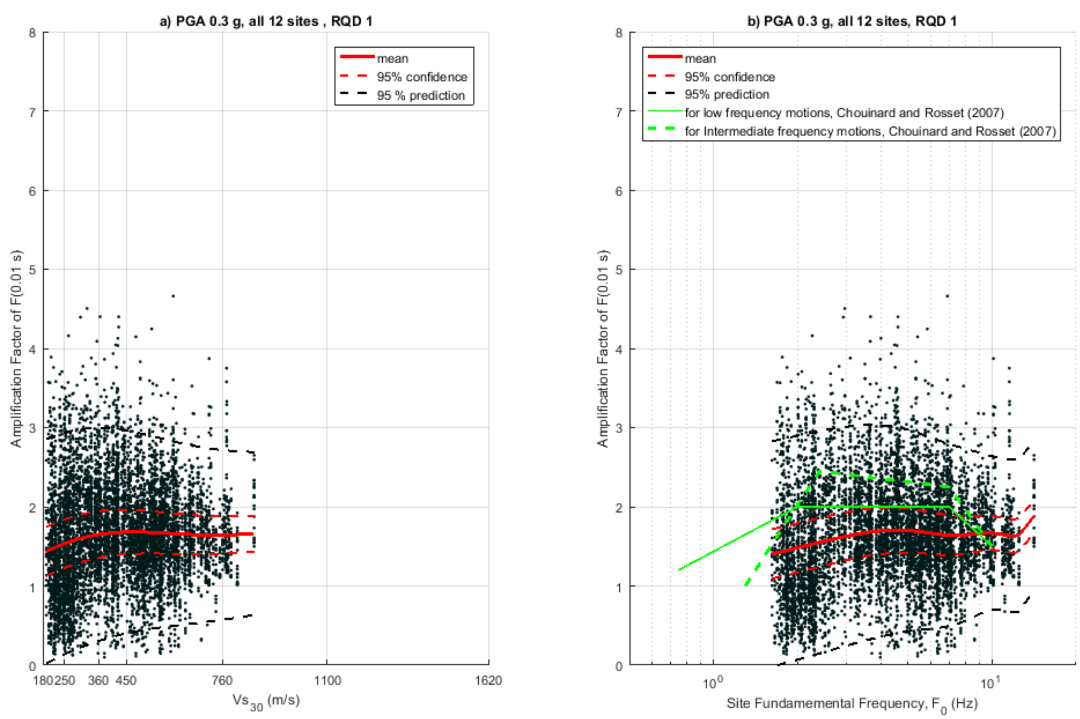

Figure 7.4: RQD 1 and PGA 0.3 g: a) relation between F(0.01 s) and Vs_{s3}, b) relation between F(0.01 s) and site fundamental frequency F_0 for randomized V_s profiles and randomized nonlinear shear modulus-damping curve.

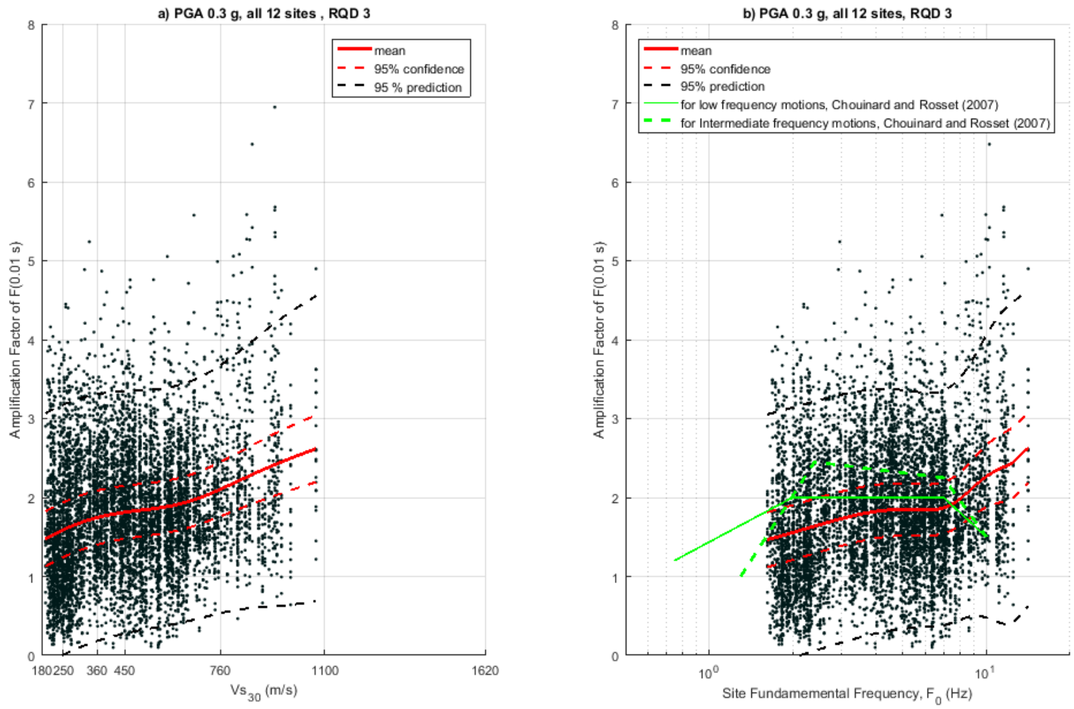

Figure 7.5: RQD 3 and PGA 0.3 g: a) relation between F(0.01 s) and V_{s30}, b) relation between F(0.01 s) and site fundamental frequency F_0 for randomized V_s profiles and randomized nonlinear shear modulus-damping curve.

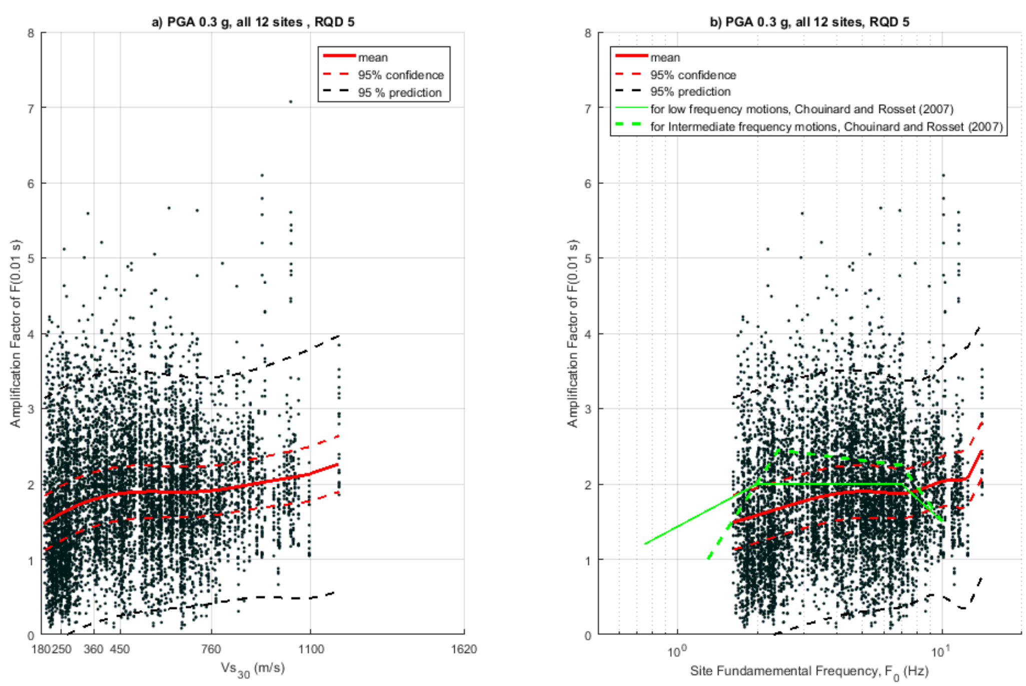

Figure 7.6: RQD 5 and PGA 0.3 g: a) relation between F(0.01 s) and V_{s30}, b) relation between F(0.01 s) and site fundamental frequency F_0 for randomized V_s profiles and randomized nonlinear shear modulus-damping curve.

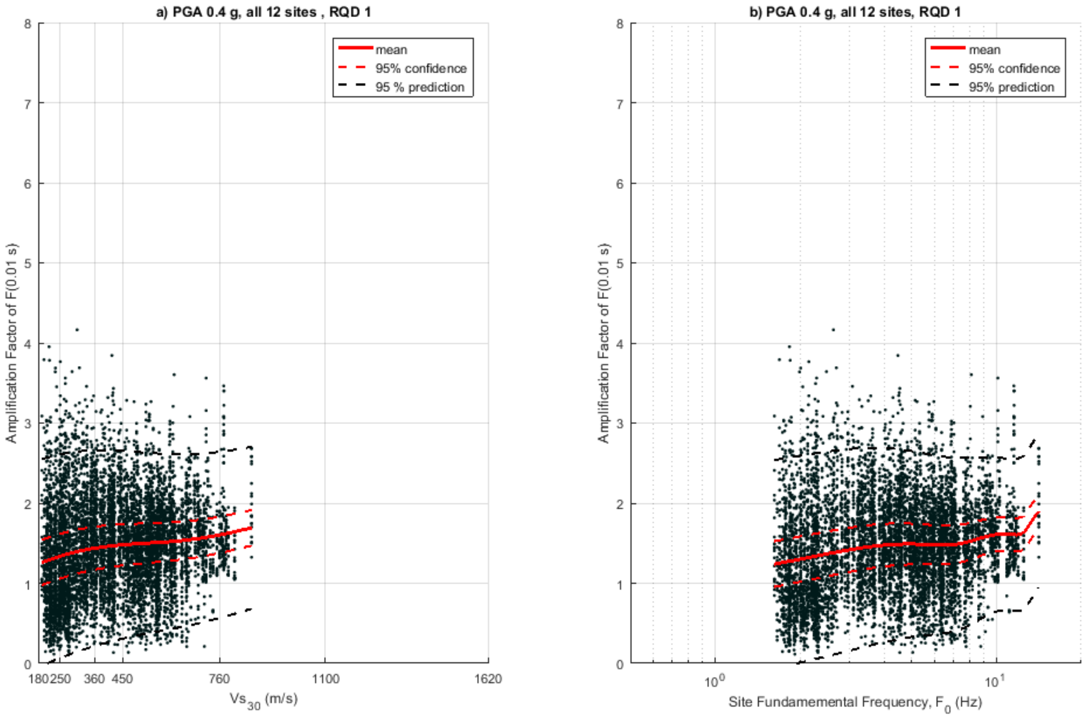

Figure 7.7: RQD 1 and PGA 0.4 g: a) relation between F(0.01 s) and V_{s30}, b) relation between F(0.01 s) and site fundamental frequency F_0 for randomized V_s profiles and randomized nonlinear shear modulus-damping curve.

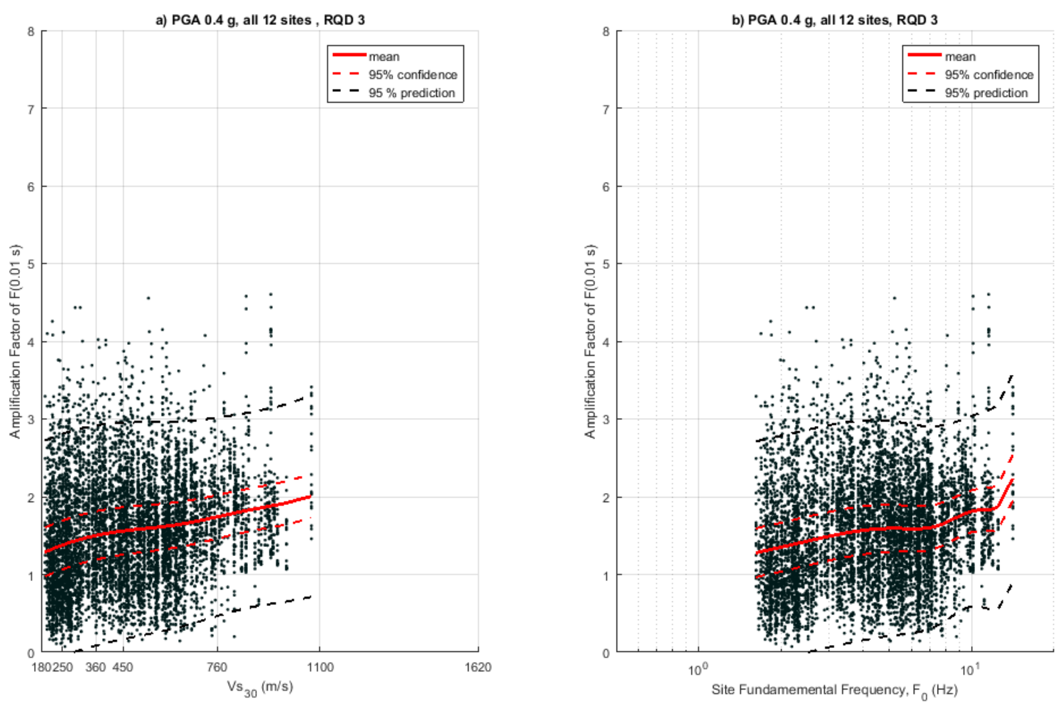

Figure 7.8: RQD 3 and PGA 0.4 g: a) relation between F(0.01 s) and V_{s30}, b) relation between F(0.01 s) and site fundamental frequency F_0 for randomized V_s profiles and randomized nonlinear shear modulus-damping curve.

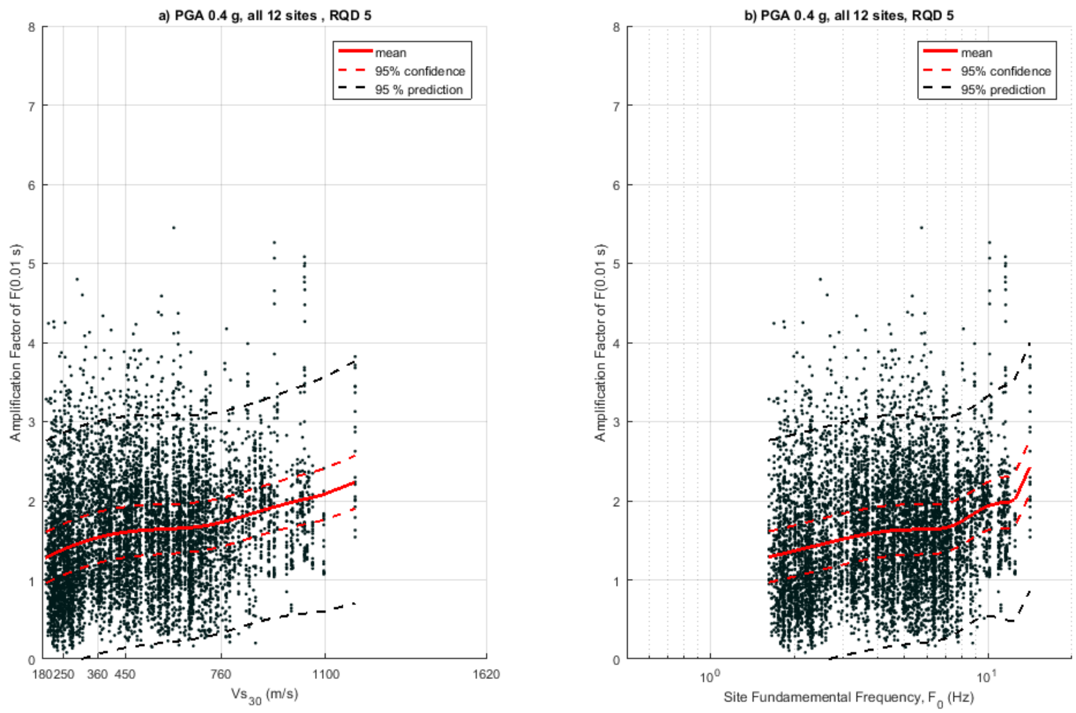

Figure 7.9 RQD 5 and PGA 0.4 g: a) relation between F(0.01 s) and V_{s30}, b) relation between F(0.01 s) and site fundamental frequency F_0 for randomized V_s profiles and randomized nonlinear shear modulus-damping curve.

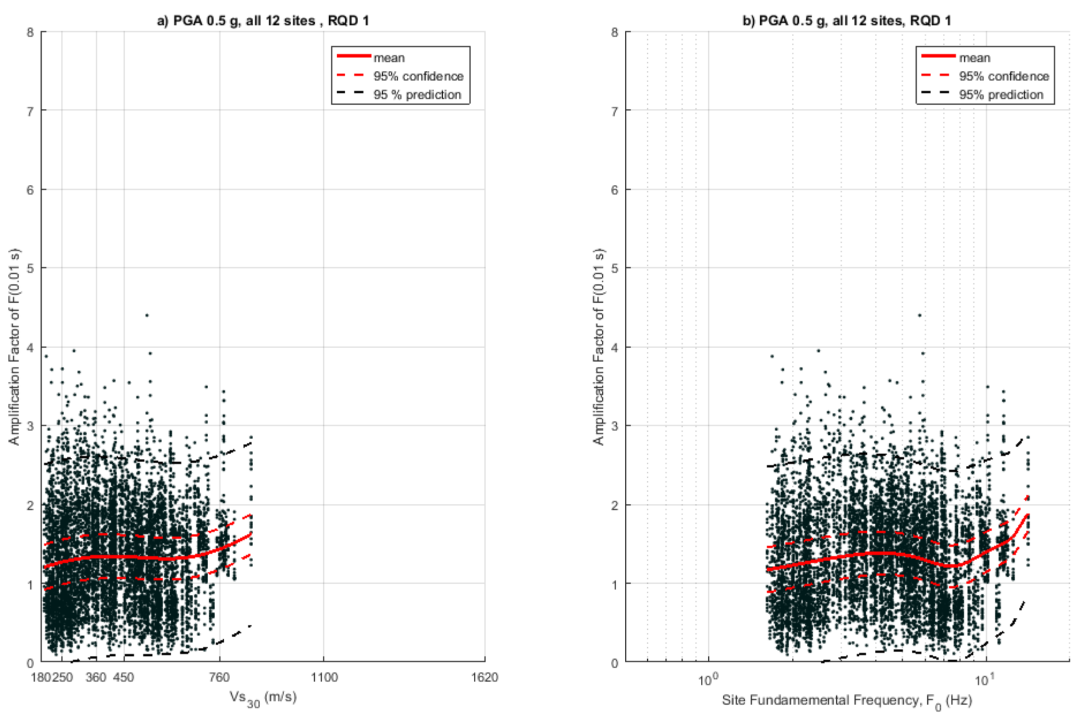

Figure 7.10: RQD 1 and PGA 0.5 g: a) relation between F(0.01 s) and V_{s30}, b) relation between F(0.01 s) and site fundamental frequency F_0 for randomized V_s profiles and randomized nonlinear shear modulus-damping curve.

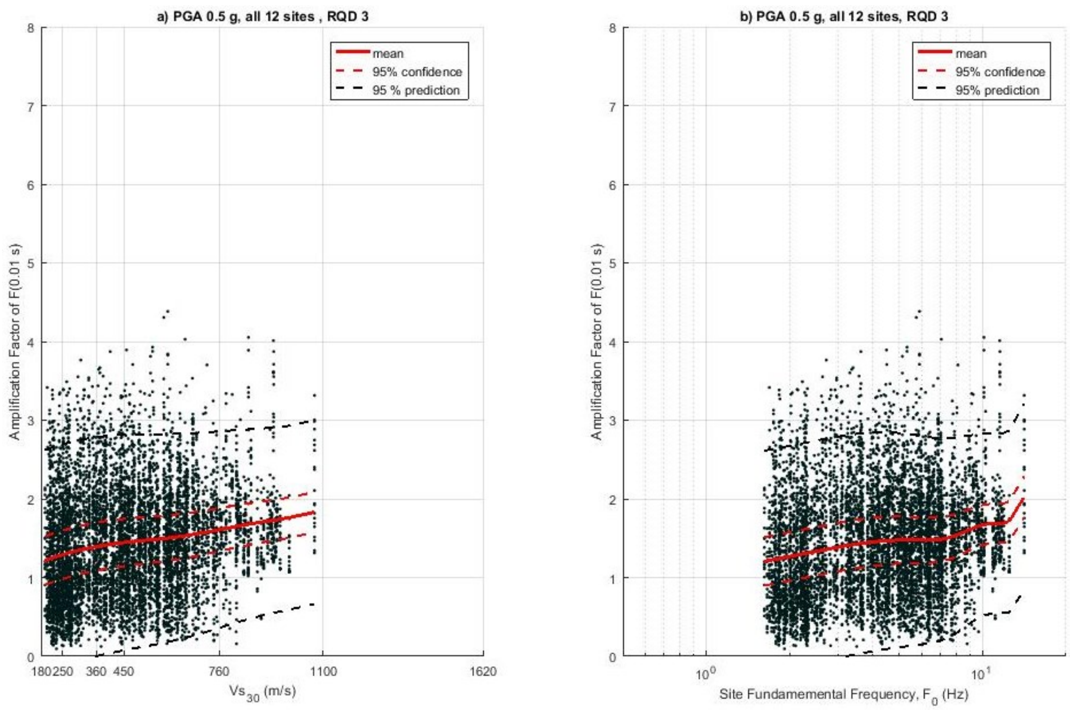

Figure 7.11: RQD 3 and PGA 0.5 g: a) relation between F(0.01 s) and V_{s30}, b) relation between F(0.01 s) and site fundamental frequency F_0 for randomized V_s profiles and randomized nonlinear shear modulus-damping curve.

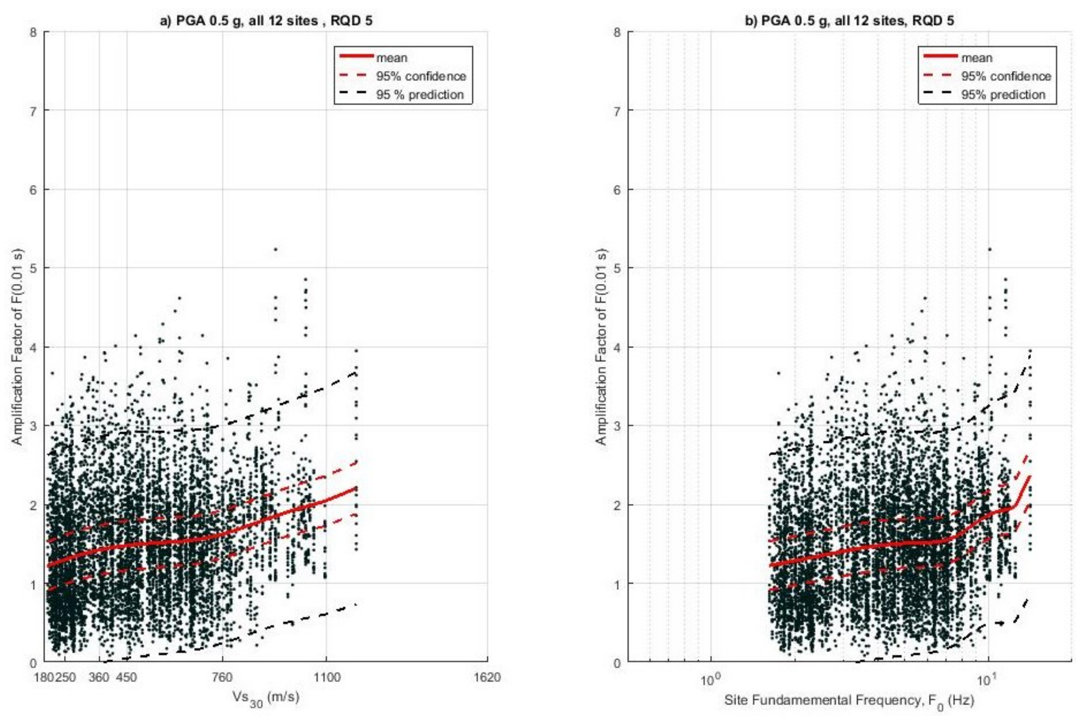

Figure 7.12: RQD 5 and PGA 0.5 g: a) relation between F(0.01 s) and V_{s30}, b) relation between F(0.01 s) and site fundamental frequency F_0 for randomized V_s profiles and randomized nonlinear shear modulus-damping curve.

8 Appendix B

Figures for F(0.2 s), F(0.5 s) and F(1 s) as a function of Vs30 for PGA 0.2 g to 0.5 g.

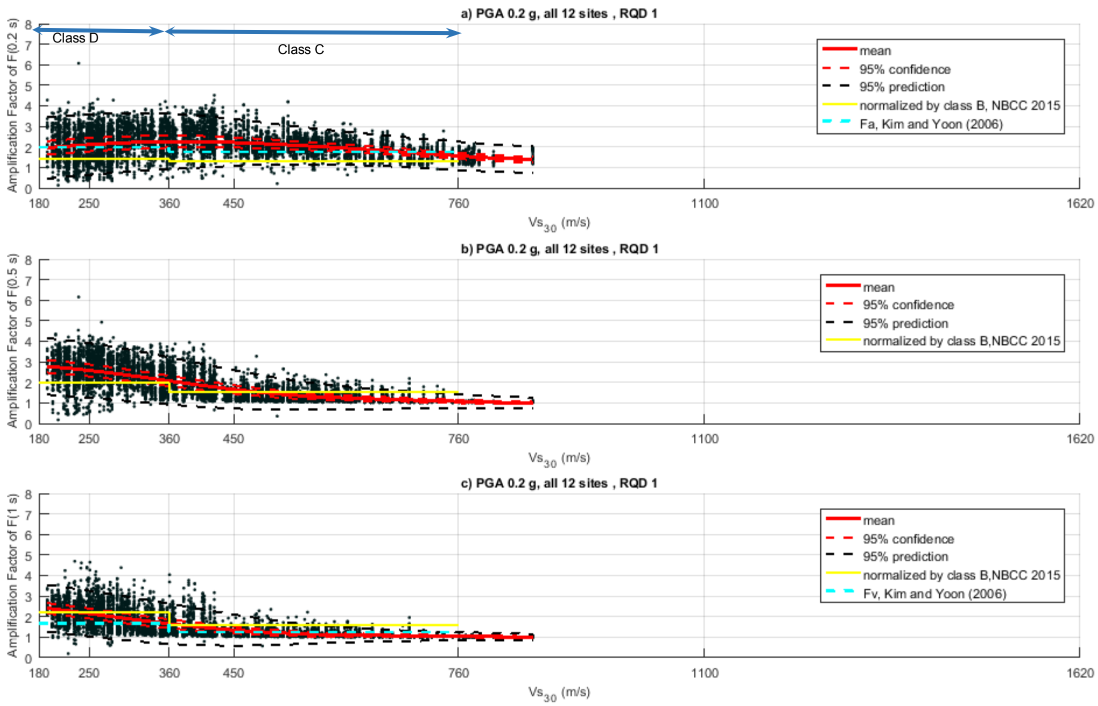

Figure 8.1: RQD of 1 and PGA 0.2 g: a) relation between F(0.2 s) and V_{s30}, b) relation between F(0.5 s) and V_{s30}, and c) relation between F(1.0 s) and V_{s30} for randomized V_s profiles and randomized nonlinear shear modulus-damping curve.

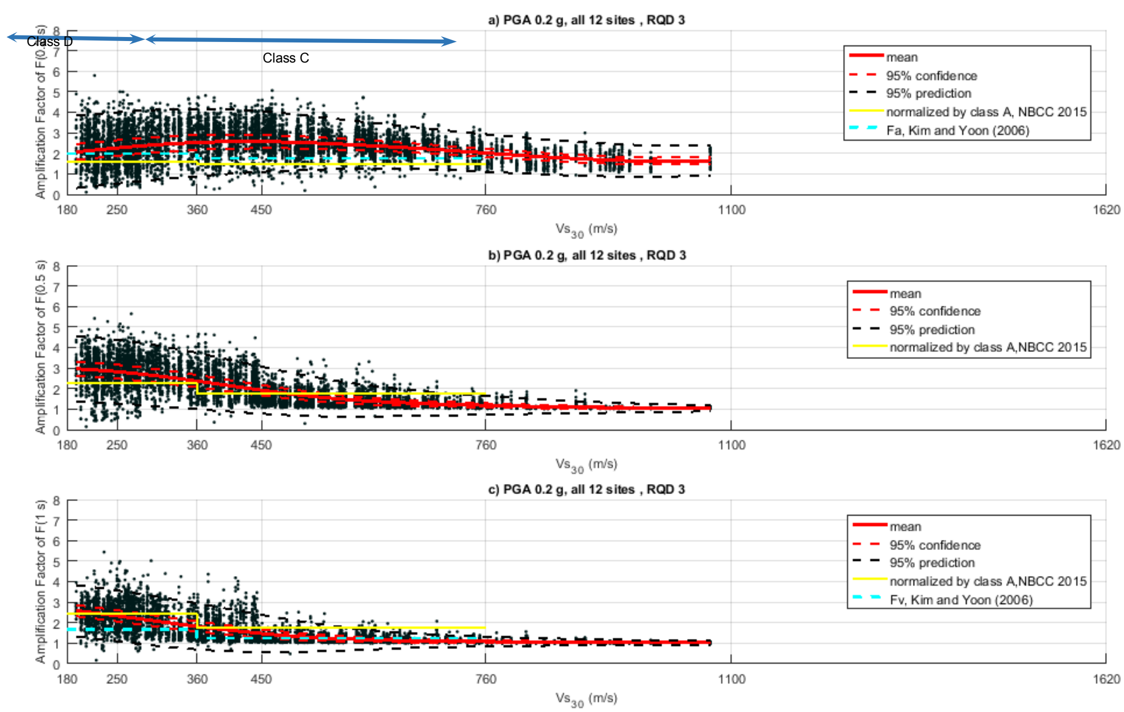

Figure 8.2: RQD of 3 and PGA 0.2 g: a) relation between F(0.2 s) and V_{s30}, b) relation between F(0.5 s) and V_{s30}, and c) relation between F(1.0 s) and V_{s30} for randomized V_s profiles and randomized nonlinear shear modulus-damping curve.

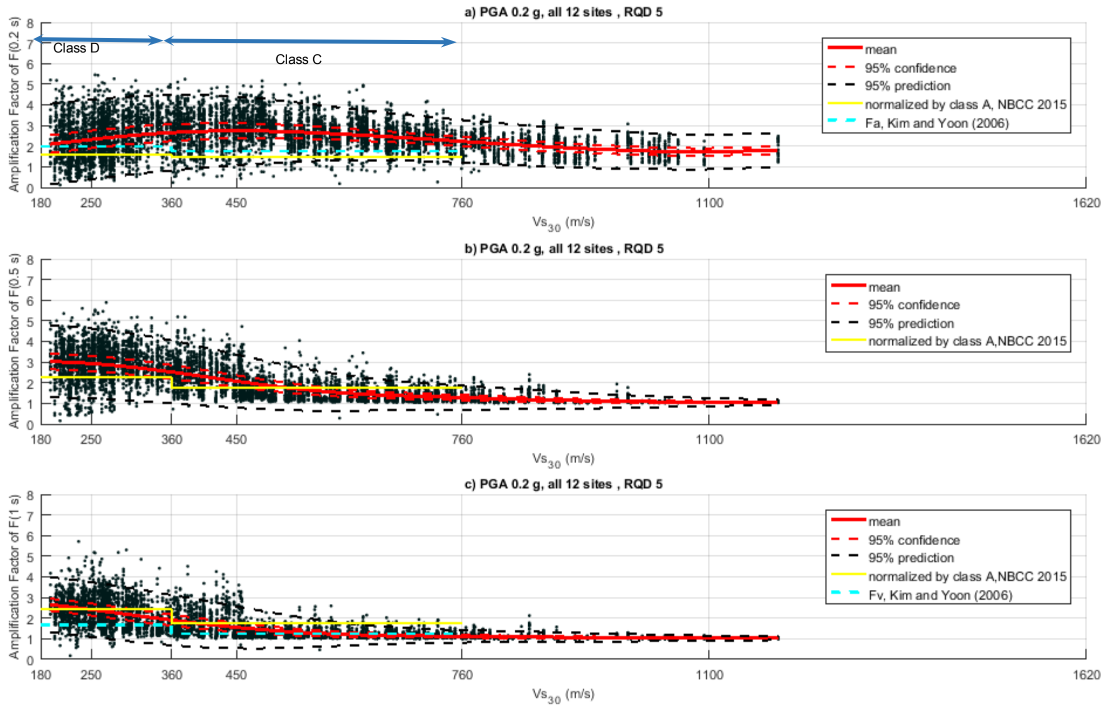

Figure 8.3: RQD of 5 and PGA 0.2 g: a) relation between F(0.2 s) and V_{s30}, b) relation between F(0.5 s) and V_{s30}, and c) relation between F(1.0 s) and V_{s30} for randomized V_s profiles and randomized nonlinear shear modulus-damping curve.

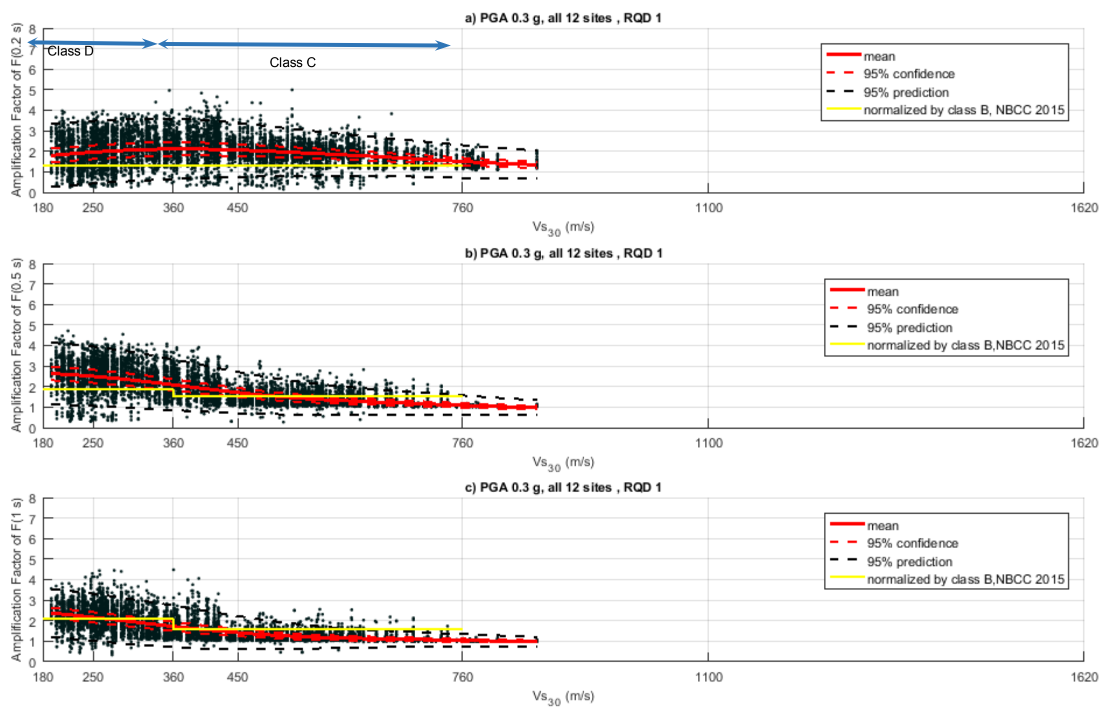

Figure 8.4: RQD of 1 and PGA 0.3 g: a) relation between F(0.2 s) and V_{s30}, b) relation between F(0.5 s) and V_{s30}, and c) relation between F(1.0 s) and V_{s30} for randomized V_s profiles and randomized nonlinear shear modulus-damping curve.

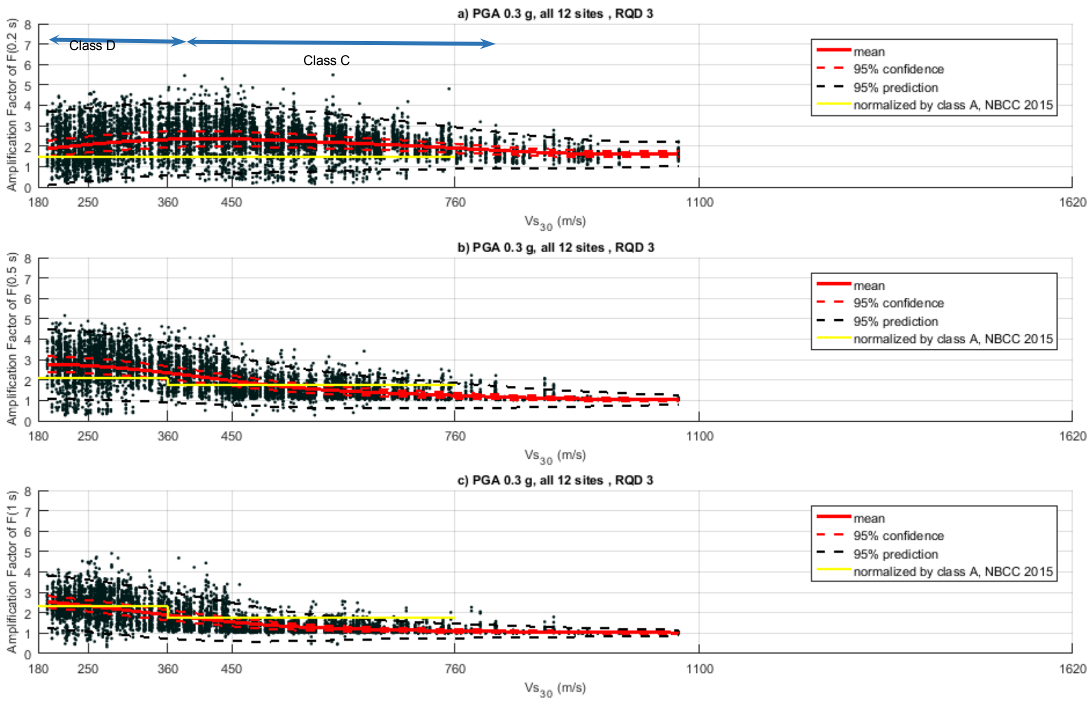

Figure 8.5: RQD of 3 and PGA 0.3 g: a) relation between F(0.2 s) and V_{s30}, b) relation between F(0.5 s) and V_{s30}, and c) relation between F(1.0 s) and V_{s30} for randomized V_s profiles and randomized nonlinear shear modulus-damping curve.

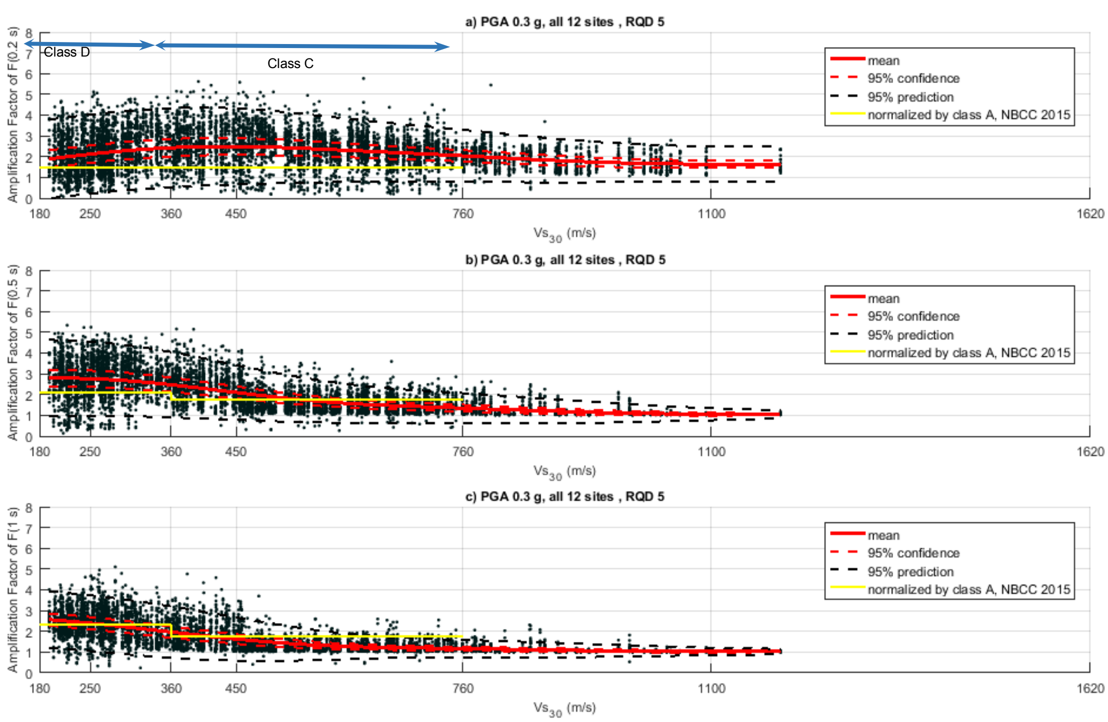

Figure 8.6: RQD 5 and PGA 0.3 g: a) relation between F(0.2 s) and V_{s30}, b) relation between F(0.5 s) and V_{s30}, and c) relation between F(1.0 s) and V_{s30} for randomized V_s profiles and randomized nonlinear shear modulus-damping curve.

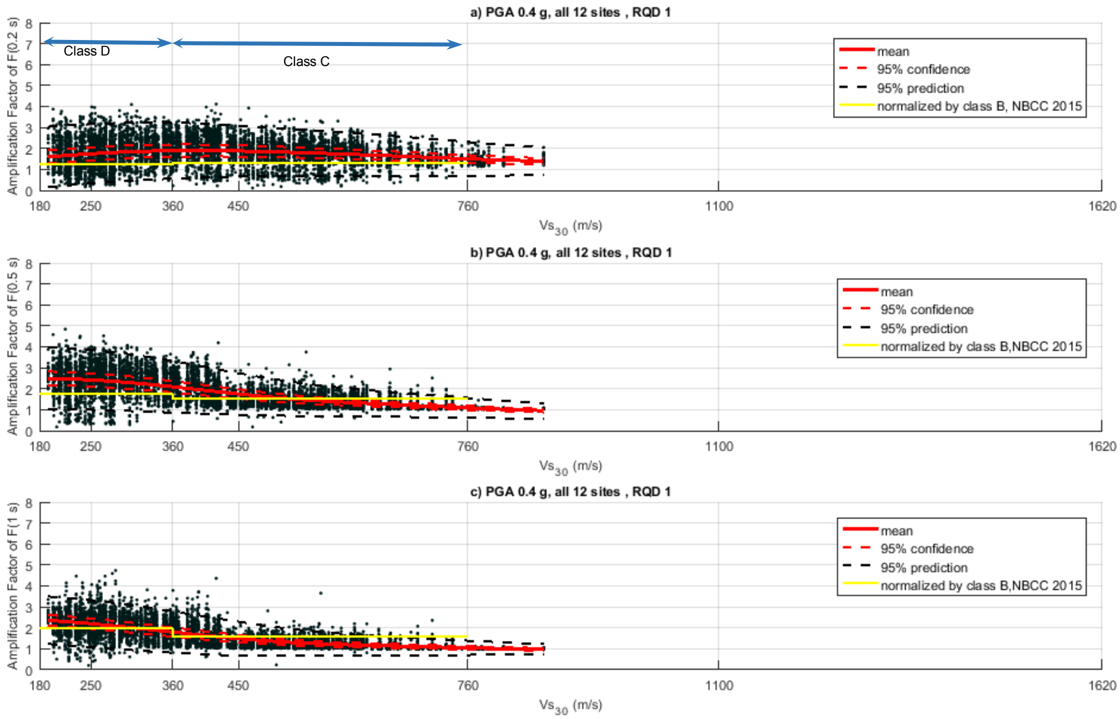

Figure 8.7: RQD of 1 and PGA 0.4 g: a) relation between F(0.2 s) and V_{s30}, b) relation between F(0.5 s) and V_{s30}, and c) relation between F(1.0 s) and V_{s30} for randomized V_s profiles and randomized nonlinear shear modulus-damping curve.

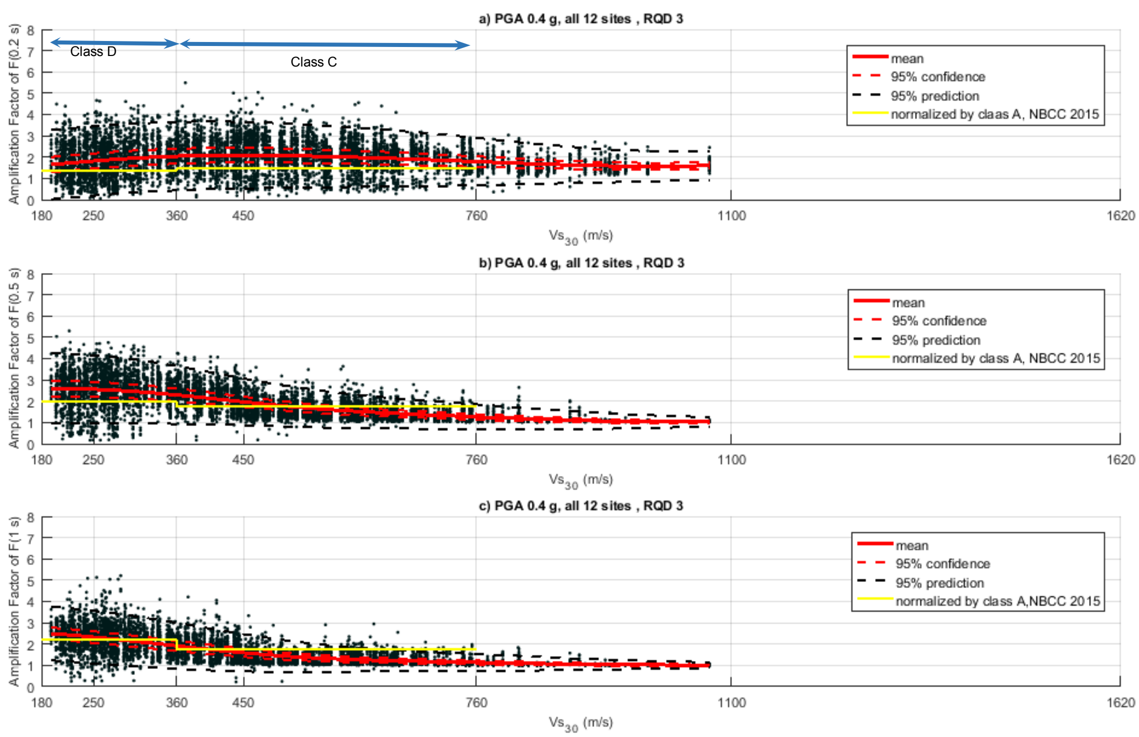

Figure 8.8: RQD of 3 and PGA 0.4 g: a) relation between F(0.2 s) and V_{s30}, b) relation between F(0.5 s) and V_{s30}, and c) relation between F(1.0 s) and V_{s30} for randomized V_s profiles and randomized nonlinear shear modulus-damping curve.

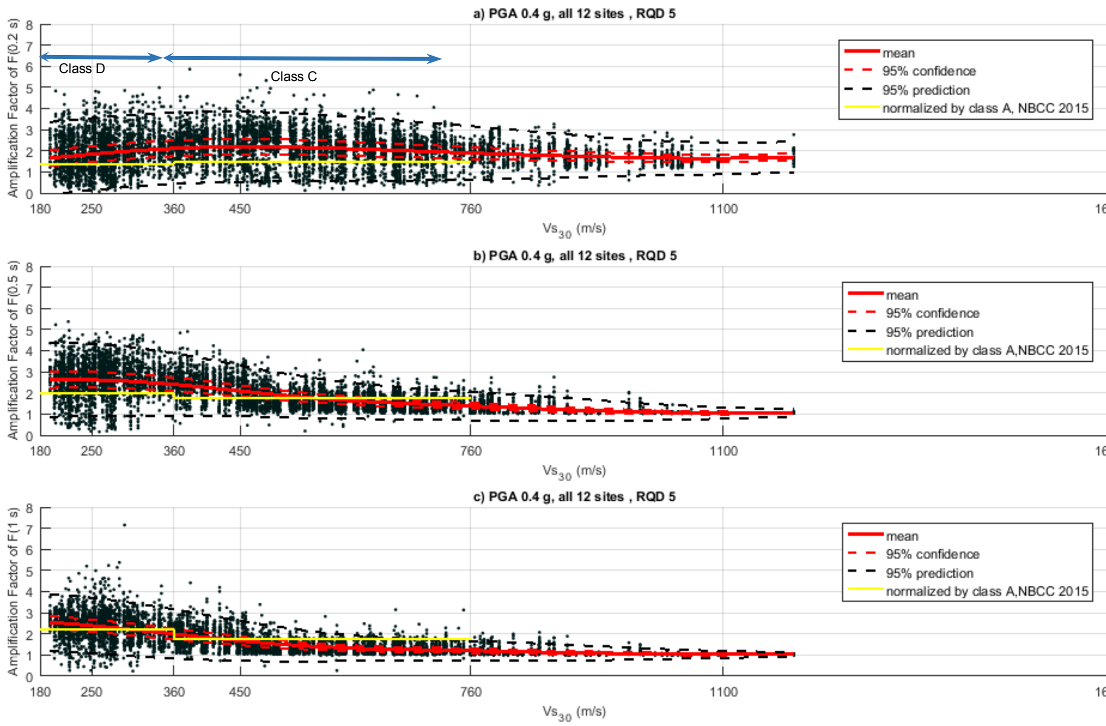

Figure 8.9: RQD of 5 and PGA 0.4 g: a) relation between F(0.2 s) and V_{s30}, b) relation between F(0.5 s) and V_{s30}, and c) relation between F(1.0 s) and V_{s30} for randomized V_s profiles and randomized nonlinear shear modulus-damping curve.

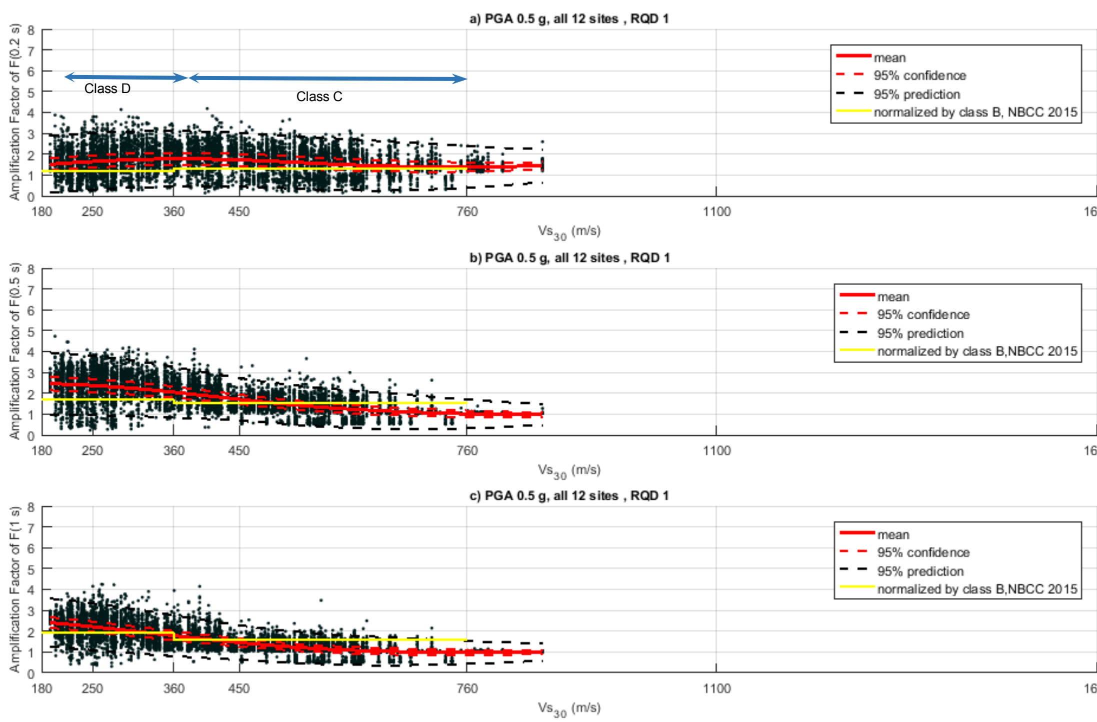

Figure 8.10: RQD of 1 and PGA 0.5 g: a) relation between F(0.2 s) and V_{s30}, b) relation between F(0.5 s) and V_{s30}, and c) relation between F(1.0 s) and V_{s30} for randomized V_s profiles and randomized nonlinear shear modulus-damping curve.

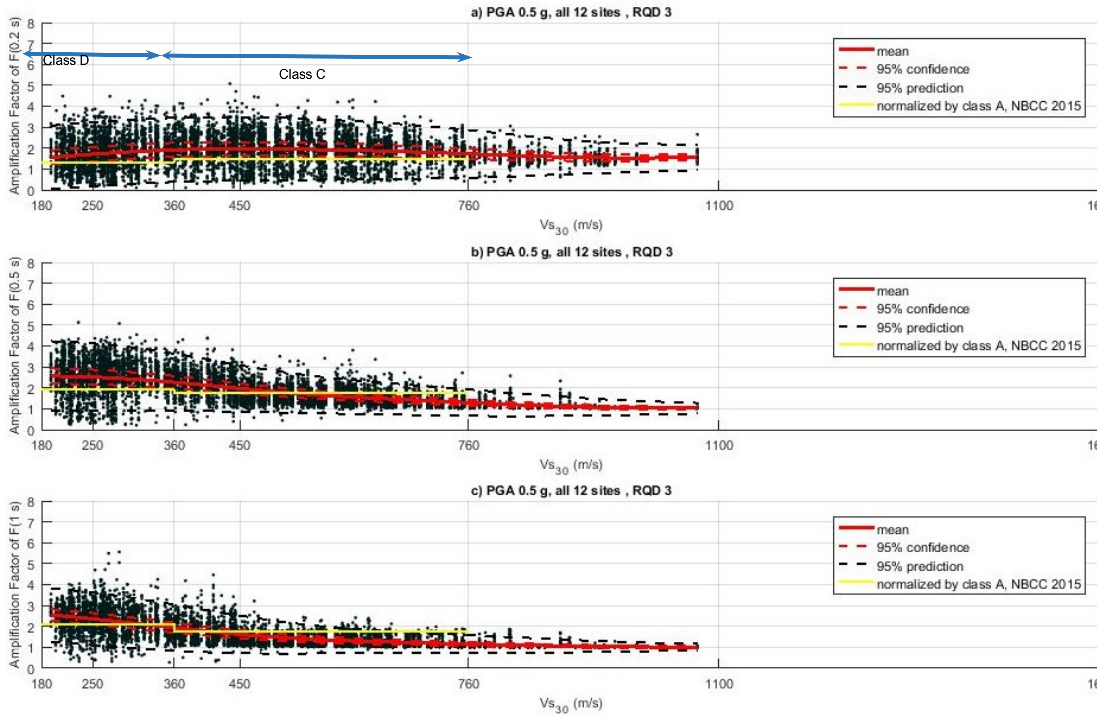

Figure 8.11: RQD of 3 and PGA 0.5 g: a) relation between F(0.2 s) and V_{s30}, b) relation between F(0.5 s) and V_{s30}, and c) relation between F(1.0 s) and V_{s30} for randomized V_s profiles and randomized nonlinear shear modulus-damping curve.

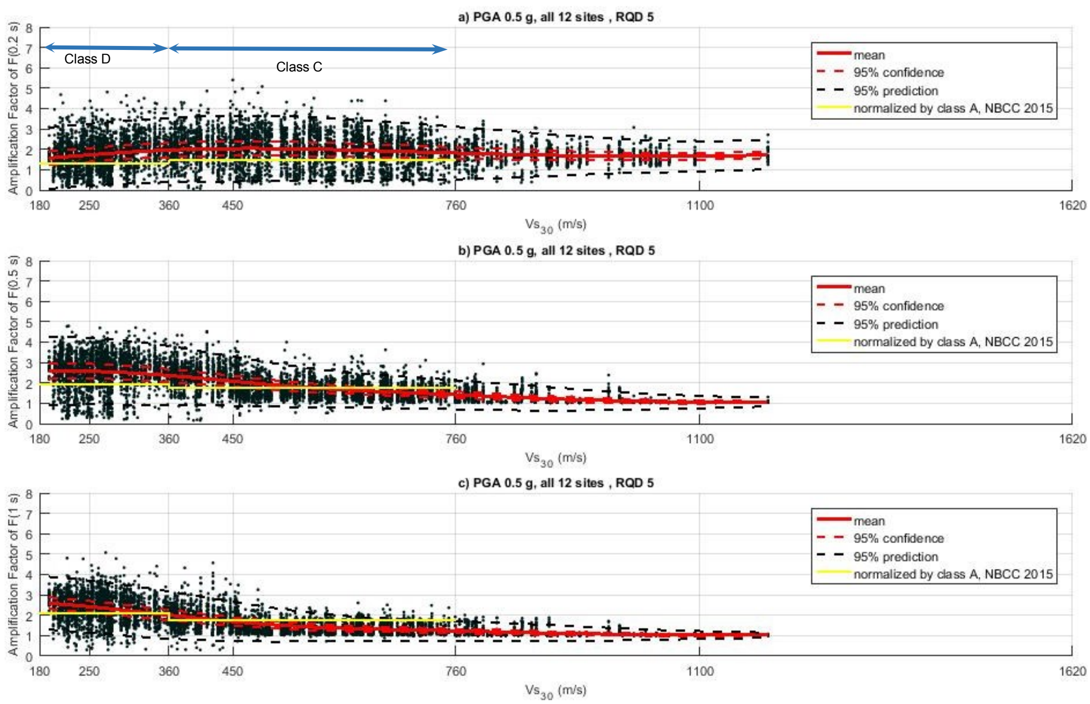

Figure 8.12: RQD of 5 and PGA 0.5 g: a) relation between F(0.2 s) and V_{s30}, b) relation between F(0.5 s) and V_{s30}, and c) relation between F(1.0 s) and V_{s30} for randomized V_s profiles and randomized nonlinear shear modulus-damping curve.

9 Appendix C

Figures for F(0.2 s), F(0.5 s) and F(1 s) as a function of site periods for PGA 0.2 g to 0.5 g.

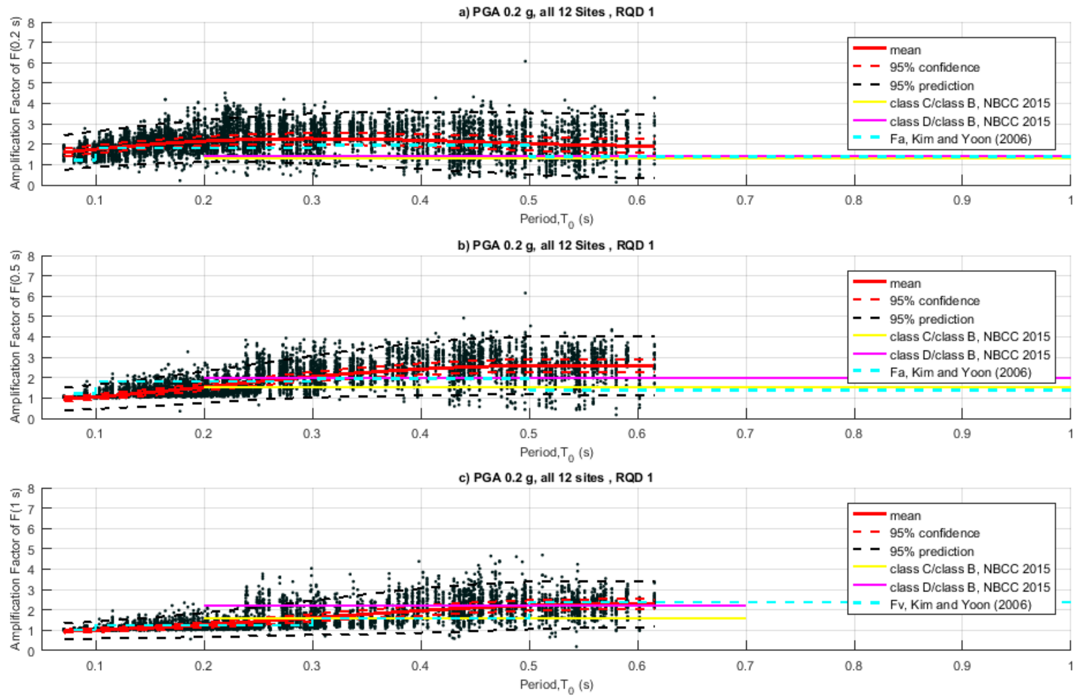

Figure 9.1: RQD 1 and PGA 0.2 g: a) relation between F(0.2 s) and T_0, b) relation between F(0.5 s) and T_0, and c) relation between F(1.0 s) and T_0 for randomized V_s profiles and randomized nonlinear shear modulus-damping curve.

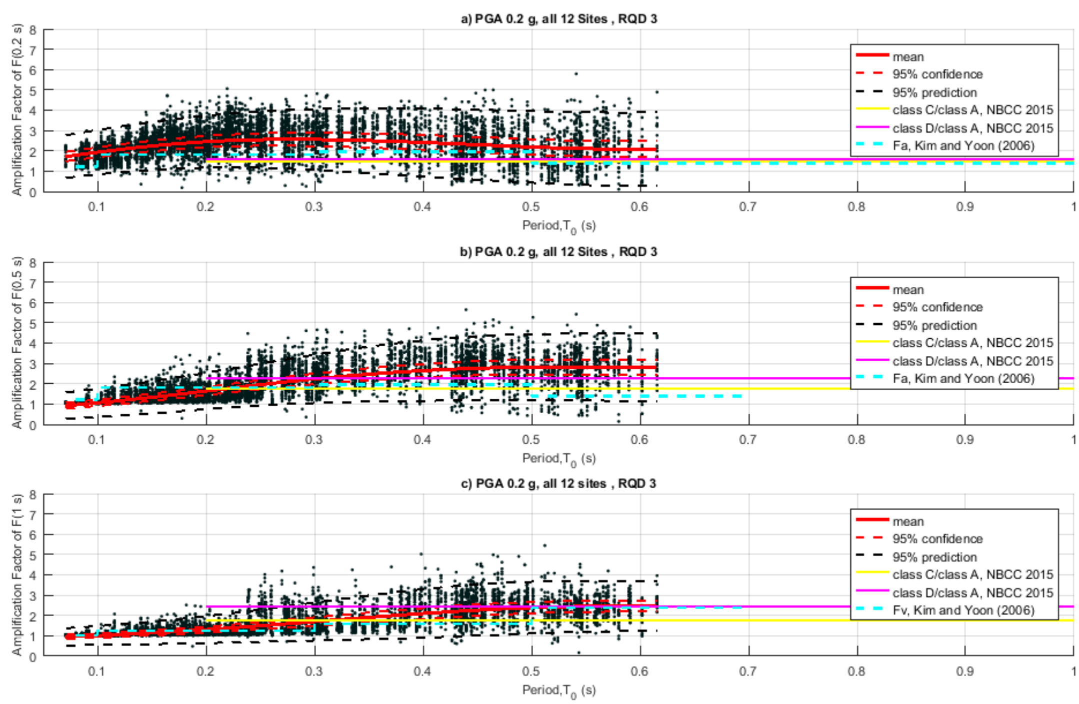

Figure 9.2: RQD 3 and PGA 0.2 g: a) relation between F(0.2 s) and T_0, b) relation between F(0.5 s) and T_0, and c) relation between F(1.0 s) and T_0 for randomized V_s profiles and randomized nonlinear shear modulus-damping curve.

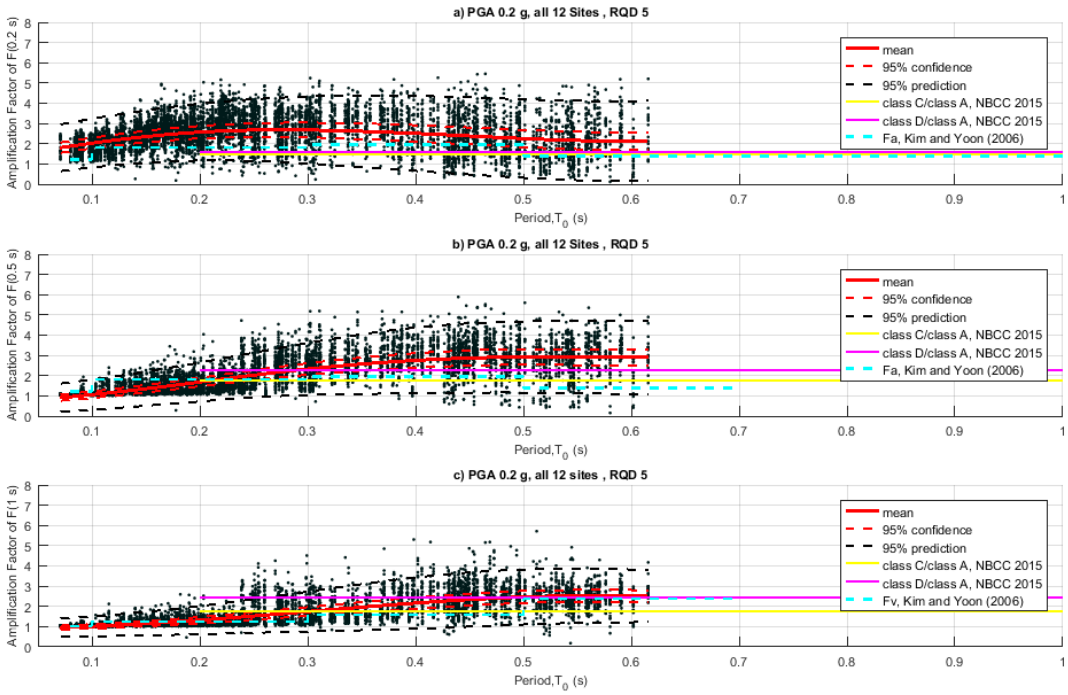

Figure 9.3: RQD 5 and PGA 0.2 g: a) relation between F(0.2 s) and T_0, b) relation between F(0.5 s) and T_0, and c) relation between F(1.0 s) and T_0 for randomized V_s profiles and randomized nonlinear shear modulus-damping curve.

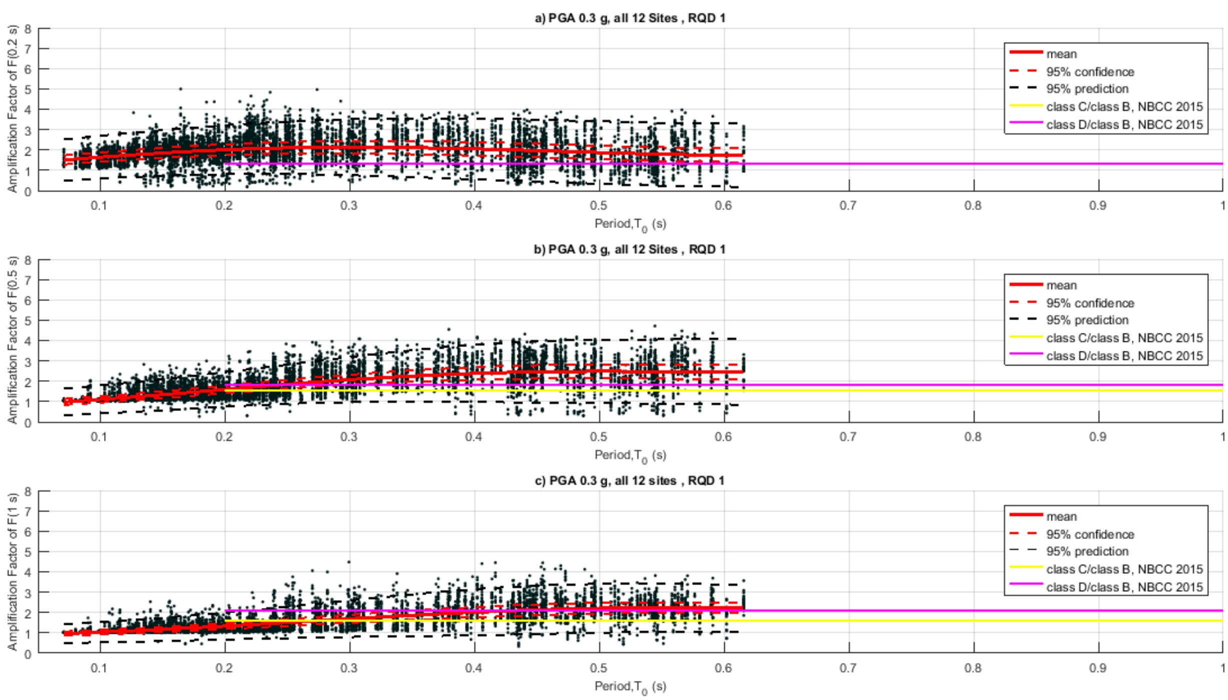

Figure 9.4: RQD 1 and PGA 0.3 g: a) relation between F(0.2 s) and T_0, b) relation between F(0.5 s) and T_0, and c) relation between F(1.0 s) and T_0 for randomized V_s profiles and randomized nonlinear shear modulus-damping curve.

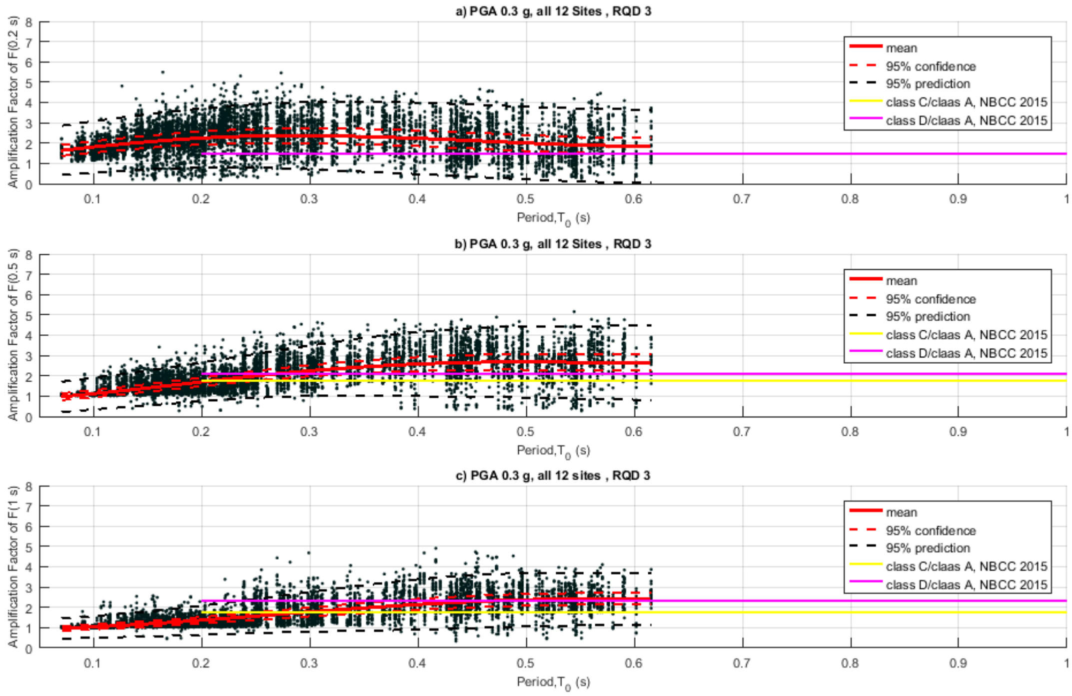

Figure 9.5 RQD 3 and PGA 0.3 g: a) relation between F(0.2 s) and T_0, b) relation between F(0.5 s) and T_0, and c) relation between F(1.0 s) and T_0 for randomized V_s profiles and randomized nonlinear shear modulus-damping curve.

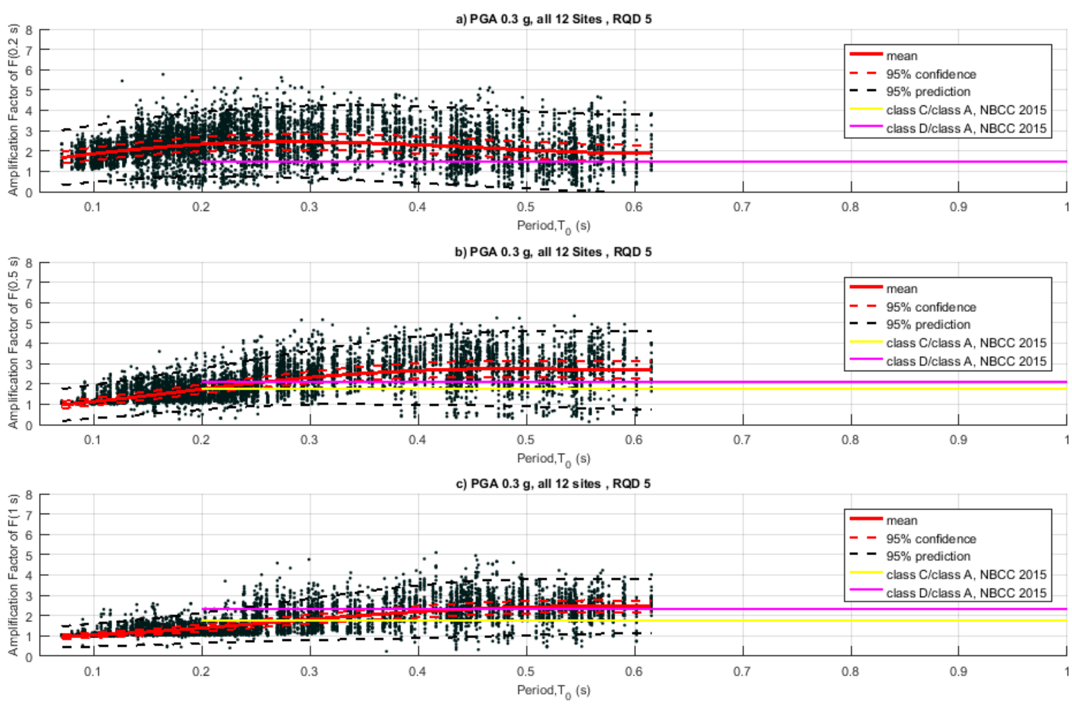

Figure 9.6: RQD 5 and PGA 0.3 g: a) relation between F(0.2 s) and T_0, b) relation between F(0.5 s) and T_0, and c) relation between F(1.0 s) and T_0 for randomized V_s profiles and randomized nonlinear shear modulus-damping curve.

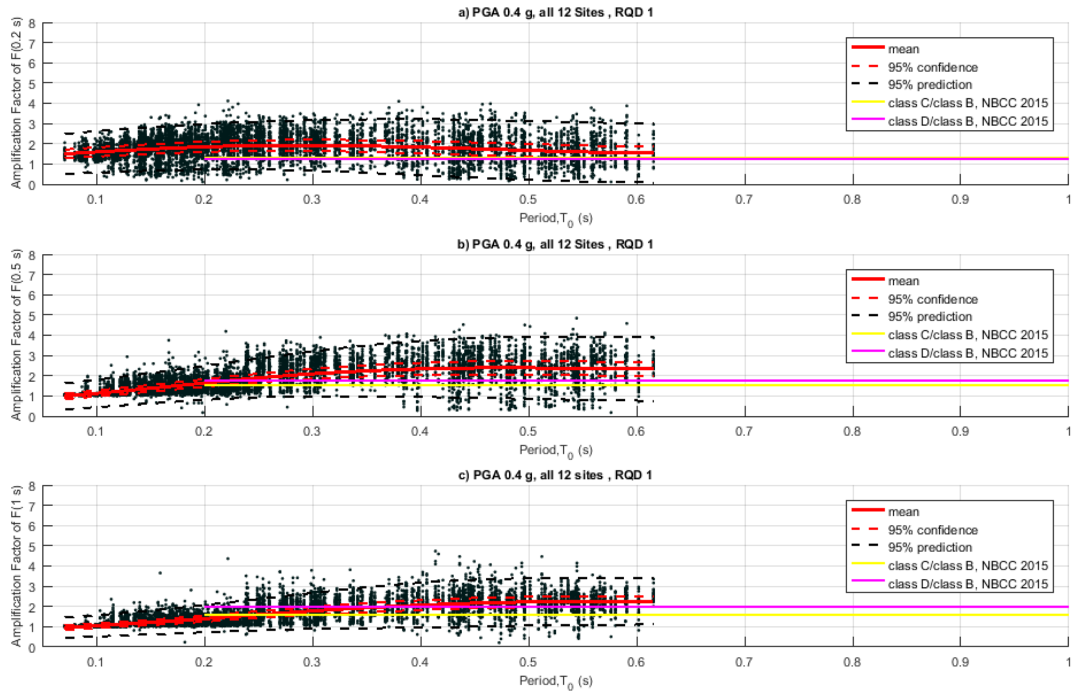

Figure 9.7: RQD 1 and PGA 0.4 g: a) relation between F(0.2 s) and T_0, b) relation between F(0.5 s) and T_0, and c) relation between F(1.0 s) and T_0 for randomized V_s profiles and randomized nonlinear shear modulus-damping curve.

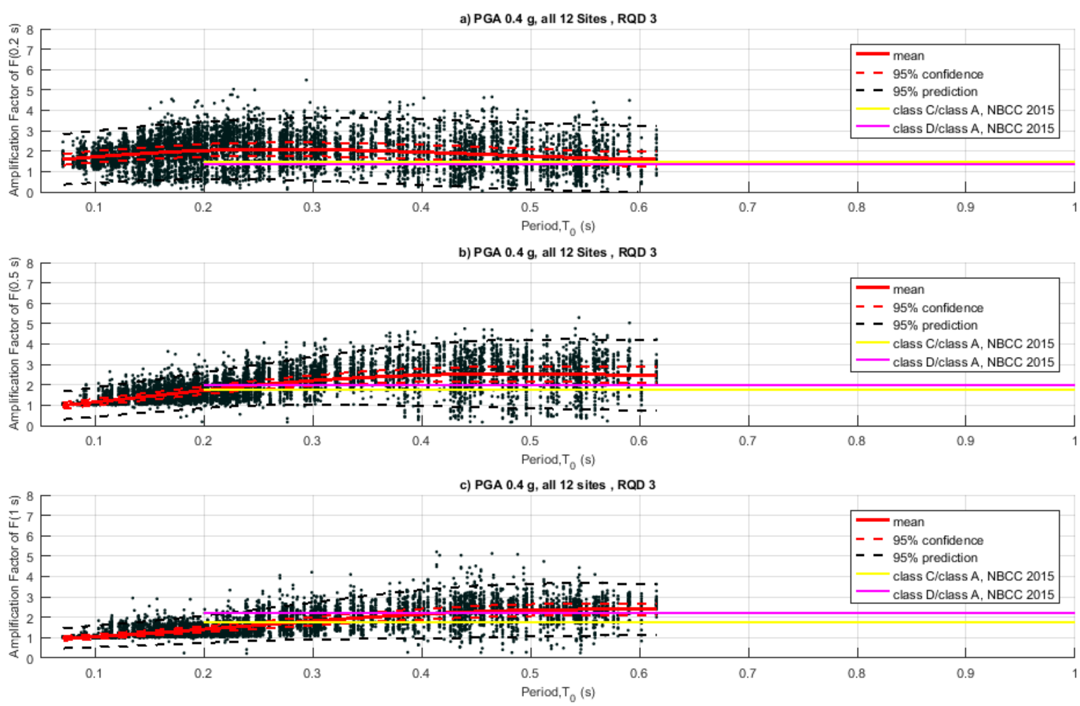

Figure 9.8: RQD 3 and PGA 0.4 g: a) relation between F(0.2 s) and T_0, b) relation between F(0.5 s) and T_0, and c) relation between F(1.0 s) and T_0 for randomized V_s profiles and randomized nonlinear shear modulus-damping curve.

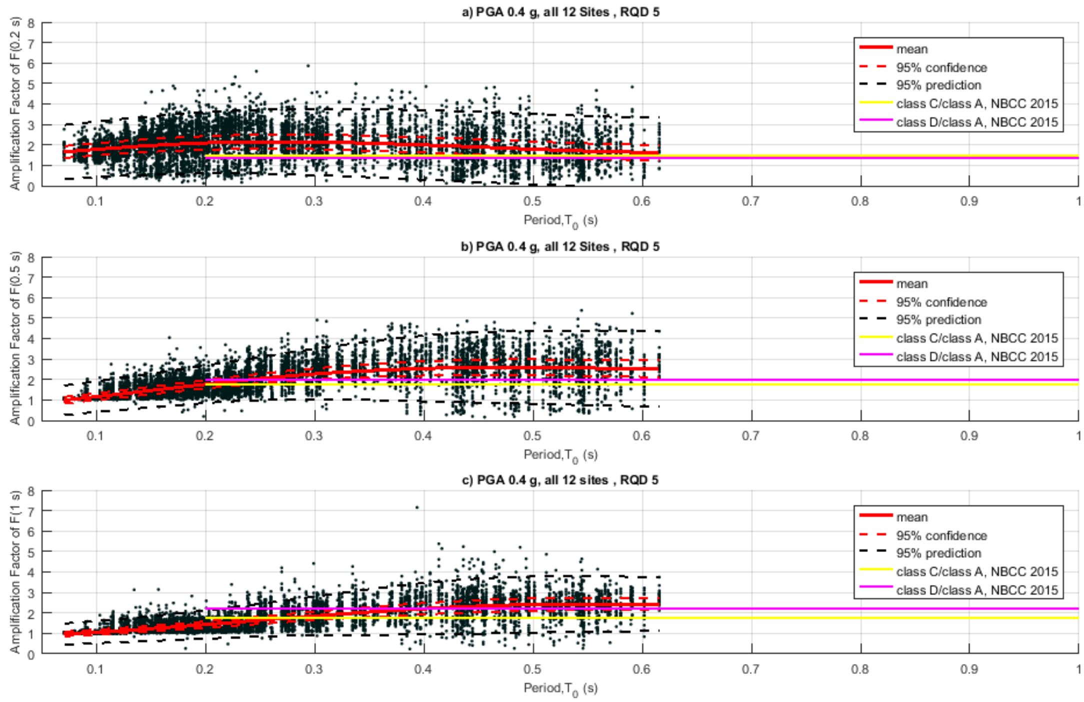

Figure 9.9: RQD 5 and PGA 0.4 g: a) relation between F(0.2 s) and T_0, b) relation between F(0.5 s) and T_0, and c) relation between F(1.0 s) and T_0 for randomized V_s profiles and randomized nonlinear shear modulus-damping curve.

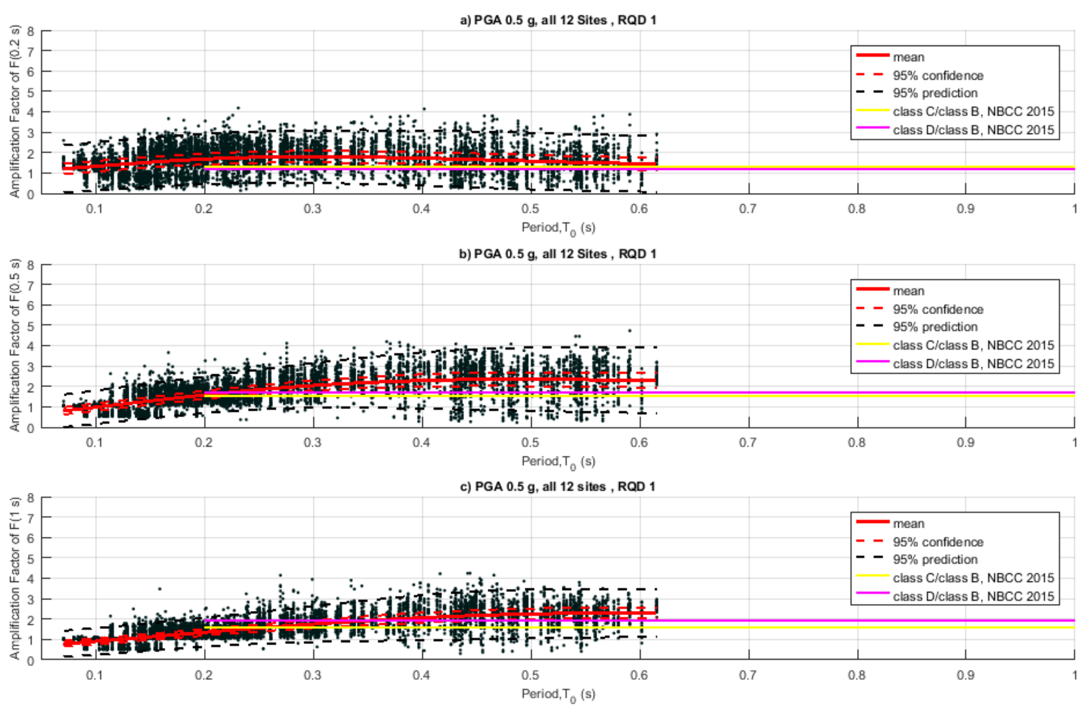

Figure 9.10: RQD 1 and PGA 0.5 g: a) relation between F(0.2 s) and T_0, b) relation between F(0.5 s) and T_0, and c) relation between F(1.0 s) and T_0 for randomized V_s profiles and randomized nonlinear shear modulus-damping curve.

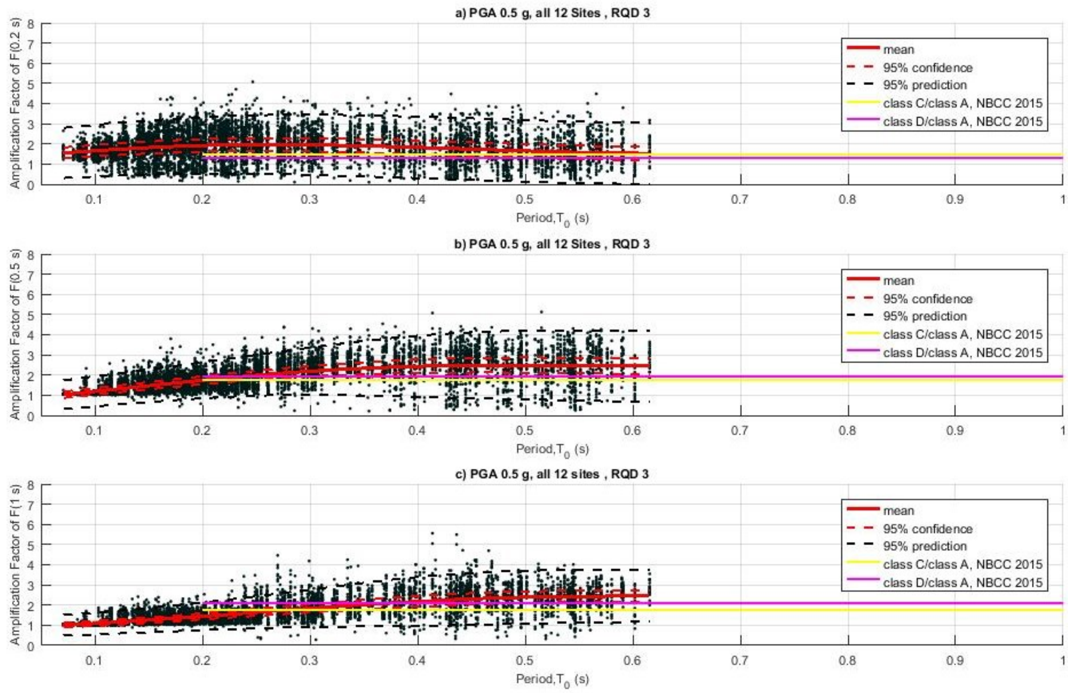

Figure 9.11: RQD of 3 and PGA 0.5 g: a) relation between F(0.2 s) and Vs_{30}, b) relation between F(0.5 s) and Vs_{30}, and c) relation between F(1.0 s) and Vs_{30} for randomized V_s profiles and randomized nonlinear shear modulus-damping curve.

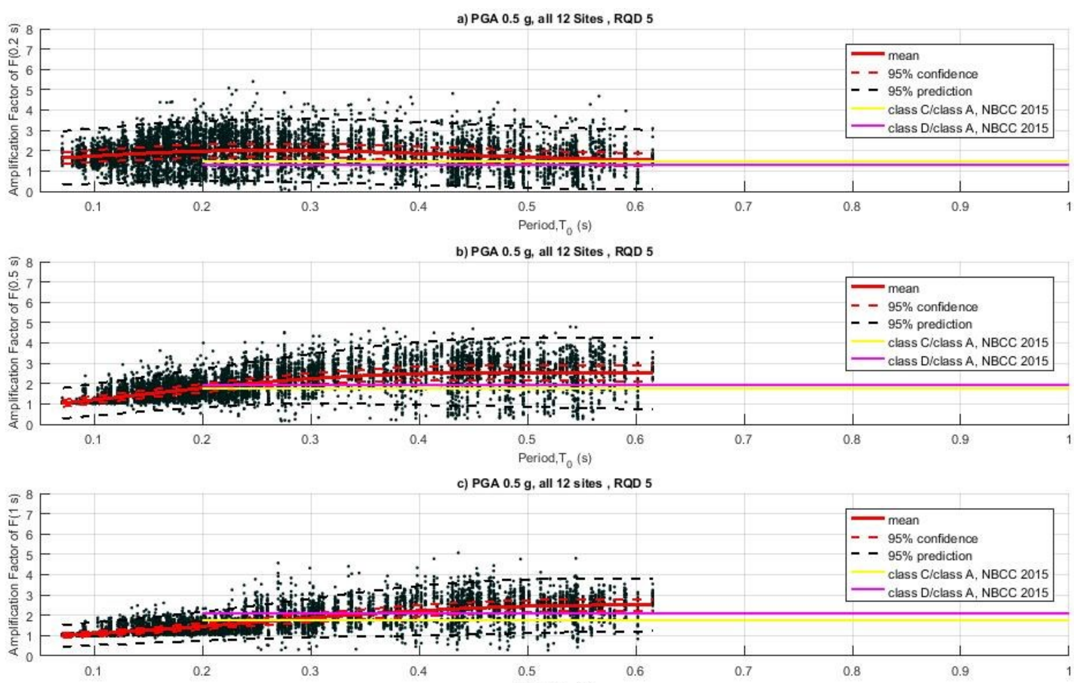

Figure 9.12: RQD of 5 and PGA 0.5 g: a) relation between F(0.2 s) and T_0, b) relation between F(0.5 s) and T_0, and c) relation between F(1.0 s) and T_0 for randomized V_s profiles and randomized nonlinear shear modulus-damping curve.

10 Appendix D

Scatter plots showing correlation between F_C and F_D calculated from the 1-D runs with randomized V_s profiles and randomized dynamic nonlinear properties for PGA 0.2 g to 0.5 g.

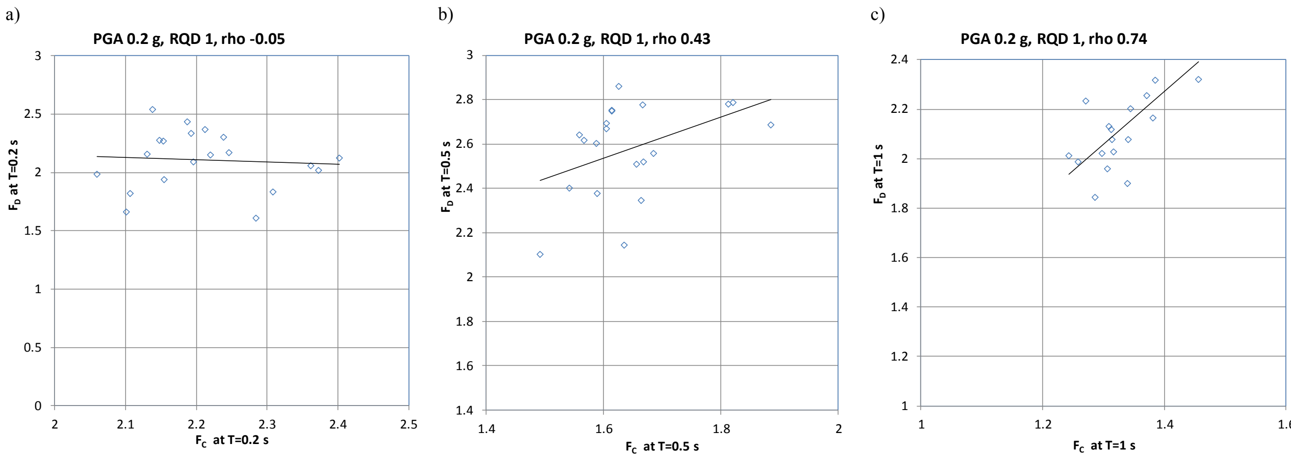

Figure 10.1: Correlation scatter plots for PGA of 0.2 g and RQD of 1(V_s= 1258 m/s) compare F_D and F_C calculated from the ground response to each of the 20 motions for T= 0.2 , 0.5 and 1.0 s for randomized V_s profiles and randomized nonlinear shear modulus-damping curve.

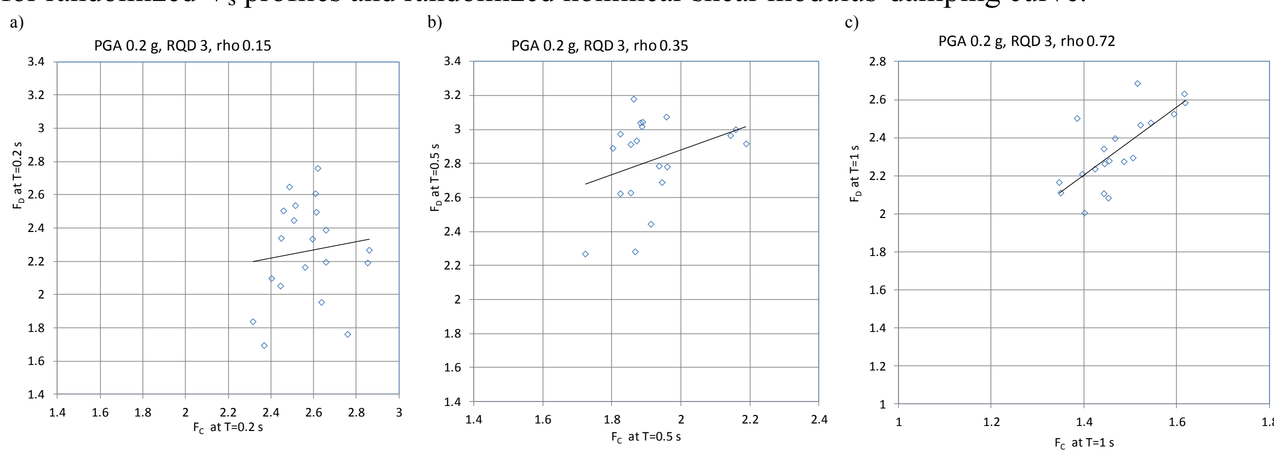

Figure 10.2: Correlation scatter plots for PGA of 0.2 g and RQD of 3 (V_s=2082 m/s) compare F_D and F_C calculated from the ground response to each of the 20 motions for T= 0.2 , 0.5 and 1.0 s for randomized V_s profiles and randomized nonlinear shear modulus-damping curve.

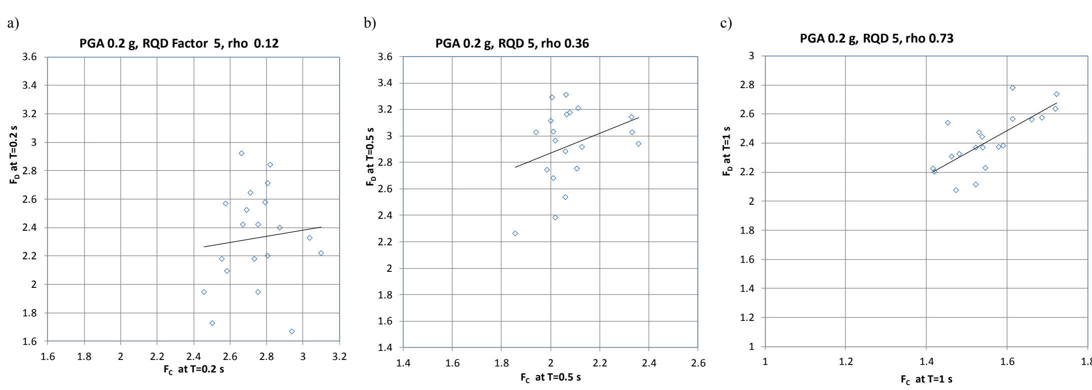

Figure 10.3: Correlation scatter plots for PGA of 0.2 g and RQD of 5 (V_s= 2926 m/s) compare F_D and F_C calculated for T= 0.2 , 0.5 and 1.0 s for randomized V_s profiles and randomized nonlinear shear modulus-damping curve.

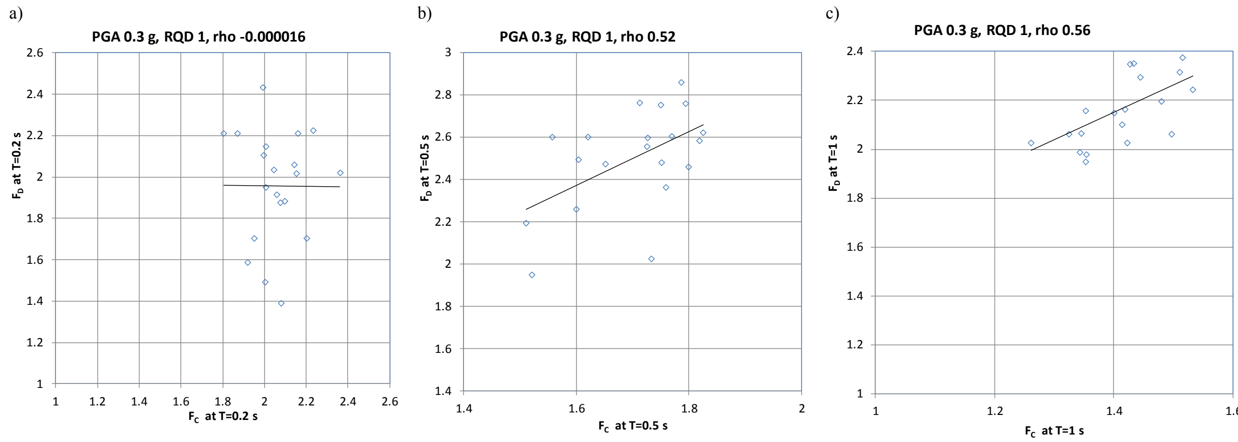

Figure 10.4: Correlation scatter plots for PGA of 0.3 g and RQD of 1 (V_s= 1258 m/s) compare F_D and F_C calculated from the ground response to each of the 20 motions for T= 0.2, 0.5 and 1.0 s for randomized V_s profiles and randomized nonlinear shear modulus-damping curve.

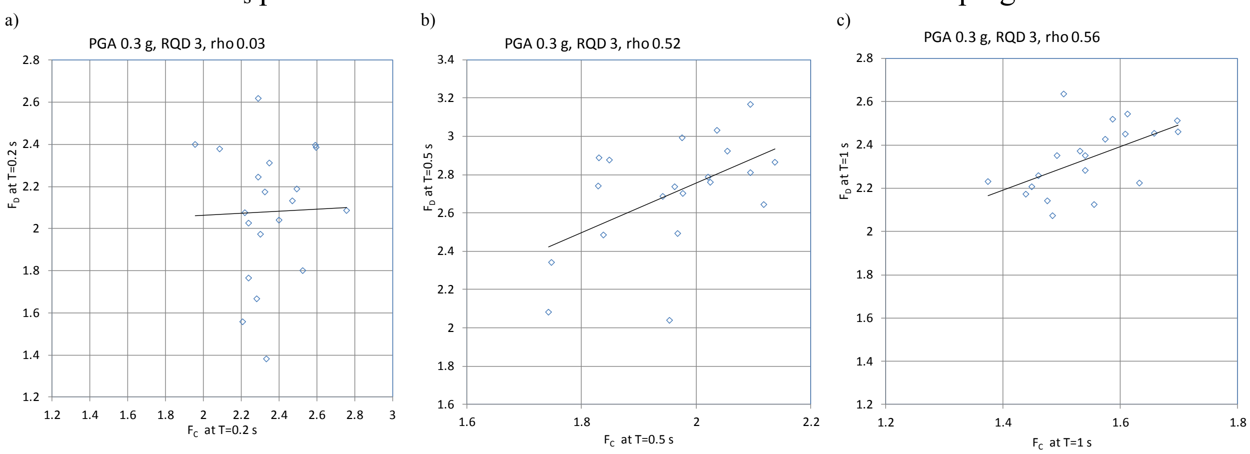

Figure 10.5: Correlation scatter plots for PGA of 0.3 g and RQD of 3 (Vs=2082 m/s) compare F_D and F_C calculated from the ground response to each of the 20 motions for T= 0.2, 0.5 and 1.0 s for randomized V_s profiles and randomized nonlinear shear modulus-damping curve.

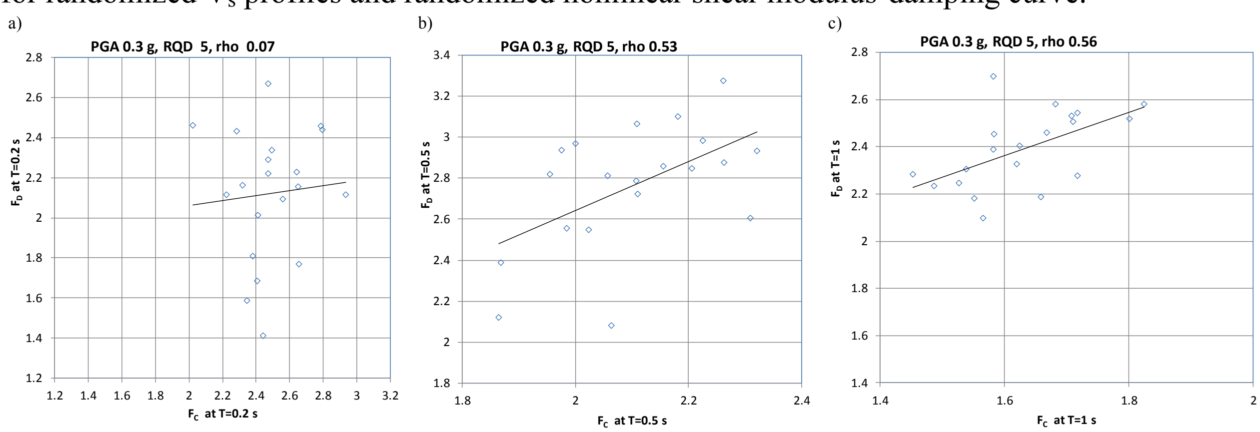

Figure 10.6: Correlation scatter plots for PGA of 0.3 g and RQD of 5 (V_s= 2926 m/s) compare F_D and F_C for T= 0.2, 0.5 and 1.0 s for randomized V_s profiles and randomized nonlinear shear modulus-damping curve.

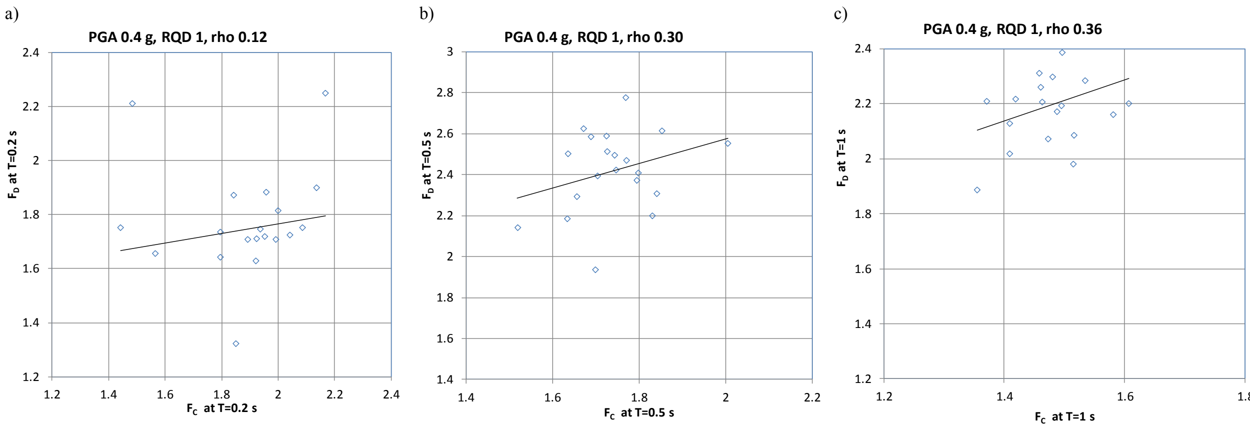

Figure 10.7: Correlation scatter plots for PGA of 0.4 g and RQD of 1 (V_s= 1258 m/s) compare F_D and F_C calculated from the ground response to each of the 20 motions for T= 0.2, 0.5 and 1.0 s for randomized V_s profiles and randomized nonlinear shear modulus-damping curve.

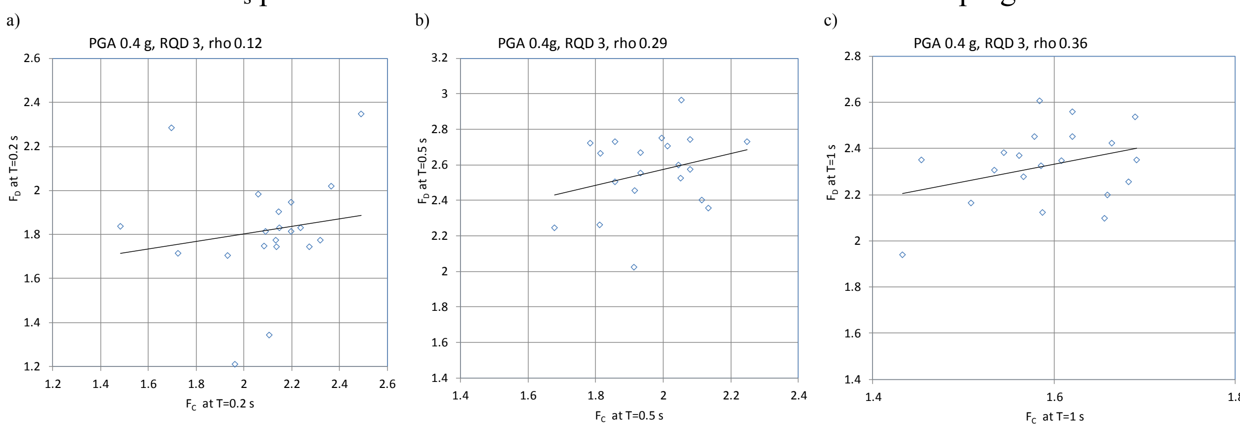

Figure 10.8: Correlation scatter plots for PGA of 0.4 g and RQD of 3 (V_s=2082 m/s) compare F_D and F_C calculated for T= 0.2, 0.5 and 1.0 s for randomized V_s profiles and randomized nonlinear shear modulus-damping curve.

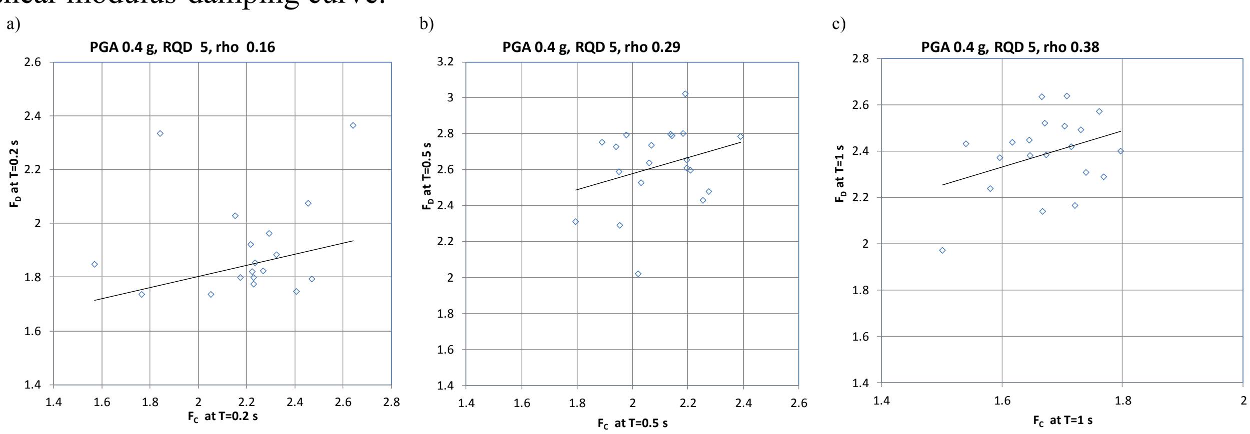

Figure 10.9: Correlation scatter plots for PGA of 0.4 g and RQD of 5 (V_s= 2926 m/s) compare F_D and F_C calculated from the ground response to each of the 20 motions for T= 0.2, 0.5 and 1.0 s for randomized V_s profiles and randomized nonlinear shear modulus-damping curve.

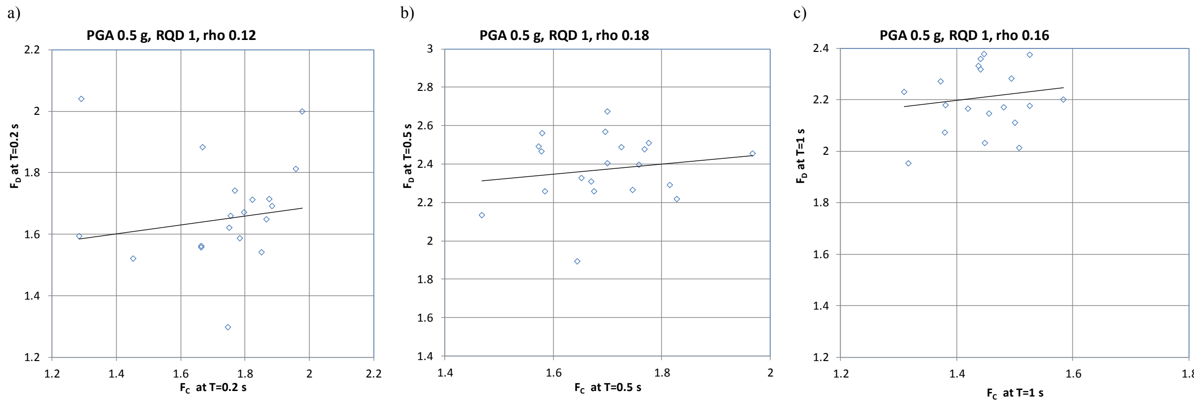

Figure 10.10: Correlation scatter plots for PGA of 0.5 g and RQD of 1 (V_s= 1258 m/s) compare F_D and F_C calculated from the ground response to each of the 20 motions for T= 0.2 , 0.5 and 1.0 s for randomized V_s profiles and randomized nonlinear shear modulus-damping curve.

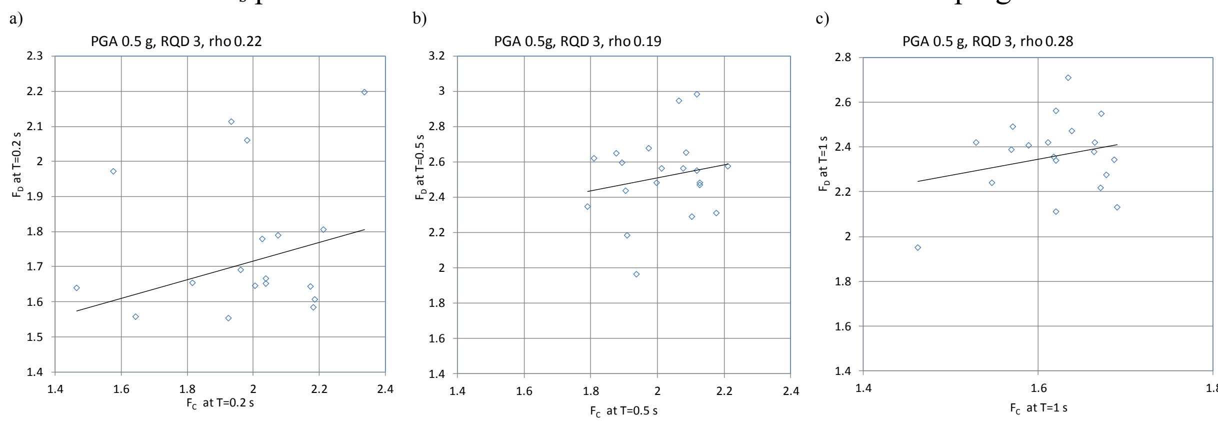

Figure 10.11: Correlation scatter plots for PGA of 0.5 g and RQD of 3 (V_s=2082 m/s) compare F_D and F_C calculated from the ground response to each of the 20 motions for T= 0.2 , 0.5 and 1.0 s for randomized V_s profiles and randomized nonlinear shear modulus-damping curve.

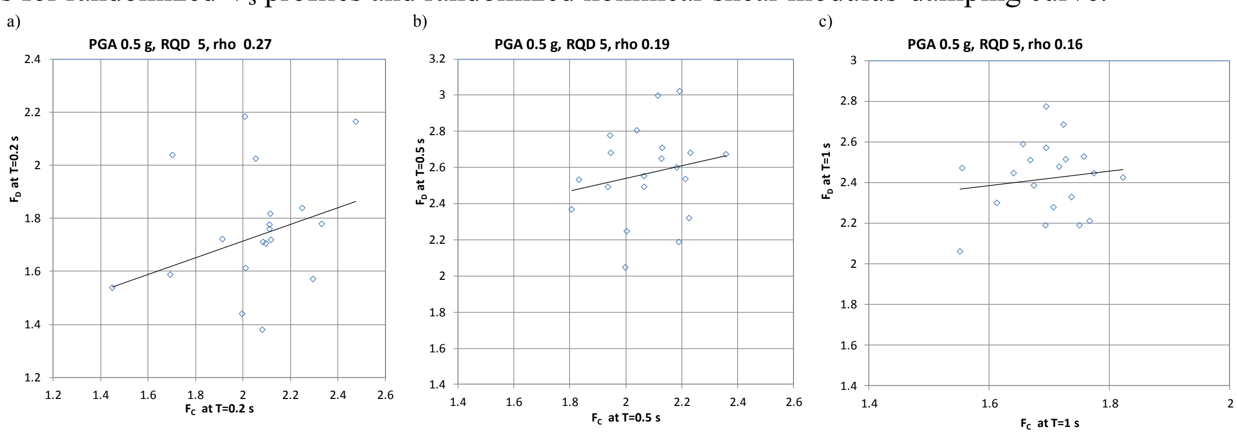

Figure 10.12: Correlation scatter plots for PGA of 0.5 g and RQD of 5 (V_s=2926 m/s) compare F_D and F_C calculated for T= 0.2 , 0.5 and 1.0 s for randomized V_s profiles and randomized nonlinear shear modulus-damping curve.

11 Appendix E

Scatter plots showing correlation between F_C and F_D calculated from the 1-D runs with randomized V_s profiles and constant dynamic nonlinear properties for PGA 0.1 g to 0.5 g.

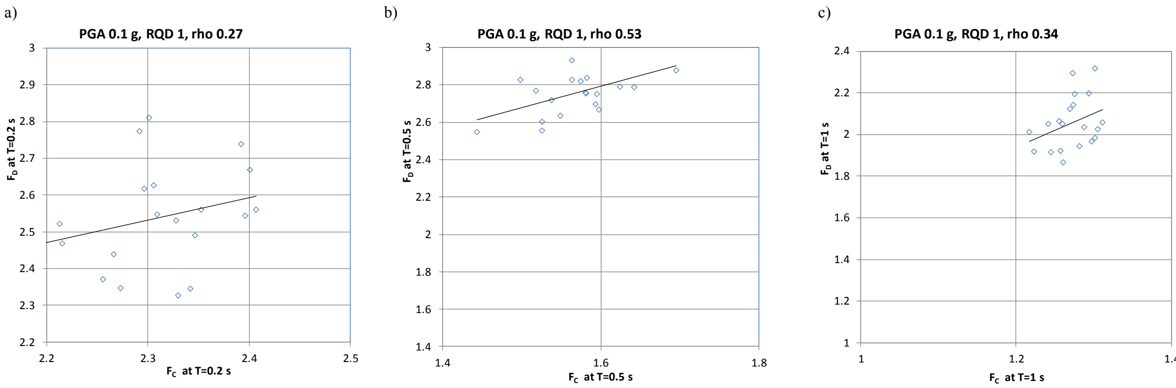

Figure 11.1: Correlation scatter plots for PGA of 0.1 g and RQD of 1, compare F_D and F_C calculated from the ground response to each of the 20 motions for T= 0.2 , 0.5 and 1.0 s for randomized V_s profiles.

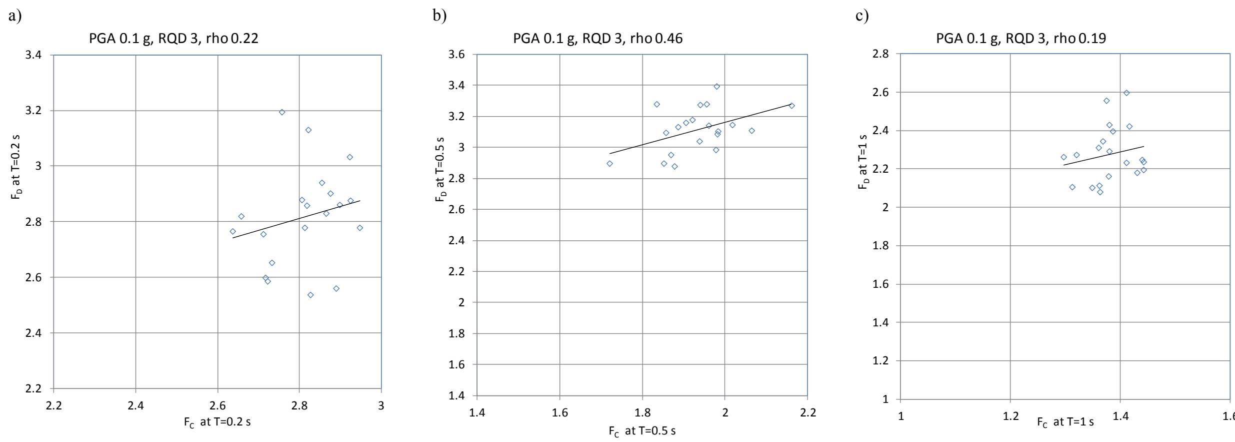

Figure 11.2: Correlation scatter plots for PGA of 0.1 g and RQD of 3 compare F_D and F_C calculated from the ground response to each of the 20 motions for T= 0.2 , 0.5 and 1.0 s for randomized V_s profiles.

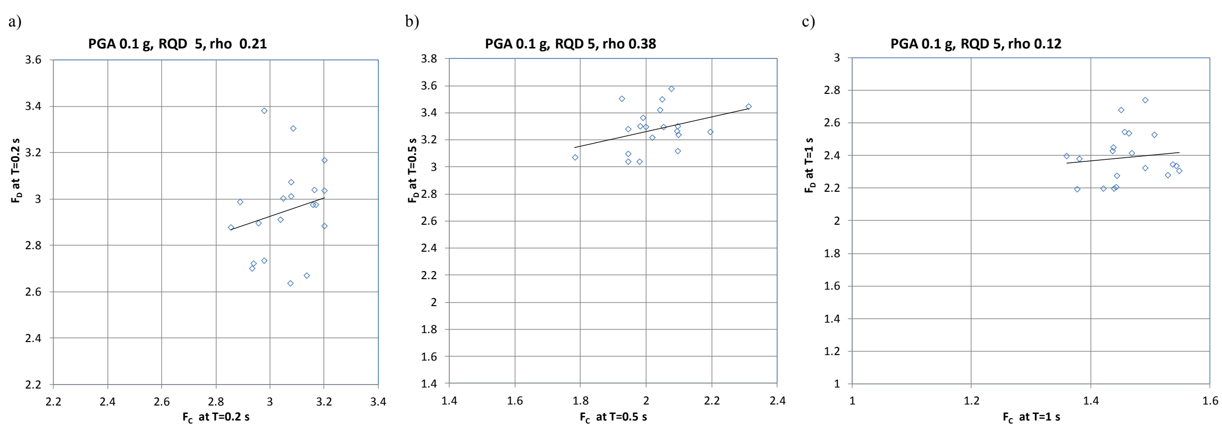

Figure 11.3: Correlation scatter plots for PGA of 0.1 g and RQD of 5 compare F_D and F_C calculated from the ground response to each of the 20 motions for T= 0.2 , 0.5 and 1.0 s for randomized V_s profiles.

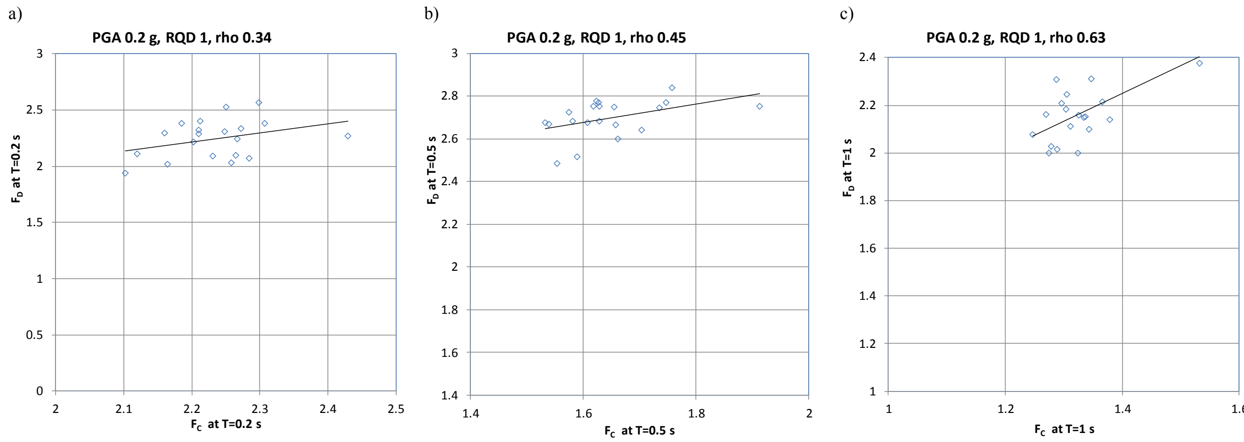

Figure 11.4: Correlation scatter plots for PGA of 0.2 g and RQD of 1 compare F_D and F_C calculated from the ground response to each of the 20 motions for T= 0.2 , 0.5 and 1.0 s for randomized V_s profiles.

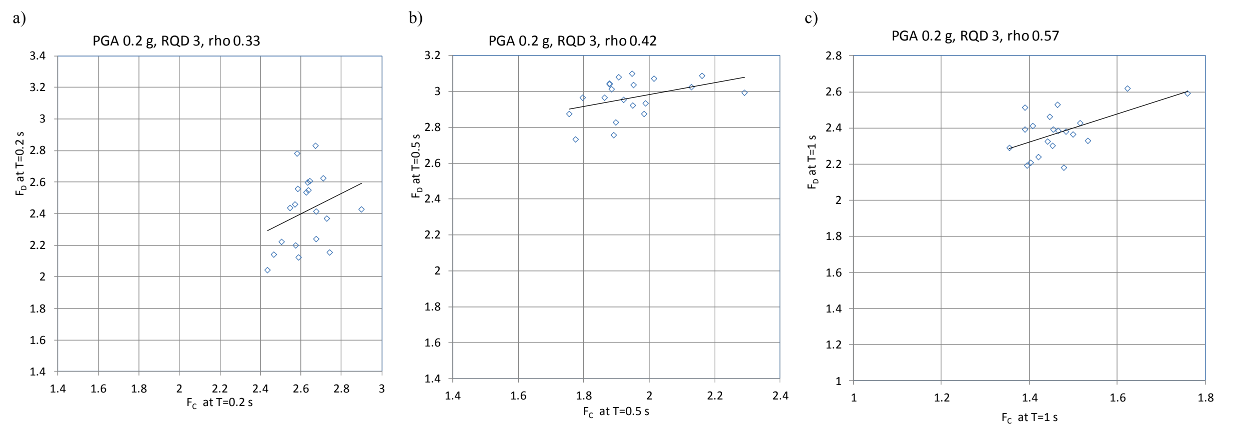

Figure 11.5: Correlation scatter plots for PGA of 0.2 g and RQD of 3 compare F_D and F_C calculated from the ground response to each of the 20 motions for T= 0.2 , 0.5 and 1.0 s for randomized V_s profiles.

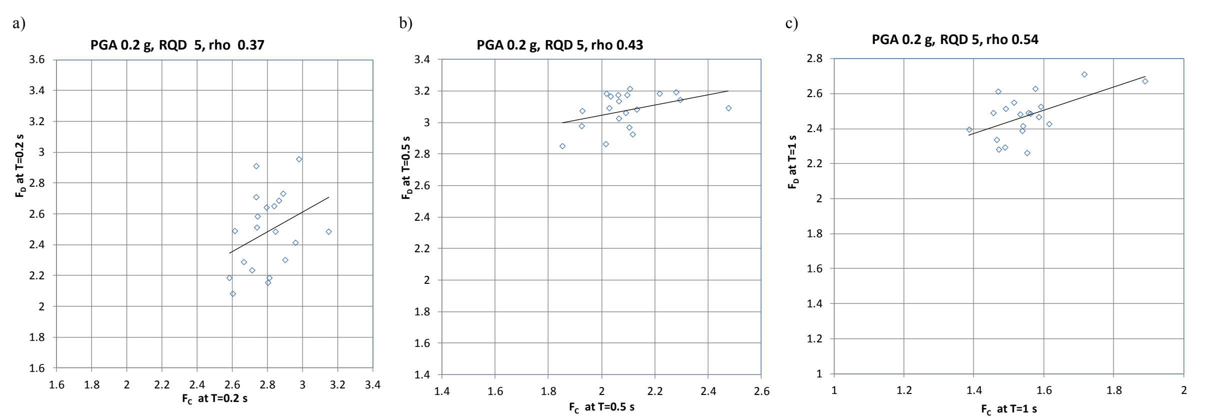

Figure 11.6: Correlation scatter plots for PGA of 0.2 g and RQD of 5 compare F_D and F_C calculated from the ground response to each of the 20 motions for T= 0.2 , 0.5 and 1.0 s for randomized V_s profiles.

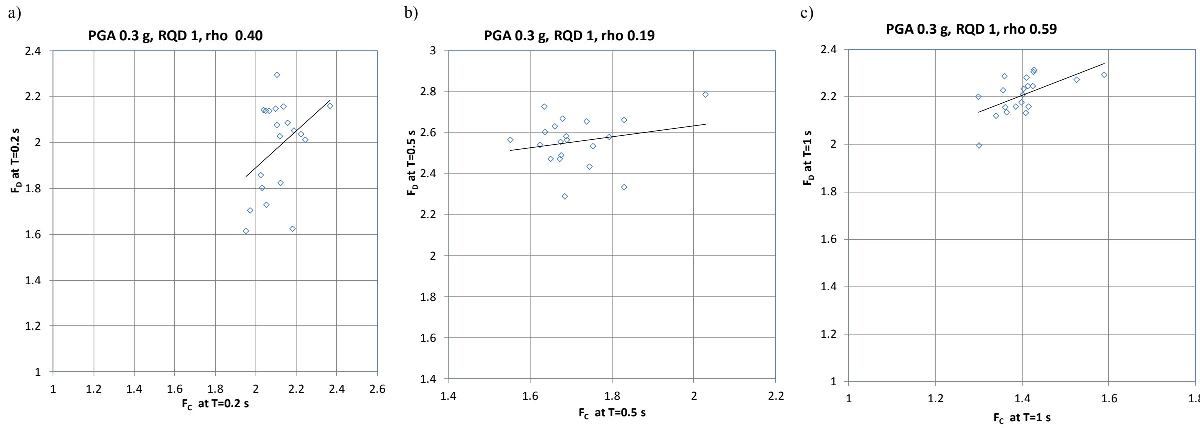

Figure 11.7: Correlation scatter plots for PGA of 0.3 g and RQD of 1 compare F_D and F_C calculated from the ground response to each of the 20 motions for T= 0.2 , 0.5 and 1.0 s for randomized V_s profiles.

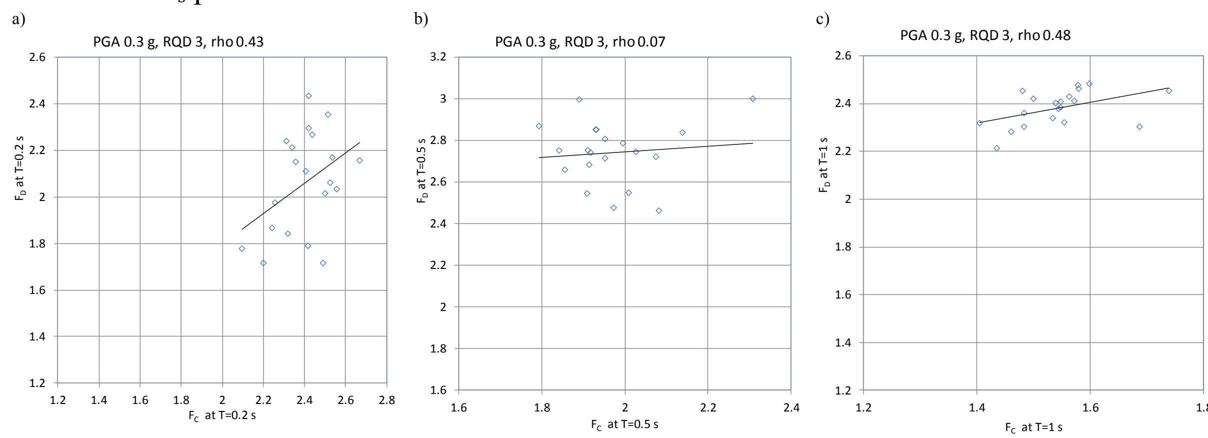

Figure 11.8: Correlation scatter plots for PGA of 0.3 g and RQD of 3 compare F_D and F_C calculated from the ground response to each of the 20 motions for T= 0.2 , 0.5 and 1.0 s for randomized V_s profiles.

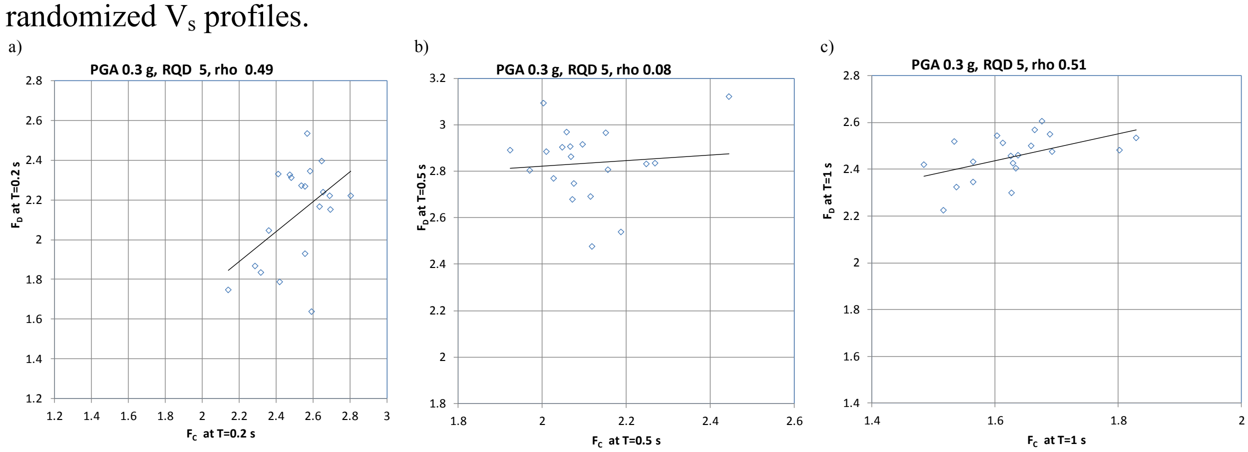

Figure 11.9: Correlation scatter plots for PGA of 0.3 g and RQD of 5 compare F_D and F_C calculated from the ground response to each of the 20 motions for T= 0.2 , 0.5 and 1.0 s for randomized V_s profiles.

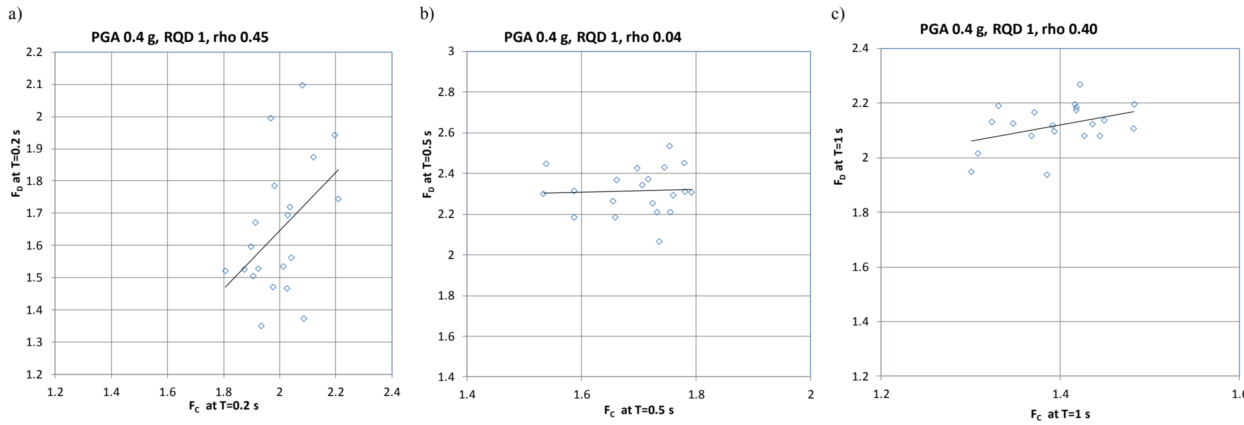

Figure 11.10: Correlation scatter plots for PGA of 0.4 g and RQD of 1 compare F_D and F_C calculated from the ground response to each of the 20 motions for T= 0.2 , 0.5 and 1.0 s for randomized V_s profiles.

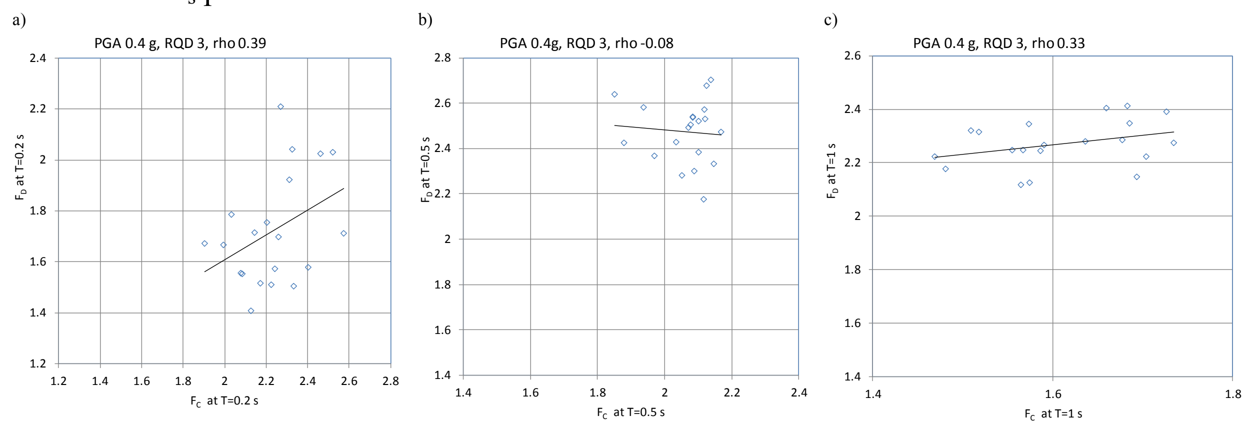

Figure 11.11: Correlation scatter plots for PGA of 0.4 g and RQD of 3 compare F_D and F_C calculated from the ground response to each of the 20 motions for T= 0.2 , 0.5 and 1.0 s for randomized V_s profiles.

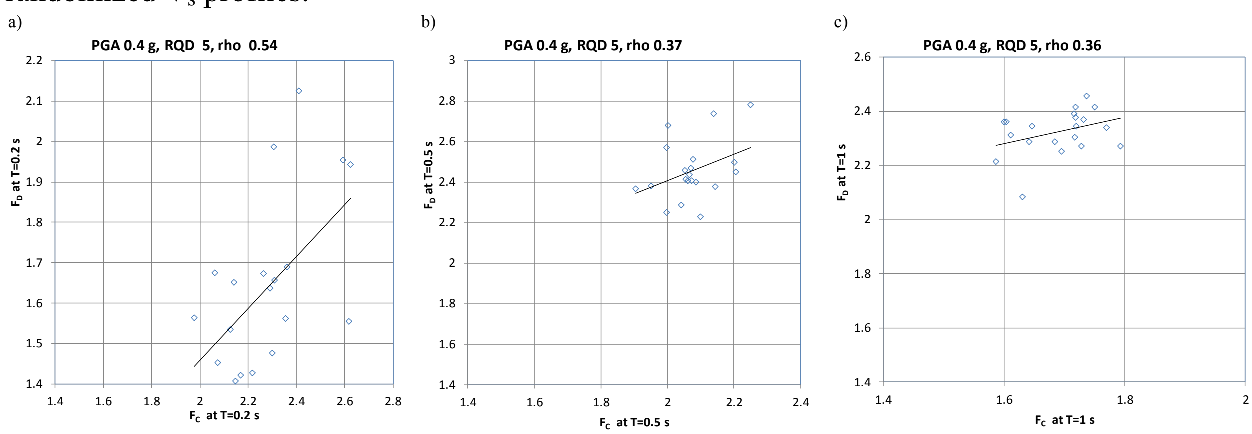

Figure 11.12: Correlation scatter plots for PGA of 0.4 g and RQD of 5 compare F_D and F_C calculated from the ground response to each of the 20 motions for T= 0.2 , 0.5 and 1.0 s for randomized V_s profiles.

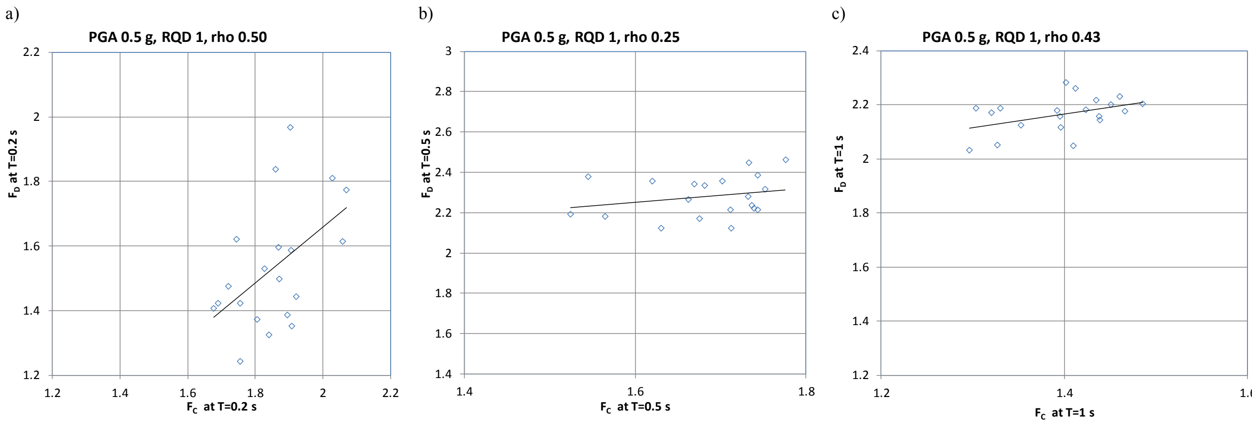

Figure 11.13: Correlation scatter plots for PGA of 0.5 g and RQD of 1 compare F_D and F_C calculated from the ground response to each of the 20 motions for T= 0.2 , 0.5 and 1.0 s for randomized V_s profiles.

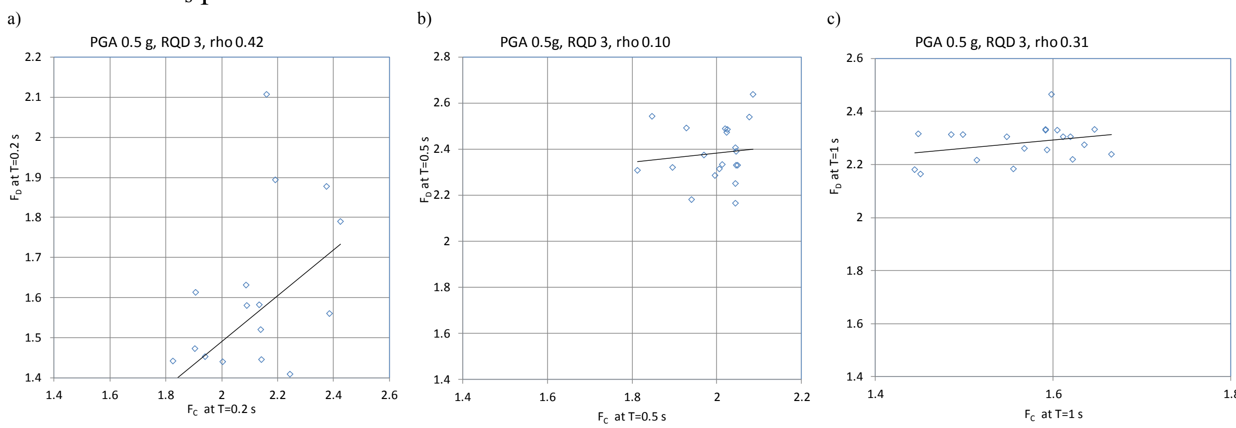

Figure 11.14: Correlation scatter plots for PGA of 0.5 g and RQD of 3 compare F_D and F_C calculated from the ground response to each of the 20 motions for T= 0.2 , 0.5 and 1.0 s for randomized V_s profiles.

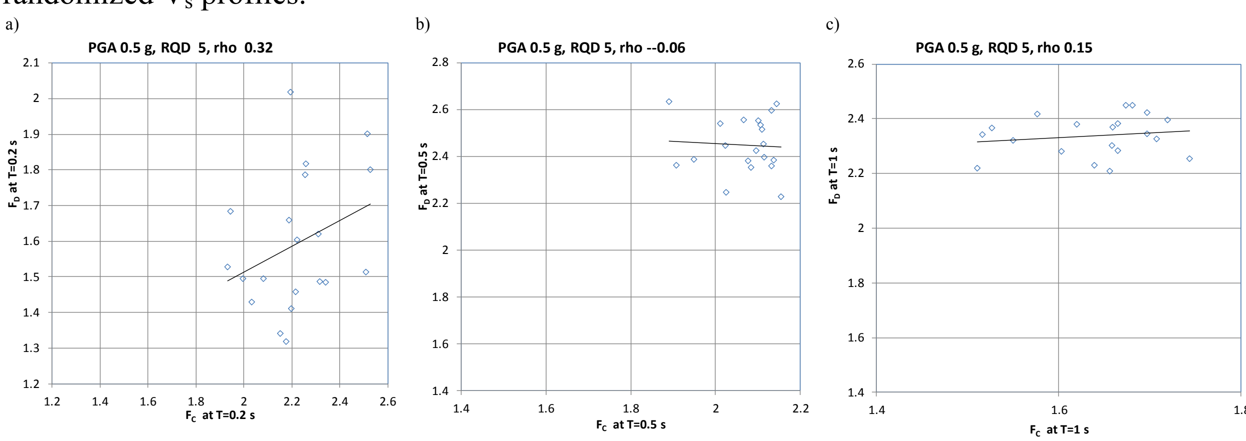

Figure 11.15: Correlation scatter plots for PGA of 0.5 g and RQD of 5 compare F_D and F_C calculated from the ground response to each of the 20 motions for T= 0.2 , 0.5 and 1.0 s for randomized V_s profiles.

12 Appendix F

Scatter plots showing correlation between F_C and F_D calculated from the 1-D runs with constant V_s profiles and randomized dynamic nonlinear properties for PGA 0.1 g to 0.5 g.

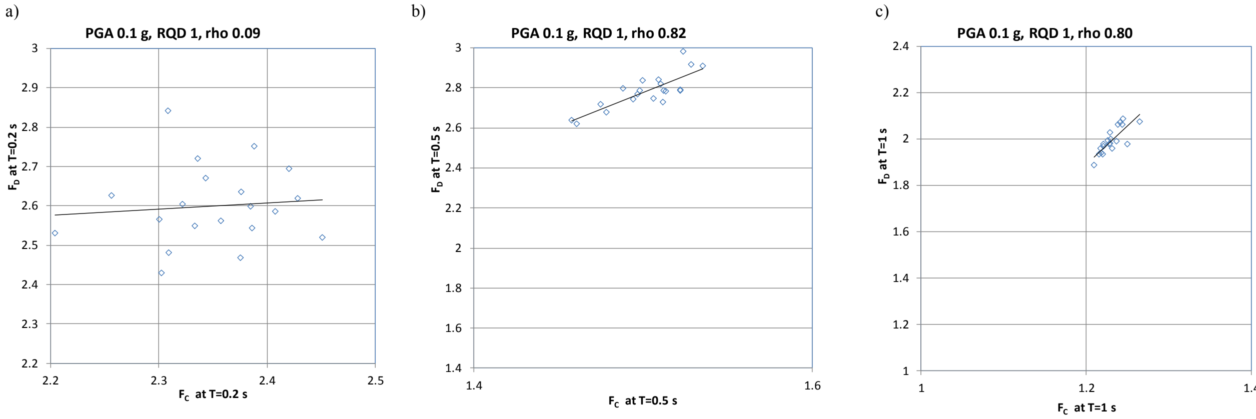

Figure 12.1: Correlation scatter plots for PGA of 0.1 g and RQD of 1, compare F_D and F_C calculated from the ground response to each of the 20 motions for T= 0.2 , 0.5 and 1.0 s for non-randomized V_s profiles.

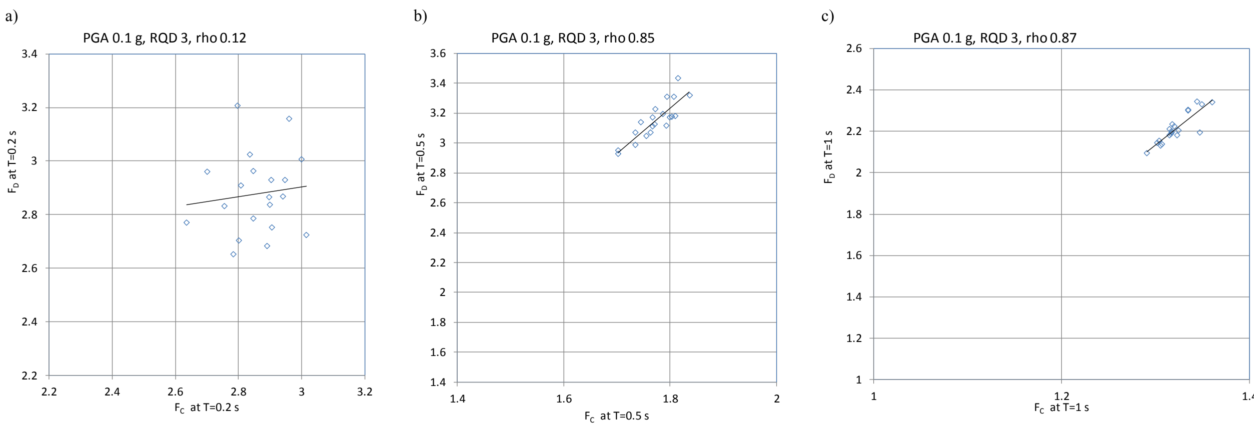

Figure 12.2: Correlation scatter plots for PGA of 0.1 g and RQD of 3 compare F_D and F_C calculated from the ground response to each of the 20 motions for T= 0.2 , 0.5 and 1.0 s for non-randomized V_s profiles.

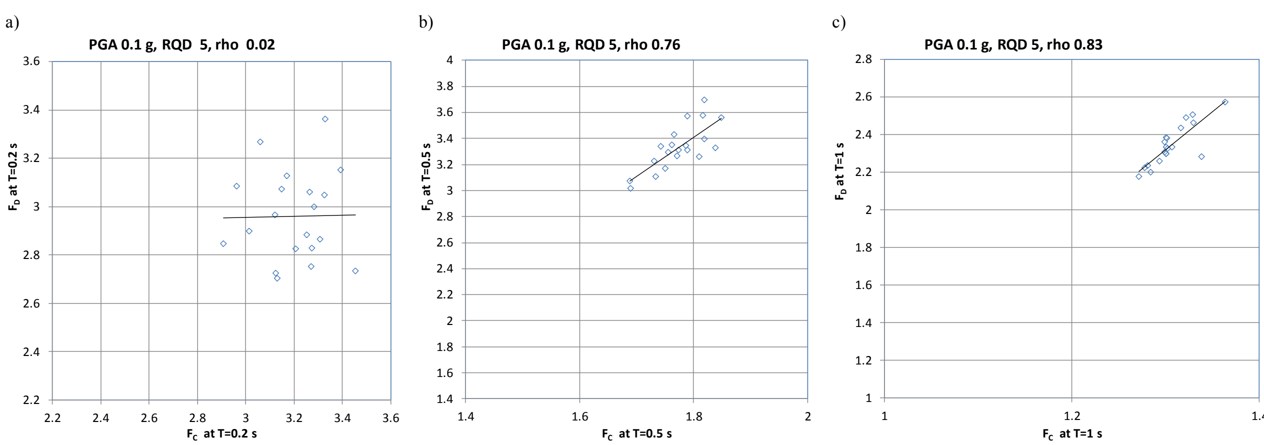

Figure 12.3: Correlation scatter plots for PGA of 0.1 g and RQD of 5 compare F_D and F_C calculated from the ground response to each of the 20 motions for T= 0.2 , 0.5 and 1.0 s for non-randomized V_s profiles.

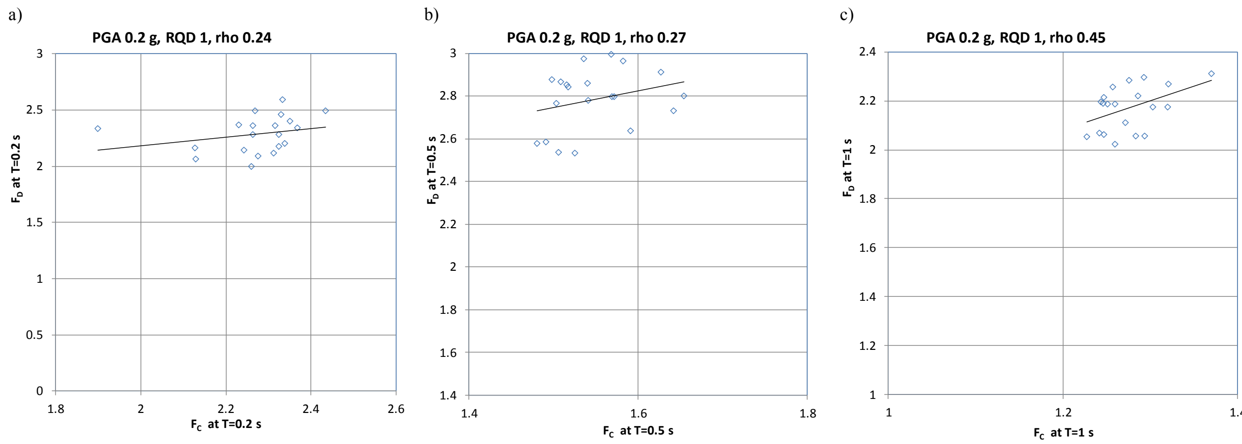

Figure 12.4: Correlation scatter plots for PGA of 0.2 g and RQD of 1 compare F_D and F_C calculated from the ground response to each of the 20 motions for T= 0.2 , 0.5 and 1.0 s for non-randomized V_s profiles.

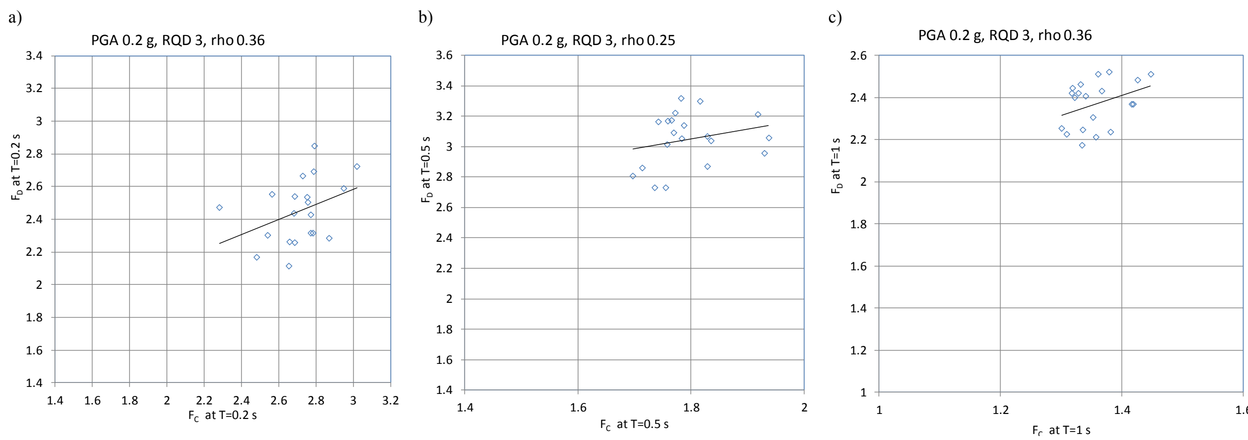

Figure 12.5: Correlation scatter plots for PGA of 0.2 g and RQD of 3 compare F_D and F_C calculated from the ground response to each of the 20 motions for T= 0.2 , 0.5 and 1.0 s for non-randomized V_s profiles.

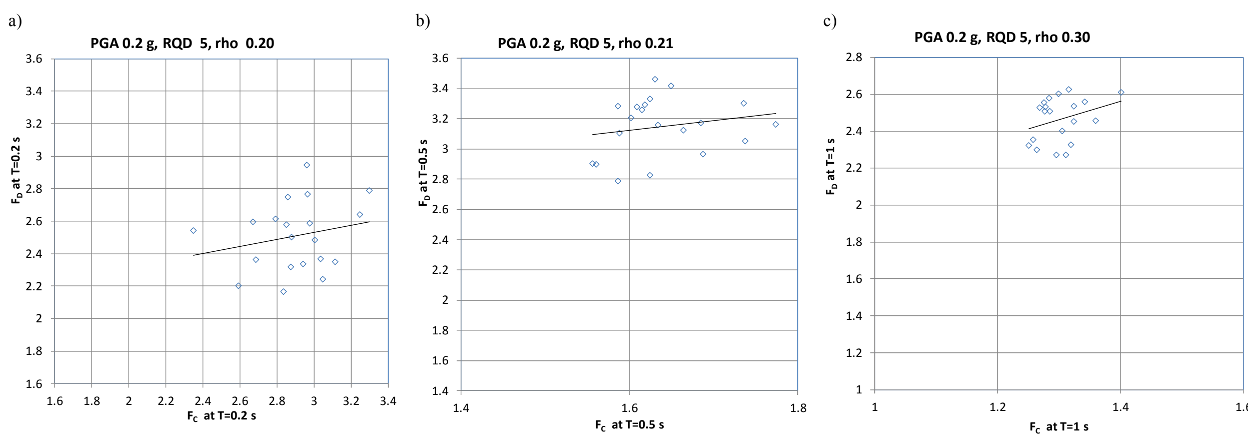

Figure 12.6: Correlation scatter plots for PGA of 0.2 g and RQD of 5 compare F_D and F_C calculated from the ground response to each of the 20 motions for T= 0.2 , 0.5 and 1.0 s for non-randomized V_s profiles.

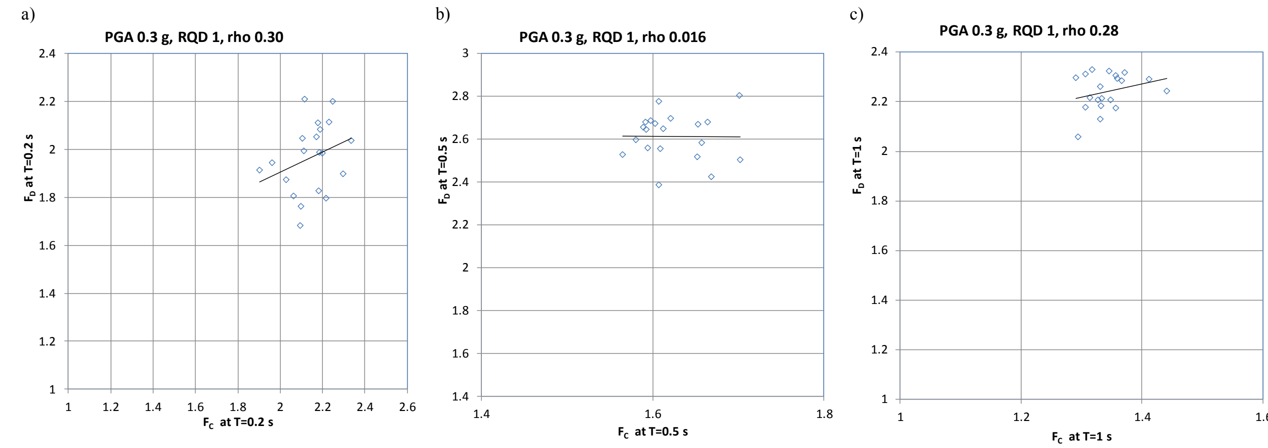

Figure 12.7: Correlation scatter plots for PGA of 0.3 g and RQD of 1 compare F_D and F_C calculated from the ground response to each of the 20 motions for T= 0.2 , 0.5 and 1.0 s for non-randomized V_s profiles.

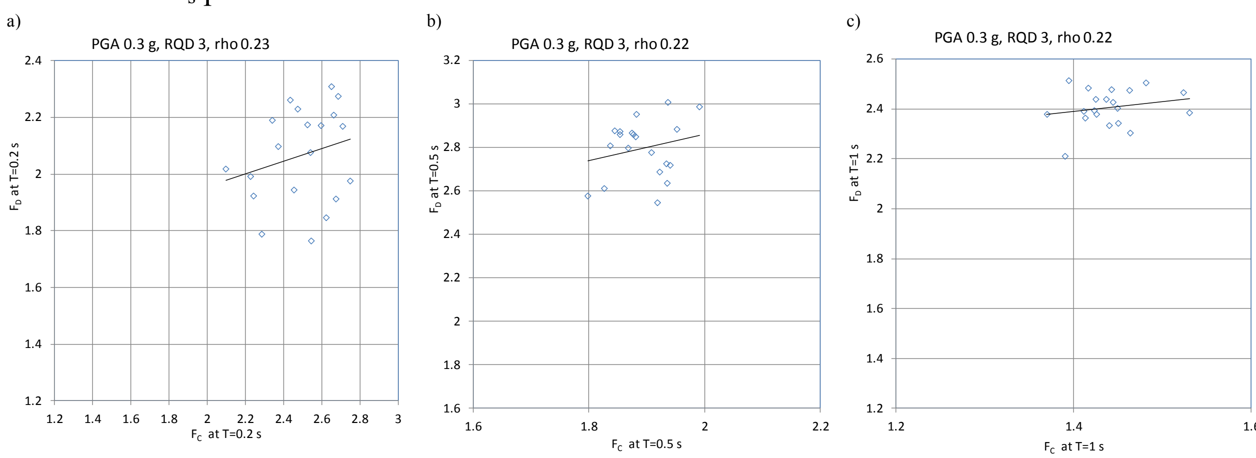

Figure 12.8: Correlation scatter plots for PGA of 0.3 g and RQD of 3 compare F_D and F_C calculated from the ground response to each of the 20 motions for T= 0.2 , 0.5 and 1.0 s for non-randomized V_s profiles.

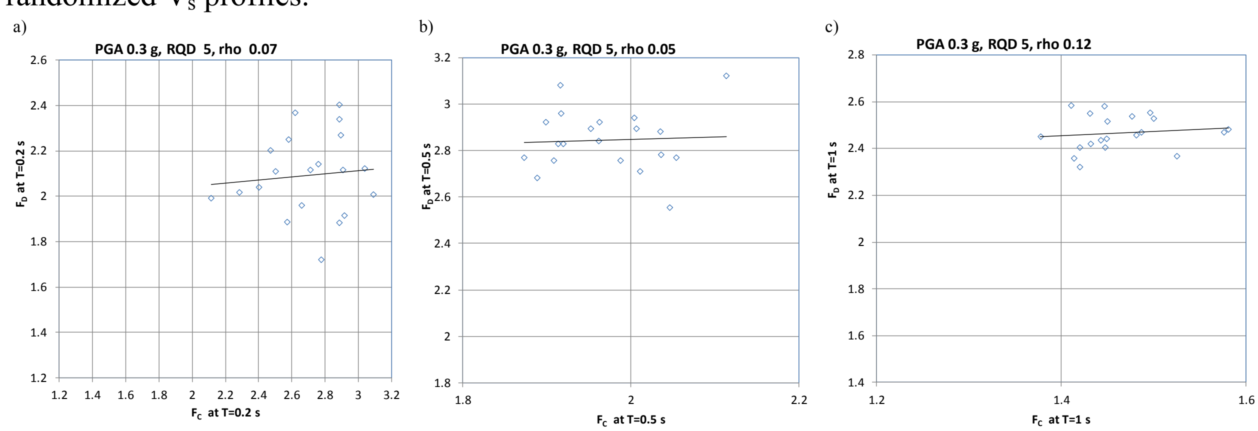

Figure 12.9: Correlation scatter plots for PGA of 0.3 g and RQD of 5 compare F_D and F_C calculated from the ground response to each of the 20 motions for T= 0.2 , 0.5 and 1.0 s for non-randomized V_s profiles.

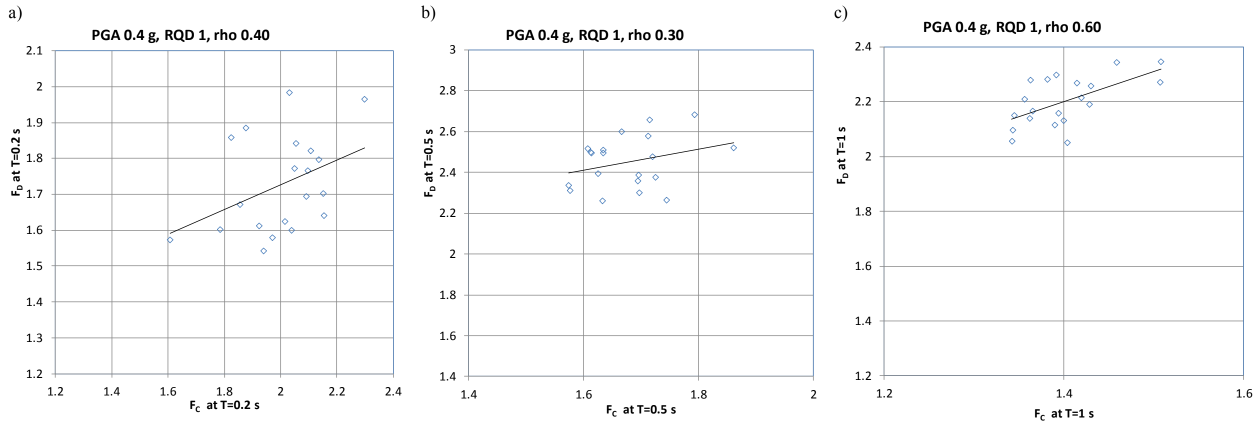

Figure 12.10: Correlation scatter plots for PGA of 0.4 g and RQD of 1 compare F_D and F_C calculated from the ground response to each of the 20 motions for T= 0.2 , 0.5 and 1.0 s for non-randomized V_s profiles.

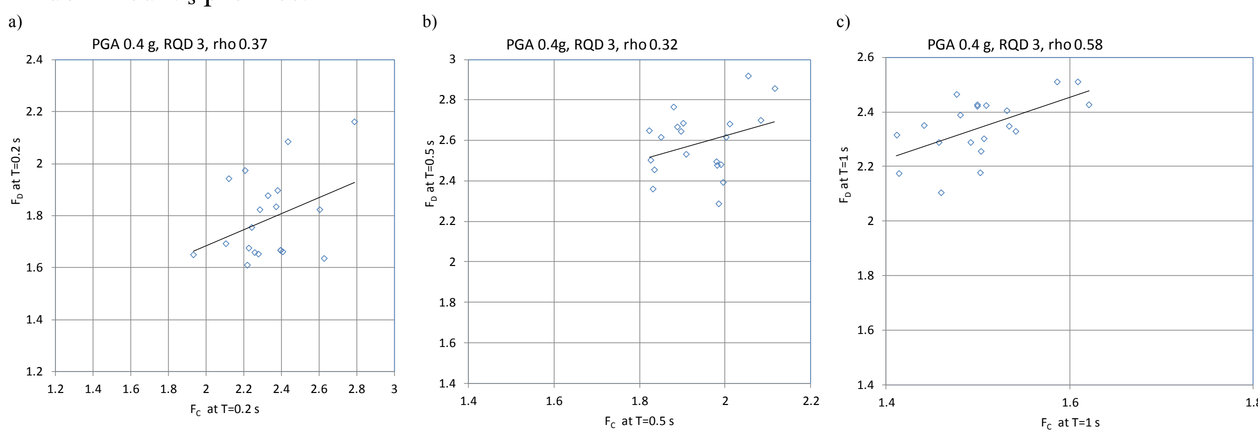

Figure 12.11: Correlation scatter plots for PGA of 0.4 g and RQD of 3 compare F_D and F_C calculated from the ground response to each of the 20 motions for T= 0.2 , 0.5 and 1.0 s for non-randomized V_s profiles.

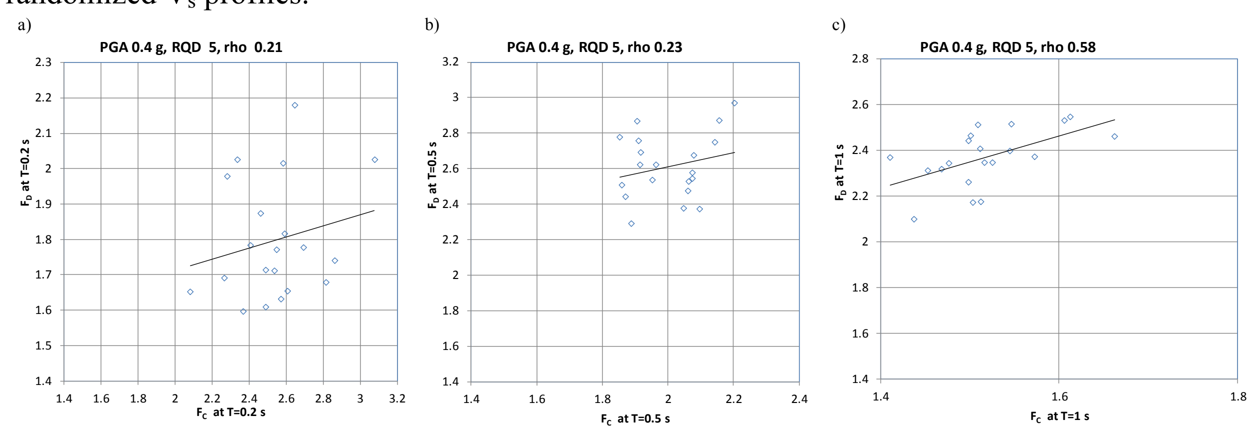

Figure 12.12: Correlation scatter plots for PGA of 0.4 g and RQD of 5 compare F_D and F_C calculated from the ground response to each of the 20 motions for T= 0.2 , 0.5 and 1.0 s for non-randomized V_s profiles.

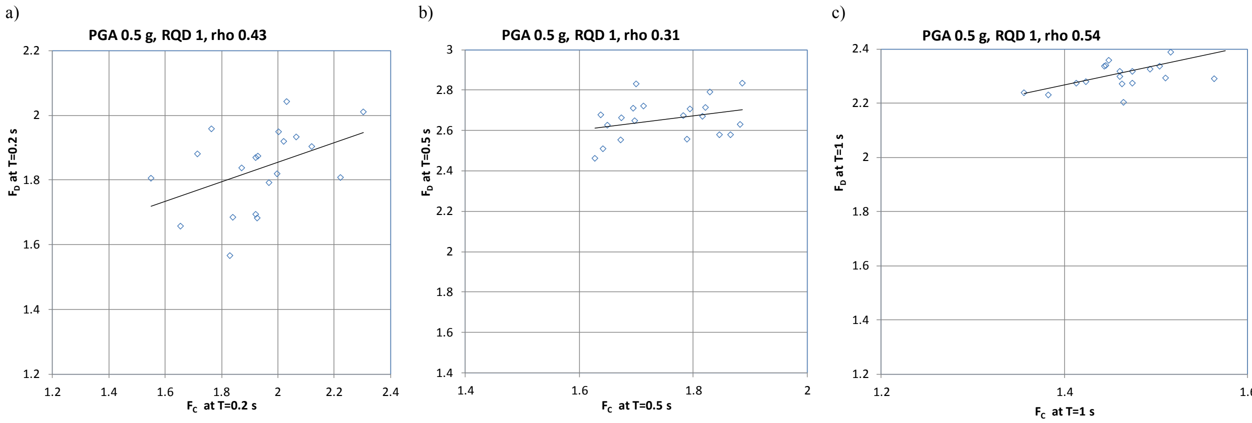

Figure 12.13: Correlation scatter plots for PGA of 0.5 g and RQD of 1 compare F_D and F_C calculated from the ground response to each of the 20 motions for T= 0.2 , 0.5 and 1.0 s for non-randomized V_s profiles.

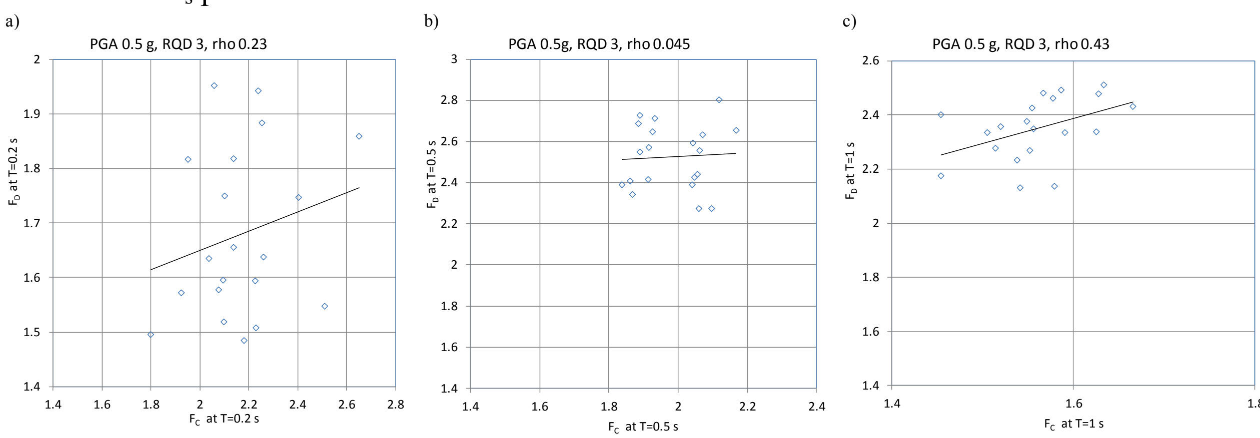

Figure 12.14: Correlation scatter plots for PGA of 0.5 g and RQD of 3 compare F_D and F_C calculated from the ground response to each of the 20 motions for T= 0.2 , 0.5 and 1.0 s for non-randomized V_s profiles.

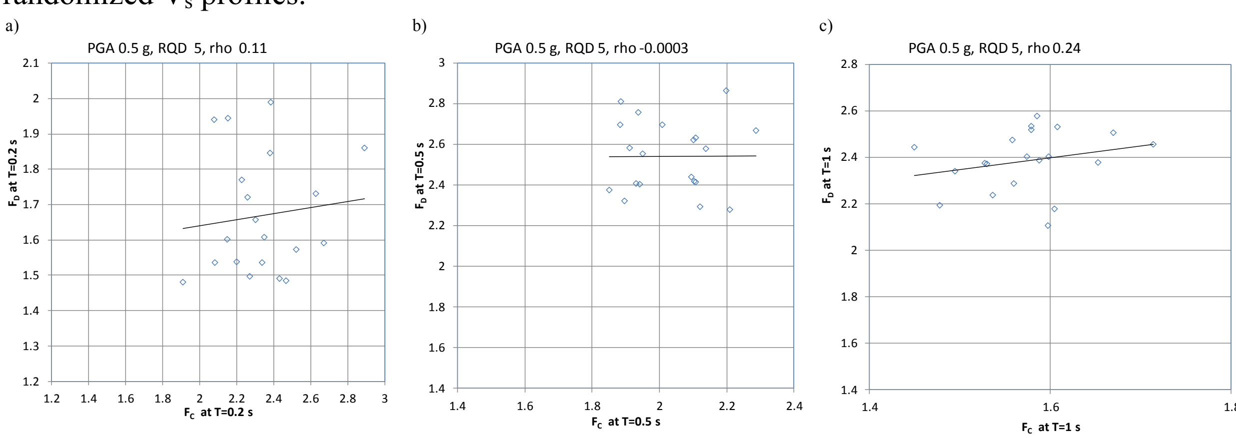

Figure 12.15: Correlation scatter plots for PGA of 0.5 g and RQD of 5 compare F_D and F_C calculated from the ground response to each of the 20 motions for T= 0.2 , 0.5 and 1.0 s for non-randomized V_s profiles.